CDF Study Report

ATHENA

Assessment of an X-Ray Telescope for the ESA Cosmic Vision Program

TABLE OF CONTENTS

1 INTRODUCTION

1.1 Background

The Hot and Energetic Universe has been selected as the Science Theme for the second large-class mission (L2), due for launch in 2028 in ESA's Cosmic Vision program. The theme poses two key astrophysical questions:

- How does ordinary matter assemble into the large-scale structures we see today?
- How do black holes grow and shape the Universe?

Understanding the Hot and Energetic Universe requires space-based observations in the X-ray band, specifically spatially-resolved X-ray spectroscopy and deep wide-field X-ray spectral imaging with performance greatly exceeding that offered by the current X-ray observatories like XMM Newton and Chandra, or by missions soon to be launched such as Astro-H and SRG/eROSITA.

The Hot and Energetic Universe has been studied in the ESA Concurrent Design Facility (CDF) previously with X-ray telescopes being studied in the IXO study (CDF-082(A) dated December 2008) and the IXO International X-Ray Telescope study (CDF-086(A) dated April 2009). IXO was also studied with two full industrial phase A studies and ATHENA_L1 has been studied both internally at ESA and externally by industry in 2011. All the above data was made available as source information for this CDF Study.

This study has been requested by SRE-FM and financed by the General Studies Program (GSP). It was carried out in the CDF by a team of specialists from ESTEC and ESOC in 9 sessions starting with a kick-off on the 16th September 2014 and ending with an Internal Final Presentation on the 23rd October 2014.

1.2 Scope

This CDF study was to build on the previous work carried out, and to particularly focus on the following:

- Maximising the effective area of the telescope taking Launcher and ESA CaC constraints into consideration
- Instrument accommodation, with particular emphasis on their thermal accommodation
- Finding the optimum solution for sharing a single Telescope between 2 instruments – more specifically, changing the focus either by a:
    - Moveable Instrument Platform (MIP)
    - Moveable Mirror Assembly (MMA)
- The SC structural design, particularly with respect to Mirror Module (MM) shock/vibration isolation
- Overall mission architecture design (including SC requirements) to satisfy the Target-of-Opportunity (ToO) response requirements
- Identifying sensible international contribution possibilities on the basis of technical and programmatic interfaces.

1.3 Previous Studies

The ATHENA mission architecture and SC design have in most respects a great deal of flight and study heritage. ESA now has much engineering and operational experience regarding Lagrange Point 2 missions, with the successful flight of Herschel, Planck and Gaia, and the forthcoming missions Euclid and Plato.

The overall mission architecture for the ATHENA mission (with the exception of the tightened ToO-response requirement) has been well defined in previous study phases, and was accordingly not the focus of the ATHENA CDF study. The ATHENA CDF study was primarily concerned with the SC design, taking the Payload (PL), including X-IFU Cooling Chain (CC) as CFI inputs.

The ATHENA SC also has many commonalities and heritage to exploit from the XMM-Newton and Chandra missions. The SC configuration is similar (dominated by the required focal length), and exploitation of certain technology items from these missions can be foreseen (e.g. telescope venting doors.)

Predecessors to the ATHENA mission (XEUS, IXO, ATHENA_L1) have been well studied (IXO to Phase A) (RD[5], RD[2], RD[51], RD[52], RD[53], RD[54]) and a lot of knowledge has been generated that can be applied to the ATHENA Phase 0/A. The requirements of the currently proposed mission (excluding ToO response) are equivalent to or encapsulated by the requirements that were applicable to the IXO/ATHENA_L1 studies (A_eff, HEW…see Table 2-1), and accordingly the general statement can already be made that the mission is technically feasible.

1.4 Document Structure

The layout of this report can be seen in the Table of Contents. The Executive Summary chapter provides an overview of the study; details of each domain addressed in the study are contained in specific chapters.

Due to the different distribution requirements, only cost assumptions excluding figures are given in this report. The costing information is published in a separate document.

2 EXECUTIVE SUMMARY

2.1 Study Flow

The mandate for this study was that it must be possible for ESA to undertake the ATHENA mission independently of any international contributions (accordingly significant technology development is underway in the critical areas of, among others, optics and CC technology RD[50]). A pre-CDF costing exercise was therefore conducted in order to identify and target a SC design-point which would result in a CaC, assuming no international contributions, close to the 1Bn (2013 EC) CaC limit. This was necessary because it is not possible to iterate the SC/Mission design in response to cost during the compressed schedule of the CDF study.

The result of this pre-costing activity indicated that targeting an ATHENA_L1-class SC (standard LV I/F, no deployable focal plane as with IXO) would be necessary to constrain the cost, and that even with this measure the CaC would be likely to significantly exceed the limit.

An additional concern was the programmatic uncertainty surrounding the availability of A5 ECA. A6 mass and volume constraints are still uncertain, and initial indications (Summer 2014) were that it would have less mass capability to L2 (~5.3t) than A5 ECA (~6.6t). Although A5 ECA was mandated as the baseline launch vehicle, targeting a reduced SC size/mass was considered a prudent measure to maintain compatibility with the eventual design of A6[1].

Therefore, the study started on September 16th 2014 based on the premise of using the standard 2624 LVA on Ariane 5 ECA. The initial sessions focused on expanding the design trade-space with respect to the possible Instrument Switch Mechanism (ISM) solutions to share the focal point between the two instruments. On session 5, a system level trade-off led to the choice of the a Movable Mirror Assembly (MMA) solution with 6 DOF for the ISM. This option was pursued and detailed in the following design sessions. The overall study flow in shown on Figure 2-1.

[1] Note now that the situation regarding A6 has now changed, with a more powerful 'heavy' version (A-64) approved for development at the ESA Council of Ministers CM-14; this would have a mass performance of 10.9t to GTO (this should translate to well over 8t to L2).

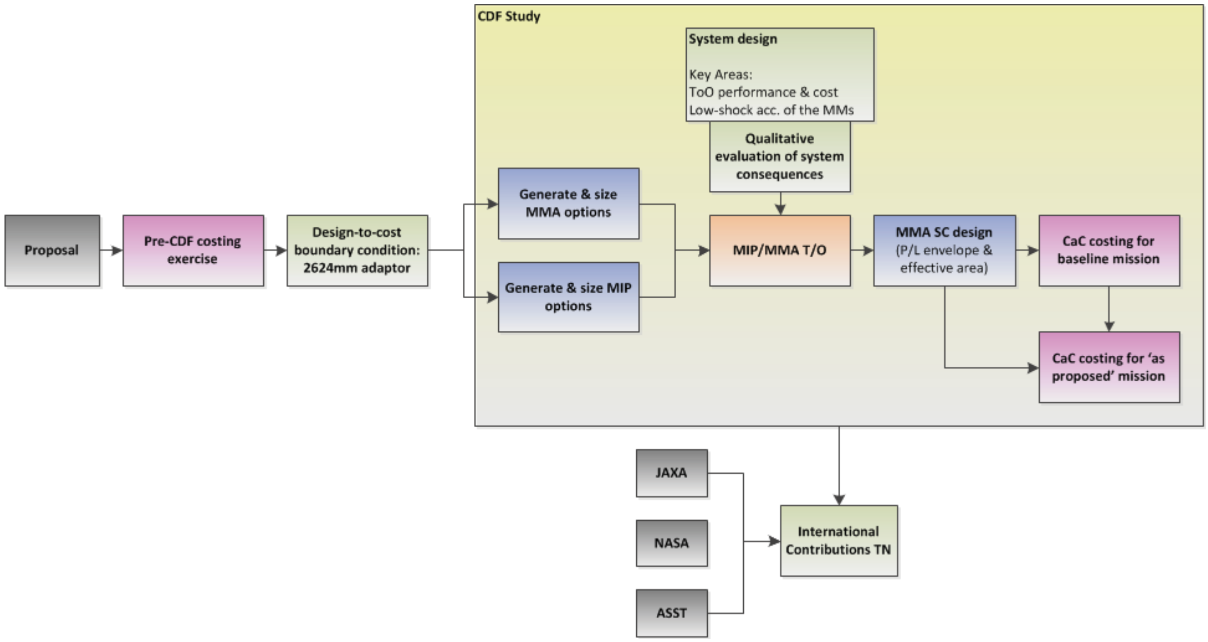

Figure 2-1: CDF study flow

2.2 Requirements and Design Drivers

There were a number of critical differences in the requirements (highlighted in red in Table 2-1) w.r.t. previous studies (see Chapter 1.3), which, when combined with programmatic boundary conditions, merit careful consideration when approaching the mission and SC design for the currently proposed L2 concept. The main considerations are outlined below.

Parameter	IXO	ATHENA_L1	ATHENA
System Requirements			
# Instruments	6	2	2
On-axis A_eff (~1keV)	2.5m^2 (@1.25keV)	1m^2 (@1.25keV)	2m^2 (@1keV)
On-axis A_eff (6keV)	0.65m^2	0.5m^2	0.25m^2
PSF HEW (on axis, <~8keV)	5''	10''	5''
AKE (a posteriori)	1'' (3σ)	1.5'' (3σ)	1'' (3σ)
ToO reaction time	<24h	<8-12h	<4h 80% of cases
Inst. Funct. Requirements			
X-IFU e_res	2.5eV	3eV	2.5eV
X-IFU FoV	2' diameter	3' diameter	5' diameter
WFI e_res	150eV	150eV	150eV
WFI FoV	18'x18'	24'x24'	40'x40'

Inst. Resource Requirements			
X-IFU (inc. CC)	(all instruments)		
Mass*	663 kg	409 kg	583 kg
Power*	1621 W	1005 W	1452 W
WFI			
Mass*	-	83 kg	288 kg
Power*	-	187 W	684 W

Table 2-1: Comparison of IXO, ATHENA_L1 and ATHENA key performance requirements

*Mass/power given are 'nominal' (design maturity margin but no system margin).

Note that the design constraint to use the 2624 LVA meant the effective area requirement at 1 keV of the mission as proposed would clearly not be met.

The following subchapters introduce the design drivers identified at the beginning of the study.

2.2.1 Payload Resource Envelope

ATHENA differs markedly from ATHENA_L1 (which had ostensibly the same instrument complement) in the resource requirements of the payloads, as can be seen from Table 2-1.

Note that the CC is considered as a CFI for the purpose of the CDF study. Also note that the CC envelope was assumed at the start of the CDF study to be an all European CC solution which is considerably more resource hungry than the JAXA equivalent.

The high resource envelope of the instruments raised the following primary concerns about the feasibility of accommodating them as-proposed:

a) **Mass accommodation:** Although the overall A5 ECA mass envelope to Lagrange Point 2 (6.6t) is less concerning, it was feared that ATHENA, having a fixed structure with a ~12m focal length, would be at best marginally compliant with the static moment requirements of the 2624mm adaptor. A pre-CDF evaluation indicated marginal compliance for the reduced version of the SC mandated by [1]. Furthermore the mass at the FPM was now comparable to the mass of the MAM, which raises the possibility that moving the MAM (using a Moveable Mirror Assembly – MMA) is an equally valid solution for switching the focal point between the two instruments.

b) **Thermal accommodation:** The power consumption (hence dissipation) of the PL as proposed is significantly larger than for ATHENA_L1, leading to a major concern that insufficient radiator area would be available at the FPM.

c) **Volume accommodation:** The increased dimensions of the PL make their accommodation under the Ogive of the fairing more challenging.

2.2.2 ToO Reaction Time

The ToO-reaction speed requirement was tightened very significantly since IXO/ATHENA_L1 – this capability was given primacy in the L2 call RD[57] as well as the SSAC paper RD[58]. Shock protection of the Mirror Modules

Previous system designs of IXO/ATHENA_L1 gave no specific attention to design solutions to reduce the shock environment seen by the MMs during launch. There was a strong motivation to do so for this study due to concerns from on-going technology development activities about the shock-levels that could be safely tolerated.

2.3 Mission

A summary of the mission architecture that resulted from the CDF evaluation is given in the IDEF0 shown in the following figure. More details can be found in the Concept of Operations document RD[7]. The Mission involves an Ariane 5 (now 6) launch to a large-amplitude Halo orbit around L2.

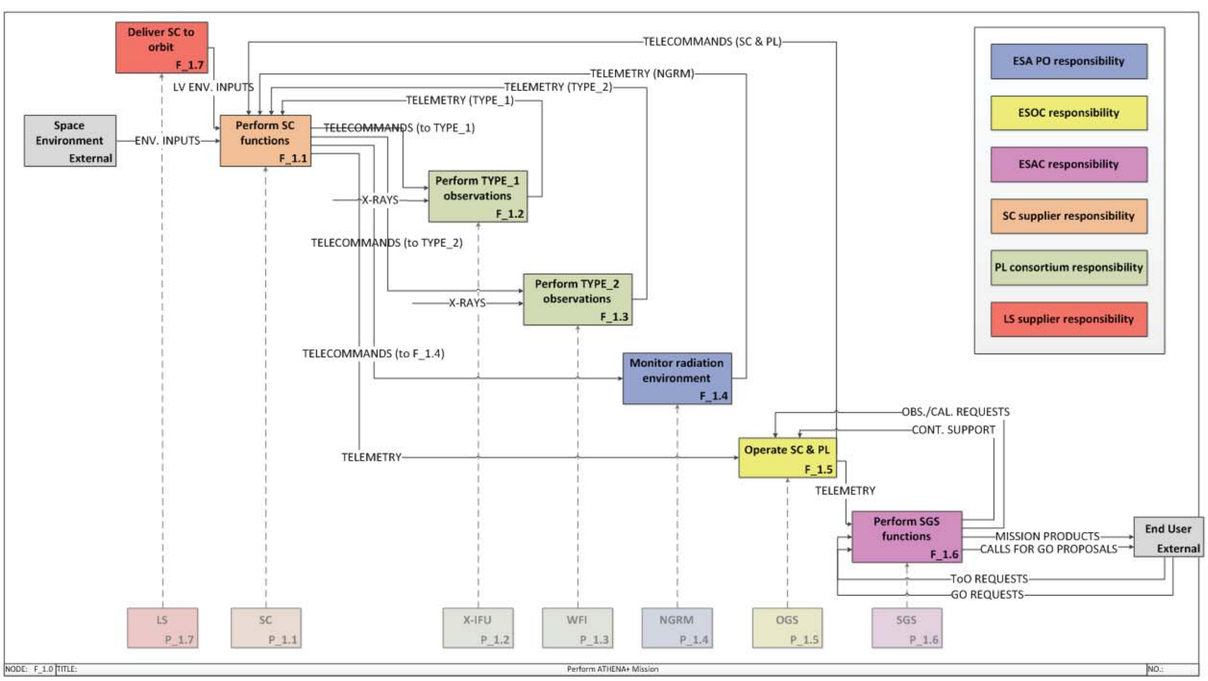

Figure 2-2: ATHENA Mission functional architecture in IDEF0 format

ATHENA Mission	
Mass (incl. Margin)	Dry mass: 5477 kg
	Propellant mass: 530 kg
	Adapter mass: 125 kg
	Wet mass: 6133 kg

Launch Date	2028
Lifetime	5 +5 (extended operations) years
Orbit	Large Halo around L2 (No Eclipse)
	Direct Insertion
Launcher	Ariane 5 ECA (2624 LVA)

Table 2-2: Baseline mission parameters

ATHENA Spacecraft			
Mass (incl. Margin)	Dry mass: 5477 kg		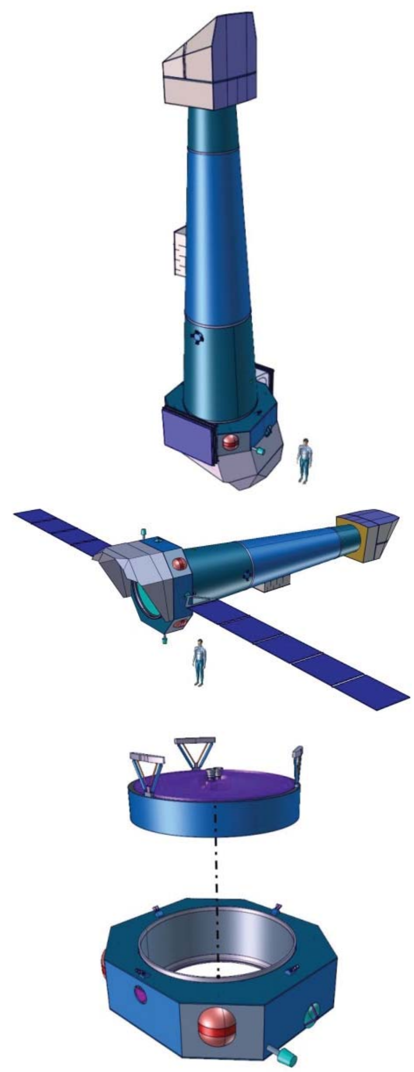
Dimensions	Height: 15 m Mirror diameter: 2570 mm Mirror effective area (1keV): 1.51 m^2 2 mm rib spacing		
System	FoR: 60 % Pitch: ±34.5°		
AOGNC	Sensors	5 Star trackers	
		2 Gyros	
		3 Sun sensors	
		On-board Metrology System	
	RCS: 22 x 1N thrusters for station keeping and fast target acquisition		
	4 x 22N thrusters for transfer manoeuvres		
	3 axis stabilized		
Thermal	Mirror heaters (2,5 kW installed power, 20 ±1 °C)		
	MLI around telescope tube		
	Instrument radiators fitted on FPM		
	Camera head instrument thermal link accomplished by heat pipes		
Mechanisms	Moveable mirror using a hexapod		
	Mirror Cover		
	Venting mechanism at FMS		
	Sun shield		
Communications	1 High gain antenna		
	2 Low gain antennas		
	x-band system		
Data handling	512 Gbit on board storage for science data		
	8 Gbit on board storage for HK data		
Structure	CFRP structure		
	Telescope with 5 stray light baffles		
Propulsion	Propellant: Hydrazine		
	4 tanks: 530 kg propellant		
Power	Fixed deployable solar array		
	4.5 kW maximum consumed power		
	Maximum time duration to survive		

ATHENA Spacecraft		
	on batteries: 2.4 h	
Instruments	X-IFU	
	WFI	

Table 2-3: Mission Summary

2.4 Technical Conclusions and Options

2.4.1 SC Design & Payload Resources

The ATHENA SC configuration is very similar to that of ATHENA_L1, with the obvious difference that it now contains a single telescope, and a mechanism to swap the instruments. The ISM trade-off resulted in the selection of a hexapod mounting of the MAM (MMA), which would isostatically support the MAM and also provide a robust and high-precision means to tilt the MAM, and thereby swap the optical axis between the focal planes of the two instruments.

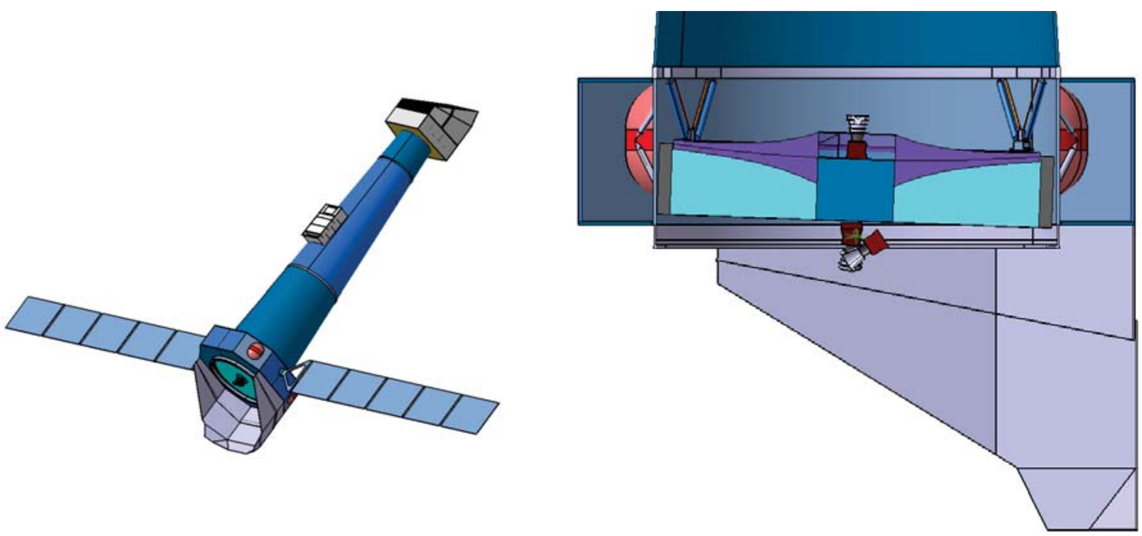

Figure 2-3: [left] The CDF SC in operational configuration, [right] view of the MAM, supported by the hexapod

The hexapod MMA design was selected through a trade-off which combined considerations of mechanism feasibility with system-level considerations. The main technical arguments in favour of the hexapod MMA are detailed in Chapter 7.2.1.

Whereas the ATHENA_L1 study did not clearly conclude on the need for On-Board Metrology (OBM), the tightened AKE requirements for ATHENA led to the inclusion of an OBM in the CDF baseline. This OBM is used as a control sensor both for the ISM and also for the AOCS s/s between observations.

2.4.2 Launch Mass

The launch wet mass of ~6.1t is significantly higher than ATHENA_L1 (~4t), which can be understood considering the significantly higher MAM mass, and also the increased mass of the PL, with associated knock-on effects for the SC. This mass is compatible with the Ariane 5 ECA envelope, and is significantly beyond the originally understood envelope for the A6 PPH version, but should be comfortably within the mass envelope of the A-64 'heavy' version, recently confirmed at the ESA Ministerial in December 2014.

2.4.3 Mission Architecture & ToO-Response

Overall the Mission Architecture is very similar to that of ATHENA_L1; daily passes of 4h duration at a single GS (New Norcia) are sufficient to handle the modest telemetry data-volume of ~75 Gbits/day in X-band. The structure of the SGS is under evaluation at the moment, but is anticipated to be Herschel-like in implementation.

Concerning the tightened ToO-Response requirement, taking into account reasonable durations for the various functions involved in responding to a ToO (including advances in automated ToO-planning, e.g. SWIFT), and the use of 3 small uplink GS to provide ~24 hour coverage, a Monte-Carlo ToO-analysis indicates that achieving a GRB-ToO observation <4 hours for 70% of pursuable targets is feasible. In combination with the CDF SC baseline FoR of 60%, this is compliant with the overall requirement for observing GRB afterglows.

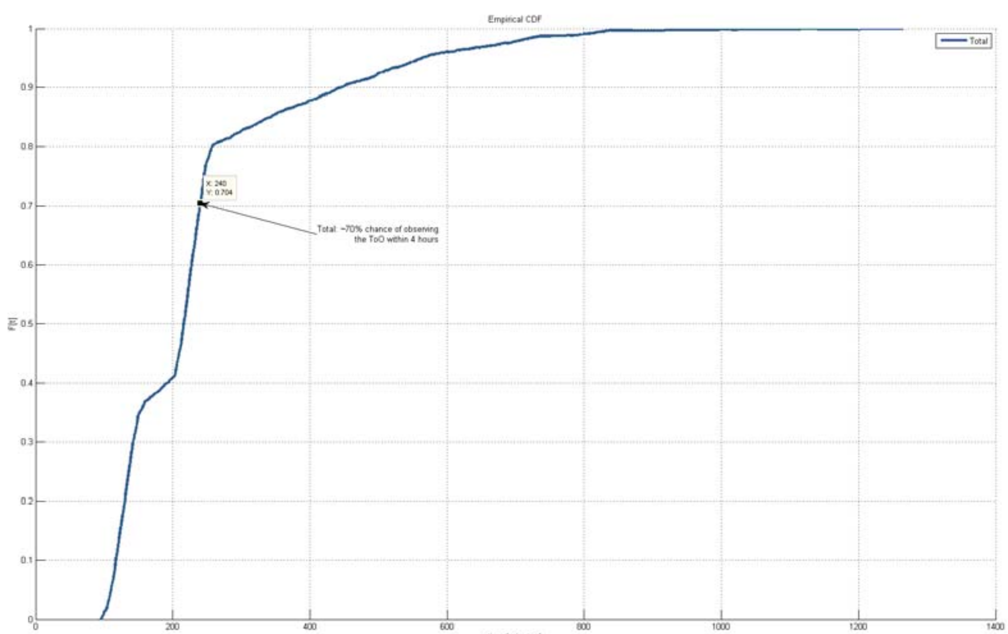

Figure 2-4: [left] ToO-response time cumulative distribution function, showing that 70% of pursuable targets are observed within 4 hours of ToO-alert receipt

2.4.4 CaC (Details in the Cost Report)

The design-to-cost point of targeting the 2624mm adaptor resulted in, as predicted, a Mission CaC significantly above the envelope. However, during the CDF study period an important programmatic commitment by CNES to take a Prime-role for the CC was confirmed, combined with a tentatively agreed CC-architecture as described in §5.3.2, mainly using JAXA technology with European components. Under the assumption that ESA/NASA are also able to agree on significant international contributions to the CaC (significant NASA involvement is already foreseen within the instruments), then the

CDF baseline should be broadly-compatible with the 1Bn€ CaC envelope, while retaining in large part of the science-case associated with 2m^2 Effective Area at 1 keV.

Fully recovering the lost 0.5m^2 Effective Area is considered out-of-scope due to the CaC-constraint. Nonetheless, the likely switch to A6 can be considered as a possible opportunity; the motivation for the A6 development is to reduce launch costs, and therefore could release some money currently allocated to the LV (assuming A5 ECA) to the SC, perhaps allowing recovery of ***some*** of the lost Effective Area. However the to-be-assumed LV cost is not clear at present (clear distinction between commercial and more expensive institutional pricing, to which an ATHENA launch would be subject, being the most important factor).

	ATHENA_L1	ATHENA
Instruments	XMS and WFI.	XMS>X-IFU. Very significant increases in the resource envelope of the instruments.
SC Configuration & Dimensions	2624mm adaptor, 11.5m Focal Length, rotating solar arrays mounted to SVM (wings).	Similar - 2624mm adaptor, 12m Focal Length, solar arrays in same location but fixed.
Telescope	2 x 0.5m^2 @ 1keV identical telescopes addressing the two instruments. Stray-light baffling and particle diverters located on disks installed in telescope tube.	1 x 1.37m^2 @ 1 keV single telescope with a movable mirror, addressing the two instruments. Straylight baffling and particle diverter still located on disks installed in telescope tube, but design changes due to movable mirror and also additional WFI chip location.
AOCS & Metrology	Thrusters for orbit control RW-off loading and safe modes, RW for nominal pointing operations. No On-Board Metrology (unclear if needed).	Similar, but with additional thrusters for fast-slew mode in support of ToO-response. On-Board Metrology considered mandatory to achieve APE and AKE performance.
CPS	Simple blow-down monopropellant system.	Similar but tank sizing and number/type of thrusters is different.
TT&C	X-band, 2xLGAs, 1xHGA.	Similar but with the HGA constantly tracking the Earth to facilitate ToO-response.
Operations	Single GS with 3h daily passes. 46% Field of Regard.	Similar, but augmented with 98% dedicated small uplink stations to facilitate ToO-response (LEOP acquisition aids at deep-space sites, e.g. NNO-2). Field of Regard enlarged to 60% to facilitate ToO-response.
MAIT	2 segment SC to facilitate use in European test facilities (LSS, LEAF…)	Similar, but split into 3 segments.

Table 2-4: Main differences between ATHENA and ATHENA_L1

3 MISSION OBJECTIVES

3.1 Background

The Hot and Energetic Universe has been selected as the Science Theme for the second large-class mission, due for launch in 2028, in ESA's Cosmic Vision program. The theme poses two key astrophysical questions:

1) How does ordinary matter assemble into the large-scale structures we see today
2) How do black holes grow and shape the Universe?

To address the first question, we must map hot gas structures in the Universe - specifically the gas in clusters and groups of galaxies, and the intergalactic medium - determine their physical properties, tracking their evolution through cosmic time. To answer the second question we must reveal supermassive black holes (SMBH), even in obscured environments, out into the early Universe, and understand both the inflows and outflows of matter and energy as the black holes grow.

The ATHENA mission has been proposed to address these themes.

3.2 Mission Justification

Because most of the baryonic component of the Universe is locked up in hot gas at temperatures of around a million degrees, and because of the extreme energetics of the processes close to the event horizon of black holes, understanding the Hot and Energetic Universe requires space-based observations in the X-ray band.

Specifically the investigations call for spatially-resolved X-ray spectroscopy and deep wide-field X-ray spectral imaging with performance greatly exceeding that offered by current X-ray observatories like *XMM-Newton* and *Chandra*, or by missions soon to be launched such as *Astro-H* and *SRG/eROSITA*. This capability requires an X-ray telescope combining unprecedented collecting area with an excellent angular resolution, and a wide field of view.

New instrumentation, providing spatially-resolved high resolution spectroscopy, will yield the physical parameters of hot gas structures out to high redshift and map the intergalactic medium in the nearby Universe. A wide field instrument performing spectrally-resolved imaging over a broad energy band is required to determine the evolution of supermassive black holes into the early Universe, and shed new light on black hole accretion and ejection processes, over a wide range of masses from Galactic compact objects to the largest supermassive black holes.

3.3 Science Objectives

The key performance parameters for the mission are derived from a set of observation templates addressing various science sub-topics. Mapping the dynamics and chemical composition of hot gas in diffuse sources requires high spectral resolution (2.5 eV) imaging with large area and low background; the same capabilities also optimise the sensitivity to weak absorption and emission features needed to uncover the hot components of the intergalactic medium. High resolution X-ray spectroscopy of distant gamma-ray bursts (GRBs) may reveal the signature of the first generation of stars, provided that the observatory can be repointed within 4 hours of an external trigger. An angular resolution lower than 5” is needed to disentangle point-source and sub-clump contaminants from the extended thermal emission in clusters, groups and galaxies. The same angular resolution is needed to resolve the dominant core emission and smaller accreting structures in galaxy clusters and groups up to redshift z~2. This resolution, when combined with the mirror effective area, also provides the necessary flux sensitivity (~10^{-17} erg cm^{-2} s^{-1} in the 0.5-2 keV band) to uncover typical accreting SMBH at z>6. The areal coverage needed to detect significant samples of these objects within a reasonable survey time demands a large field of view instrument, combined with excellent off-axis response for the X-ray optics. The spectral resolution of the same instrument will reveal the most obscured black holes at the peak of the Universe’s activity at z=1-4. High timing resolution and high count rate capability will shed new light on nearby accreting black hole systems.

A single X-ray telescope with a fixed 12 m focal length, based on ESA’s Silicon Pore Optics (SPO) technology, provides an exceptionally high ratio of collecting area to mass, while still offering the necessary angular resolution. It also benefits from a modular design highly amenable to mass production, necessary to achieve the unprecedented telescope collecting area. The telescope focuses X-ray photons onto one of two instruments at a time. In combination with the telescope, these two instruments provide the capabilities required to meet the Hot and Energetic Universe science goals.

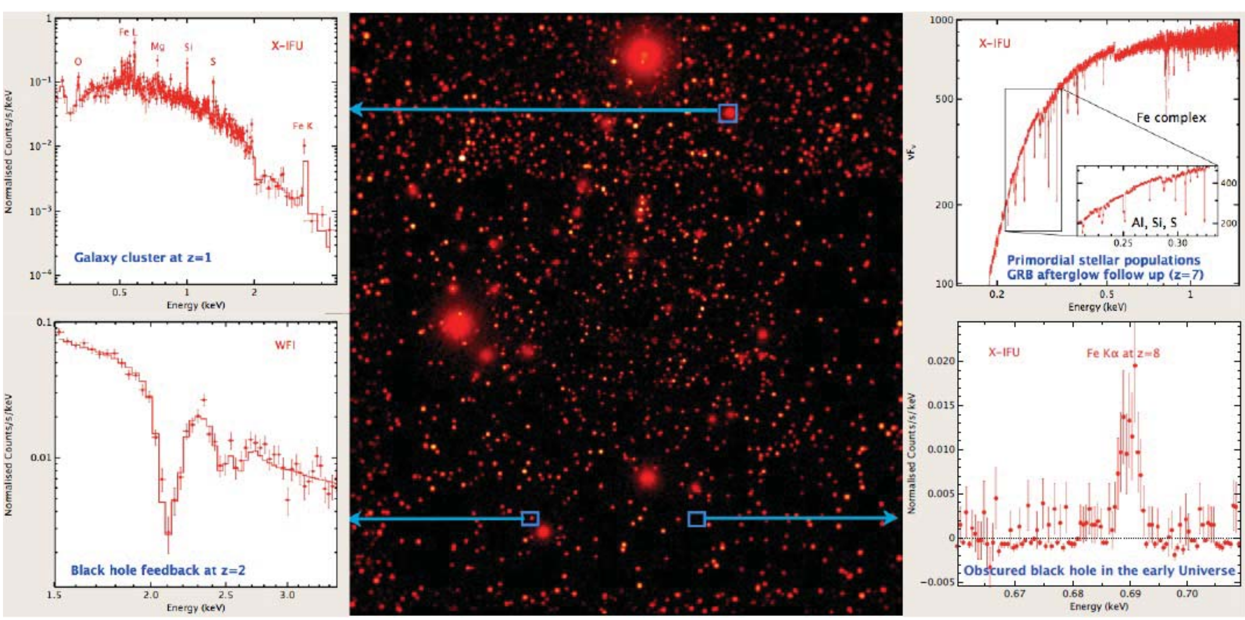

Figure 3-1: ATHENA will provide revolutionary advances in our knowledge of the Hot and Energetic Universe. The central panel is a simulated deep WFI observation, while the four surrounding spectra illustrate advances in different science areas, none of which are possible with current facilities.

3.4 Mission Requirements

ATHENA will predominantly perform pointed observations of celestial targets. There will be around 300 such observations per year, with durations ranging from 1 ks to 1 Ms, with typical duration of 100 ks per pointing. This routine observing plan will be interrupted by ToO (e.g. GRBs and other transients) observations at a typical rate of twice a month.

The required orbit location at L2 provides a stable environment and high observing efficiency. ATHENA has a baseline mission lifetime of 5 years, although for such an ambitious mission, consumables should be sized to enable an extension of at least 5 more years.

Pointing requirements are set by the need to locate the optical or near-IR counterparts of very faint X-ray sources, and to cross-identify structures in the X-ray images at other wavebands. An absolute pointing error of 3” (3σ) is required, and the on-ground a posteriori reconstructed astrometric measurements accuracy should be better than 1” (3σ).

Telescope and Payload performance requirements can be summarised as follows:

Telescope	
Effective area at 1 keV	2 m^2
Effective area at 6 keV	0.25 m^2
PSF HEW	5” on axis
(at E<8 keV)	10” at 25’ radius
X-IFU	
X-IFU spectral resolution	2.5 eV
X-IFU energy calibration accuracy (rms)	0.4 eV
X-IFU field of view	5’ diameter
X-IFU low energy threshold	0.2 keV
X-IFU total optical blocking filter attenuation	Factor 10^{12} at 1200 Å
WFI	
WFI field of view	40’ x 40’
WFI spectral resolution at 6 keV	150 eV
WFI count rate capability at	1 Crab=2.4 x 10^{-9} ergs s^{-1} cm^{-2}
80% throughput	(2-10 keV)
Charged particle background, Determined to within a few %	<5 x 10^{-3} (cts/m^2/s/keV)
Reconstructed astrometric error	1” (3σ)
Absolute astrometric error	3” (3σ)

This Page Intentionally Blank

4 MISSION ANALYSIS

4.1 Requirements and Design Drivers

Subsystem requirements		
Req. ID	**STATEMENT**	**Parent ID**
MA-010	Residual acceleration during operational phase < $6 \cdot 10^{-12}$ km/s^2	

4.2 Assumptions and Trade-Offs

The operational orbit for ATHENA was a-priori defined as an orbit about the Sun-Earth Libration Point 2 (SEL2). Other orbit options were not considered for the mission during this CDF study, although they are discussed briefly in a technical note which addresses the uncertainty surrounding A6 performance RD[56].

The launch is envisioned using an Ariane 5 from the Kourou spaceport in French Guiana. The Ariane 5 ECA launcher can lift up to 6,600 kg (payload + payload adapter) into the transfer orbit towards SEL2. The duration of the powered ascent phase is about 1510 seconds, followed by an upper-stage re-orientation phase in case a specific separation attitude is required, e.g. Sun-pointing of the solar panels prior to separation.

4.3 Baseline Design

The baseline orbit for ATHENA is a large amplitude quasi-Halo orbit about the co-linear Sun-Earth Libration Point 2 (SEL2). A typical example of such an orbit is shown in Figure 4-1. Libration Point orbits are best depicted in a rotating coordinate frame. Here the x-axis is along the Sun-Earth line, the z-axis is normal to the ecliptic plane and the y-axis supplements the system to be a right-hand coordinate system. The origin of the system is located in the Earth’s centre.

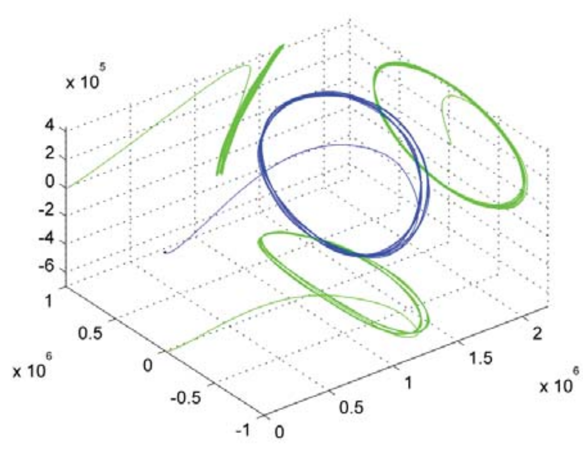

Figure 4-1 : Example of a large amplitude quasi-halo orbit about the Sun-Earth Libration Point 2

The chief advantages of orbits about SEL2 are (I) a constant thermal environment, since they can be designed to be eclipse free, and (II) a limited communication distance. Another advantage for astronomy missions is that the Sun, Earth and Moon are all located in one hemisphere as seen from the SC.

Such an orbit can be reached via a so called 'free' transfer trajectory, not requiring any deterministic orbit insertion manoeuvre after Earth departure. The SC travels on the so called stable manifold toward its operational orbit about SEL2. A typical transfer trajectory on the stable manifold of the target orbit is depicted in Figure 4-2. The full stable manifold of the target orbit is shown. Some parts of the manifold intersect with the near-Earth environment (the Earth is at the origin), where the launcher can place the SC on the stable manifold of the target orbit.

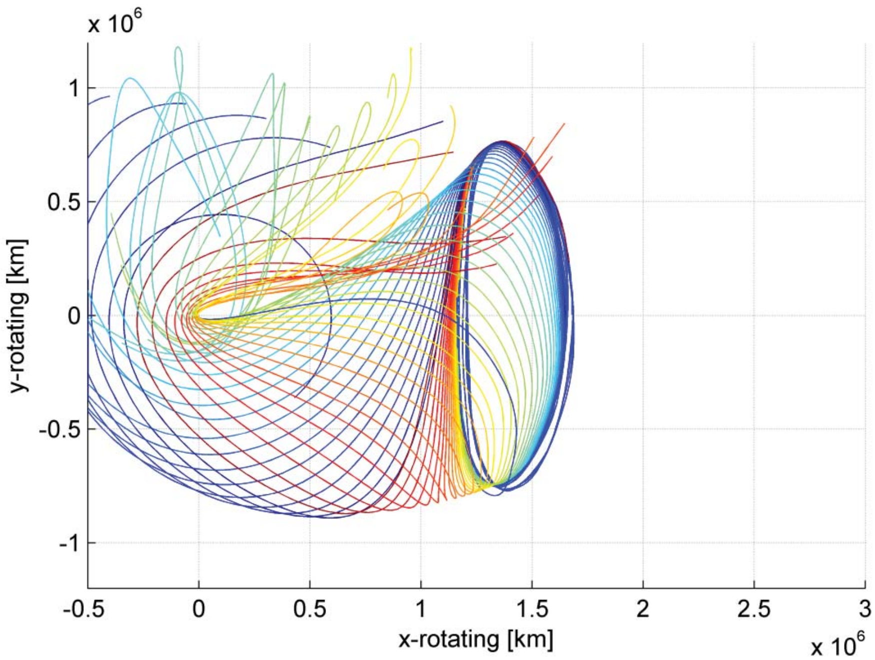

Figure 4-2: Stable manifold and free transfer option to an SEL example orbit. The free transfer trajectory is the single blue line passing through the inner libration point orbit region

It is assumed that the launch vehicle will directly insert the SC on the transfer trajectory. The in-and out-of-plane amplitudes (Ay and Az) of the SEL2 orbit are then not prescribed, but depend on the launch date and launch hour. The size of a SEL2 orbit is often described by the so called Sun-SC-Earth angle (SSCE). The minimum SSCE angle is defined by the free transfer condition and is near 28°. If smaller SSCE angles are required for operational reasons, an orbit insertion manoeuvre must be performed. This is usually required for spinning SC, where the Earth has to be kept close to the antenna pattern (e.g. Planck and Gaia). For 3-axis stabilized missions as ATHENA, there is usually no constraint. However for ATHENA an upper limitation of 33° SSCE angle has been proposed to limit design parameters such as the mechanism requirements on the SC HGA, and also the maximum declination with respect to the Earth's equator, which is important to ensure visibility from ground stations (GS) in the northern and southern hemisphere.

Solutions with an eclipse in the transfer trajectory are excluded from the launch window, and the achieved SEL2 orbit is eclipse free.

With a fixed launcher program the perigee velocity of the transfer orbit is also fixed. However, for each day of the year the free transfer requires a specific perigee velocity. In addition there is a dispersion in the final osculating perigee velocity. Due to these effects the SC will therefore initially not travel on the stable manifold of the libration point orbit and thus a small manoeuvre is required to correct the SC state and put it onto the stable manifold. This manoeuvre is time-critical and is thus performed as soon as possible after the launch. In order to have enough time to track the SC and estimate the state vector an execution 24 hours into the mission is foreseen, but to account for any problems with the SC or ground segment an execution on day-2 (48 hours into the mission) is budgeted. Inaccuracies in this manoeuvre will be corrected on day-5 and day-20. The third manoeuvre concludes the transfer. The SC can now be assumed to be on the SEL2 orbit, where station-keeping continues.

The SEL2 operational orbit is inherently unstable and requires regular but small maintenance manoeuvres. The total ΔV allocated for the orbit maintenance manoeuvre depends on the station-keeping interval and the capability of the AOCS to deliver pure torque or torque only together with a change in the SC velocity.

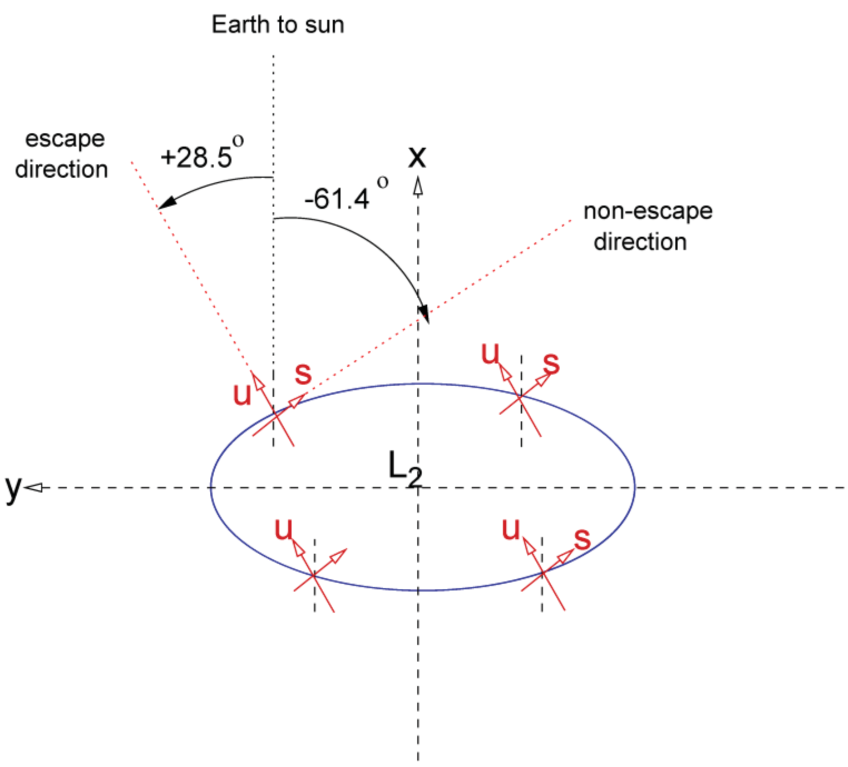

Figure 4-3: Stable and unstable direction derived from linear theory for station-keeping considerations

Station-keeping manoeuvres are assumed in the unstable direction of the linear theory. This direction is depicted in Figure 4-3.

A typical station-keeping ∆V evolution example is provided in Figure 4-4. The yearly station-keeping ∆V highly depends on the residual accelerations of the SC. To be more precise, it depends on the unknown residual acceleration of the SC, since known components can be taken into account, similar to the solar radiation pressure. The difference in the allocation can easily by different by orders of magnitude, e.g. the largest station-keeping manoeuvre of Herschel was larger than the station-keeping allocation of Gaia for an entire year. Gaia, being a spinning SC, had well predictable residual acceleration, while the attitude of 3-axis stabilised Herschel could by definition not be known a-priori.

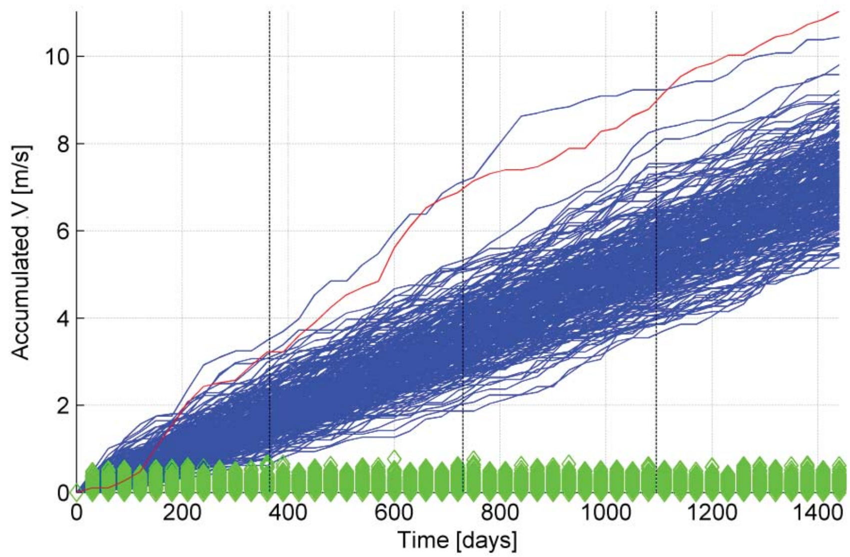

Figure 4-4:Example Station Keeping ∆V evolution for four years. The blue curve shows the accumulated ∆V and the green diamonds indicate the size of each individual station-keeping manoeuvre. The red curve depicts the worst case trajectory out-of the Monte-Carlo simulation set

Another important aspect during the operational phase is the visibility of the SC from ground stations around the world to allow Target of Opportunity (ToO) observations. Ideally a contact to the SC is available 24/7. Figure 4-5 shows the elevation of the SC with respect to different ground stations around the world for minimum, maximum and zero declination cases.

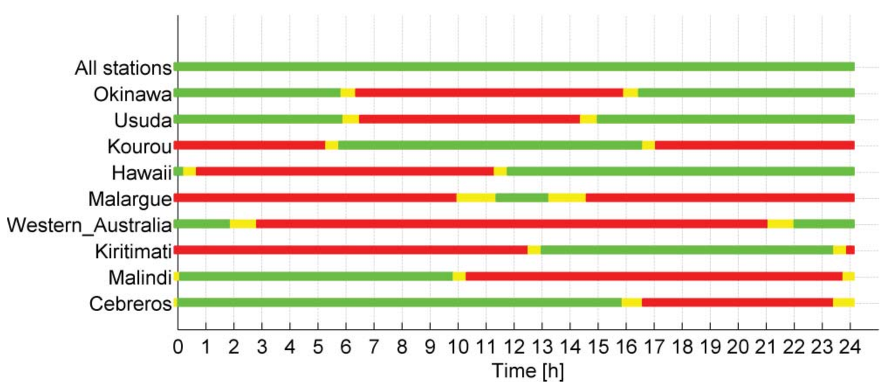

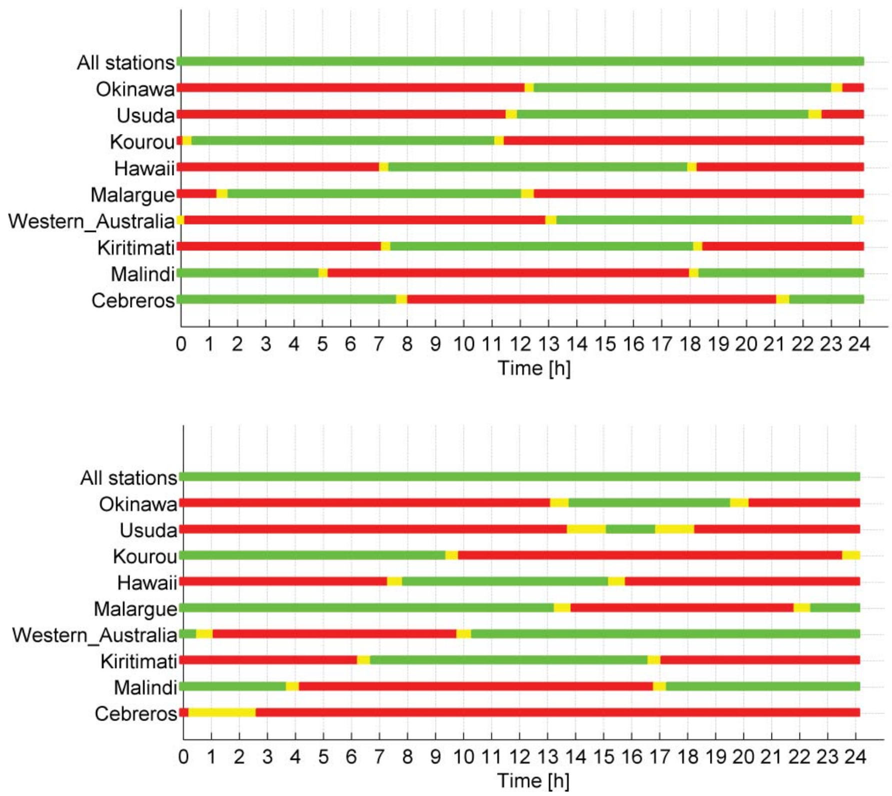

Figure 4-5: SC visibility from ground stations around the world for maximum declination (top), zero declination (middle) and minimum declination (bottom); elevations above 10° are marked in green, between 5 and 10° in yellow and elevations with less than 5° are marked in red

After the scientific operational phase the SC must be disposed of. A standard disposal strategy for libration point missions has not been defined yet, but in general three different kinds of disposal strategies are possible:

- Heliocentric disposal
- Earth return
- Lunar impact.

The heliocentric disposal has been applied to the Herschel and Planck missions and is currently still the baseline for Gaia. A lunar impact had been studied for Herschel. The Earth return option can either be controlled or uncontrolled. An uncontrolled re-entry can only be performed, if the parts of the SC possibly reaching the ground do not exceed the on-ground casualty risk as defined in the Space Debris Mitigation Policy for Agency Projects.

For ATHENA a heliocentric disposal is the current baseline. An allocation for the disposal manoeuvre of 10 m/s has been made. This manoeuvre of up to 10 m/s is to ensure a fast departure into the solar system. A second, later manoeuvre can decrease the likelihood of a return to the Earth-Moon system. No additional allocation beyond the remaining part of the 10 m/s is made for this manoeuvre, however, the remaining fuel on board can be used to increase this so called Jacobi raise manoeuvre. This manoeuvre is more efficient at greater distances. The initial manoeuvre ensures that a larger distance is reached reasonably fast to limit operations time for the disposal.

4.4 Budgets

The main Mission Analysis budget is the ΔV budget. With almost no deterministic ΔV, the budget strongly depends on the assumptions for the launcher dispersion and the residual acceleration of the SC while in the operational orbit.

ΔV requirements		
Manoeuvre	**Value [m/s]**	**Comment**
Perigee velocity correction	12.7	Assuming 1.5 m/s perigee velocity correction capability
TCM#1 (mainly launcher dispersion correction)	36.3	Ariane 5 launcher dispersion considered
TCM#2 & #3 Transfer correction	2.8	
Station-keeping 5 years	5.43	ONLY VALID FOR RESIDUAL ACCELERATION < $6 \cdot 10^{-12}$ km/s²
Station-keeping 5 years	5.43	ONLY VALID FOR RESIDUAL ACCELERATION < $6 \cdot 10^{-12}$ km/s²
Moon eclipse avoidance	0.0	Not required due to orbit design
Decommissioning (Heliocentric Disposal)	10.0	
Safe Mode DeltaV 5 years	1.08	Two safe modes per year assumed with residual acceleration level < $6 \cdot 10^{-12}$ km/s²
Safe Mode DeltaV 5 years	1.08	
Operational contingency	TBD	Depends on contingency scenarios to be covered
Sum (10 years)	>74.82	

Table 4-1: ΔV summary table. The total ΔV strongly depends on the station-keepings assumptions. This table is only valid for a SC with a residual acceleration of less than $6 \cdot 10^{-12}$ km/s²

The ΔV values presented in this table are so called geometric or impulsive ΔV values. They do not take any losses into account, e.g. manoeuvre decomposition losses, ramping losses or gravity losses are not accounted for. The so called effective ΔV depends on the propulsion system design. On SC with attitude limitations, such a loss in efficiency can be drastic, e.g. some manoeuvre direction on Gaia had efficiencies as low as 30 %.In addition the ΔV values do not contain any margins. Applicable margins must be added to the different types of ΔV.

4.5 Options

Two alternative options with respect to the transfer and the operation orbit are briefly discussed, a small size Lissajous orbit with limited SSCE angle and the indirect transfer, reducing the criticality of the day-2 manoeuvre.

4.5.1 Small Lissajous Orbit

In case a constraint on the amplitude sizes is added a small Lissajous orbit could be an alternative to the large amplitude orbit reachable via the free transfer trajectory. Then an orbit insertion ΔV is required at SEL2 arrival. The size of this orbit insertion manoeuvre depends on the maximum Sun-SC-Earth angle allowed. The transfer is then similar to the one of Gaia RD[4].

4.5.2 Indirect Transfer

The indirect transfer option removes the criticality of the day-2 manoeuvre described above by inserting the SC into an intermediate HEO prior to the insertion onto the stable manifold of the destination orbit. Dependant on the propulsion system layout an increase in payload mass could also be achieved RD[3].

This Page Intentionally Blank

5 INSTRUMENTS

5.1 Requirements and Design Drivers

The ATHENA model instrument suite comprises two key elements:

- The X-ray Integral Field Unit (X-IFU), an advanced actively-shielded X-ray micro-calorimeter spectrometer for high-spectral resolution imaging, utilising cooled Transition Edge Sensors
- The Wide Field Imager (WFI), a Silicon DEPFET Active Pixel Sensor camera with a large field of view, high count-rate capability and moderate resolution spectroscopic capability.

Subsystem requirements		
Req. ID	**STATEMENT**	**Parent ID**
INS-010	X-IFU spectral resolution 2.5 eV X-IFU energy calibration 0.4 eV X-IFU field of view 5' diameter X-IFU low energy threshold 0.2 keV X-IFU total optical blocking Factor 10^{12} at 1200 Å	
INS-020	WFI field of view 40' x 40' WFI spectral resolution at 6 keV 150 eV WFI count rate capability at 1 Crab=2.4 x 10^{-9} ergs s^{-1} cm^{-2} 80% throughput (2-10 keV) Charged particle background Determined to within a few % <5 x 10^{-3} (cts/m2/s/keV) Reconstructed astrometric error 1” (3σ) Absolute astrometric error 3” (3σ)	

5.2 Assumptions and Trade-Offs

The X-IFU and WFI instruments considered during the study are based on the reference payloads described in the mission proposal. The X-IFU CC, which was originally considered to be provided by ESA, is now under the responsibility of the X-IFU prime with elements of the CC to be provided by ESA and JAXA. Several architectures have been considered (pure European and different configurations with Japanese coolers). The baseline presented here is one of the most efficient, drawing maximum heritage from Astro-H by re-using the same coolers and enables the use of European coolers currently under development.

5.3 Baseline Design

5.3.1 Wide Field Imager (WFI)

5.3.1.1 Detector Concept

The technology and design of the WFI for ATHENA builds on the strong heritage of the wide field imagers proposed for the International X-ray Observatory and for ATHENA_L1. The heart of the camera is formed by a set of arrays of DEPFET (DEpleted P-channel Field Effect Transistor) active pixels integrated onto common 450 μm thick silicon bulks. Similar sensors have been developed for the Mercury Imaging X-ray Spectrometer (MIXS) for ESA's BepiColombo mission to Mercury to be launched in 2016 and will also be used in a variety of ground-based experiments (e.g., European X-ray Free Electron Laser).

A DEPFET is a combined detector-amplifier structure (Figure 5-1). Every pixel consists of a p-channel Metal-Oxide Semiconductor Field Effect Transistor (MOSFET), which is integrated onto a fully (sideways) depleted silicon bulk. With an additional deep-n implantation, a potential minimum for electrons, the so-called internal gate, is generated and laterally constrained to the region below the transistor channel. Incident X-ray photons interact with the bulk material, and generate a number of electron hole pairs proportional to the incident photon energy. Holes are removed over the backside contact while electrons are collected in the internal gates of the pixels nearest to the photon interaction site. The conductivity of the MOSFET channel will be modulated by their presence. The change in conductivity is proportional to the number of charge carriers and therefore a measure of the energy of the incident photon. The internal gate and the nearby clear gate and clear contact form an n-channel MOSFET, enabling the removal of collected charges by applying sufficient voltages.

The internal gate persists regardless of the presence of a transistor current. Thus, each row of pixels can be turned off during a certain exposure time, and only turned on for readout on demand. The amount of integrated charge can then be sensed by turning on the transistor current and measuring the conductivity before and after the charge removal. The difference in conductivity is then proportional to the amount of charge collected in the internal gate.

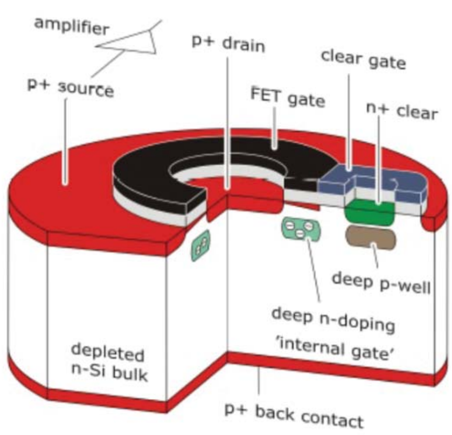

Figure 5-1: Cutaway display of a circular MOS-type DEPFET

The prototype devices designed for IXO have circular transistor geometry. A cutaway of a DEPMOSFET pixel is shown in Figure 5-2. Figure 5-2 and Figure 5-3 show microscope photographs of a fully processed matrix pixel and of a pixel sensor.

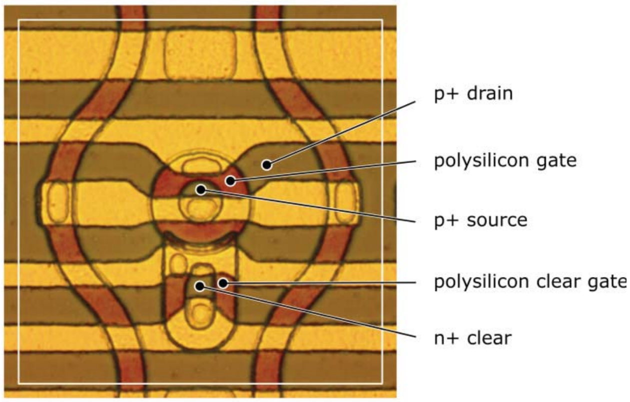

Figure 5-2: Microphotograph of a 75 µm pixel with a circular DEPFET in the centre and the ClearFET structure below. At the periphery, column-separating structures are visible. The gate length of the DEPFET is < 5 µm, the gate width is ~45 µm

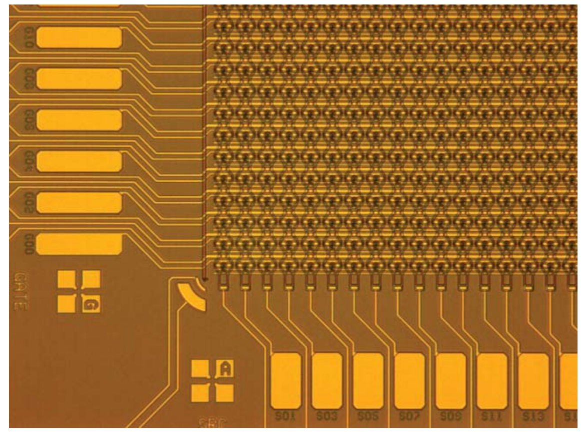

Figure 5-3: Corner of a 64 × 64 pixel sensor composed of DEPFETs as shown in Figure 5-2. The bright rectangles are bond pads for the connection to readout and control chips

In normal operation mode, photons hitting the sensor during the moments of integration or clear will receive an incorrect energy association. This leads to an increased background level and a spectral distortion. In order to suppress these events, a shutter can be implemented into each active pixel. Two layout concepts are currently studied. Both include an additional highly n-doped contact serving as sink for electrons produced during read out and a potential-barrier to avoid electrons from the internal gate. These so-called gateable DEPFETs have all the benefits of the normal sensors and at the same time provide a fast built-in shutter. Using recently produced prototypes a shielding of the collection anode up to 10^{-4} was achieved. Simulations predict that values of 10^{-5} and better can be reached with an optimised geometry. In addition to the shutter capability, pixel layouts containing an intermediate storage region are in development. Here, charge generated during the readout is not lost but accumulated and preserved for later processing. This capability completely obviates dead times and the distortion of the spectral resolution while maximising the throughput (Figure 5-4). First test devices have been produced and the proof of principle has been demonstrated.

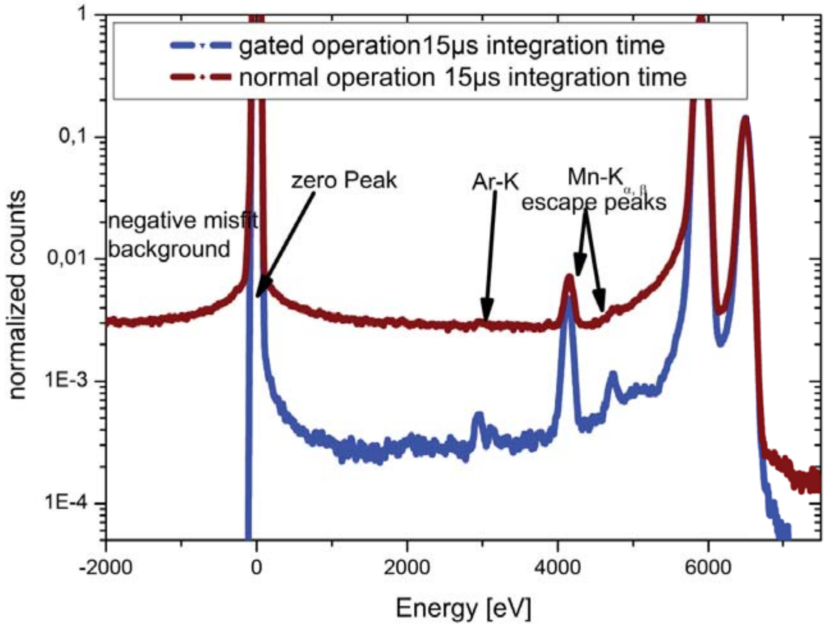

Figure 5-4: Impact of the gateable DEPFET technology demonstrated by ^{55}Fe spectra measured with a macropixel in gated (blue) and normal (dark red) operation mode. Without shutter, charges deposited during the integrations will cause energy misfits. If happening during the first integration, a lower energy is derived, leading to a higher background signal. Charges during the second integration lead to negative differences and produce background at apparent negative energies

The benefits of using a DEPFET based sensor are listed below:

- The DEPFET is a fully depleted device, the full Wafer thickness of 450 μm helps to increase the quantum efficiency in the energy range above 7 keV
- DEPFET based devices are sideways depleted devices, which provides for an unobstructed, homogeneous entrance window with 100% fill factor and excellent QE in the low energy range
- The local charge storage capability allows for a large variety of flexible readout modes, which allow observing objects in a large range of brightness without being limited by pileup
- The very low readout capacitance of the DEPFET allows for very low readout noise and thus excellent energy resolution even at high speed
- The sensor is area efficient compared to CCD based sensors, as no frame store area is needed
- The sensor permits faster readout compared to CCD based sensors, as no charge transfer is needed. This avoids furthermore out-of-time events (photons hitting the sensor during charge transfer and showing therefore wrong position)
- The sensor is radiation hard and power efficient, as the pixels are turned on only during readout.

5.3.1.2 Focal Plane Design

The WFI will combine in a single focal plane array excellent wide field survey power with its high-count rate and timing capabilities. Due to the physical size, this cannot be realized with a single chip on a monolithic wafer. Instead, the current design foresees an array of multiple sensor chips, which together fill the field of view provided by the ATHENA MA.

Several different layout options are currently studied. One possibility for the ATHENA system baseline FoV of 40' x 40' is depicted in Figure 5-5. Here, the large field of view is formed by 4 quadrants. Each quadrant consists of a 512 x 512 pixel matrix with 130x130μm² pixels. At 12m Focal Length the selected pixel size properly samples (factor 2.2) the 5" on-axis PSF, but actually achieves a better position resolution because of event splitting over up to four pixels.

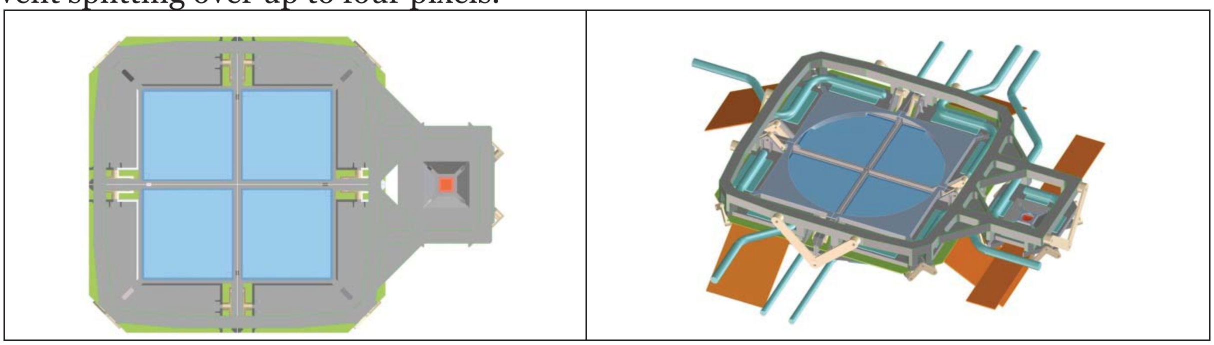

Figure 5-5: Layout of the DEPFET sensor arrays in the focal plane as seen from the front (left) and back (right). The large detector array (shown in blue) covers the 40 arcmin field of view. The fast timing detector is shown in red. The large area DEPFET APS (shown in blue) has to be subdivided in four quadrants because of its physical size. The fast timing detector (shown in red) uses a gateable DEPFET with intermediate analog storage region per pixel. The cold sensors chips are thermally decoupled from the frontend electronics (Veritas2 and Switcher ASICs). Each detector is connected via a flexlead to the dedicated detector electronics box. Cooling is accomplished by heat pipes which are linked to the respective radiators for the sensors, the frontend electronics and the electronics boxes

The fast timing sensor is located nearby the large area detectors. It is a 64 x 64 matrix of 130x130μm² pixels (TBC) covering a field of view of approx. 147" x 147". The selected pixel size properly samples (factor 2.2) the 5" on-axis PSF and at the same time retains the high count-rate capability.

5.3.1.3 Front End Electronics

The WFI focal plane array requires two different front-end Application-Specific Integrated Circuit (ASIC) devices, the control front end (CFE) and the analogue front end (AFE). Pixels are controlled by toggling a sequence of voltages on the gate, clear gate, and clear contacts of each row, and sensing the current through each column. Here, the correct voltage sequence is applied by the SWITCHER CFE, shown exemplary in Figure 5-6 (left and right of the active pixel sensor array). The AFE will be low-noise multi-channel signal amplifier/shaper circuit with integrated sequencer and serial analogue output (VERITAS2). VERITAS2 implements a trapezoidal filter function with a single fully-differential amplifier. The trapezoidal filter function is the time-limited optimum filter for white series noise, which is dominant at the foreseen readout speed.

The most important feature established with VERITAS2 is, additional to the source-follower, the drain-readout. This is made possible by a low-noise current-to-voltage converter placed in front of the preamplifier. The main advantage of the drain-readout is that all the nodes of the DEPFET are at a fixed potential and the readout speed of the system is not limited by the resistor-capacitor (RC) time constant of the input of the readout chain. This capacitance comprises the input capacitance of the preamplifier and the parasitic capacitance associated to the DEPFET source line. Coupling the ASIC in the drain-readout mode with a DEPFET array, it will be possible to obtain a readout time per row of about 2.5 µs. The outputs of the analogue channels of VERITAS2 are serialized by a 64:1 multiplexer with a clocking speed up to 20 MHz and sent to a fast fully differential output buffer. The architecture allows window-mode readout of the pixel matrices making it possible to address selectively arbitrary sub-areas of the DEPFET matrix or even to readout different sub-areas at different speeds.

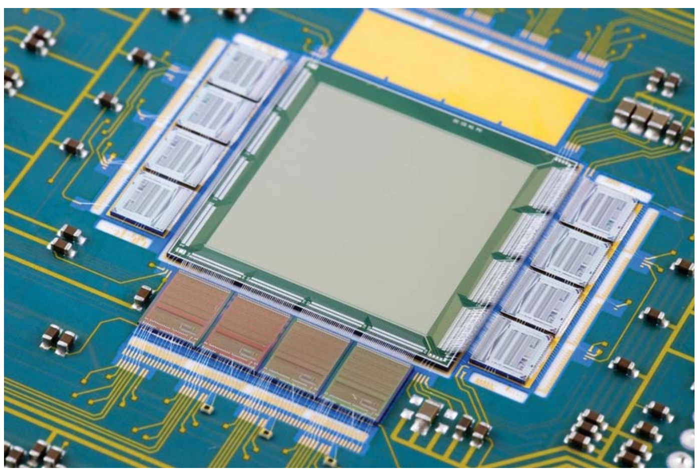

Figure 5-6: DEPFET hybrid with a prototype 256 x 256 sensor chip in the center, four banks of CFE SWITCHER control chips left and right, and four AFE ASIC readout chips at the bottom

5.3.1.4 Signal Processing

Before the information about a detected X-ray photon can reach the astronomer, a number of processing steps is required. The block diagram of the electronics system is presented in Figure 5-7 and a concept design of the instrument architecture is shown in Figure 5-11**.** After passing through the X-ray mirror system, a photon is collected in the active pixel array and subsequently converted into a charge. After a first amplification in the DEPFET itself the signal is further amplified and shaped in the AFE VERITAS2 and there converted into an analogue voltage signal. The DEPFET arrays and front end electronics are mounted in the camera head, which provides the structural stability, shielding and required cooling resources. The signal is then transferred to the pre-processor using a flex-lead. The pre-processor contains the analogue-to-digital-converters (ADCs) digitizing the output from the VERITAS2 ASIC. This digitization takes places in so-called ADC clusters, cards hosting multiple ADCs and field-programmable gate arrays (FPGAs). Furthermore, the frame processor performs the necessary offset calculation and subtraction, common mode correction, noise and threshold calculation, as well as pattern recognition and event identification. The instrument control and power unit (ICPU) merges the data streams of the 4+2 modular detector units and performs data compression.

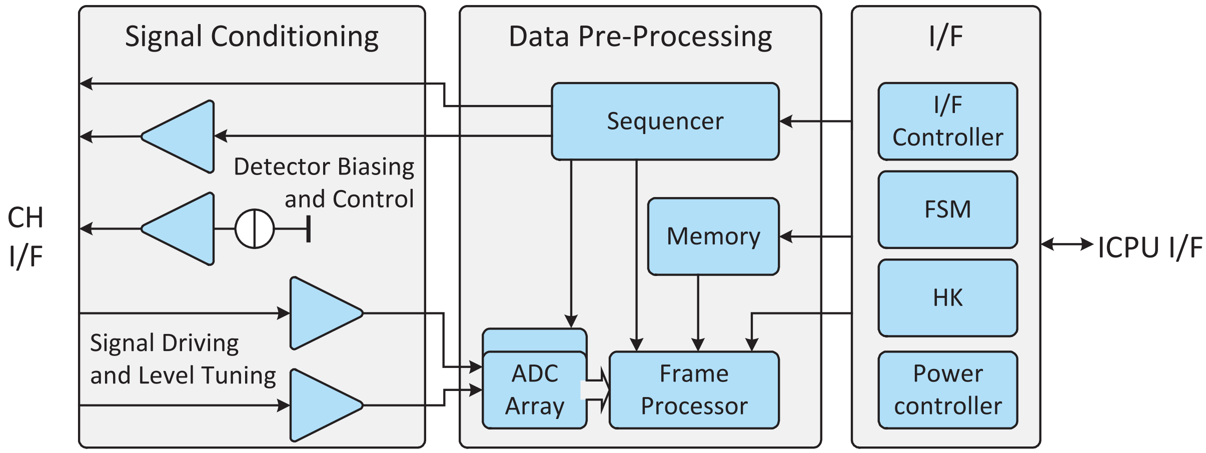

Figure 5-7: Overview of the detector electronics system with the blocks for signal conditioning, the data pre-processing, and the interfaces to the ICPU

The electronic system responsible for controlling the instrument is located in the instrument power and control unit (ICPU) box. The ICPU performs all data interface tasks with the SC and receives the telecommands from the ground stations. It also acts as the power interface to the SC, and performs the filter wheel control.

5.3.1.5 Filters and Quantum Efficiency

The sideways depletion utilised for the DEPFETs provides for an unobstructed, homogenous entrance window with 100% filling factor and excellent quantum efficiency (QE) at low energies (Figure 5-8). This low energy sensitivity is conserved by the use of a 70nm thin SiO_2/Si_3N_4 entrance window. The 450 µm thickness of the depleted Si bulk provides also a high QE above 10keV, thus the overall accessible energy range comprises approx. 0.1-15 keV.

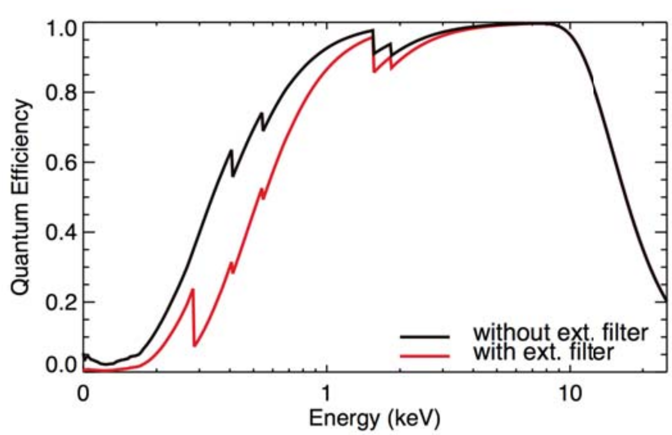

Figure 5-8: QE of the DEPFET sensor as function of energy without (black curve) and with (red curve) external blocking filter for optical/UV light

However, the large effective area ATHENA mirror will focus in addition to the X-ray photons also a significant amount of optical and UV light on to the detector. Most of these photons will be blocked by the multi-layer entrance window located directly on top of the active pixel sensors and by an additional thin (e.g., 70 nm) Al layer deposited on top of that. For the remaining optical/UV photons two alternative approaches are currently studied. The thickness of the on-chip filter could be chosen such that even for optically bright sources optical loading is sufficiently reduced. Alternatively, a thin Al-layer (e.g. 40 nm) on top of a substrate foil (e.g. 350 nm polymer carrier) in a filter wheel could be used (see Figure 5-9). The latter could rotate in and out of the photon path to facilitate observations where the low-energy response is scientifically critical. However, the physical size of the field of view places strong requirements on the stability and longevity of such a thin filter.

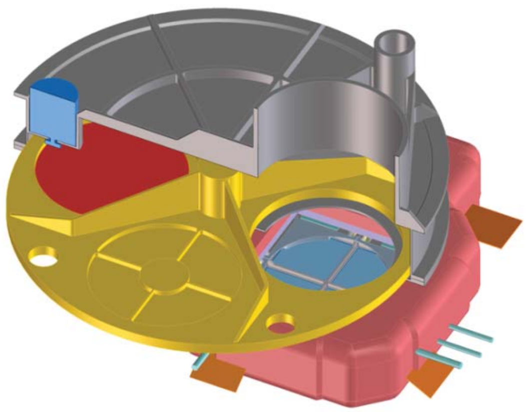

Figure 5-9: Filter wheel concept with X-ray baffle. The thin and large-area filters need to be protected against the acoustic noise occurring during launch. For this, a trade-off of the protection mechanism has to be performed with the following options: (1) filter in protected parking position in filter wheel (no depressurisation), (2) local protection of filter (depressurised), (3) WFI+FW in depressurised vacuum chamber

5.3.1.6 Instrument configuration

Figure 5-11 and Figure 5-12 show 3D sketches of the instrument configuration. The overall payload is divided into the following subsystems

- Camera Head
  - 1 Large DEPFET Array (4x 512x512 pixels)
  - 1 Fast DEPFET Array (64x64 pixels).
- Detector Electronics
- Instrument Control and Power Unit
- Filter Wheel
- Primary Structure
- Camera Head Radiator
- Detector Electronics + ICPU Electronics Radiator.

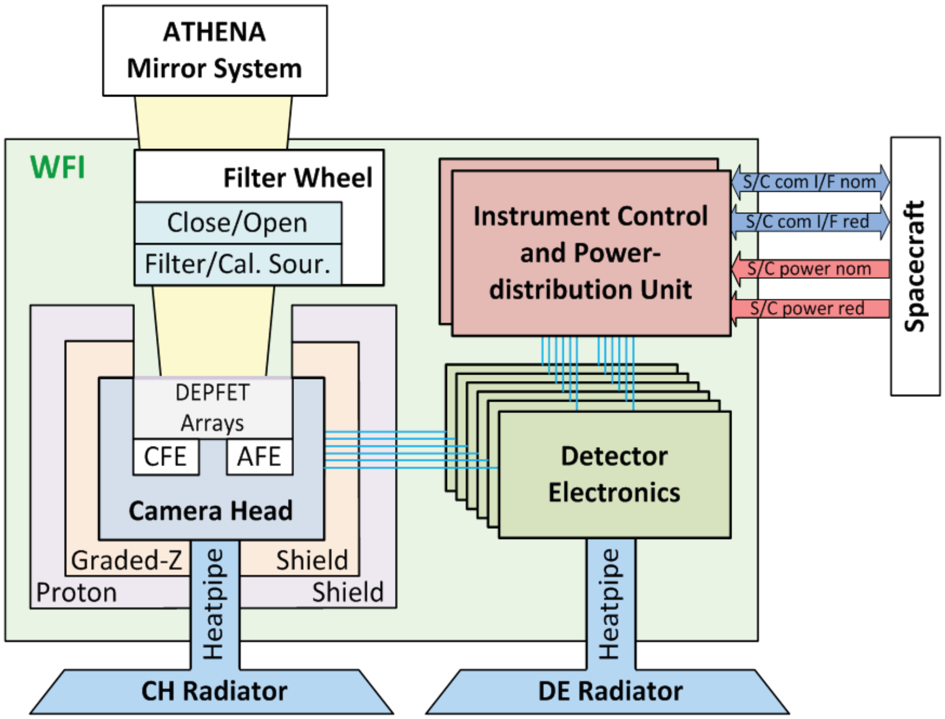

Figure 5-10: WFI functional Block Diagram

The WFI detector assembly is mounted to a base-plate that also carries the WFI filter-wheel. The camera head is de-coupled from the baseplate, which is in turn de-coupled from the instrument platform. All detector electronics boxes are mounted directly to the primary structure close to the camera head, while the ICPU electronics boxes can be positioned at the opposite side of the baseplate.

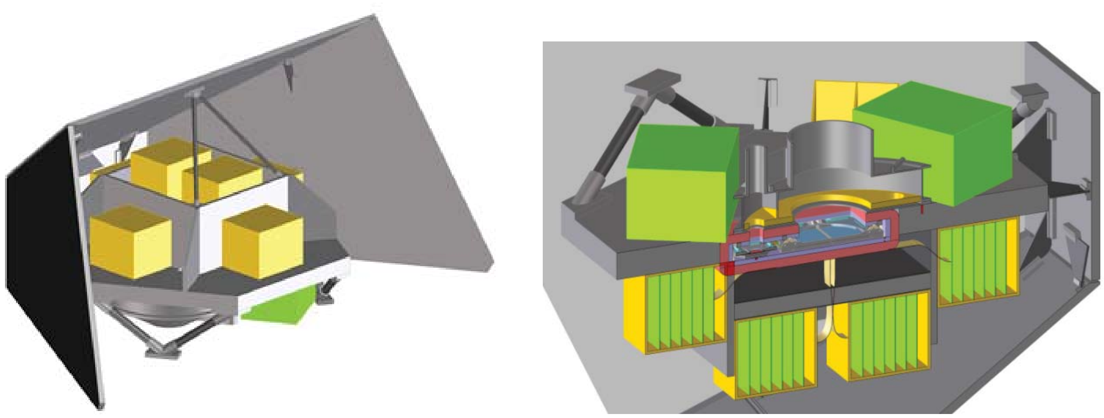

Figure 5-11: Overview over the instrument configuration with the detector electronic boxes shown in yellow and the ICPU in green

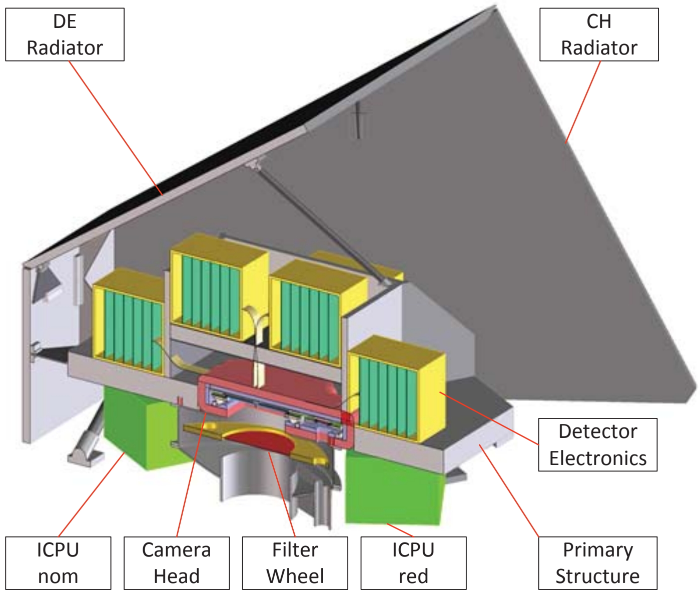

Figure 5-12: Cut through the WFI concept drawing. At its heart lies the camera head hosting the sensors and front end electronics. On top of the camera head lies the X-ray baffle and filter wheel. Flex-leads connect to the electronic boxes holding the detector electronics

The camera head holds the FPA and its front end electronics, provides the required structural stability, proton and graded Z-shield, and the required cooling resources. The FPA consists of two detectors: one detector with four large-area sensors to span the FoV of 40' x 40' and a second detector, located beside the large array, that is specifically designed for observations of bright sources. The DEPFET sensors will be thermally decoupled from the front end electronics boards since only the sensors require cooling to -80 C. A filter wheel is mounted in front of the camera head.

Six Detector Electronics (DE) boxes are mounted close to the camera head, one for each of the 4 large detectors and one for each of the two halves of the fast detector. The event processing is accomplished in the detector electronics for each detector. The data streams are then merged into one ICPU (Instrument Control and Power Units in cold redundant configuration) which performs data compression before sending the science and housekeeping data into the mass memory on-board the SC.

Each detector board, containing the DEPFET sensor and the AFE and CFE ASICs, is connected to the detector electronics by a short (about 25 cm) flex-lead. The detector electronics contains the main sequencer driving the AFE and CFE ASICs, the ADCs digitizing the AFE's output and a high-throughput data processing pipeline. The serial analogue data from the VERITAS ASICs is digitised by one ADC per ASIC.

The power conditioners of the detector electronics generate the required power for the various WFI subsystems from the SC provided supplies. In addition, it switches power supplies on demand. Hereby, it has to be distinguished between adjustable voltages and 'commandable' voltages. 'Commandable' voltages can be commanded in states ON and OFF, while adjustable voltages can also be adjusted in a certain range, which is important to e.g. compensate radiation damage effects in oxides. All voltage channels can be read back via slow control for housekeeping purposes.

5.3.2 The X-Ray Integral Field Unit (X-IFU)

The X-IFU instrument delivers:

- Spectroscopic imaging of extended sources, enabling the measurement of hot gas bulk motions through line shifts, distribution of heavy elements, ionisation state etc.
- Weak line sensitivity to detect absorption lines from material associated to or intervening towards bright local and distant X-ray sources, as well as to detect emission/absorption features from a number of chemical elements.
- Capability to obtain physical properties of Hot and Energetic Universe sources by delivering precise line energies, emission/absorption line shapes, line intensities and line ratios in multiplets.

The X-IFU will provide spatially resolved spectra with an energy resolution of 2.5 eV in the energy range 0.2 – 12 keV over a 5' diameter field of view.

5.3.2.1 Detection Principle and Readout Scheme

The X-IFU detector is a large array of X-ray absorbers on top of Transition Edge Sensors (TES). The TES micro-calorimeter senses the heat pulses generated by X-ray photons when they are absorbed and thermalised. The temperature increases sharply with the incident photon energy and is measured by the change in the electrical resistance of the TES, which must be cooled to temperatures less than 100 mK (the thermal bath is at 50 mK) and biased in its transition region between super conducting and normal states (Figure 5-13).

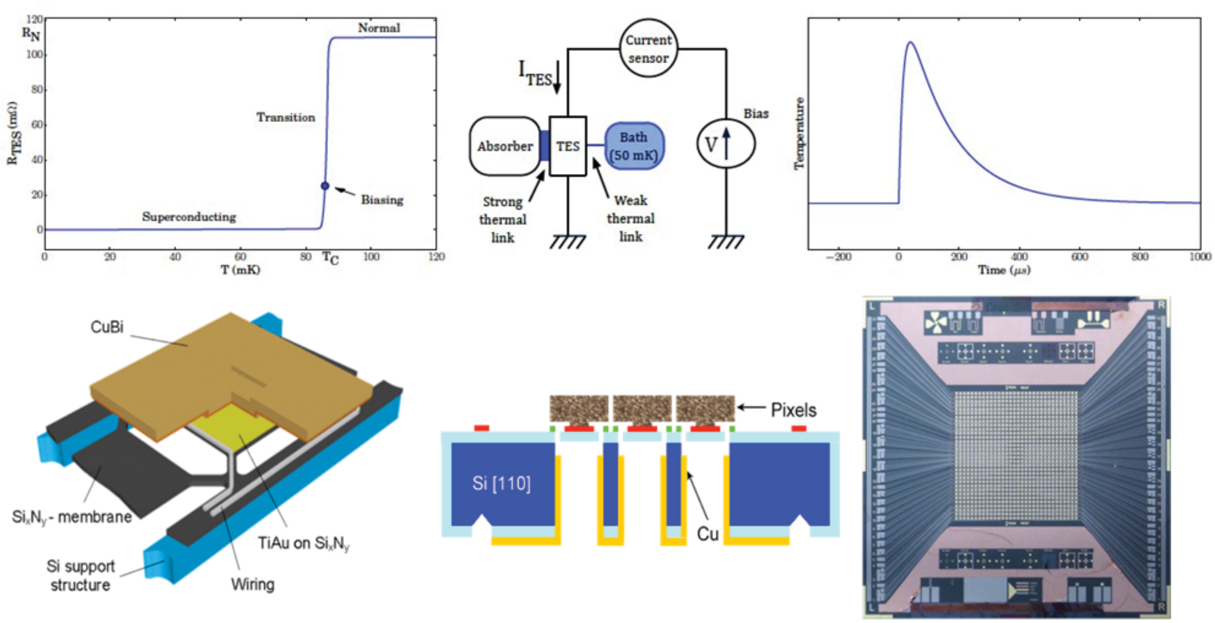

Figure 5-13: top): Principle of a Transition Edge Sensor (TES) acting as a micro-calorimeter. Left panel) The TES is cooled and voltage-biased to lie in its transition between its superconducting and normal states. Middle panel) The absorption of

an X-ray photon heats both the absorber and the TES through the strong thermal link. Right) The change in temperature (or resistance) with time shows a fast rise (due to the strong link between the absorber and the TES) and a slower decay (due to the combination of a weak link with the 50 mK thermal bath and a negative electrothermal feedback). bottom) Prototype TES developed at SRON for the X-IFU

Two options are under consideration for the X-IFU sensors: Ti/Au bilayer TES with Cu/Bi absorbers or Mo/Au bilayer TES with Au/Bi absorbers. The absorber has a size of 250 x 250 μm^2, and the pitch is 265 µm. The shape of the TES array is subject to optimisation, but for mosaicked observations (these will be required for some of the core science) a square geometry would be preferred. Either absorber can achieve the correct stopping power at 1 keV and provide the low heat capacitance required for high spectral resolution. The small current of the TES is read out using a low noise amplifier chain consisting of a superconducting quantum interference device (SQUID) in the cold front end electronics (CFEE), SQUID array amplifiers at 2K and a semi-conductor low-noise amplifier in the warm front end electronics (WFEE). Multiplexing allows the reduction of the number of readout channels and hence the thermal load on the cooling chain. For Frequency Domain Multiplexing (FDM), a single comb signal AC-biases each pixel with a specific carrier matching the resonant frequency of an LC circuit (see Figure 5-13 image 2).

De-modulation of the summed signal in the digital readout electronics (DRE) enables the reconstruction of the shape of the signal in each pixel. With a frequency range of ~ 1 to 5 MHz and a carrier separation of 100 kHz, up to 40 pixels can be multiplexed in a single readout channel. To match the X-IFU field of view requirement (5' diameter), in its current design, 3840 equal size pixels are required. These are read out in 96 channels of 40 pixels each. The first stage SQUID needs to be linearised with a high gain feedback loop. A so-called base-band feedback technique ensures that the feedback signal carrier is properly phased with the TES signal carrier at the SQUID input (accounting for propagation delays of the signal in the harness and digital electronics processing delays). The TES biasing, the SQUID multiplexer control, the data digitization, the generation of the feedback signals and the de-multiplexing of the signals take place in the digital readout electronics (DRE-DEMUX), which also contains the event processor (DRE-EP). The latter includes two major functions: event triggering and pulse analysis (see Figure 5-13 image 3).

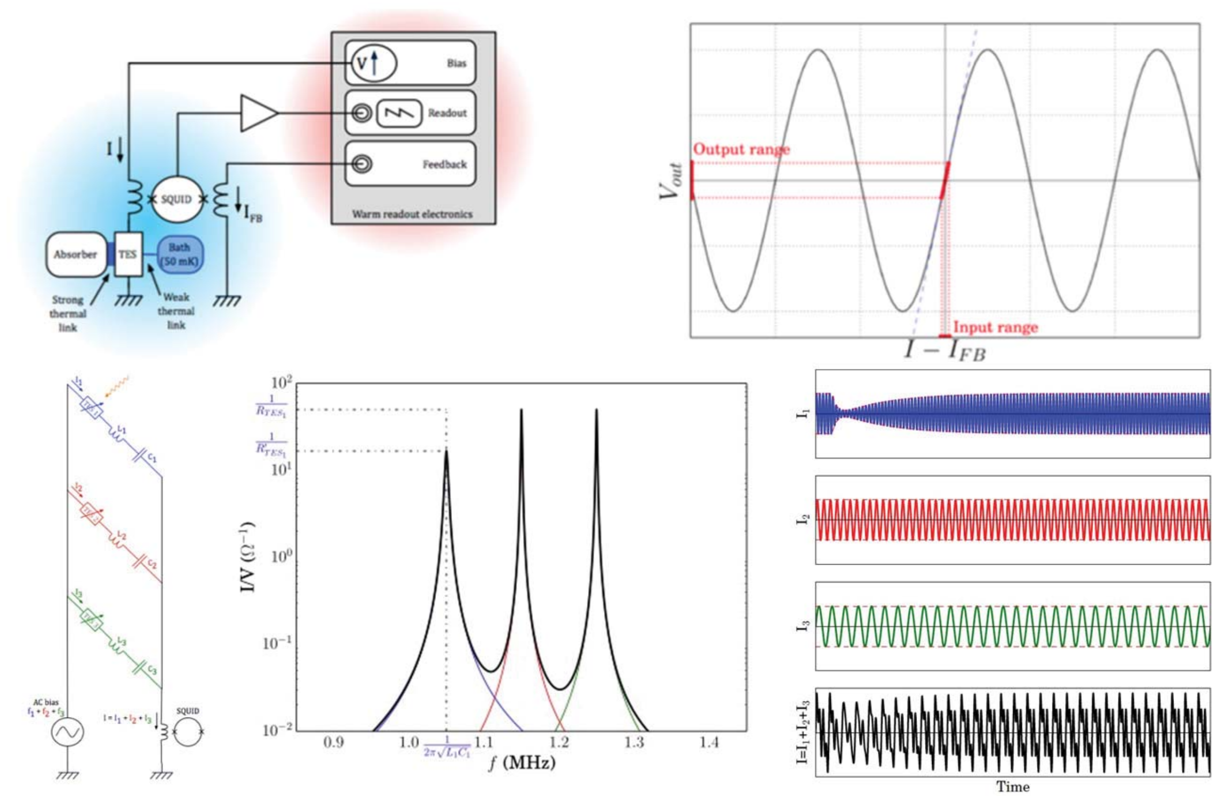

Figure 5-14: top) **A SQUID amplifier is highly non-linear, showing a sinusoidal response. It's linearisation is achieved with the use of a high gain feedback loop (so that the SQUID sees the difference between the TES and the feedback signals: the difference being small). Base-band feedback ensures that the feedback signal carrier is properly phased with the TES signal carrier at the SQUID input (accounting for propagation delays of the signal in the harness and digital electronics processing delays).** bottom) **Illustration of Frequency Domain Multiplexing principle: Left) The schematics of a 3-pixel channel. Each pixel is biased at a specific frequency (f1, f2 and f3), each matching the resonant frequency of an LC circuit. For each pixel, the TES current is modulated by the temperature/resistance variation induced by the absorption of an X-ray photon. The bottom panel shows the summed current readout by a single SQUID**

Close underneath the TES array (less than 1 mm), an active Cryogenic Anti-Coincidence detector (CryoAC) must be placed to screen the particle background. This CryoAC is also based on TES technology, implementing a large area of Silicon absorbers with Iridium TES. This choice has the advantage, in addition to sharing several commonalities with the main TES array, of exploiting a fast component of the TES response, when working in the so called a-thermal regime. The energy released by the absorption of a photon, or lost by a particle in the absorber is rapidly converted into an athermal phonon population, not yet in thermal equilibrium with the system. These phonons can be then partly detected in the TES, giving rise to a fast contribution or thermalise in the absorber by inelastic scattering processes at the crystal surfaces leading to a temperature rise of the absorber and therefore delivering a slower, thermal contribution to the signal.

The CryoAC is constituted by a 4 pixels TES-array and the related cryogenic SQUID and warm electronics. The warm electronics are divided into two boxes: the CryoAC WFEE (Front End Electronics) which assembles the TES biases, the SQUIDs biases, both in DC, plus the FLL; the CryoAC BEE (Back End Electronics), which provides commands to the CryoAC WFEE and digitizes the analog scientific signal from the CryoAC WFEE. As usual the electronics also manages commands and HKs.

The main requirements for the CryoAC, derived by imposing a rejection rate of the primary particles larger than 99%, are a low energy threshold of 20 keV, a size ~20 x 20 mm, and a rise time less than 30 µs (the size of the CryoAC TES is subject to optimization). To further reduce the residual background (inside the TES-array band), it is foreseen to insert a Kapton liner at 50 mK between the Niobium shield and the TES-array. The number of charged particles is sufficiently small that processing of the anticoincidence data can be performed on the ground.

The Instrument Control Unit is responsible for operating the instrument with the desired settings. The power distribution unit (PDU) distributes the raw power over the different electronic boxes. For the WFEE and the CryoAC WFEE, which have severe electromagnetic compatibility (EMC) requirements, the power conversion is done in a dedicated power supply unit (PSU).

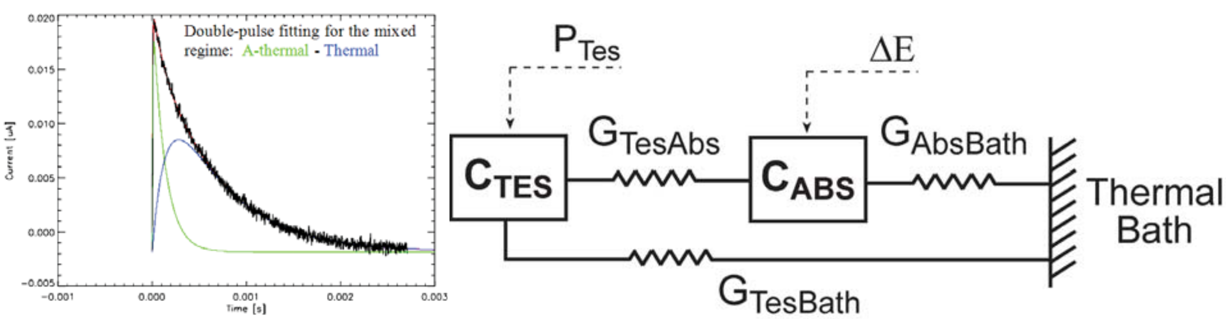

Figure 5-15: left) The signal produced by the TES CryoAC showing a fast (1µs) rise, due to the athermal component (model in green) then followed by the slower thermal component (in blue). right) thermal model of the system, with which the thermal behaviour is consistent

The focal plane assembly provides the thermal and mechanical support to the sensor and the anti-coincidence detector. In addition it accommodates the cold electronics and provides the appropriate magnetic shielding. A magnetic field attenuation of $1.6x10^5$ has been achieved by two shields: a super conducting Nb shield and a cryo-perm shield at 4 K and by an appropriate cooling sequence to avoid the trapping of magnetic flux. The focal plane assembly requires two optical blocking filters to reject the thermal and IR load on the detector (Figure 5-16). The current best estimate of the mass of the focal plane assembly is about 2 kg.

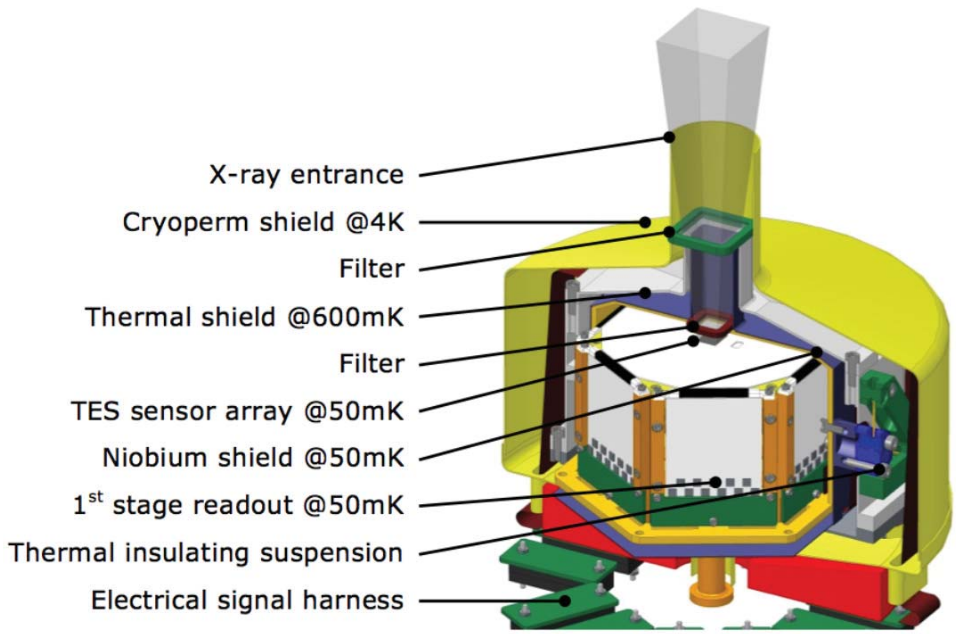

Figure 5-16: Schematic drawing for the focal plane assembly (purple: detector at 50 mK; gray: intermediate temperature stage (between 0.3 and 1.0 K); yellow: outer shield (between 2 and 4 K)

5.3.2.2 50mK cooling

To operate the cryogenic detector at 50 mK , the focal plane assembly needs to be coupled to a sub-Kelvin cooler. The development status of a 50mK cooler is currently at an advanced stage. This hybrid cooler is based on the combination of a 300 mK sorption stage (similar to the one flown on Herschel) and a small adiabatic demagnetization stage. A first engineering model has been developed in the framework of an ESA TRP focused on IXO (Figure 5-17). Duty cycles of 77% have been achieved for a hold time of 31 hours and 1 μW heat lift at 50 mK. A second engineering model developed for the Safari instrument on-board SPICA has been designed to withstand static loads of 120 g and random vibration level of 21 g RMS, with a mass of 5 kg. It has been sized to provide net heat lifts of 0.4 and 14 μW respectively at 50 and 300 mK, for an overall cycle duration of 48 hours and a duty cycle objective of over 75%.

Figure 5-17: ESA TRP 50 mK Cooler (1 µW @ 50 mK and 10 µW @ 300 mK, 77% duty cycle efficiency)

Besides the Sorption/ADR hybrid, other sub-kelvin coolers as e.g. closed cycle dilution refrigerators and multistage ADR coolers could be considered. All these coolers require pre-cooling around 2K. This will be provided by the X-IFU CC.

5.3.2.3 Cryogenic architecture

Based on the XMS studies performed by JAXA and European industry for IXO/ATHENA_L1 and the ADR/sorption cooler developed by CEA, one can deduce the parasitic loads for the various temperature stages as:

- ~2W at 100-120K
- Shield cooler (15-25K) = 350mW + non-operational cooler (200mW PT/50mW ST)
- 2K: 10mW + parasitics (1mW) + non-operational cooler (1-3mW), requires (150mW pre-cooling at 15K, derived from RAL 2K cooler development)
- 4.5K: 10mW (ADR/Sorption) + 5mW (parasitic) = 15mW + non-op cooler (1-3mW), requires (~100mW pre-cooling at 18K, derived from Planck 4K JT cooler).

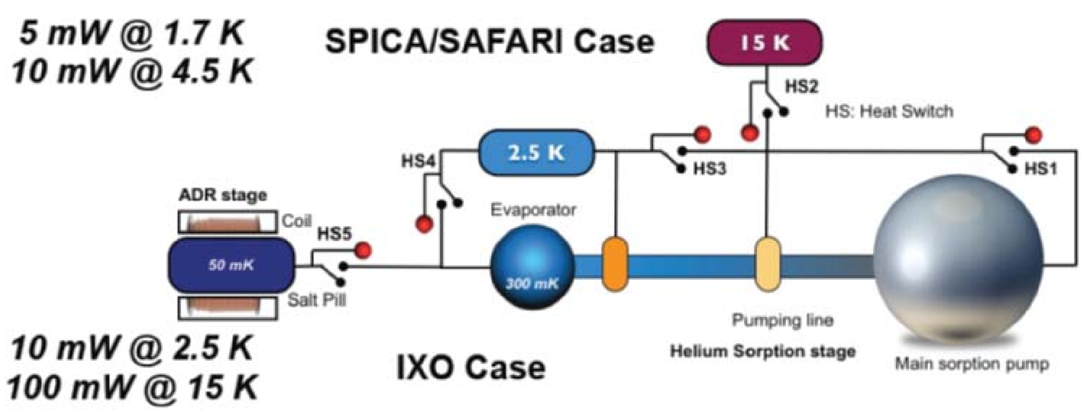

Figure 5-18: 50mK cooler and pre-cooling required for the different configurations

In addition to these loads, sufficient margins in cooling capacity (50-100% at this stage) must be available. The following European and Japanese coolers are considered:

- 2-stage Stirling cooler JAXA: 200mW at 20K and 1W at 83K, 90W input power
- 15K Pulse Tube Air Liquide: 300mW at 15K and 1-2W at ~100K, 300 W input power (prediction based on BB results with active Phase shifter)
- JAXA 1.7K JT: provides 10mW, requires 4 Stirling pre-cooler in redundant config (from SPICA). Loss from JT line (20K-2K) ~1mW
- JAXA 4K JT: provides 50mW, requires 3 Stirling pre-coolers in redundant config. 2 Stirling pre-coolers in case of lower cooling power. Loss from JT line (20K-4K) ~1mW
- RAL 2K JT: provides 20mW, requires 1 15K PT pre-cooler. Cold redundant config without cross coupling of pre-cooling stages at 15K possible (only limited degradation over lifetime expected). Loss from JT line (100K-2K) ~3mW
- RAL 4K JT: provides 20mW, requires 1 15K PT pre-cooler. Cold redundant config without cross coupling of pre-cooling stages possible (only limited degradation over lifetime expected). Loss from JT line (100K-4K) ~3mW or (20K-4K) ~1mW.

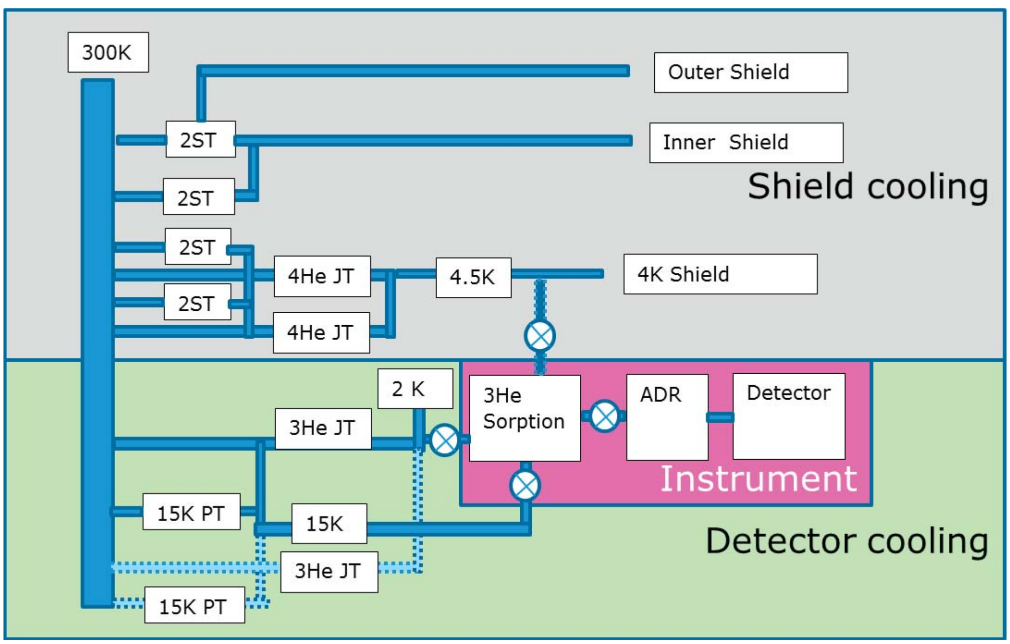

Figure 5-19: Thermal schematics of European/Japanese cooling chain from room temperature to 50 mK

The power consumption for the X-IFU CC, assuming the use of the RAL 2K cooler and the Air Liquide 15K Pulse Tube cooler for the detector cooling and the Japanese coolers for the shield cooling, is illustrated in Table 5-1.

Cooler	Power to compressor	Cooling power	Needed cooling power	Margin
Shield cooler	2x50 = 100W	200-450mW (17-25K)	400mW	12%
4K JT pre-cooler	2x50 = 100W	200mW at 18K	150mW	33%
4K JT cooler	2x50 = 100W	20mW at 4K	16mW	25%
15K PT pre-cooler	1x200 = 200W	200mW at 15K	150mW	33%
2K JT cooler	1x100 = 100W	20mW at 2K	14mW	42%
Total	600W			

Table 5-1: Estimated electrical power to the compressors of the JT and Pulse Tube/Stirling cooler(for nominal operation) during observation

During recycling, the input power to the 15K JT pre-cooler might increase by ~100W. Including a 20% development margin, this results in ~850W total input power, which also covers different configurations.

The harness between the room temperature electronics and the focal plane has a major impact on the thermal design. The cooling power has been estimated using the reference design parameters from the ATHENA ATHENA_L1 study. A first assessment has shown that the increased pixel-count will be compensated by the FDM, resulting in a smaller harness.

5.3.2.4 Instrument optical design

The optical design of the instrument is simple: the detector plane, which is inside the Dewar on the central axis, should be within the specified accuracies from the focal point of the X-ray mirrors. In addition the optical design includes a number of functions/units which are specified in this section.

5.3.2.4.1 Filter wheel

The filter wheel position may be selected per observation according to necessity for additional optical light blocking, calibration source deployment, safety or intense source observations. The filter wheel shall accommodate a TBD number of filters. Depending on the needs and on the necessity to reduce the overall size of the filter wheel, some of these filters which are dedicated to the study of point sources only may restrict the field-of-view to the central source.

The following filters are under consideration and are being studied by the consortium with inputs from the X-IFU science team:

- An open position (which gives the best sensitivity)
- A closed position to protect the instrument in case of emergencies and periods of high radiation, and to help in the determination of the non-x-ray background
- A position which includes a Be filter of thickness 30-50 µm, which suppresses part of the low energy photons, ensuring full spectral resolution for bright X-

ray sources when the lowest energy bins are not crucial and maximal count rate above 2 keV must be preserved

- A neutral-density filter, composed of a thick Molybdenum disk with many small holes, such that the transmission is independent of energy, allowing the observation of bright sources even at the lowest energies, while fully preserving the imaging capabilities
- A beam diffuser to spread the X-ray beam on a large number of pixels in case of strong point sources. The beam diffuser is made of a bended multi-channel plate which has its own specific energy response and is effective at low energies (<2 keV)
- An optical filter (to suppress light from the objects which are observed). Optical filters are typically made of an extremely thin layer of aluminium (a few tens of nm) deposited on a thin plastic film (about 200 nm). Optical filters may also be added to the neutral-density filter and to the beam diffuser
- A (presumably) open position equipped with Fe55 radioactive sources, in order to complement, or add further redundancy to the active X-ray calibration sources.

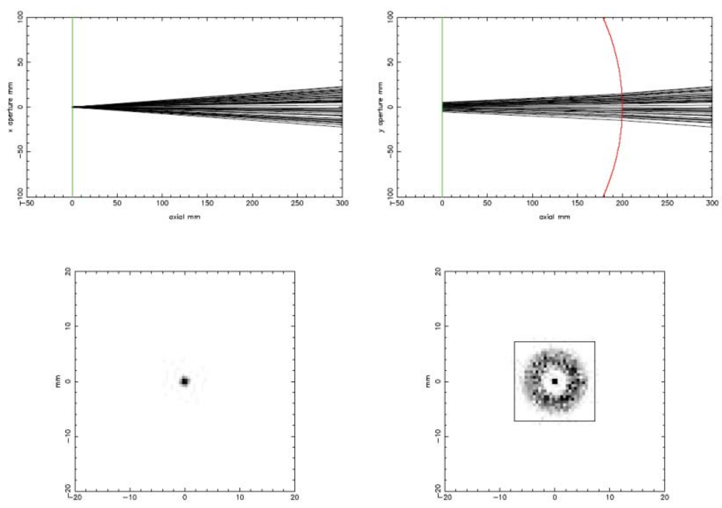

Figure 5-20: Effect of a beam diverter (bended multi-channel plate) on the PSF. Left: nominal case; right: after insertion of the beam diverter. Clearly the beam is spread over a larger number of pixels but at the expense of a limited efficiency of the beam diverter itself (order 30-40%)

In order to observe bright stars it will be necessary to reduce the optical light of such objects by inserting an additional optical blocking filter in the beam (as this also reduces the X-ray throughput this filter will only be used for optically bright objects). The effect of bright sources has been estimated using a number of bright sources and calculating the contribution of their optical/UV intensity to the energy resolution of the detector taking into account the large collecting area, the relatively fast detector response time (4.5 msec record length) and requiring that the contributions of the optical/UV light to the degradation of the X-ray energy resolution has to be significantly less than 1 eV. We have calculated this for the assumed thin (goal) filters in the Dewar as this is the worst case for the optical load. In Figure 5-21 we give the total transmission for various bright stars. With an additional optical filter of 60 nm Al on 200 nm polyimide bright stars can be observed without noticeable resolution degradation. Of course there is a penalty in terms of the low energy X-ray response of the detector which also reduces. Inclusion of such filter in the beam diffuser is under discussion.

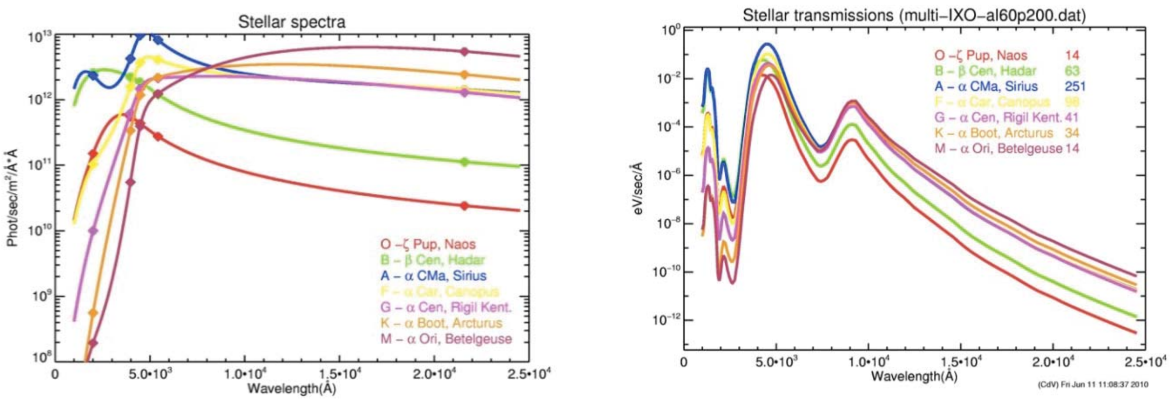

Figure 5-21: Spectra for a number of very bright stars (left) and the noise induced by transmitted light after inclusion of the thin Dewar filters and an optical filter in the filter wheel assembly of 60 nm Al on 200 nm polyimide. The numbers in this plot (at the right top) give the additional contribution to the energy resolution in eV/sec (note that the typical record length is 4.5 ms)

The baseline for the filter wheel is to mount it on the Dewar, but this needs to be reassessed based on the mechanical constraints (allowed volume) of the SC and telescope. Typical dimension of a filter covering the full field of view is ~120 mm in diameter assuming a mirror diameter of 3 meter, (but some margin is included for as the aperture cylinder has not yet been designed in detail) and the distance between the detector and the filter wheel of ~0.31 m. The filter wheel assembly is about 500 mm in diameter. The vacuum door of the Dewar will be integrated with the filter wheel. This is illustrated in Figure 5-22. Note that in this figure the choice of filters is not yet definitive and the diameters are only selected to show some of the options.

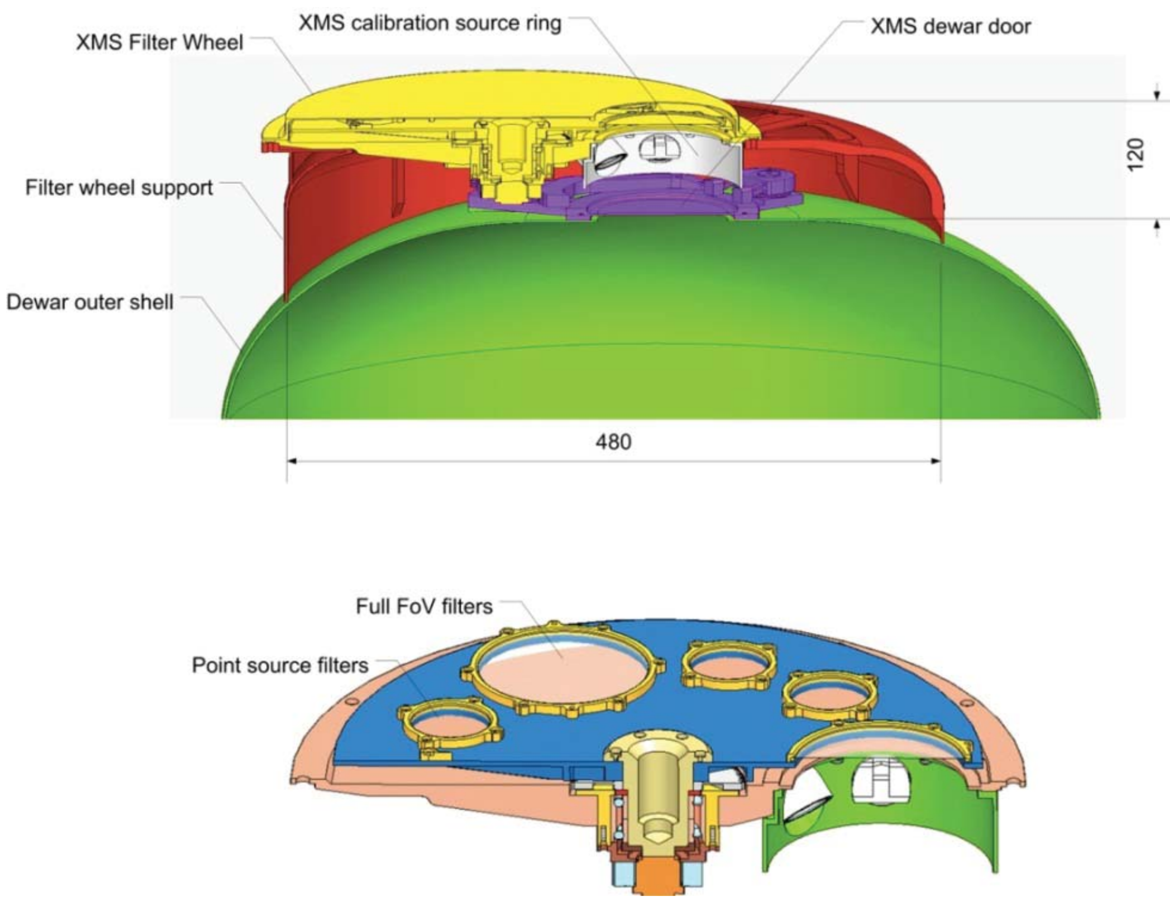

Figure 5-22: Overview of the filter wheel assembly. The top panel is showing the different components. In the bottom panel a cross cut is given showing clearly the large filters for the full FoV and smaller filters for point sources as was planned for IXO. Choice of filters (bright source and/or polarization) is TBD

Optical thermal/blocking filters

In order to allow the X-ray beam to reach the array of micro-calorimeters at the focal plane, a clear path has to be opened in the cryostat thermal and structural shields surrounding the cold stage, identified as the aperture cylinder. Optical blocking filters (OBF) need to be mounted on such shields to reduce the radiation heat-load from warmer surfaces onto the detector array. The micro-calorimeters operating as thermal detectors are also sensitive to photons at lower energies than X-rays. Although the detector does not trigger on individual low energy photons, the statistical fluctuation of the absorbed energy during the effective X-rays detection time, can introduce a degradation of the energy resolution of the detector known as shot noise. The OBF need to prevent the shot noise due to out of band radiations from the cryostat to deteriorate the intrinsic energy resolution of the detector. The OBF also significantly reduces the out of band radiation from target sources and background in the telescope field of view. However, particularly bright sources in the UV/VIS/IR (e.g. massive O stars, planets, QSO’s, etc.) may need the use of additional optical filters in the filter wheel which will be mounted at the entrance of the cryostat aperture cylinder.

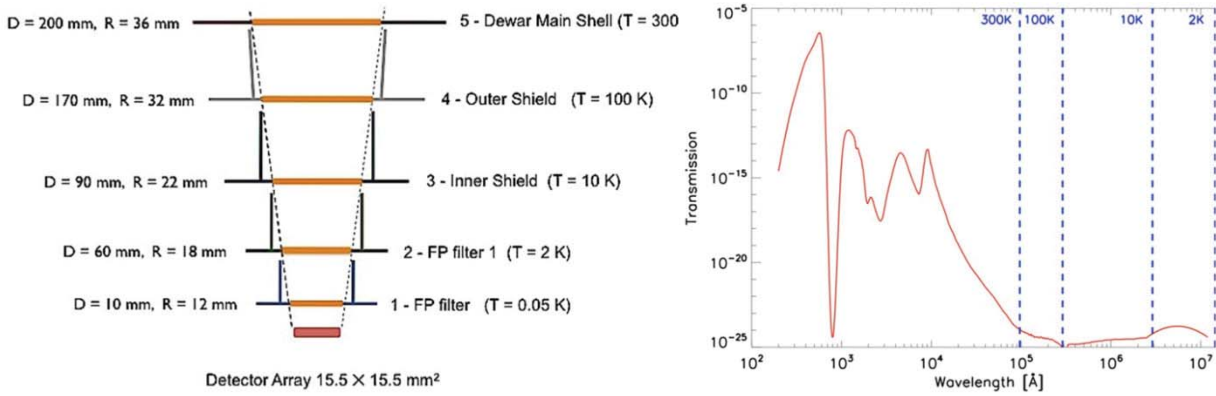

Figure 5-23: Left) Adopted scheme for the optical blocking filters in the cryostat aperture cylinder. The filter temperatures, distances from the detector array (D), and radii (R) are shown in the schematic drawing. Right) Calculated total transmission for the full set of five filters. Superimposed in the plots are the wavelengths of the peak thermal emission from the cryostat shields

The baseline design of the OBF for the X-IFU experiment, which is largely based on the investigation conducted during the IXO-XMS study phase and ASTRO-H development, consists of 5 identical filters for a total of 2800Å of polyimide and 2100 Å of aluminium, with the two outer and larger diameter filters supported by a 10 µm thick integrated polyimide grid. The optical performance of a more transparent OBF design, aimed at increasing the low energy response, consisting of 5 identical filters with a total of 2250 Å of polyimide and 1000 Å of aluminium, with a mesh with 97% open area, similar to the one adopted for ASTRO-H, to mechanically support the two larger diameter filters will also be evaluated.

5.3.2.5 Instrument configuration

The configuration of the instrument includes the cryostat, the electronics for the detector, the electronics to operate the cryo-coolers and control electronics. The detector is located inside a Dewar, which is cooled by a set of cryo-coolers with its dedicated drive electronics. The Dewar, together with its cryo-coolers is called the X-IFU cryo. The Front End Electronics (FEE) is galvanically well connected to the detector. The amplified signals from the FEE are passed to the Digital Electronics / Event Processing (DE/EP) unit where the data is digitized, the feedback signal is generated and the (demodulated) triggered event data, including triggers from the anti-coincidence detector are selected and subsequently processed to extract the relevant event parameters (e.g. energy, time stamp, and event grade). The Instrument Control Unit (prime or redundant) is responsible for operating the instrument with the desired settings and also monitors the health of the instrument. It uses SpaceWire for its communications. The Power Distribution Unit distributes the raw power over the cooler drives and the electronic boxes and the conversion is done inside these electronic boxes. Only for the FEE, with its severe EMC requirements, the power conversion is done in a separate unit (PSU). Some units are cold redundant whereas in most cases parallel signal chains are implemented (warm redundancy). This system overview is shown in Figure 5-24.

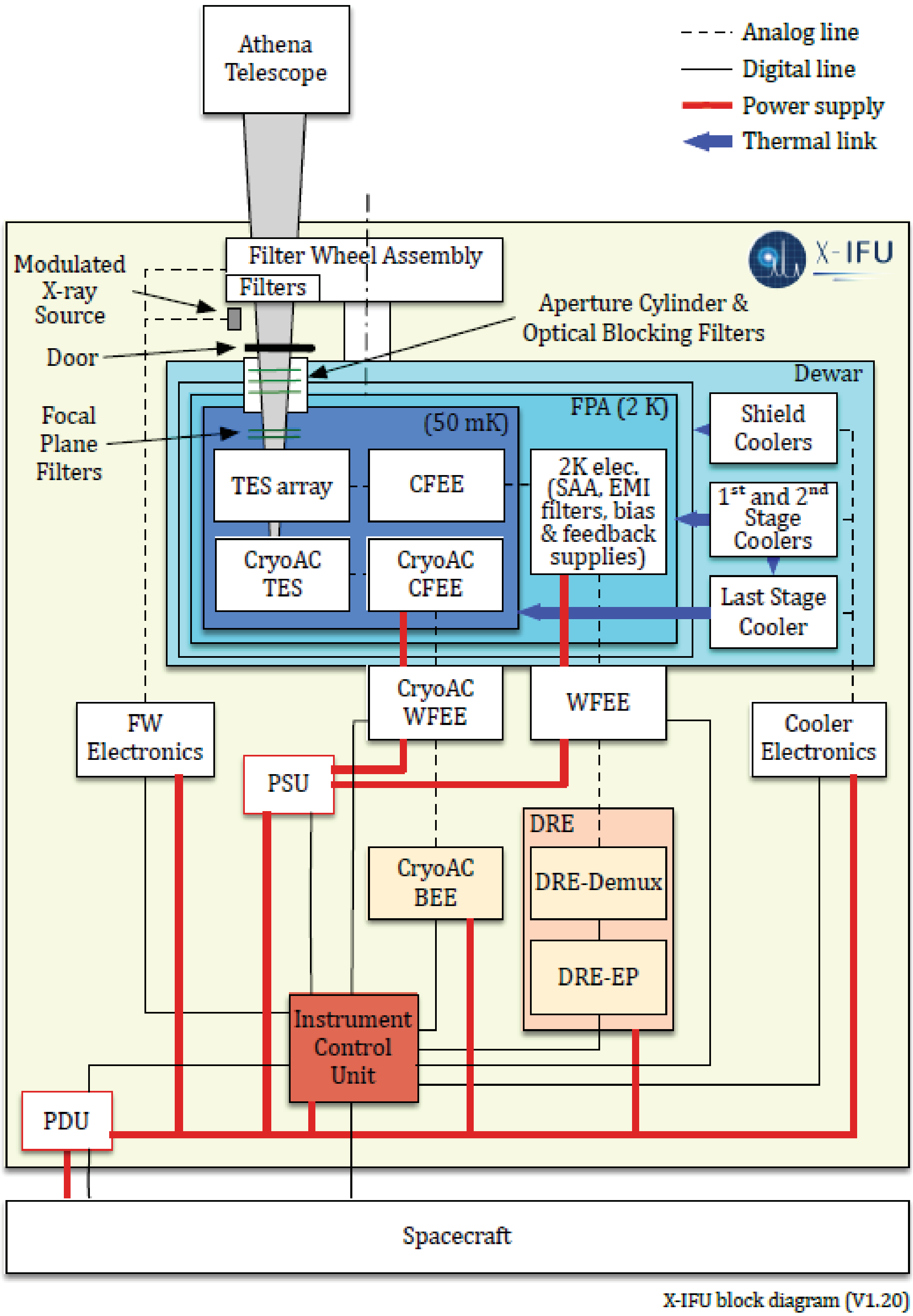

Figure 5-24: X-IFU block diagram. The TES array, its anticoincidence and the SQUIDs are at 50 mK. The front-end electronics consists primarily of the LNAs. The instrument control unit provides the interface with the SC

A description of the instrument configuration, starting from the top of the functional block diagram is given in Table 5-2:

Unit	Redundancy	Comments
Filter Wheel (FW)	n/a	The filter wheel is mounted on the Dewar. It will include a TBD number of positions (see below).
Modulated X-ray source (MXS)	n/a	The Modulated X-ray source is a ring with 4 (TBD) commandable calibration sources including the relevant HV power supplies (11 kV). It will be controlled by the filter wheel electronics.
Dewar door	n/a	The Dewar will be launched under vacuum with ambient temperature and this requires a door which closes the entrance window. It will be located underneath the filter wheel.
Aperture cylinder	n/a	An internal baffle to be mounted on the Dewar to contain optical blocking filters.
Focal plane assembly (FPA)	n/a	Focal Plane Assembly (main TES array, CryoAC TES, their cold front end electronics, 2K electronics, SQUID array amplifiers) will be mounted in the Dewar.
Dewar	n/a	The Dewar contains the cryo-chain and the FPA: the vacuum vessel, the cryogenically cooled shields and the cooling chain down to 50 mK. It also includes the support structure and the harness between ambient temperature and 2 K.
Filter Wheel electronics	Cold	Electronics to control the FW and the MXS.
CryoAC Warm Front End Electronics (CryoAC WFEE)	Warm	The anti-co electronics contains all relevant electronics for the CyroAC detector (e.g. bias setting, read-out amplifier, ..). This has to be part of the same faraday cage as the Dewar and the WFEE and should therefore also be located close to (< 0.5 m) or directly attached to the Dewar.
Warm Front-End Electronics (WFEE)	Warm	The WFEE accommodates the low-noise-amplifiers (LNA) used to amplify the SQUID outputs. This box also contains the DC-bias sources for the SQUIDs. The box is galvanically (<better than 1 mΩ) integrated with the cryostat (either by bolting directly on the cryostat or by a < 0.5m cable) to form a Faraday cage.

Unit	Redundancy	Comments
Shield, 1st & 2nd stage coolers & last stage coolers	See text	The assumption for the cooling chain is that it is based on a set of redundant shield coolers down to 4K , redundant 2K JT coolers with dedicated pre-cooler and 1 Sorption-ADR last stage cooler.
Cooler electronics	Warm	Drive electronics to operate the coolers (shield coolers, pre- coolers, 2K coolers, last stage cooler).
Digital Readout Electronics (DRE)	Warm	The digital readout electronics digitizes the continuous data stream, generates the feedback to the SQUID, derives the energy and the grade of the photon. Each unit handles independently the data of one quadrant of the detector. The DRE units can be located at a certain distance (typically 1 – 2 m) from the WFEE.
Power Supply Unit (PSU)	Warm	The Power Supply Unit provides regulated and well shielded secondary power to the sensitive WFEE and the CryoAC WFEE.
Power Distribution Unit (PDU)	Cold	The Power Distribution Unit distributes the raw SC power to the various electronics units, with the exception of the WFEE and the CryoAC WFEE.
Instrument Control Unit (ICU)	Cold	It can autonomously set-up and control the instrument. It will also autonomously take action if instrument HK parameters get out of limit. It interfaces with the SC (data handling, TM/TC) and performs critical health checks on the instrument.

Table 5-2: Units for the X-IFU FPA and their redundancy pattern

5.4 List of Equipment

	mass (kg)	mass margin (%)	mass incl. margin (kg)
FPM	**718.30**	**21.26**	**871.00**
WFI	**240.00**	**20.00**	**288.00**
WFI_CH	51.10	20.00	61.32
WFI_CHR	16.10	20.00	19.32
WFI_DE_0	5.40	20.00	6.48
WFI_DE_1	5.40	20.00	6.48
WFI_DE_2	5.40	20.00	6.48
WFI_DE_3	5.40	20.00	6.48
WFI_DE_4	5.40	20.00	6.48
WFI_DE_5	5.40	20.00	6.48

WFI_DER	34.20	20.00	41.04
WFI_FW	39.80	20.00	47.76
WFI_HarMis	30.50	20.00	36.60
WFI_ICPU_0	11.00	20.00	13.20
WFI_ICPU_1	11.00	20.00	13.20
WFI_PrimStruc	13.90	20.00	16.68
XIFU	**478.30**	**21.89**	**583.00**
XIFU_CryoAC_BEE	2.10	50.00	3.15
XIFU_CryoACWFEE	1.20	50.00	1.80
XIFU_Dewar	233.20	23.30	287.54
XIFU_DRE_0	32.50	20.00	39.00
XIFU_DRE_1	32.50	20.00	39.00
XIFU_DRE_2	32.50	20.00	39.00
XIFU_DRE_3	32.50	20.00	39.00
XIFU_FSDE	24.00	20.00	28.80
XIFU_FW	8.50	20.00	10.20
XIFU_FWE	2.90	20.00	3.48
XIFU_ICU	8.80	20.00	10.56
XIFU_LSDE	13.50	20.00	16.20
XIFU_PDU	2.00	30.00	2.60
XIFU_PSU	1.50	30.00	1.95
XIFU_SCDE	16.00	20.00	19.20
XIFU_SSDE	14.60	20.00	17.52
XIFU_WFEE	20.00	20.00	24.00
Grand Total	**718.30**	**21.26**	**871.00**

Table 5-3: Mass budget for the instruments

Power (W)		
	P_on	P_stby
WFI	**631.30**	**48.00**
WFI_CH	72.20	48.00
WFI_CHR	0.00	0.00
WFI_DE_0	72.60	0.00
WFI_DE_1	72.60	0.00
WFI_DE_2	72.60	0.00
WFI_DE_3	72.60	0.00
WFI_DE_4	72.60	0.00
WFI_DE_5	72.60	0.00
WFI_DER	0.00	0.00
WFI_FW	1.00	0.00
WFI_HarMis	0.00	0.00

WFI_ICPU_0	61.25	0.00
WFI_ICPU_1	61.25	0.00
WFI_PrimStruc	0.00	0.00
XIFU	**1544.00**	**0.00**
XIFU_CryoAC_BEE	15.00	0.00
XIFU_CryoACWFEE	5.00	0.00
XIFU_Dewar	850.00	0.00
XIFU_DRE_0	93.25	0.00
XIFU_DRE_1	93.25	0.00
XIFU_DRE_2	93.25	0.00
XIFU_DRE_3	93.25	0.00
XIFU_FSDE	79.00	0.00
XIFU_FW	2.00	0.00
XIFU_FWE	9.00	0.00
XIFU_ICU	20.00	0.00
XIFU_LSDE	27.00	0.00
XIFU_PDU	5.00	0.00
XIFU_PSU	21.00	0.00
XIFU_SCDE	53.00	0.00
XIFU_SSDE	60.00	0.00
XIFU_WFEE	25.00	0.00
Grand Total	**2175.30**	**48.00**

Table 5-4: Installed power for the instruments

Power (W)	Com	FSlew	Lau	Man	Obs WFI	Obs XIFU	Safe	SlSlew	SwIn
WFI	284.75	0.00	0.00	0.00	569.50	569.50	0.00	0.00	0.00
XIFU	1053.36	1020.57	0.00	1175.00	1210.90	1159.61	180.13	1020.57	1175.00
Grand Total	**1338.11**	**1020.57**	**0.00**	**1175.00**	**1780.40**	**1729.11**	**180.13**	**1020.57**	**1175.00**

Table 5-5: Power budget per system mode as defined in chapter 7.3.3

	height (m)	length (m)	width (m)	Can be moved from FPM	Constraints
WFI					
WFI_CH	0.12	0.41	0.31	No	
WFI_CHR	1.58	0.90	0.04	No	
WFI_DE_0	0.19	0.22	0.20	No	
WFI_DE_1	0.19	0.22	0.20	No	
WFI_DE_2	0.19	0.22	0.20	No	

WFI_DE_3	0.19	0.22	0.20	No	
WFI_DE_4	0.19	0.22	0.20	No	
WFI_DE_5	0.19	0.22	0.20	No	
WFI_DER	1.14	2.02	0.95	No	
WFI_FW	0.11	0.00	0.00	No	
WFI_HarMis	0.00	0.00	0.00	No	
WFI_ICPU_0	0.19	0.26	0.20	Yes	Max distance of 10 m from Detector Electronics
WFI_ICPU_1	0.19	0.26	0.20	Yes	Max distance of 10 m from Detector Electronics
WFI_PrimStruc	0.53	0.00	0.00	No	
XIFU					
XIFU_CryoAC_BEE	0.26	0.26	0.12	Yes	
XIFU_CryoACWFEE	0.23	0.23	0.06	Yes	Max distance of 2 m from Dewar
XIFU_Dewar	0.00	0.00	0.00	No	
XIFU_DRE_0	0.32	0.41	0.59	Yes	Max distance of 2 m from Warm Front Electronics
XIFU_DRE_1	0.32	0.41	0.59	Yes	Max distance of 2 m from Warm Front Electronics
XIFU_DRE_2	0.32	0.41	0.59	Yes	Max distance of 2 m from Warm Front Electronics
XIFU_DRE_3	0.32	0.41	0.59	Yes	Max distance of 2 m from Warm Front Electronics
XIFU_FSDE	0.37	0.35	0.16	Yes	
XIFU_FW	0.00	0.00	0.00	No	
XIFU_FWE	0.17	0.17	0.17	Yes	
XIFU_ICU	0.35	0.35	0.31	Yes	
XIFU_LSDE	0.37	0.35	0.17	Yes	
XIFU_PDU	0.21	0.21	0.17	Yes	
XIFU_PSU	0.19	0.19	0.19	No	
XIFU_SCDE	0.37	0.35	0.16	Yes	
XIFU_SSDE	0.37	0.35	0.31	Yes	Max distance of 2 m from Dewar
XIFU_WFEE	0.37	0.35	0.31	Yes	

Table 5-6: Dimensions and configuration constraints on instrument equipment

6 OPTICS

6.1 Requirements and Design Drivers

The requirements and design drivers for the optics are not yet specified, apart from those described by the general requirements and design drivers specified as part of the mission or system.

6.2 Assumptions and Trade-Offs

The main assumption is that the X-ray telescope is built using Silicon Pore Optics (SPO). This enables a modular design using Mirror Modules (MMs).

6.3 Baseline Design

The baseline design is described in detail in RD[7]. A summary of the main features is given below.

- The maximum width of Mirror Modules (MM) is 6 cm for radii below 0.5 m, 10 cm for radii above 0.5m. This is in contrast to previous studies where 10 cm was used throughout and is based on results from studies where MMs at the inner radius were produced. This assumption might need to be refined later (e.g. by allowing for a smooth increase)
- A design consisting of 2x35 plates stacked closely together, of which 68 are reflecting
- Spacing between the MMs is 7 mm radially and 16.8 mm azimuthally
- Additional space is reserved to obtain a 6 petal-like structure. This additional space is also 16.8 mm. This additional space also results in aligning MMs in a 6-fold symmetry. This space can be used to easily route thermal wiring, star tracker harness, and add structural stiffening, etc. without impacting effective area
- 1 mm rib pitch. A larger rib pitch is currently under investigation and could be implemented in future design iterations
- 0.170 mm plate thickness, 0.605 mm plate separation
- Focal length of 12 m (baseline)
- Coating: Iridium with 8nm B_4C overcoat.

The lay-out of the MMs is shown in Figure 6-1. One detail which is not included in the calculations of effective area and vignetting is the lay-out of the MMs in the Wolter-Schwarzschild design. However, this has no or a negligible impact on the effective area results. The Wolter-Schwarzschild lay-out is chosen to optimise off-axis PSF performance and is not addressed here. The Wolter-Schwarzschild design means that the mid-plane of the MMs are arranged on a spherical surface with a radius equal to the focal length (with a very small modification to the internal kink-angle of the MMs). More details can be found in RD[8]. Note that this curved mid-plane **is** taken into account for the configuration aspect during the CDF study for which it is important.

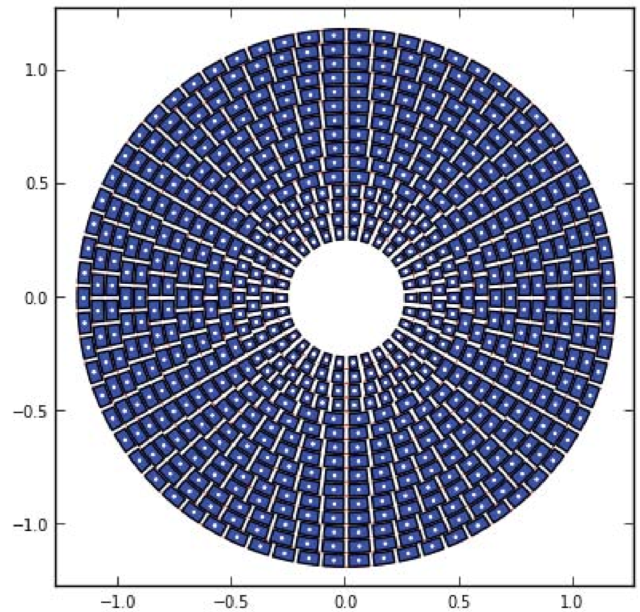

Figure 6-1: Lay-out of the Mirror Modules with 15 rows (units are in m) Note the smaller Mirror Modules at the centre and the 6-fold symmetry

The rationale of the assumption of 1 mm rib pitch, and the impact on effective area, warrants some elucidation. During the last ~10 years of technology development MMs have been developed and studied using a 1 mm rib pitch. A 1 mm rib pitch is therefore considered as well studied and considered a safe (and perhaps slightly conservative) baseline. Mirror modules with larger rib-pitch are currently under development and will become the baseline if successful.

With a rib thickness of 0.170 mm this leaves 0.830 mm of reflecting material in-between the ribs, i.e. a fractional reflective area of 83%. If the rib pitch is increased to 2 mm, the fractional area is increased to 91.5% (94.3% for 3 mm rib pitch). This corresponds to relative gains of effective area of 10% (2 mm) and 13.6% (3 mm). In the ATHENA proposal a 3 mm rib spacing (corresponding to 3.17 mm rib pitch) is used, mainly to limit vignetting effects. However, as is shown in Figure 6-2 vignetting improves dramatically from 1 to 2 mm rib pitch, but going to 3 mm rib pitch only adds a small improvement. The vignetting curves in Figure 6-2 were calculated with a geometrical model, which assumes small grazing incidences angles and ignores (small) variations of the incidence angles and, and hence squared reflectivities, as a function of off-axis angles. Furthermore the model approximates at the MM level (as opposed to the pore level), i.e. it calculates the performance of pores at the middle radius. Especially for the innermost MMs the performance changes rapidly with radius in a non-linear way and therefore the average performance can be slightly different from the performance of a pore at the middle radius; the curves were confirmed (to within a few %) by ray-tracing results which show slightly less vignetting (not shown).

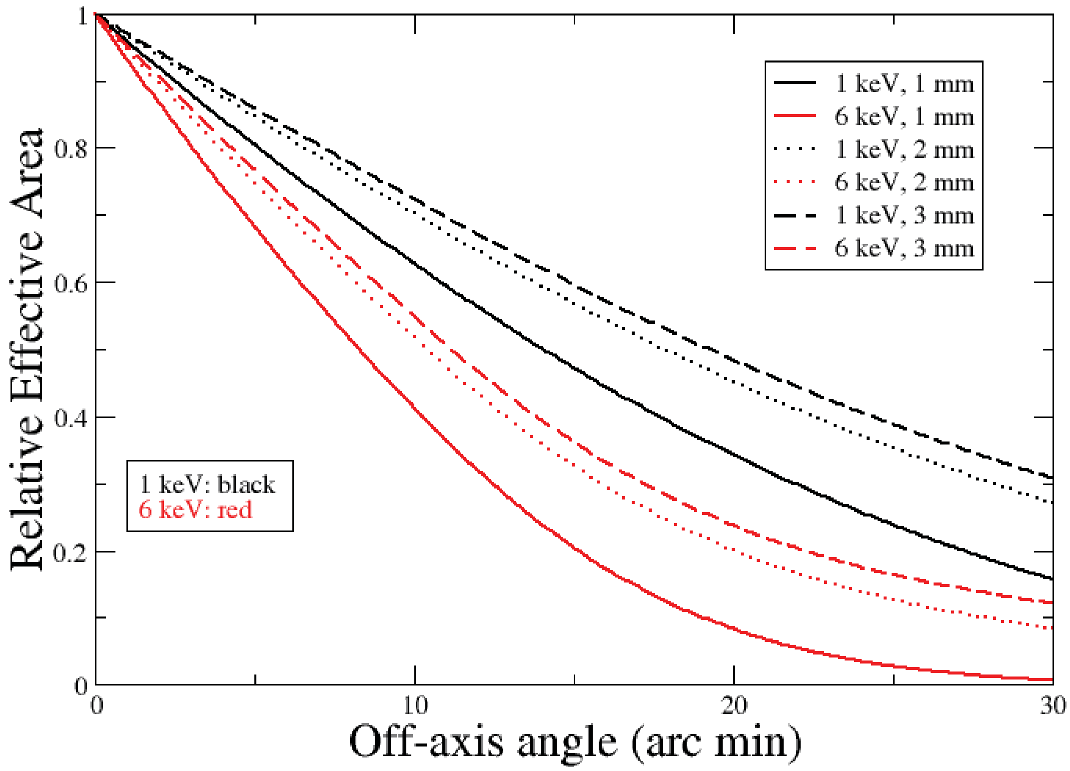

Figure 6-2 : Estimated vignetting, using an approximate model, at two energies (1 keV and 6 keV, black and red) for three rib pitches (1, 2, and 3 mm) for a telescope design with 15 rows

From the perspective of maximising total off-axis area, but more importantly from vignetting considerations, it is clear that an increased rib pitch is needed. Whether the 3 mm rib pitch in the proposal is feasible remains to be studied. However, given the modest additional increase in vignetting and effective area from 2 to 3 mm it is recommended an improvement of the rib pitch to around 2 mm will be the subject of Technology Development Activities (which is already foreseen for MMs at the inner radii).

During the CDF study the approximate effective area at 1 and 6 keV was calculated for each MM in each ring. Within OCDT a quick assessment of the total area was therefore possible by specifying the number of MMs in each ring. In Figure 6-3 the total effective area curves (including 10% assumed losses) are displayed for the various options in the legend.

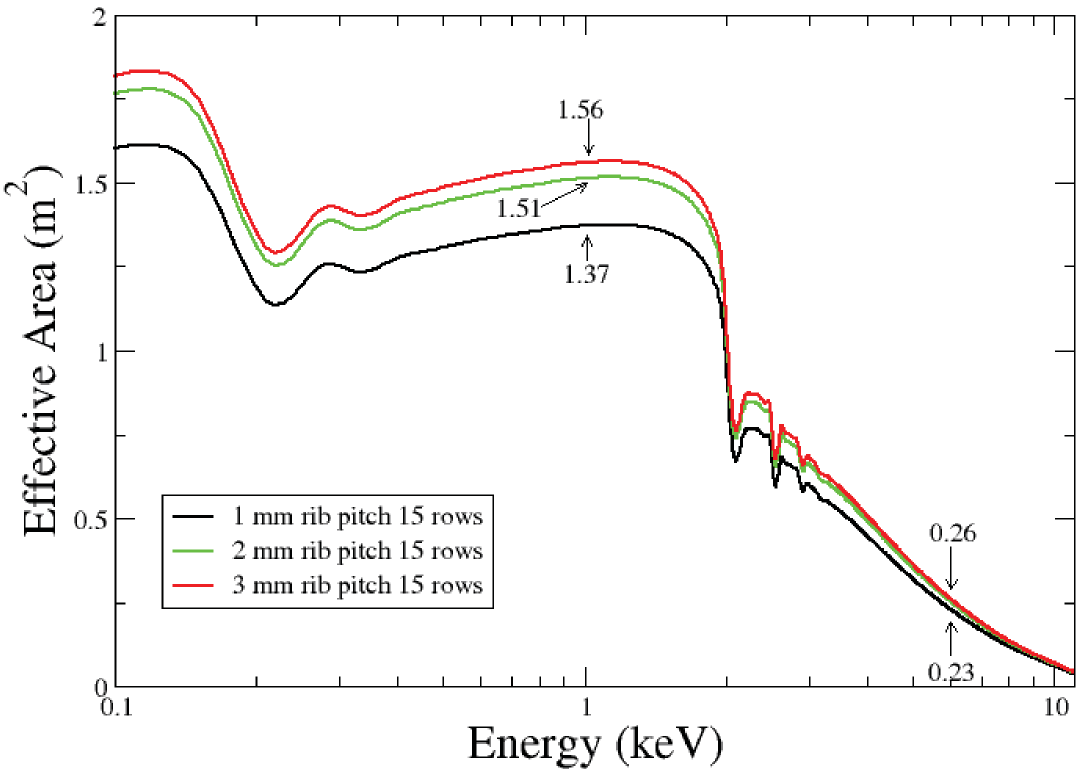

Figure 6-3: Effective area curves for 15 rows and 1, 2, and 3 mm rib pitch. Note that 3 mm rib pitch corresponds to 2.83 mm rib spacing

Details of the MMs can be found in Table 6-1.

Row	Width (mm)	Length (mm)	Number of MMs	Middle radius (m)
1	37.096	101.504	30	0.286
2	50.158	83.388	30	0.348
3	49.838	70.762	36	0.411
4	49.613	61.460	42	0.473
5	89.363	54.321	30	0.535
6	82.476	48.671	36	0.597
7	77.571	44.087	42	0.659
8	86.892	40.294	42	0.722
9	82.053	37.104	48	0.784
10	90.205	34.383	48	0.846
11	85.538	32.036	54	0.908
12	92.782	29.990	54	0.970

Row	Width (mm)	Length (mm)	Number of MMs	Middle radius (m)
13	88.326	28.191	60	1.032
14	94.845	26.597	60	1.095
15	90.608	25.175	66	1.157
			Total:678	

Table 6-1: Details on the Mirror Modules. The length in this table is the length of both the parabolic and hyperbolic stack along the optical axis. Total length is twice this value

6.4 Mirror Module Displacement Tolerances

The individual MMs have to be accurately co-aligned in order to form a common focus. The co-alignment of the MMs will be affected by different effects like the accuracy of the integration procedure, mechanical displacements (settling) during launch, gravity release, thermal properties of the telescope and other error-sources. In order to quantitatively assess the impact of a degrading co-alignment on the point spread function and effective area the following analysis was performed.

In order to reach a telescope performance of 5 arcsec HEW, an error allocation was used which allocates 4.3 arcsec to each MM and values between 0.5 arcsec and 2 arcsec to several effects (integration, mechanical, thermal, gravity, etc.) which can cause unwanted displacements and rotations. The allocations are combined by root sum squaring resulting in the 5 arcsec requirement. It is important to note, that an error contribution of for example 1 arcsec corresponds to a degradation of the HEW from 4.3 arcsec (perfect co-alignment) to (4.3^2+1^2)^0.5 arcsec = 4.41 arcsec.

A numerical analysis was performed to calculate the maximum movement of the PSF (assumed as a 2D Gaussian with 4.3 arcsec HEW) on the focal plane which still leaves 50% of energy inside a 4.41 arcsec circle centred on the optical axis. For 12 m focal length and a resulting 58 µm/arcsec ratio on the focal plane, the calculated maximum is 34.5 µm. For error allocations of 0.5 arcsec or 2 arcsec, the resulting translation maximum is 17 µm and 70 µm.

Error [arcsec]	PSF HEW [arcsec]	$(PSF^2+Error^2)$^0.5 [arcsec]	Max translation [µm]
0.5	4.3	4.33	17
1	4.3	4.41	34.5
2	4.3	4.74	70

Table 6-2: Maximum translation of a 4.3 arcsec PSF on the focal plane for different error allocations

A translation of the PSF on the focal plane can be caused by moving a MM along its 6 degrees of freedom (3 translations and 3 rotations). Translations of the MM in x or y direction directly cause the same movement of the PSF. Translations of the MM along the z axis do not shift the PSF, but cause a small degradation in resolution. A first numerical assessment of defocusing a MM came to the conclusion that a 500 µm shift can be tolerated. A rotation α around its local z-axis of a MM located at a radial position R results in a translation of the PSF of αR. For a 1.2 radius, 10 µm correspond to a 1.7 arcsec z-rotation. Rotations of a MM around its local x or y axis have a low influence on the PSF translation and degradation (which will have to be quantified in more detail by ray tracing in future studies) but these rotations result in vignetting and effective area degradation. The tolerable loss of effective area for this calculation was assumed to be 1%. As the maximum x or y rotation depend on the radial position (due to different plate lengths). The following table provides values for inner and outer radii together with other displacement allocations.

DOF	Displacement	Comment
dx+dy	20 µm	dx and dy added vectorial
dz	500 µm	
Rot x	20 arcsec	Inner MM at 0.25 m; for 1% eff area loss
Rot y	6 arcsec	Inner MM at 0.25 m; for 1% eff area loss
Rot x	30 arcsec	Outer MM at 1.2 m; for 1% eff area loss
Rot y	18 arcsec	Outer MM at 1.2 m; for 1% eff area loss
Rot z	1.7 arcsec	At 1.2 m radius, for smaller radii r multiply with 1.2/r

Table 6-3: Displacement allocations for MM with 4.3 arcsec HEW PSF and 1 arcsec RSS error allocation

The values dx, dy, dz and rot z are listed for a 1 arcsec RSS error allocation but can be scaled linearly for 0.5 arcsec or 2 arcsec allocations. The values rot x and rot y are listed for 1 % loss of effective area and can also be scaled linearly for different loss limits.

6.5 List of Equipment

	mass (kg)	mass margin (%)	mass incl. margin (kg)
MM_Ring01	16.65	0.00	16.65
MM_Ring02	17.42	0.00	17.42
MM_Ring03	18.20	0.00	18.20
MM_Ring04	18.83	0.00	18.83
MM_Ring05	18.29	0.00	18.29
MM_Ring06	18.93	0.00	18.93
MM_Ring07	19.53	0.00	19.53

	mass (kg)	mass margin (%)	mass incl. margin (kg)
MM_Ring08	19.76	0.00	19.76
MM_Ring09	20.47	0.00	20.47
MM_Ring10	20.64	0.00	20.64
MM_Ring11	21.32	0.00	21.32
MM_Ring12	21.50	0.00	21.50
MM_Ring13	22.22	0.00	22.22
MM_Ring14	22.35	0.00	22.35
MM_Ring15	23.07	0.00	23.07
Grand Total	**299.19**	**0.00**	**299.19**

Table 6-4: Mass budget of the optics subsystem

Note: The mass margin of the individual MM rings is already included in the mass allocation.

6.6 Technology Requirements

A detailed technology development plan for the Silicon Pore Optics technology is currently implemented which covers the following technical areas:

- Inner mirror modules
- Outer mirror modules
- Improving the HEW performance to below 5 arcsec
- Demonstrating the MM integration and alignment into the mirror structure
- X-ray coatings
- Industrialisation of mirror plate manufacturing (including coating)
- Further development of simulation tools
- Extending existing X-ray metrology facilities (incl. adapting for 12 m focal length)
- Environmental qualification of an engineering model MM
- Stray-light simulation and baffling.

More information on these technology developments can be found in RD[23].

This Page Intentionally Blank

7 SYSTEMS

7.1 System Requirements and Design Drivers

The ATHENA requirements flow down is shown in Figure 7-1. The CDF study focused on the design of the SC, mission and science operations. The instruments (WFI and X-IFU) were considered as an input to the study, their expected/desired specifications have been taken as guidelines for the design of the SC.

The requirements were provided by the customer prior to the study sessions in the form of several documents:

- The Science Requirements Document (SciRD RD[10]) derived from the initial proposal from the ASST RD[14]
- The Mission Requirements Document (MRD (RD[11]))
- The preliminary SC Requirements Document (SRD RD[12])
- The Concept of Operations (ConOps RD[13]) document, describing the mission boundary conditions in Part A, and the reference mission architecture and profile, comprising a single launch into an L2 halo orbit with an Ariane launch vehicle in Part B.

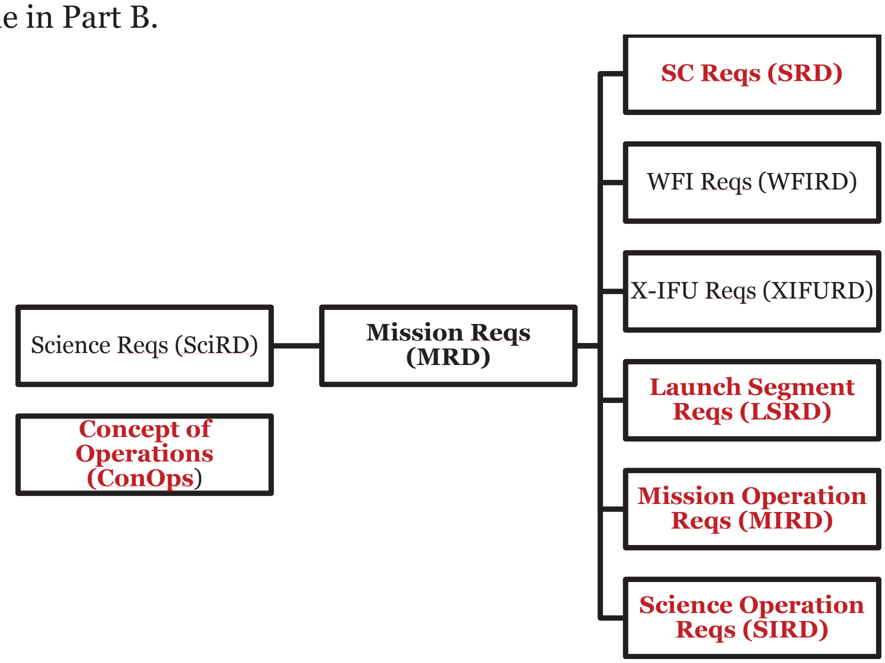

Figure 7-1: ATHENA requirements flow down structure, in red are the requirements relevant to the study

The following tables enumerate some of the sizing requirements for the overall system as defined in the beginning of the study. They were mostly taken from the SRD (RD[12]) whenever the flow down of the requirement had been done, or the MRD (RD[11]) if the flow down was still inexistent.

This subset of requirements focuses on the ones which were more relevant at overall system level and applicable to all system and subsystem-level options.

Mission requirements		
GROUP	**Req. ID**	**STATEMENT**
Mission lifetime	R-MIS-120	The ATHENA Mission shall launch in 2028.
	R-MIS-130	The ATHENA Mission shall be compatible with an overall lifetime of 10.25 years.
	R-MIS-170	The ATHENA Mission shall include a Nominal Operations Phase (NoP) of 5 years in duration.
	R-MIS-180	The ATHENA Mission shall include an Extended Operations Phase (EoP) of 5 years in duration.
Orbit	R-MIS-20	The ATHENA Mission shall include a Space Segment operating in a halo orbit around the second Lagrangian point of the Sun-Earth system (L2).
Launcher	R-MIS-30	The ATHENA Mission baseline launcher shall be Ariane 5 ECA.
Technology Readiness	R-MIS-780	The ATHENA Mission shall achieve a TRL-level of 5 for all elements by the start of Phase B2.
Payload	R-MIS-40	The ATHENA Mission shall include a single telescope common to the Narrow-Field and Wide-Field channels.
	R-MIS-50	The ATHENA Mission shall include a Narrow-Field channel implemented by a single X-IFU instrument provided by the Payload Consortium.
	R-MIS-60	The ATHENA Mission shall include a Wide-Field channel implemented by a single WFI instrument provided by the Payload Consortium.

Table 7-1: Mission requirements

<table>
<tr><th colspan="3">SC requirements</th></tr>
<tr><th>Req. ID</th><th>STATEMENT</th><th>Parent ID</th></tr>
<tr><td>R-SC-20</td><td>The SC shall be compatible with the reference mission design as described in the CReMA (RD[16]), characterised by the following maximum/minimum parameters:
<table>
<tr><th>Parameters</th><th>Value</th></tr>
<tr><td>Maximum SSCE angle</td><td>33 deg</td></tr>
<tr><td>Maximum declination</td><td>43.03 deg</td></tr>
<tr><td>Minimum declination</td><td>-42.86 deg</td></tr>
<tr><td>Maximum distance from Earth</td><td>1770000 km</td></tr>
</table></td><td>R-MIS-20</td></tr>
<tr><td>R-SC-310</td><td>The SC shall be able to perform any type of observation within a Field of Regard of 50% of the sky. The anticipated FoR is a spherical segment +/- 30° from the plane orthogonal to the sun-line).</td><td>R-MIS-570</td></tr>
<tr><td>G-SC-310</td><td>The SC shall be able to perform any type of observation within a Field of Regard of 60% of the sky. The anticipated FoR is a spherical segment roughly +/-35° from the plane orthogonal to the sun-line).</td><td>SCI-OBS-G-01</td></tr>
</table>

R-SC-320	The SC shall support continuous observing for all observations of 100ks.	SciRD
R-SC-330	The SC shall offer a minimum observing duration of 1ks.	SciRD
R-SC-400	The SC shall be able to downlink to the OGS the entire generated science telemetry as defined by the reference Observation Plan given an average down-link period of 3 hours per day, with a maximum latency of 4 (TBC) days.	ConOps Part B MTB [DDF_1.0]
R-SC-410	The SC shall preferentially downlink the science telemetry from a ToO-observation within 24 hours of the end of the observation.	ConOps Part B MTB [DDF_1.0]

Table 7-2: SC requirements

In the scope of the study a series of Key Performance Indicators (KPI) were defined to assess the performance of different system level solutions. These were divided into technical and non-technical indicators (Figure 7-2).

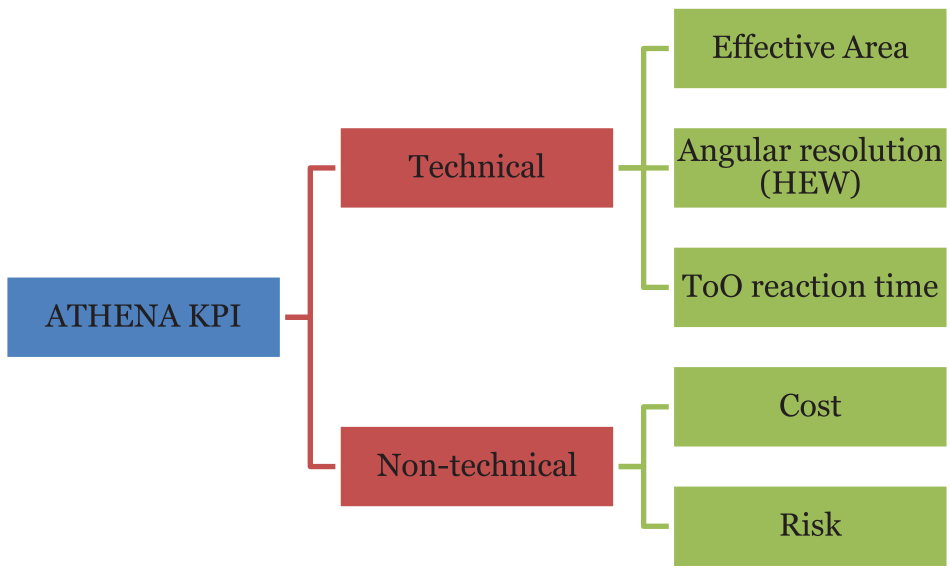

Figure 7-2: ATHENA mission KPI

The non-technical indicators were not strictly formalized into requirements at the system level but rather as assumptions and constraints (mentioned in chapter 7.2).

The following subsections detail the requirements associated with the different technical indicators, along with their preliminary breakdown allocation.

7.1.1 Effective Area

The effective area is the area that must be used when calculating the physical properties of sources in the sky (e.g. flux, surface brightness). Reflectivity and vignetting, among other effects, cause the geometric area of a telescope to be reduced to a smaller "effective area".

The effective area of observations at an x-ray energy e [$A_{eff\_WF}(e)$], is a product of the effective area provided to the focal plane by the SC [$A_{eff\_SC}(e)$], a vignetting correction factor [$V(e)$] in the case of the specification of the integrated effective area over the FoV, and the Quantum Efficiency of the instrument [$Q(e)$], including all effects at instrument-level (detector and filter). Therefore $A_{eff}(e)$ can be written as:

$$A_{eff}(e) = A_{eff\_SC}(e).V(e).Q(e) \qquad \textbf{Equation 1}$$

The anticipated overall $Q(e)$, with and without a filter in the optical path, for the X-IFU and the WFI, are shown in Figure 7-3 and Figure 7-4. From these, requirements at 1 and 6keV have been extracted.

For the on-axis response, $V(e) = 1$. For the FoV-averaged response, the following expression applies:

$$V_{FoV}(e) = \frac{2}{(20')^2}\int_0^{20'} V(e,\theta).\theta d\theta \qquad \textbf{Equation 2}$$

This integral yields the values presented in Table 7-3.

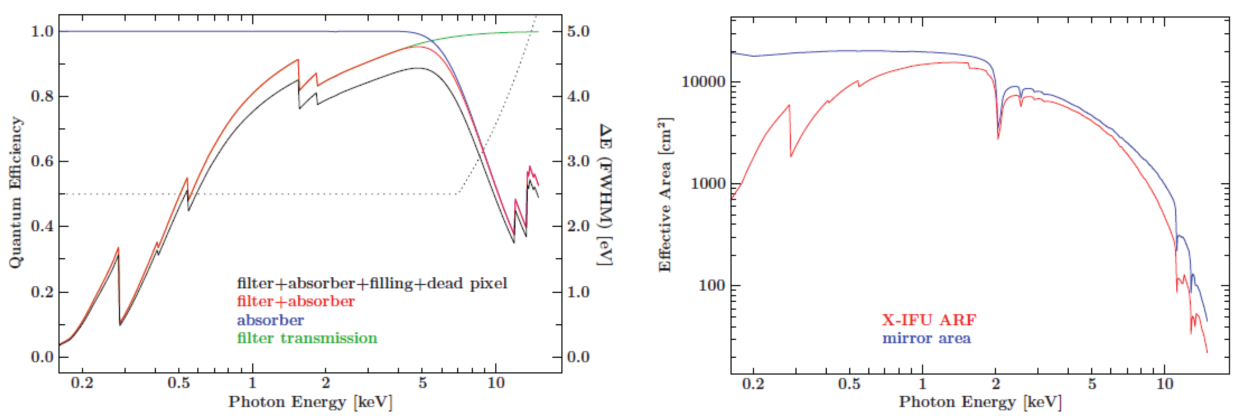

(a) QE of the combination of filter attenuation, filling factor, dead pixel fraction, and absorber efficiency. The plot also displays the energy resolution of the instrument.

(b) ARF in comparison to the effective area of the telescope.

Figure 7-3: (a) Anticipated X-IFU QE (black line=overall) and (b) Effective Area as a function of energy compared to the anticipated SC (telescope) Effective Area

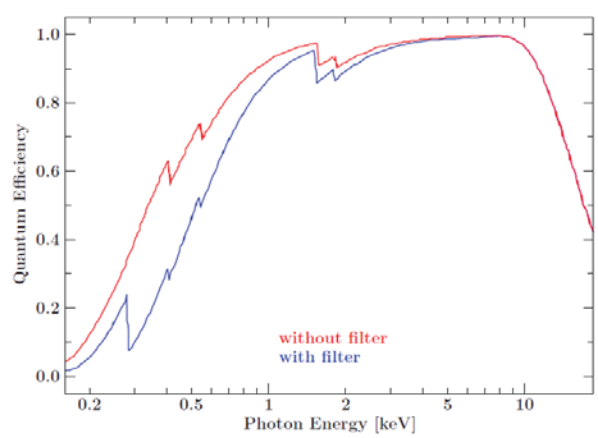

Figure 7-4: WFI anticipated QE with and without filter as a function of energy

E [keV]	V_FoV [%]
1	69.4
2	60.9
3	57.9
6	39.8
10	25.4
15	20

Table 7-3: Average vignetting over the Wide-Field FoV at different energies

The requirements in the MRD (or SciRD) have been broken down (Figure 7-5) to identify the contributions of the instruments (impacting $Q(e)$) and, the SC (impacting $A_{eff\_SC}(e)$, and $V(e)$).

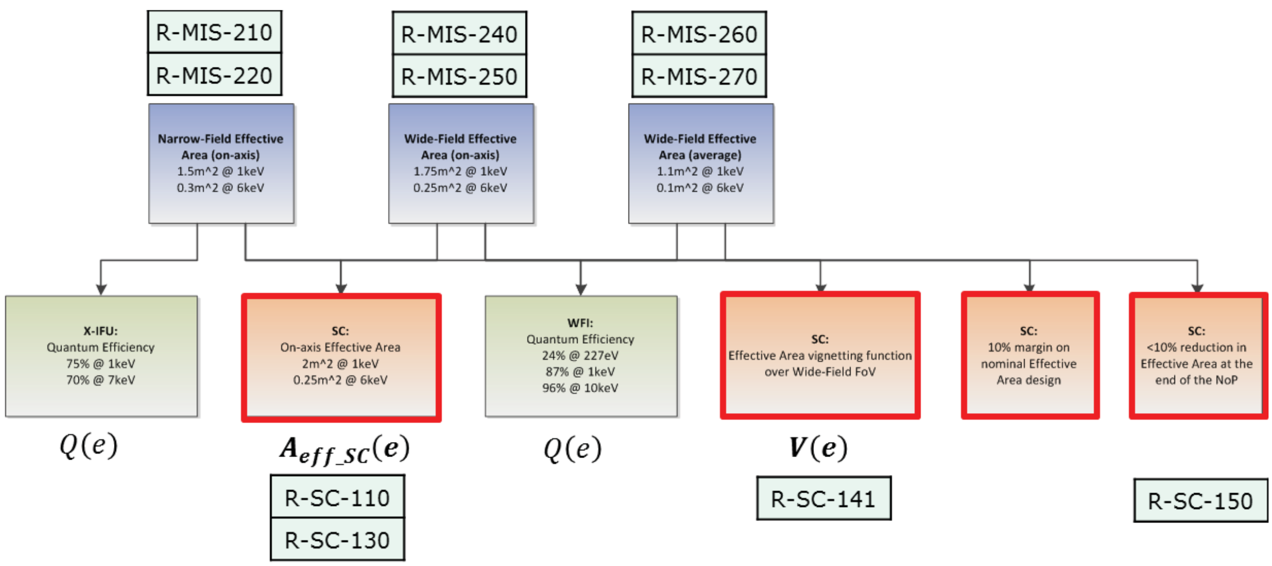

Figure 7-5: Effective area requirements breakdown at the beginning of the study

Since during the study the focus was on the SC design, the applicable requirements were the ones on Table 7-4.

Effective area requirements		
Req. ID	**STATEMENT**	**Parent ID**
R-SC-110	The SC should provide both X-IFU and WFI with an on-axis Effective Area of 2 m^2 at 1 keV.	MTB [DDF_1.0]
R-SC-130	The SC shall provide both X-IFU and WFI with an on-axis Effective Area of 0.25m^2 at 6 keV.	MTB [DDF_1.0]
R-MIS-210	ATHENA shall perform Wide-Field observations with an average Effective Area integrated over the Field of View of at least 1.1m^2 at 1 keV. (Not sizing)	SciRD

R-MIS-220	ATHENA shall perform Wide-Field observations with an average Effective Area integrated over the Field of View of at least 0.1m^2 at 6 keV. (Not sizing)	SciRD
R-SC-141	The SC shall provide an average vignetting over the Wide-Field governed by the following expression in Equation 2.	MTB [DDF_1.0]
R-SC-150	The SC shall restrict Effective Area loss to 10% below 3keV at the end of the mission.	MTB [DDF_1.0]

Table 7-4: Applicable effective area requirements on the SC

Due to a cost constraint, the initial point design was set at the highest possible mirror to fit the standard 2624 Ariane 5 LVA (section 7.2). This led to a de-scope of requirement R-SC-110 from the onset of the study, and a mirror with 15 MM rows adding up to $A_{eff\_SC}(1\ keV) \cong 1.37m^2$.

7.1.2 Angular resolution (HEW)

For ATHENA the image quality was specified in terms angular resolution, and characterised with the Half Energy Width (HEW) of the Point Spread Function (PSF) at different energy point sources. Table 7-1 aggregates the angular resolution requirements for the different energy ranges.

Angular resolution requirements		
Req. ID	**STATEMENT**	**Parent ID**
R-SC-160	The SC shall provide, for all observations, an on-boresight angular resolution of 5'' Half Energy Width (HEW), over an energy range of 0.1 - 7keV, at the focal plane of the instrument.	SciRD
G-SC-170	The SC should provide, for all observations, an on-boresight angular resolution of 3'' HEW, over an energy range of 0.1 - 7keV, at the focal plane of the instrument.	SciRD
R-SC-180	The SC shall provide, for all observations, an on-boresight angular resolution of 20'' HEW, over the energy range 7 - 15 keV, at the focal plane of the instrument.	SciRD
R-SC-190	The SC shall provide, for all observations, at 25' off-axis, an angular resolution of 10'' HEW, over the energy range 0.1-7keV, at the focal plane of the instrument.	SciRD

Table 7-5: Angular resolution requirements

The image quality (HEW) includes many contributors, including defocusing, MM internal distortion, as well as the impact of lateral and longitudinal motion of the detector with respect to the target line-of-sight (incl. mainly jitter of both mirror boresight and detector-to-mirror deflection - RPE). A preliminary HEW budget with the allocations for the MM, MA and SC is provided in Table 7-6 (RD[16]).

Mirror Module	Allocation ["]
MM internal	4.3
Mirror Assembly	
Gravity	1
TED	1
moisture release	1
MM alignment	1
MA & telescope tilt	0.5
MA & telescope focus	0.5
SC	
RPE	1
De-focus (gnd to flight)	1
HEW	**5.0**

Table 7-6: Preliminary HEW budget (RMS addition)

7.1.3 Target of Opportunity

One of the main objectives of ATHENA is to be able to perform Target of Opportunity Observations (ToOs) to follow-up transient phenomena of high scientific interest such as Gamma-Ray Bursts and X-ray transient afterglows (RD[10]). This need translated itself into a mission requirement in terms of ToO reaction time. The requirement on ToO reaction time is understood to consider the time starting from receipt of an un-validated ToO-alert by the SGS, until the subsequent commencement of TYPE_1 (Narrow-Field – with X-IFU) observations of the ToO.

ToO requirement		
Req. ID	**STATEMENT**	**Parent ID**
R-MIS-550	The ATHENA Mission shall perform Narrow-Field observations of a GRB-ToO within 4 hours (goal of 2 hours) of the receipt of an external ToO alert for 80% of pursued ToO alerts.	MTB [DDF_1.0]

Table 7-7: ToO requirement

This requirement was derived from the need to obtain 10 suitable GRBs per year with sufficient fluence 4 hours after the trigger, out of a pool of 200 GRBs per year expected from external GRB triggers (12% assumption). Those 200 GRBs per year translates to a Field of Regard (FoR),defined as the fraction of observable sky at any time, of 50% and an efficiency sufficient to get the X-IFU on target in at least 80% of the cases.

At the beginning of the study the requirement had been broken to the tier-1 items in the Product Tree (SGS, OGS, SC, and X-IFU) as shown in Figure 7-6.

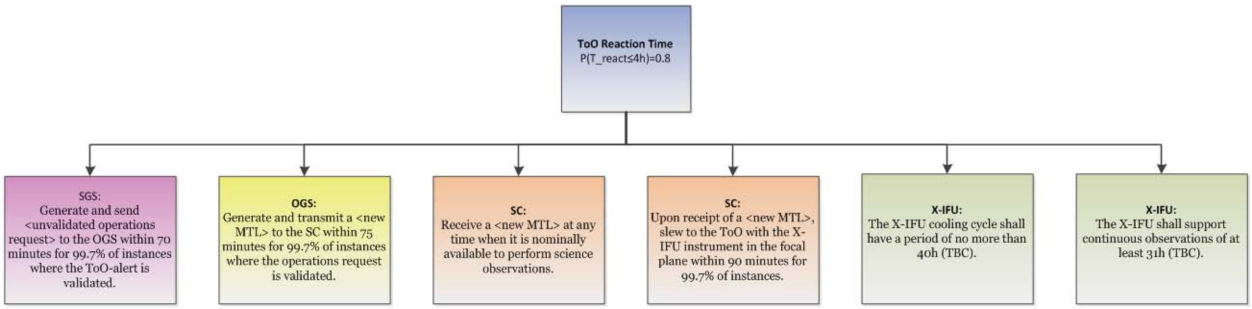

Figure 7-6: ToO reaction time requirement breakdown at the beginning of the study

7.2 System Assumptions and Trade-Offs

In addition to the technical requirements, there were a series of programmatic and budgetary assumptions set at the beginning of the study:

- **ESA only mission**. The mandate for the ATHENA CDF study was to design a mission independently of any international contributions (European technology development is underway in the critical areas such as optics and CC technology). Different possibilities for international collaboration were compiled in separate document using the inputs from the CDF study team. This document was made available to the ASST and provides ideas on possible contributions by JAXA and NASA on elements up to 20% of the CaC limit
- **1Bn€ (2013 EC) CaC limit** to comply with the target cost mandated from management, in the range of a L-class mission
- **SC compliant with the largest standard A5 ECA LVA (2624mm)**. A costing exercise was conducted prior to the CDF study which showed that the previous financial constraint would imply a standard LVA to constrain both the SC mass and cost. This meant that the 2 m^2 requirement on effective area at 1 keV (R-SC-110) could not be met from the onset of the study.

At the beginning of the CDF study a number of design drivers were identified:

(1) Identify and evaluate (through a system level trade-off) different design solutions for an Instrument Switch Mechanism (ISM) to share the focal point between the 2 instruments.

(2) Design a configuration compliant with an Ariane 5 ECA launch to L2 in terms of mass (mass envelope of 6600 kg), fairing accommodation, structural frequency modes, and allowable static moment at the LVA I/F.

(3) Design a configuration ensuring thermal accommodation at the FPM. The power consumption (hence dissipation) of the payloads as proposed was significantly larger than for ATHENA_L1, leading to a major concern that insufficient radiator area would be available at the FPM.

(4) Consolidate the pointing requirements by revisiting the assumptions behind their specification and choosing a design solution that ensures design compatibility (possibly with involving the use of OBM.

(5) Ensure the mechanical accommodation of the MMs by identifying design solutions to reduce the shock environment seen by the MMs during launch.

(6) Establish SGS, OGS architectures, and a SC design compliant with the ToO reaction time requirement.

Drivers	Chapter
1	Systems (Chapter 7.2.1)
2	Configuration (Chapter 8) Static moment (Chapter 23.1)
3	Thermal (Chapter 11) Configuration (Chapter 8)
4	AOGNC (Chapter 14)
5	Optics (Chapter 6)
6	Systems (Chapter 7.2.2)

Table 7-8: Index of the design drivers

The design drivers are approached in the chapters referenced by Table 7-8.

At system level there were 2 main trade-offs:

- The mechanism to share the focal point between the instruments
- The selection of an architecture to respond to a ToO.

7.2.1 Trade-off on ISM

To change the instrument in the focal point two system options were identified in this study:

- MIP (Movable Instrument Platform)
- MMA (Movable Mirror Assembly).

During the course of the study 2 MIP and 3 MMA mechanisms were identified as being possible options for the SC.

The MIP mechanisms need to be able to account for a linear stroke of around 0.75 m. For the MMA this means a change in mirror angle of approximately 3.5°.

The following subsections introduce the different configurations approached during the study. Their specific characteristics, advantages and disadvantages are explained in the sections below.

7.2.1.1 MIP 1-DOF

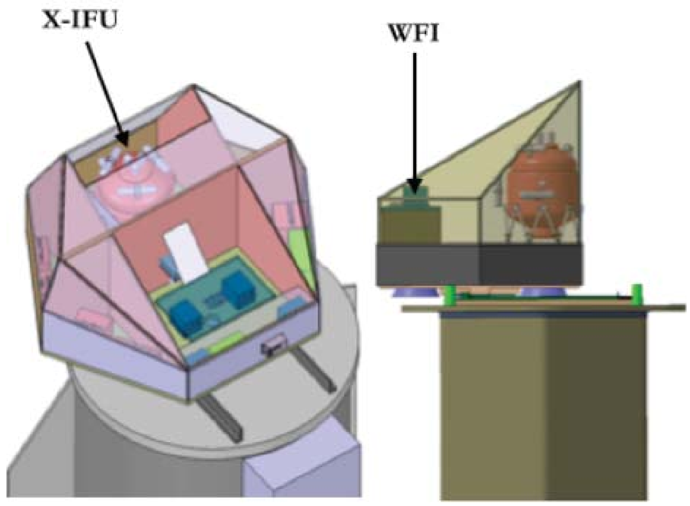

Figure 7-7: Example of a MIP 1 DOF

The MIP 1-DOF is a sliding table which contains the instruments. The examples shown in the above figure are taken from the L2 proposal.

7.2.1.2 MIP 3-DOF

The MIP 3-DoF mechanism provides the 3 translations along orthogonal axes. One translation motion with a range of 750 mm, similar to the 1-DoF MIP, on top of the base stage, fine-adjustment motions of the order of 1 mm and resolution better than 0.05 mm can be accomplished by orthogonal stages.

7.2.1.3 MMA 1-DOF using a hinge driven mechanism

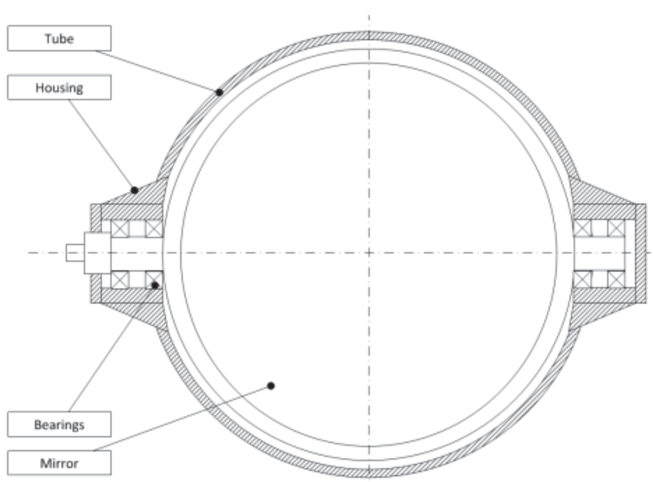

Figure 7-8: MMA 1-DOF using a hinge driven mechanism

In this mechanism the mirror rotation is driven by a motor on the hinge itself.

7.2.1.4 MMA 1-DOF using a hinge and spindle

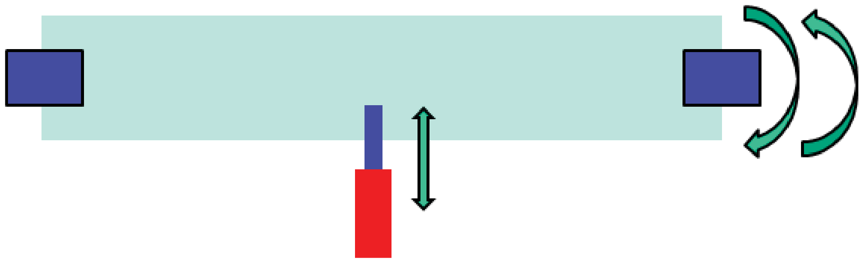

Figure 7-9: MMA 1-DOF using a hinge and spindle to drive the rotation

The rotation in this mechanism is driven using a spindle at the side of the mirror.

7.2.1.5 MMA 6-DOF

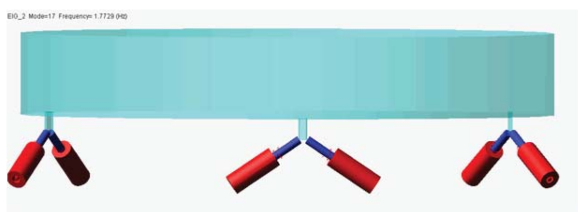

Figure 7-10: MMA 6 DOF hexapod option.

The Hexapod or Steward Platform mechanism is a design solution which allows the motion of the mirror along 6-DoF: tilt around two axes, piston, decentring along two lateral directions, and rotation around the mirror axis. The motion is realised by the axial extension of 6 linear actuators (legs or pods).

Tier 1 Criteria	Tier 1 Weights	Tier 2 Criteria	Tier 2 Weights	MIP 1 DOF	MIP 3 DOF	MMA 1 DOF (Hinge)	MMA 1 DOF (Hinge + Spindle)	MMA 6 DOF (Hexa pod)
Cost	0.15	Mechanism Mass	0.25	2	1	4.5	4.5	3
		AOGNC Mass Indirect (SC)	0.03	3	3	3	3	3
		Structural Mass Indirect (SC)	0.15	2	1	3.5	3.5	5
		Thermal Mass Indirect (SC)	0.2	1.5	1.5	4	4	4
		Power Mass Indirect (SC)	0.02	3	3	3	3	3
		Propulsion Mass	0.1	3	3	3	3	3

Tier 1 Criteria	Tier 1 Weights	Tier 2 Criteria	Tier 2 Weights	MIP 1 DOF	MIP 3 DOF	MMA 1 DOF (Hinge)	MMA 1 DOF (Hinge + Spindle)	MMA 6 DOF (Hexa pod)
		Indirect (SC)						
		AIT Cost	0.2	2	1	4	4	4
		Straylight and Non X-Ray radiation Mass Indirect	0.05	4	5	1.5	1.5	3
Risk	0.15	Heritage	0.33	5	4	2.5	2.5	1
		Failure tolerance	0.33	1	4	2.5	2.5	5
		TRL	0.33	3	3	3	3	3
Aeff	0.35	Effective area at low energies	0.75	4.5	4.5	1.5	1.5	3
		Effective area at high energies	0.25	3	3	3	3	3
HEW	0.2	Telescope focus	0.50	2	4.5	2	2	4.5
		Mirror assembly distortion	0.50	4.5	4.5	2	2	2
ToO Reaction Time	0.05	Instrument switch time	0.5	1.5	1.5	4	4	4
		Slew time	0.5	1.5	1.5	4	4	4
FoV	0.1	Volume Accommodation at FPM	0.50	2	1	4	4	4
		CoG position	0.50	1.5	1.5	4	4	4
			Total	**3.1**	**3.3**	**2.6**	**2.6**	**3.3**

Table 7-9: Results of ISM trade-off

Comments on Table 7-9:

- The Tier-1 criteria came directly from the KPIs of the mission (Figure 7-2)

- Tier-1 weights were agreed between Study Manager, Study Scientist and Science Team (particularly the X-IFU team)
- Tier-2 weights for cost were agreed with cost specialists
- Tier-2 weights for risk were agreed with risk specialists
- After the iteration in the session, the criteria in red were found irrelevant for this trade-off.

The following subsections detail the ranking of the ISM options for the different criteria.

7.2.1.6 Cost

7.2.1.6.1 Mechanism mass

- The two MMA 1 DOF options (with the hinge and hinge + spindle) should have more or less the same mass, the hinge should have a similar size in both options and the mass of the rotational actuator should be similar to the spindle. The lower number of components for these options made them the ones with the lowest expected mass.
- The MMA 6 DOF (hexapod) solution requires more components than the other MMA options and should therefore be heavier than those.
- The MIP options should generally be more massive, requiring more components and higher strokes, which should therefore lead to a higher mass. The added complexity for the MIP 3 DOF makes it the one with the highest expected mass.

Assumptions: We assume we have off-loading devices in the design of the mechanism. The mass of the mechanism includes the off-loading devices.

7.2.1.6.2 Indirect impact on AOGNC and Propulsion masses

- Switching from a MMA to a MIP solution will increase the MOI, which may require larger RWs to slew the SC (for repointing or pursuing ToOs).
- All the options scored the same in these criteria, which make them irrelevant in the trade-off.

7.2.1.6.3 Indirect impact on Structures mass

- Increasing the DOFs of the mechanism will allow correction for structural deformations, which will decrease engineering effort for the FMS and other structural components. For this reason the MMA 6 DOF (hexapod) solution, scores the best in this criteria.
- In addition to this, using the MMA 6 DOF option will probably not require an additional interface ring at the Mirror Assembly to pass the stress loads (which was deemed necessary for the MMA 1 DOF options).
- The MIP options should require considerable additional mass to support the expected sturdier mechanism, which is also at the top of the launch stack, therefore requiring more structural mass in the FMS. This factor is aggravated for the MIP 3 DOF, making it the worst option as far as this criteria is concerned.

7.2.1.6.4 Indirect impact on Thermal mass

- The MIP options require a more complex heat transfer solution to transport PL heat across the plane of the mechanism (heat pipes with flexible lines), which will ultimately lead to a higher mass and cost.

7.2.1.6.5 Indirect impact on Power mass

- The additional mass of longer harnesses to enable the longer translation of the MIP options was considered irrelevant.

All the options scored the same in these criteria, which make them irrelevant in the trade-off.

7.2.1.6.6 AIT cost

- The asymmetric configuration of the MIP solutions, their higher volume, and overall complexity should make them more difficult to integrate and test. Therefore, the MIP options score worse than the MMA options in this criterion.

7.2.1.6.7 Indirect impact on Straylight and Non X-Ray radiation mass

- The MMA options should require two separate sets of magnetics diverters, one for each instrument.
- The baseline disk configuration for the straylight baffles will require an additional hole at least in the baffle closer to the detector plane in the MMA options. This configuration is less optimal than in the MIP options. This fact will probably require more shielding material as compensation.
- The above reasons make the MIP options better in this criterion.
- Having more DOFs will allow placing the detectors exactly in the optimal point for which the baffle was designed, this is the reason why the options with more DOFs score (relatively) better than the ones with only 1 DOF.

7.2.1.7 Risk

7.2.1.7.1 Heritage

- The translational mechanism of both MIP options has some heritage from Chandra (even though for completely different mass ranges). This is the reason they score better than the MMA options.
- The expected added complexity of the MMA 6 DOF (hexapod) vs. the MMA 1 DOF options, make it the worst w.r.t this criteria.

7.2.1.7.2 Failure tolerance

Assumption: This criterion refers to not only operation with no failures during the lifetime, but also operation with an acceptable degradation.

- In a degraded scenario, higher DOF gives you the ability to compensate for failures and still maintain some scientific return. In the 1 DOF options, if the mechanism fails (for instance between the 2 FoV of the different instruments) there is a total loss for the mission.

- A hexapod design seems to be potentially more reliable because, even though it should have more components, it is free of single point failures.

7.2.1.7.3 TRL

- All low level TRLs, because there are no similar mechanisms in the same range of masses (higher than 1000 kg).

All the options scored the same in these criteria, which make them irrelevant in the trade-off.

7.2.1.8 Aeff

7.2.1.8.1 Effective area at low energies

- The MMA 1 DOF options could require an additional structural ring which will require removing at least one ring of the Mirror Assembly, which makes these options the worse in this criteria (note that this was avoided in the eventual design).
- The MMA 6 DOF (hexapod) solution, should not require the structural ring, but could require the removal of some Mirror Modules at the interface of the different actuators.
- The MIP options are optimal in terms of effective area because Mirror Assembly geometric area would be optimal.

Assumptions: The loss of effective area due to vignetting effects in the MMA options are not considered for this criterion because we assume this will be passed as a requirement for the accuracy of the mechanism (+ OBM). All options shall therefore be designed to minimize this effect to a certain threshold (currently set at 1% A_eff loss).

7.2.1.8.2 Effective area at high energies

This criterion was considered a second order effect on potential focal length reduction in the MIP options. For consistency reasons, it was discarded from the trade-off.

7.2.1.9 HEW

7.2.1.9.1 Telescope focus

- The options with higher DOFs allow you to change the position of the focal point in the z direction which should allow compensation for any length changes in the FMS and other structural elements throughout the SC lifetime.
- Enabling focusing improves HEW, this is the reason why options with higher DOFs score better than the ones with only 1 DOF in this particular criteria.

7.2.1.9.2 Mirror assembly distortion

- Placing the mechanism in the mirror could create additional stresses in the mirror assembly which can lead to distortions over the lifetime (the number of expected cycles is in the order of 5000). These distortions will penalise the angular resolution.

- For the above reason, the MMA options score worse than the MIP options in this criterion.

7.2.1.10 ToO reaction time

7.2.1.10.1 Instrument switch time

- If a response to a ToO alert requires switching from the WFI to the X-IFU, the time to switch instrument should be subtracted from the nominally available 4 hours to pursue the ToO.
- Since the MIP option mechanisms have higher strokes, it is expected that they require more time to switch instruments, which make them the worse options w.r.t. this criterion.

7.2.1.10.2 Slew time

- The asymmetric configuration of the MIP options, along with its expected higher masses for the mechanism, shall increase the MOI of the SC.
- For the same configuration of thrusters and RWs, a higher MOI will lead to higher slew times, this is the reason why the MIP options score worse in this criteria.

7.2.1.11 FoV

This measures the impact that the mechanism choice can have in restraining the size of the instruments.

7.2.1.11.1 Volume accommodation at the FPM

- Placing the mechanism at the FPM will reduce the available volume for the instruments, which can lead to a reduction of the size of the instruments. This is the reason why the MIP options score worse than the MMA options in this criterion.

7.2.1.11.2 CoG position

- Increasing the mass at the FPM will move the CoG upwards in the FMS which might induce a constraint in the mass of the instruments to comply with the static moment requirement of the launcher. This is the reason why the MMA options score better than the MIP options in this criterion.

7.2.2 ToO-Response Analysis

The second trade-off at system level was the choice of baseline architecture to respond to ToO observation requests.

To accomplish this, a model was developed (RD[9]) evaluating the overall compliance of the ATHENA mission to the GRB ToO-response requirement (R-MIS-550) , namely that the Cumulative Distribution Function of the system response times should exhibit the property:

$$P(T_{react} \leq 4 \text{ hours}) = 0.8$$

This requirement corresponds to a FoR of 50%; in the case that a 60% FoR can be achieved for the SC design (is this confirmed as the baseline), the requirement is reduced to 0.67.

7.2.2.1 Analysis Description

A Functional Flow Block Diagram (FFBD) was defined which specifies the logical sequence and dependencies of sub-functions needed to perform the overall function of responding to a ToO-alert. For each function defined in the FFBD, there is a Probability Density Function (PDF) or Probability Mass Function (PMF), which defines the function duration. A Monte-Carlo model, for each of a user-defined number of iterations, generates a random ToO-alert on a random day during the mission operational phase. For each run the model then takes a sample from the PDF/PMF for each function, and constructs a timeline of events for that iteration. The model then returns a Cumulative Distribution Function (CDF) for the intermediate and total durations. This allows compliance with the ToO reaction-time requirement, which is expressed in CDF form, to be assessed.

7.2.2.1.1 Functional Flow Specification

The response architecture is defined using an enhanced Functional Flow Block Diagram (FFBD), specifying the sequential flow of functions within the ToO-response function, as well as the flow of information between them. The FFBD is shown in Figure 7-12; *Notes:*

Immediately upon receipt of the <unvalidated ToO-alert>, i.e. after SGS_1, a pre-warning is sent to:

- *The on-call scientist responsible for SGS_3 (in practise because SGS_2 is of very short duration, the benefit of this is marginal, but does help to improve the response-time)*
- *The ECC at ESOC is responsible for the scheduling of the uplink*
- *The on-call engineer at ESOC responsible for validating the <unvalidated operations request> (OGS_2) and generating the new MTL (OGS_4).*

The FFBD prescribes that the SC switches the focal plane (if necessary) prior to slewing to the ToO, rather than performing these steps in parallel (this avoids multiple control-loops [1xISM, 1xAOCS] operating simultaneously).

7.2.2.2 Function Duration Specification

The duration rules governing each of the functions shown in the FFBD are explicitly prescribed in (RD[9]). They were defined taking into account input from ESOC, ESAC, PL and SC specialists. A summary of the duration specifications is given in the following table.

Function	Prescription (all durations/times are specified in minutes)
SGS	
ToO_1 (this is the generation of the random ToO event for each iteration).	ToO alert is received at an isotropically random day of the week and time of day.
Function: Receive <unvalidated ToO-request> Designation: SGS_1	1
Function: Validate <unvalidated ToO-request> Designation: SGS_2	5
Function: Generate <unvalidated operations-request> Designation: SGS_3	5
Function: Send <unvalidated operations request> Designation: SGS_4	1
Function: Ready On-call scientist Designation: SGS_5	Up to 2h15m. The on-call scientist is available outside working hours via remote connection. The duration of this function takes into account the time of day, taking into account commuting times, time taken to establish a remote connection to ESAC etc.
OGS	
Function: Receive <unvalidated operations request> Designation: OGS_1	1
Function: Ready on-call engineer Designation: OGS_6	Up to 2h. The on-call engineer is available outside of working hours, but has to return to work to perform their functions. The duration of this function takes into account the time of day, taking into account commuting times, and also the possibility of SPACONs from other missions being able to cover for the on-call engineer outside of normal working hours.
Function: Validate <unvalidated operations request> Designation: OGS_2	5
Function: Schedule GS Designation: OGS_3	30
Function: Generate <new MTL> Designation: OGS_4	60
Function: Send <new MTL> Designation: OGS_5	15 minimum, up to several hours. A 15 minute duration for the uplink sequence is assumed. The baseline Ground Stations are New Norcia, Malargue and Cebreros. The duration until the next station AoS is calculated from an AoS/LoS algorithm supplied by ESOC, which operates on a sample day from the operational phase (NoP/EoP) of a reference mission trajectory, also supplied by ESOC. The simulation also takes into account the possibility that the uplink stations are being used for LEOP campaigns on other missions.
SC	
Function: Receive <new MTL> Designation: SC_1	1
Function: Update <SC MTL> Designation: SC_2	1

Function	Prescription (all durations/times are specified in minutes)
Function: Swap Focal Plane Designation: SC_3	40% chance of 10. There is a 40% chance that the instruments need to be swapped over, based on the Mock Observing Plan.
Function: Slew SC Designation: SC_4	0 to 45. The ToOs are isotropically distributed in the sky, so the required slew angle is a uniform random angle between 0 and 180 degrees. The SC is assumed to be able to slew & settle at an effective rate of 4 degrees/s (this is compatible with the AOCS design).
Function: Regenerate CC Designation: SC_5	0 to 8 hours. The X-IFU Cooling Chain has a cooling cycle of 32h ON and 8h OFF. Accordingly there is a 20% chance that the X-IFU is regenerating (CC=OFF).
Function: Observe ToO Designation: SC_6	No duration (objective reached).

Table 7-10: ToO-Response function duration summary

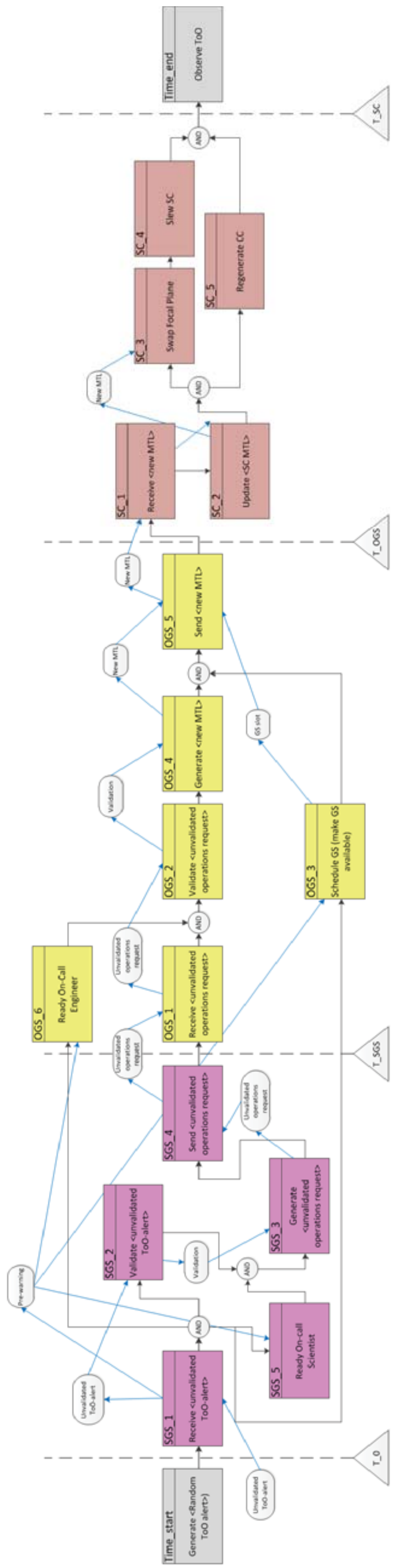

Figure 7-11: ToO-alert FFBD

7.2.2.3 Results & Discussion

Note: All results presented here are for Monte-Carlo simulations with n=5000 runs.

7.2.2.3.1 Baseline

Figure 7-13, Figure 7-14, Figure 7-15 and Figure 7-16 show the SGS, OGS, SC and Total duration CDFs corresponding to the baseline FFBD and function duration prescription. The main features of the CDFs are indicated in the figures. From Figure 7-16 it can be seen that the total CDF exhibits the property $P(T_{react} \leq 4\,hours) = 0.70$, and so modestly exceeds the requirement associated with a 60% FoR (but not for 50%). We can also note that the fastest possible response time is 95 minutes (starting point of the CDF curve in Figure 7-16), representing the case where:

- SGS/OGS functions occur during ESAC/ESOC working-hours
- an uplink GS is immediately available and visible to the SC
- The X-IFU instrument is already in the focal plane and it's CC is operating
- ~No slew manoeuvre is required (the ToO is very close to the nominal target).

Conversely response-times can extend to well beyond the 4 hours required, corresponding to less-favourable cases where commuting times, coverage gaps, large slew angles and CC-regeneration times all conspire together.

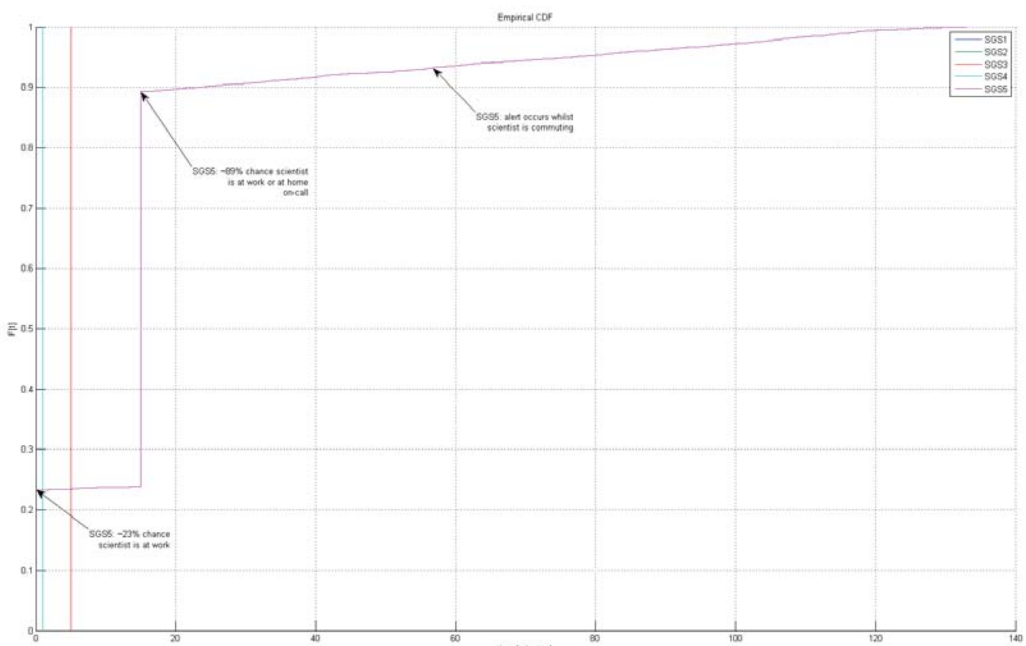

Figure 7-12: SGS function duration CDFs

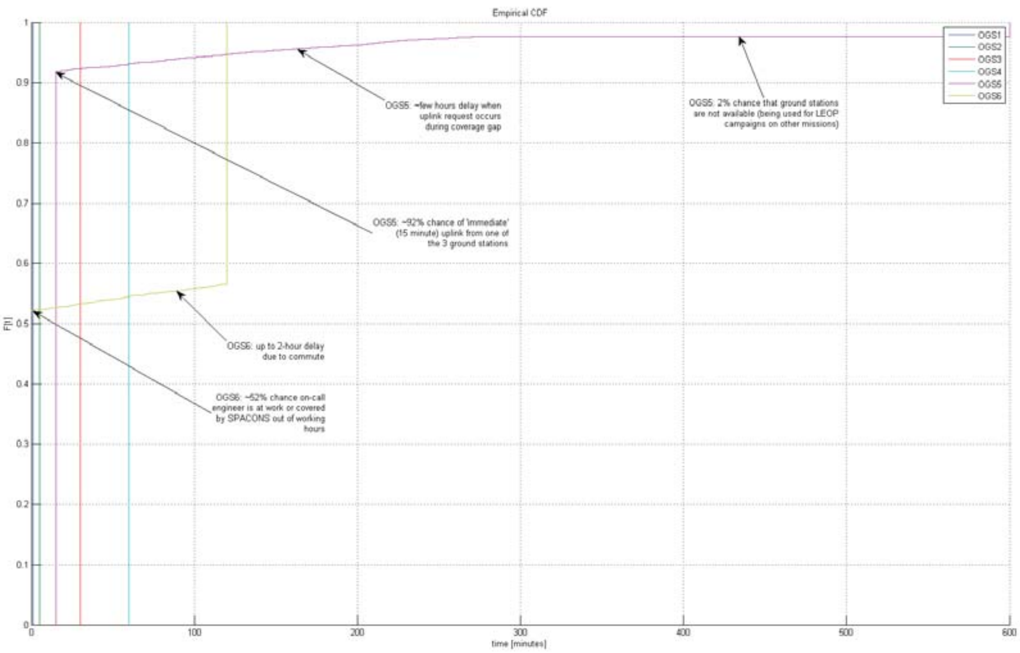

Figure 7-13: OGS function duration CDFs

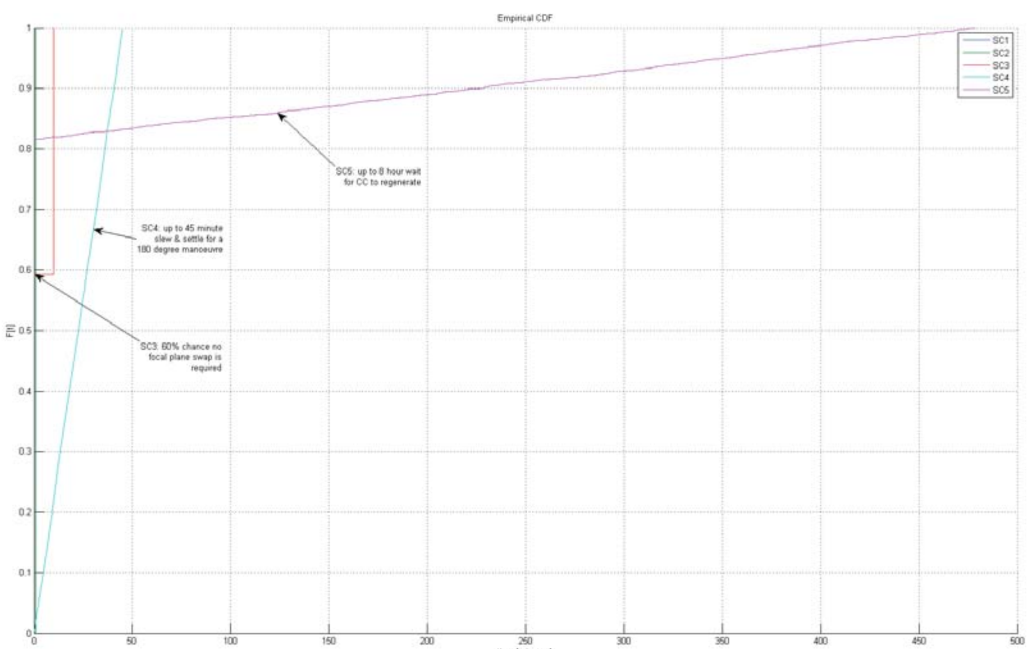

Figure 7-14: SC function duration CDFs

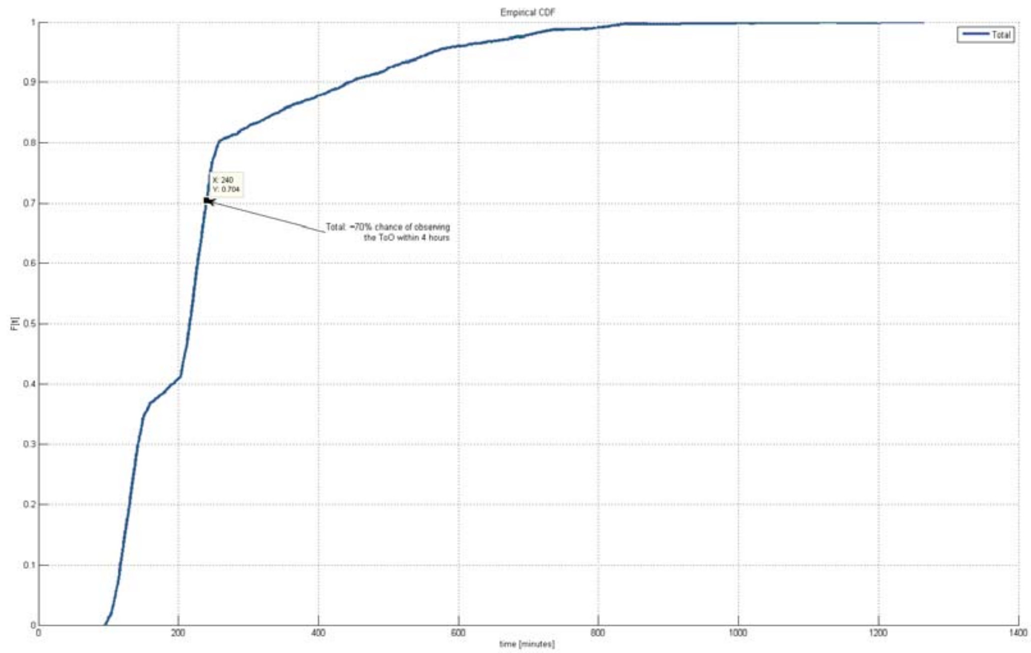

Figure 7-15: Total function duration CDF

7.2.2.3.2 Alternatives

A few alternative simulations are presented, modifying some of the key parameters from the baseline prescription, to evaluate their effect. This is not an exhaustive analysis, but is intended to provide some initial insight into the performance of the system and possibilities for alternative implementations.

The following cases are presented:

- Figure 7-17: The total duration CDF, as the baseline but with Cebreros GS removed
- Figure 7-18: The total duration CDF, as the baseline but with Malargue GS removed
- Figure 7-19: The total duration CDF, as the baseline but with Cebreros GS removed and the commuting times for functions SGS_5 & OGS_6 reduced to 90 minutes
- Figure 7-20: The OGS function CDFs, corresponding to Figure 7-19.

The following main observations can be made:

Under the assumption that other SGS and OGS functions are suitably constrained in duration, the main determinants of the reaction-time are (i) OGS_6 (Ready on-call engineer), OGS_5 (send <new MTL>) and SC_3 (configure payload; specifically the CC cooling-cycle.)

In the current prescription, where OGS_2 requires that an on-call engineer travels into work during non-working hours for 38% of cases, this travel time (commute, currently 120 minutes) is critically important to the overall performance. Something as simple as ensuring the on-call engineer lives close to ESOC will have a big impact on the overall performance of the system.

Quasi-continuous (~24h) uplink coverage for OGS_5 is mandatory to meet the requirement, but this does not necessarily need to be provided by the 3 GS of the baseline. We can see from the OGS_5 CDF in Figure 7-20 that without Cebreros, NN and Malargue GS still achieve a guaranteed coverage for ~84% of instances; this is only a modest reduction from the guaranteed coverage of ~92% of instances achieved by the baseline (see OGS_5 CDF in Figure 7-14). This is because Cebreros at -4.4° longitude is more-or-less in the middle of NN (116.2°) and Malargue (-69.4°), which are nicely spaced (~174° apart, i.e. nearly optimal in longitude for a 2 GS solution). Accordingly, despite Cebreros being a Northern hemisphere GS (latitude=+40.5°), unlike both NN (-31.0°) and Malargue (-35.8°), and therefore having better coverage when the SC is at high +ve declinations, it does not provide much benefit.

Overall, the removal of Cebreros results in a very modest reduction in overall performance from the baseline ~70% (Figure 7-16) to ~67% (Figure 7-17). For comparison, Figure 7-18 shows that the removal of Malargue GS is more serious, reducing the guaranteed uplink to ~60%.

Furthermore, if out-of-working hour dependencies with durations comparable to the requirement are introduced in the ESAC/ESOC functions (as is the case in the baseline, in particular for ESOC where the on-call engineer must travel into work to perform their function), then employing a GS at Cebreros brings little benefit because it will, to a large extent, not be able to see the SC during ESAC/ESOC working hours (Cebreros is close to ESAC/ESOC in longitude, and so cannot see the SC at L2 during ESAC/ESOC daytime) and hence cannot contribute to achieving fast reaction times under 4 hours.

The absence of Cebreros can be more than compensated by a modest shortening of the commuting-time. The initial levelling in the Total CDF at ~200 minutes in Figure 7-16 is driven by the commuting times, mainly at ESOC, and shortening the commuting time will have the significant impact of shifting the following steep section of distribution to the left, improving the performance significantly. This effect can be seen in Figure 7-19, where the commuting time has been modestly reduced to 90 minutes, and Cebreros removed, and the overall performance is actually better than the baseline at ~76%.

Although not presented here, clearly any improvement in other parameters (e.g. reducing the regeneration cycle of the CC, or increasing the agility of the SC) will bring a significant improvement to the performance statistics. In particular, shortening the CC regeneration cycle will improve the amount of time available for subsequent observation of the ToO. For the current baseline the X-IFU will have a >90% chance of being able to observe a particular ToO for more than 3 hours. Any constraints on the minimum observing time need to be discussed with the scientists, and captured in requirements if necessary, as this may affect the statistics very significantly.

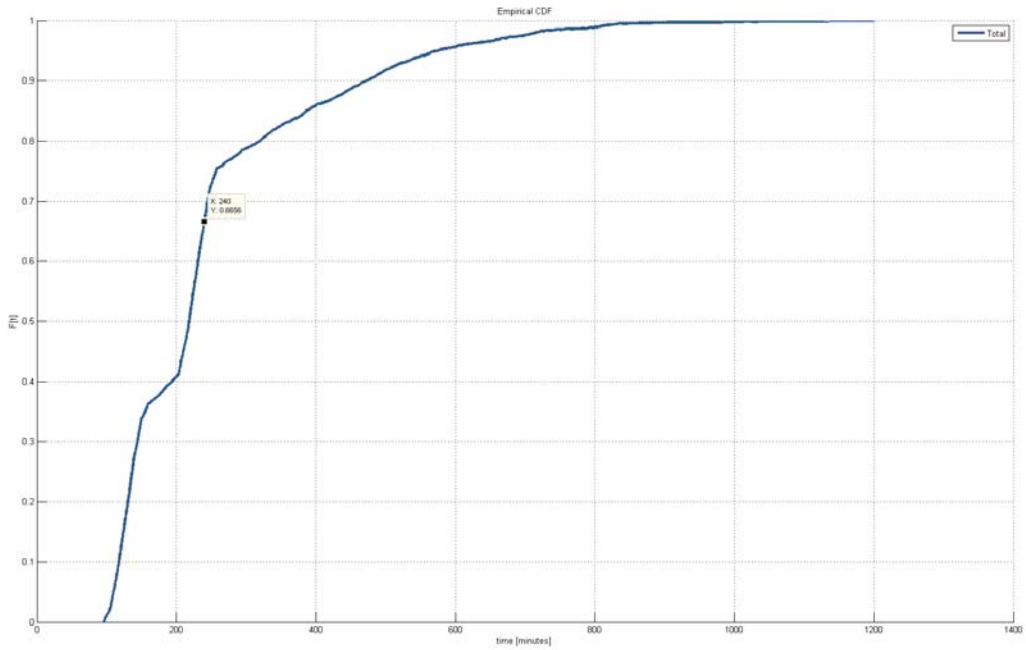

Figure 7-16: Total function duration CDF, as baseline but with Cebreros removed

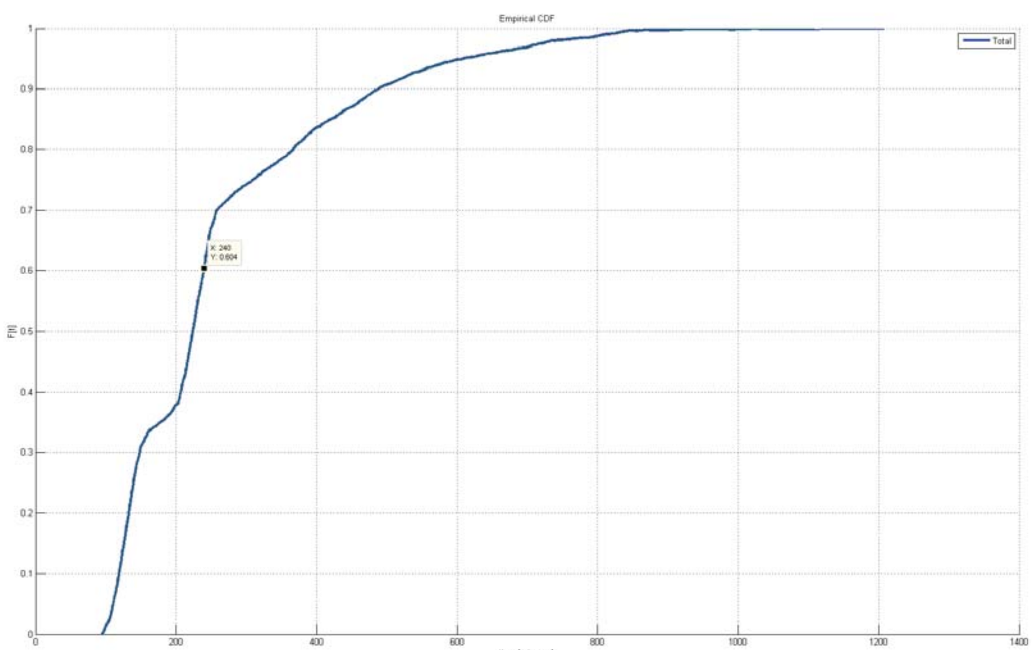

Figure 7-17: Total function duration CDF, as baseline but with Malargue removed

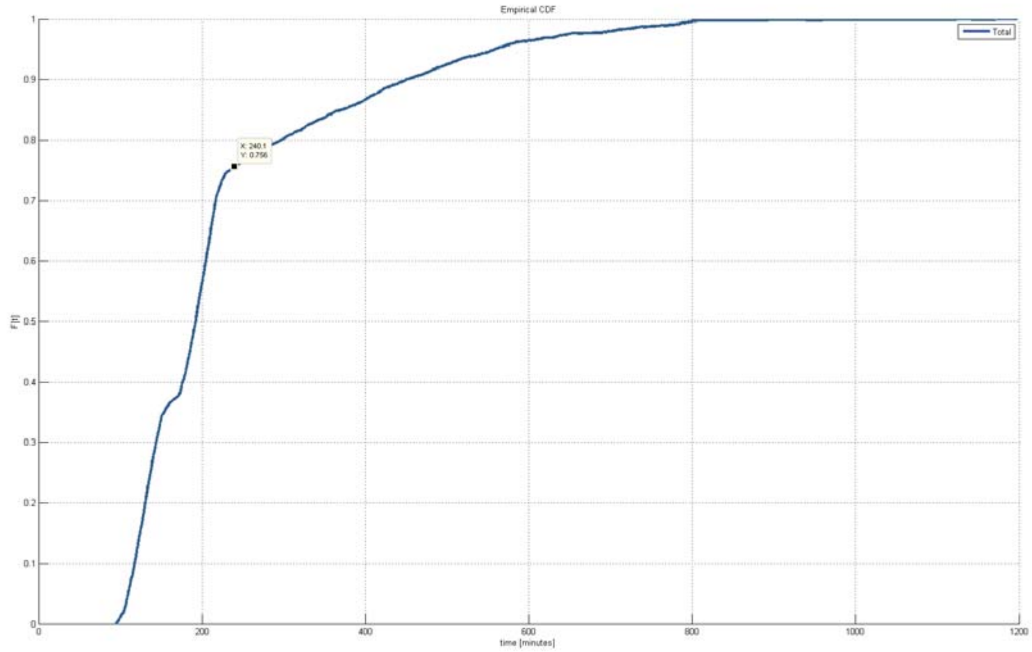

Figure 7-18: Total function duration CDF, as baseline but with Cebreros removed and C=90 minutes for SGS5 & OGS6 (baseline C=120)

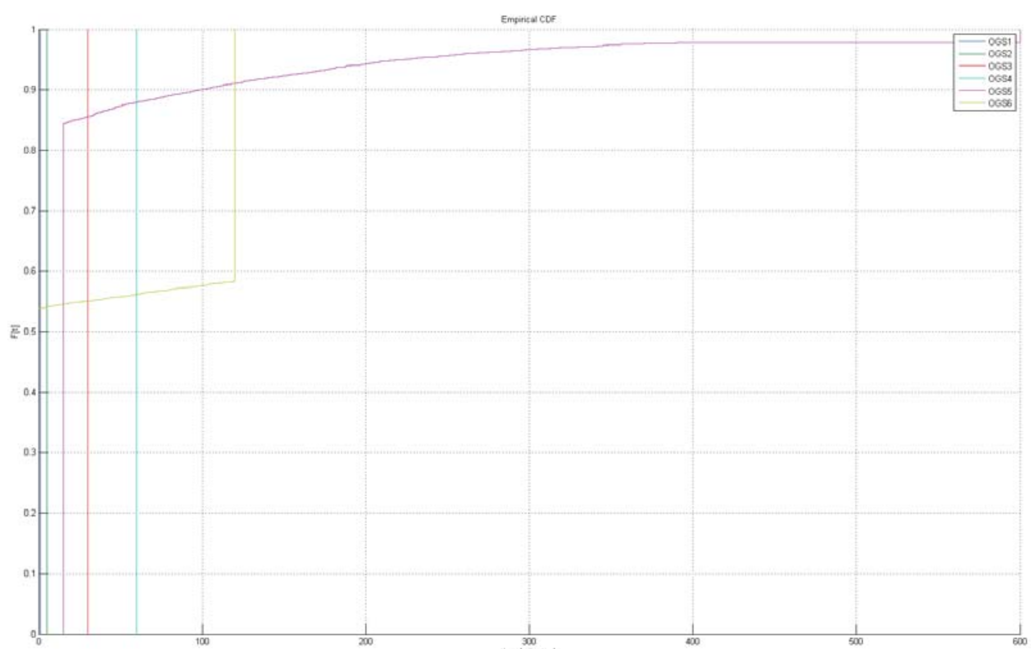

Figure 7-19: OGS function duration CDFS, corresponding to Figure 7-19

7.2.2.4 Conclusions

The form of the FFBD and the function duration specifications for the baseline have been consolidated prior to and during the CDF study, and have resulted in the architecture and results presented. The system exhibits the property:

$$P(T_{react} \leq 4\text{ hours}) = 0.70$$

Therefore modestly exceeding the requirement of:

$$P(T_{react} \leq 4\text{ hours}) = 0.67$$

Which is corresponding to a baseline FoR of 60%, but does not meet the requirement corresponding to a FoR of 50%. Should the Phase A SC designs from the industrial Primes have difficulty in achieving a 60% FoR, then significant improvements may be needed.

The main conclusion at the moment is that the baseline uplink GS at Cebreros provides marginal benefit, and depending on the cost to the ATHENA mission of using it (up to the estimated ~4M€ development cost, plus operations) could perhaps be dropped from the baseline, in favour of more 'value for money' improvements, such as reducing commuting times.

Note: the model prescribed in this report can only be considered as a starting point, for subsequent refinement during Phase A, on the basis of inputs from across the ATHENA mission.

7.3 System Baseline Design

7.3.1 Overview

ATHENA Mission	
Mass (incl. Margin)	Dry mass: 5477 kg
	Propellant mass: 530 kg
	Adapter mass: 125 kg
	Wet mass: 6133 kg
Launch Date	2028
Lifetime	5 +5 (extended operations) years
Orbit	Large Halo around L2 (No Eclipse)
	Direct Insertion
Launcher	Ariane 5 ECA (2624 LVA)

Table 7-11: Mission baseline design

ATHENA Spacecraft			
Mass (incl. Margin)	Dry mass: 5477 kg		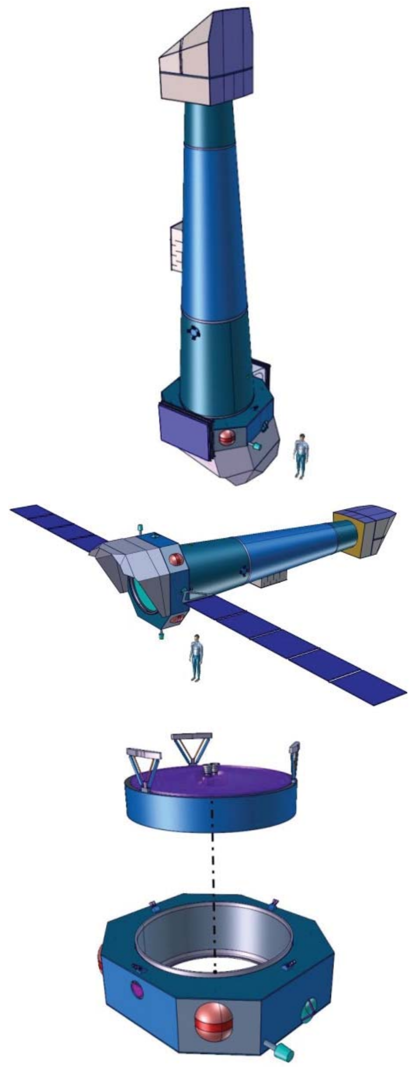
Dimensions	Height: 15 m Mirror diameter: 2570 mm Mirror effective area (1keV): 1.51 m^2 2 mm rib spacing		
System	FoR: 60 % Pitch: ±34.5°		
AOGNC	Sensors	5 Star trackers	
		2 Gyros	
		3 Sun sensors	
		On-board Metrology System	
	RCS: 22 x 1N thrusters for station keeping and fast target acquisition		
	4 x 22N thrusters for transfer manoeuvres		
	3 axis stabilized		
Thermal	Mirror heaters (2,5 kW installed power, 20 ±1 °C)		
	MLI around telescope tube		
	Instrument radiators fitted on FPM		
	Camera head instrument thermal link accomplished by heat pipes		
Mechanisms	Moveable mirror using a hexapod		
	Mirror Cover		
	Venting mechanism at FMS		
	Sun shield		
Communications	1 High gain antenna		
	2 Low gain antennas		
	x-band system		
Data handling	512 Gbit on board storage for science data		
	8 Gbit on board storage for HK data		
Structure	CFRP structure		
	Telescope with 5 stray light baffles		
Propulsion	Propellant: Hydrazine		
	4 tanks: 530 kg propellant		
Power	Fixed deployable solar array		
	4.5 kW maximum consumed power		
	Maximum time duration to survive on batteries: 2.4 h		
Instruments	X-IFU		
	WFI		

Table 7-12: Spacecraft baseline design

7.3.2 Model Decomposition

The ATHENA product tree has been decomposed in the OCDT in the 5 following first tier products:

- FPM, containing the instruments, electronic boxes, cooling chains and radiators (1243 kg)
- MAM, containing the mirror, mirror structure, mirror heaters and interface from the ISM to the FMS (1158 kg)
- FMS, the telescope tube including the baffles/diverters and the venting mechanism (580 kg)
- ISM, the MMA 6-DOF hexapod (42.6 kg)
- SVM, containing the other equipment to support the main function of the SC (1539 kg).

7.3.3 System Modes

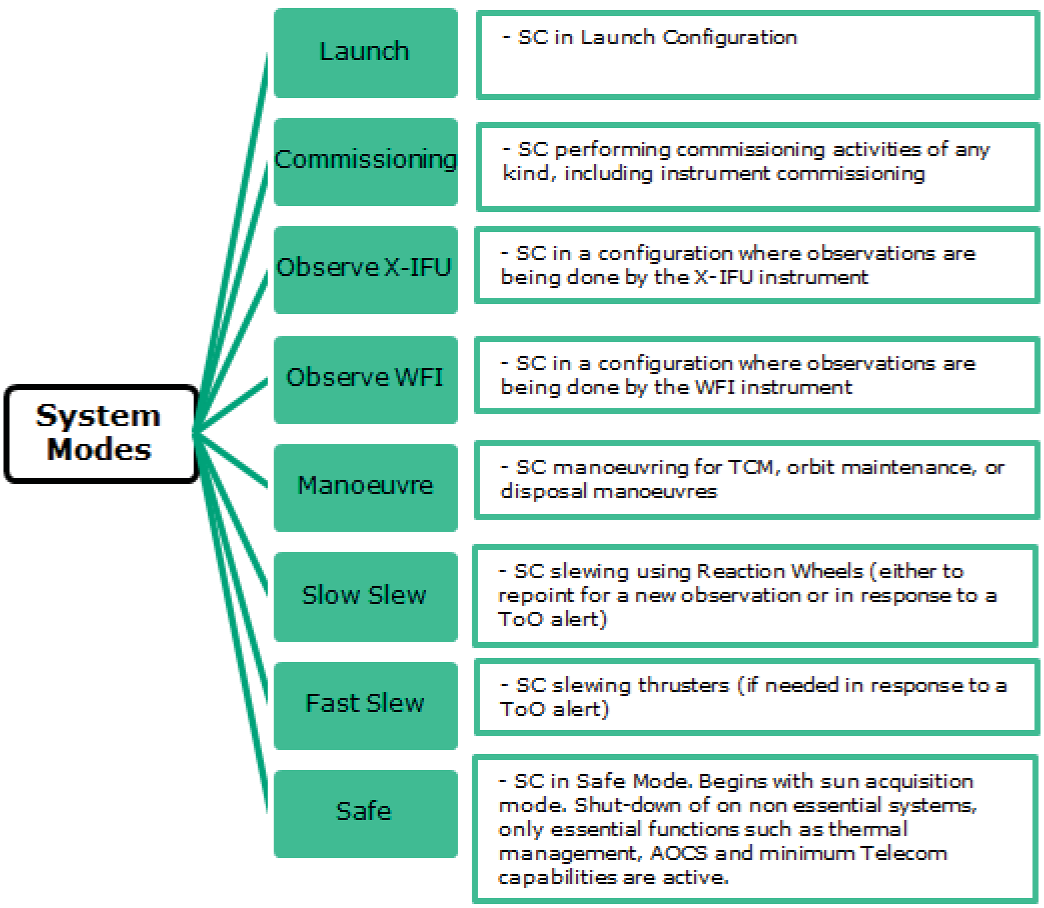

Table 7-13: ATHENA spacecraft system modes used in the scope of the CDF

7.3.4 Delta-V Budget

Manoeuvre	Delta V [m/s]	Delta V Margin [%]	Delta V with margin [m/s]
Perigee Velocity Correction	12.70	5.00	13.34
Trajectory Correction Manoeuvre 1	36.30	5.00	38.12
Trajectory Correction Manoeuvre 2	2.80	100.00	5.60
Trajectory Correction Manoeuvre 3	2.80	100.00	5.60
Nominal Operations Phase Station Keeping	6.51	100.00	13.02
Extended Operations Phase Station Keeping	6.51	100.00	13.02
Disposal	10.00	5.00	10.50
AOCS manoeuvres	28.00	100.00	56.00
		Total DeltaV	66.50

Table 7-14: ATHENA mission delta V budget

7.3.5 Mass Budget

Table 7-12 summarises the mass budget for the ATHENA subsystems

Subsystem	Mass (kg)	Mass margin (%)	Mass margin (kg)	Mass + margin (kg)
AOGNC	59.00	6.67	3.93	62.93
COM	19.80	17.12	3.39	23.19
CPROP	83.34	4.40	3.67	87.01
DH	38.00	10.00	3.80	41.80
GSO	0.00	0.00	0.00	0.00
INS	718.30	21.26	152.70	871.00
MEC	288.02	16.18	46.60	334.62
MIS	0.00	0.00	0.00	0.00
OPT	371.19	19.40	72.00	443.19
PWR	253.00	20.00	50.60	303.60
STR	1549.30	20.00	309.86	1859.16
SYE	310.41	0.00	0.00	310.41
TC	189.72	20.00	37.94	227.66
Totals	**3880.07**	17.64	684.49	**4564.56**
			System Margin	20.00 %
			Dry Mass incl. system margin	**5477.47**
			Adapter Mass	125.00
			Dry Mass + Adapter	5602.47
			Propellant	**520.00**
			Propellant mass margin	10.40
			Total Wet mass	**6132.87**

Table 7-15: ATHENA SC mass budget aggregated per subsystem

7.3.6 List of Equipment

	#	Mass (kg)	Mass margin (%)	Mass margin (kg)	Mass + margin (kg)
AOGNC		**59.00**	**6.67**	**3.93**	**62.93**
GYRO_Sireus	2	0.80	10.00	0.08	0.88
int_metrology_transmitt_elec	2	1.38	20.00	0.28	1.66
int_metrology_transmitt	2	1.38	20.00	0.28	1.66
RW_RDR68_3	4	7.60	5.00	0.38	7.98
RW_WDE8_45	4	1.25	5.00	0.06	1.31
STR_HydraEU	4	1.85	5.00	0.09	1.94
STR_HydraOH	5	1.37	5.00	0.07	1.44
SUN_MoogBrad_CSS	3	0.22	5.00	0.01	0.23
COM		**19.80**	**17.12**	**3.39**	**23.19**
EPC	2	1.40	10.00	0.14	1.54
HGA_ATHL	1	3.00	20.00	0.60	3.6
LGA	2	0.30	5.00	0.02	0.32
RFDU	1	5.00	20.00	1.00	6
TRASP_Tx_MOD_Rx_DED	2	3.20	20.00	0.64	3.84
TWT	2	1.00	10.00	0.10	1.1
CPROP		**83.34**	**4.40**	**3.67**	**87.01**
Feed_Line	1	10.00	0.00	0.00	10
Fill_Dr_Val	7	0.07	5.00	0.00	0.07
Latch_Valve	2	0.55	5.00	0.03	0.58
Press_Transd	2	0.22	5.00	0.01	0.23
Prop_Filter	1	0.77	5.00	0.04	0.81
Prop_Tank	4	15.50	5.00	0.78	16.28
Thr_Pair_1N	12	0.58	5.00	0.03	0.61
Thr_Pair_22N	2	0.79	5.00	0.04	0.83
DH		**38.00**	**10.00**	**3.80**	**41.8**
CDMU	1	11.00	10.00	1.10	12.1
PDHU	1	15.00	10.00	1.50	16.5
RIU	1	6.00	10.00	0.60	6.6
RTU	1	6.00	10.00	0.60	6.6
INS		**718.30**	**21.26**	**152.70**	**871**
WFI	1	240.00	20.00	48.00	288
XIFU	1	478.30	21.89	104.70	583
MEC		**288.02**	**16.18**	**46.60**	**334.62**
ADPM	1	5.00	18.00	0.90	5.9
Hexapod	1	36.00	18.33	6.60	42.6
Mirror_Cover	1	137.00	20.00	27.40	164.4
SADS	1	21.80	10.00	2.18	23.98
Sun_Shield	1	72.00	10.97	7.90	79.9

	#	Mass (kg)	Mass margin (%)	Mass margin (kg)	Mass + margin (kg)
Venting_Mech	1	16.22	10.00	1.62	17.84
OPT		**371.19**	**19.40**	**72.00**	**443.19**
MM_Ring01	1	16.65	0.00	0.00	16.65
MM_Ring02	1	17.42	0.00	0.00	17.42
MM_Ring03	1	18.20	0.00	0.00	18.2
MM_Ring04	1	18.83	0.00	0.00	18.83
MM_Ring05	1	18.29	0.00	0.00	18.29
MM_Ring06	1	18.93	0.00	0.00	18.93
MM_Ring07	1	19.53	0.00	0.00	19.53
MM_Ring08	1	19.76	0.00	0.00	19.76
MM_Ring09	1	20.47	0.00	0.00	20.47
MM_Ring10	1	20.64	0.00	0.00	20.64
MM_Ring11	1	21.32	0.00	0.00	21.32
MM_Ring12	1	21.50	0.00	0.00	21.5
MM_Ring13	1	22.22	0.00	0.00	22.22
MM_Ring14	1	22.35	0.00	0.00	22.35
MM_Ring15	1	23.07	0.00	0.00	23.07
Stry_Baffles_Div	1	72.00	100.00	72.00	144
PWR		**253.00**	**20.00**	**50.60**	**303.6**
Bat18650HC	2	37.00	20.00	7.40	44.4
PCDU	1	25.00	20.00	5.00	30
SA	2	77.00	20.00	15.40	92.4
STR		**1549.30**	**20.00**	**309.86**	**1859.16**
FMS_Str	1	468.50	20.00	93.70	562.2
FPM_Str	1	240.00	20.00	48.00	288
MirStr	1	650.00	20.00	130.00	780
SVM_Str	1	190.80	20.00	38.16	228.96
SYE		**310.41**	**0.00**	**0.00**	**310.31**
Har	1	310.41	0.00	0.00	310.31
TC		**189.72**	**20.00**	**37.94**	**227.66**
MAM_Heat	1	65.80	20.00	13.16	78.96
MLI_Tele	1	39.30	20.00	7.86	47.16
SVM_TCS	1	14.40	20.00	2.88	17.28
TheBaf	1	0.00	0.00	0.00	0
XIFU_Cool_Rad	1	40.46	20.00	8.09	48.55
XIFU_Ebox_Rad	1	17.16	20.00	3.43	20.59
X-IFU_Th_Link	1	12.60	20.00	2.52	15.12
Grand Total		**3880.07**	**17.64**	**684.49**	**4564.56**

Comments:

- The restriction to the 2624mm LVA limited the number of mirror module rings to 15, their masses are given by a model which already includes margins

- The structural mass of the mirror cover and the sunshield were included in the equipment list with the short names: Mirror_Cover and Sun_Shield, under the Mechanisms domain of expertise
- The thrusters mass corresponds to a pair (nominal and redundant). There are a total of twelve 1N pairs, and two 22N pairs
- The Harness mass was assumed to be 8% of the total dry mass of the SC, and was considered under the responsibility of the system domain of expertise
- Under the baseline design, the Thermal baffle function is provided by mirror structure itself, this is the reason why no mass is allocated to it.

This Page Intentionally Blank

8 CONFIGURATION

8.1 Requirements and Design Drivers

The following list of requirements applies to the configuration discipline to achieve the ATHENA mission objectives.

SubSystem requirements		
Req. ID	**STATEMENT**	**Parent ID**
CFG-010	The configuration shall comply with the constraints of the Ariane 5 launcher and long fairing.	
CFG-020	The Interface for the Launcher to SC shall be the 2624 standard adapter.	
CFG-030	The configuration shall accommodate the Mirror, Instruments and equipment in order to comply with the mission objectives, power, thermal, propulsion and communication requirements.	
CFG-040	The configuration shall take into account the limitations due to AIV constraints.	
CFG-050	The configuration shall provide an unobstructed field of view for all instruments and equipment.	
CFG-060	The configuration shall provide unobstructed position for the thrusters to fulfil the mission requirements without contamination of relevant parts of the SC.	
CFG-070	Mission orbital and attitude constraints shall be taken into account to provide the required thermal and stray-light shielding	

8.2 Assumptions and Trade-Offs

In order to achieve the mission objectives and configuration requirements, the Ariane 5 long fairing volume has been used to its maximum volumetric capability. In addition the service module (SVM) has been constructed around an optimal design for the Pore-Optics Mirror, to maximise the area of the mirror within the selected 2624 launcher adapter. Furthermore clear major sub-systems have been established for programmatic reasons.

The initial instrument positioning has been based on the currently available design and dimensions, and shall be optimised in the following phases of development. Similarly an initial equipment layout has been derived to achieve a conceptual design. The next development phases shall assess and optimise these against the mission requirements.

8.3 Baseline Design

Figure 8-1 shows the ATHENA SC (SC) in launch configuration with and without the Ariane 5 launcher long fairing. The large SC fits within the available volume with sufficient margin to spare. At the lower part near the interface adapter with the launcher the spacing is narrower and will need to be monitored during the development phases.

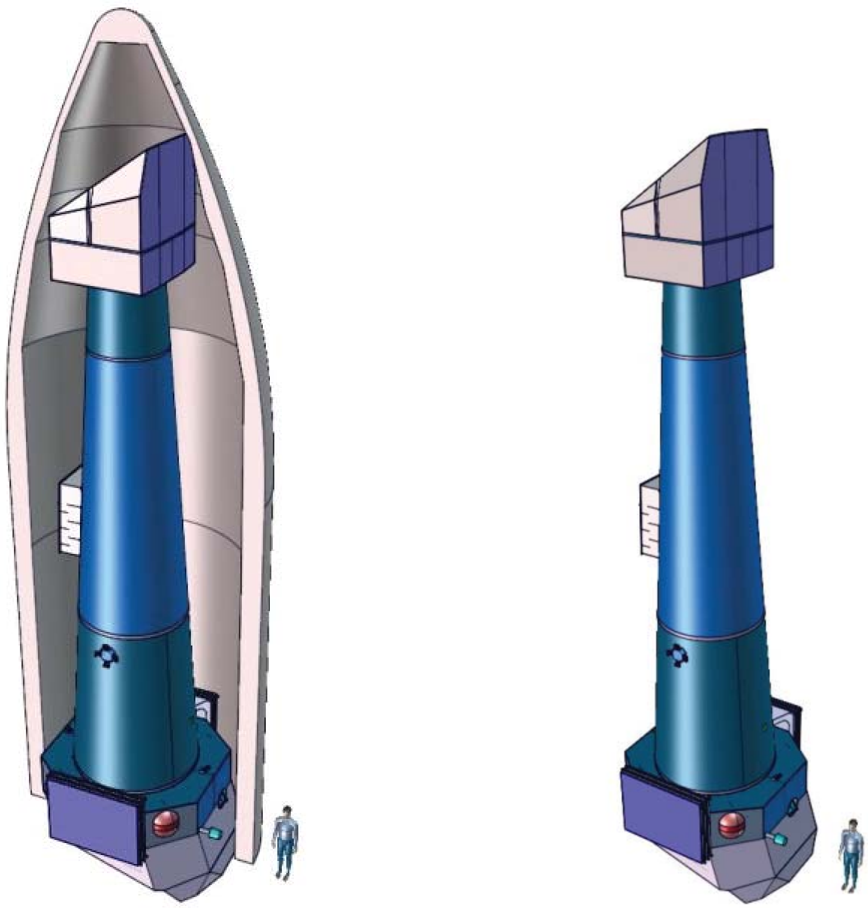

Figure 8-1: ATHENA SC in stowed configuration

Figure 8-2 shows a general view of the ATHENA deployed SC.

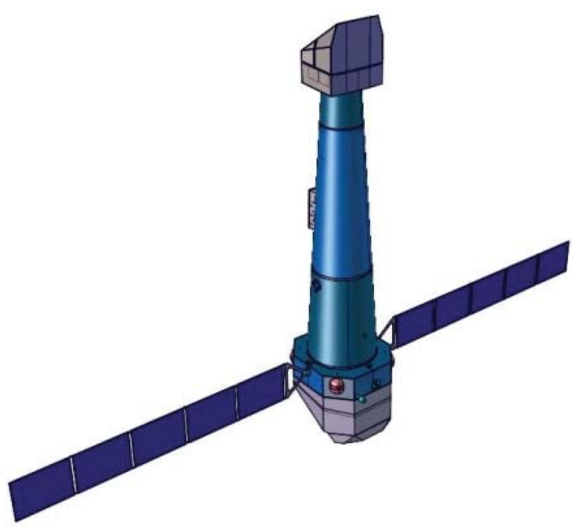

Figure 8-2: ATHENA SC in deployed configuration

Another view of the deployed ATHENA SC is shown in Figure 8-3.

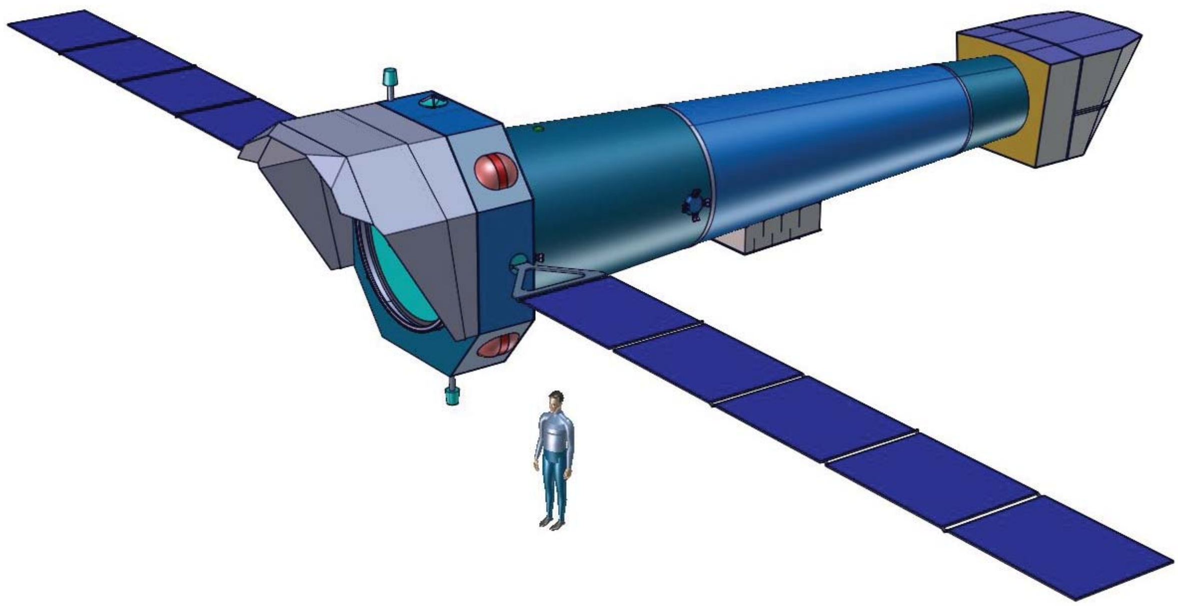

Figure 8-3: ATHENA deployed configuration 2

In Figure 8-4 the System level division is shown for the SC. The following elements are distinguishable; Service Module (SVM), Mirror Assembly Module (MAM) , Focal Plane Module (FPM). This decomposition is slightly different than the description in the system chapter.

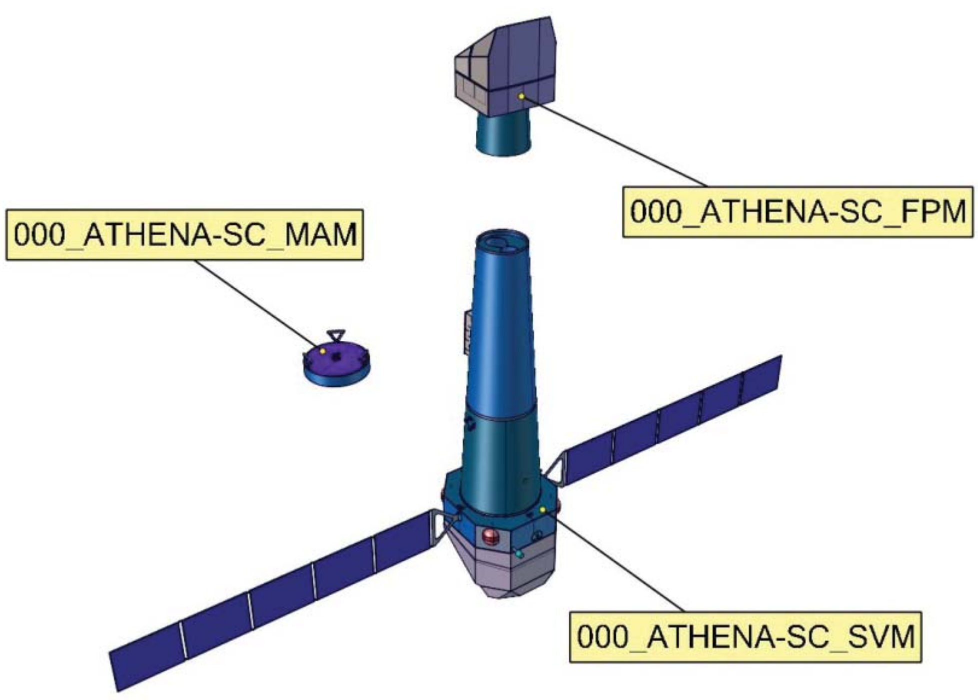

Figure 8-4: Major Product tree sub-systems

Apart from the system level definition of the major sub-systems, there is also a more practical division of the SC.

Figure 8-5 shows the SVM with the lower part of the Fixed Metering Structure (FMS), which also internally (not shown) includes the MAM.

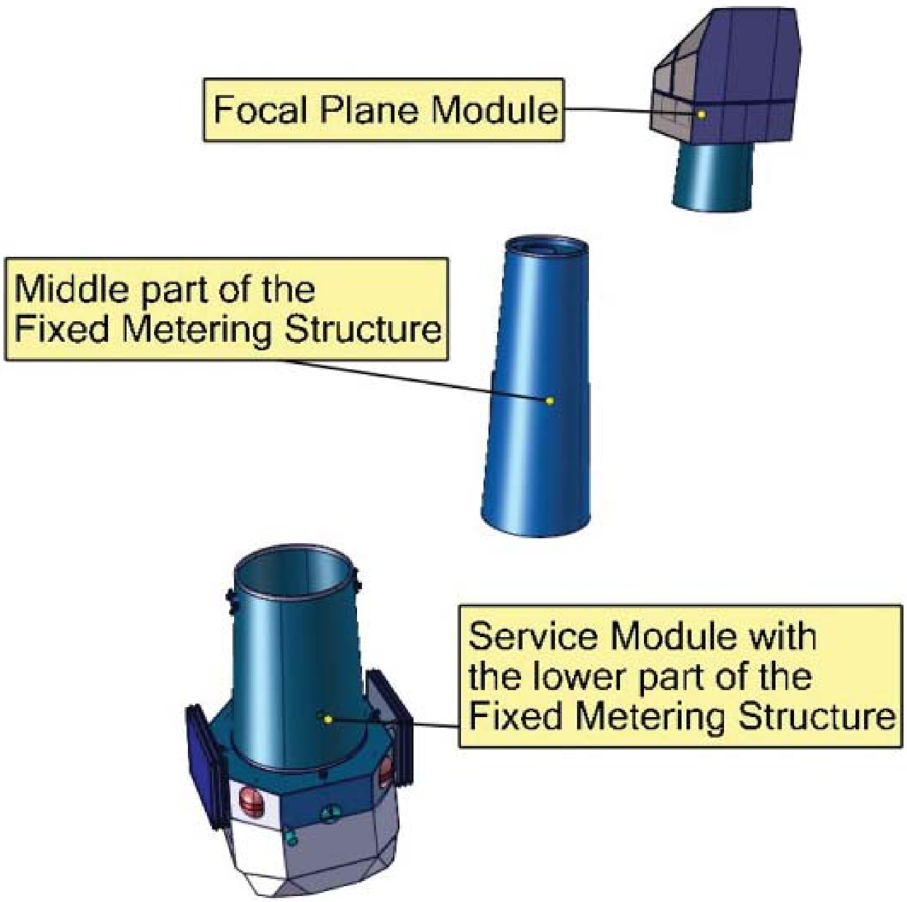

Figure 8-5: Configuration sub-division for AIV purposes

Furthermore the FPM is shown as a separate unit, and then the middle part of the FMS. This middle part of the FMS does not have any electronic units instrumentation, it is only the structure between the upper and lower part of the SC. It does include some internal baffles. The separation in this fashion is needed for AIV and transportation purposes. The SC is very large, and test centres for various tests (e.g. mechanical, thermal, functional) cannot all be performed with the complete SC assembly.

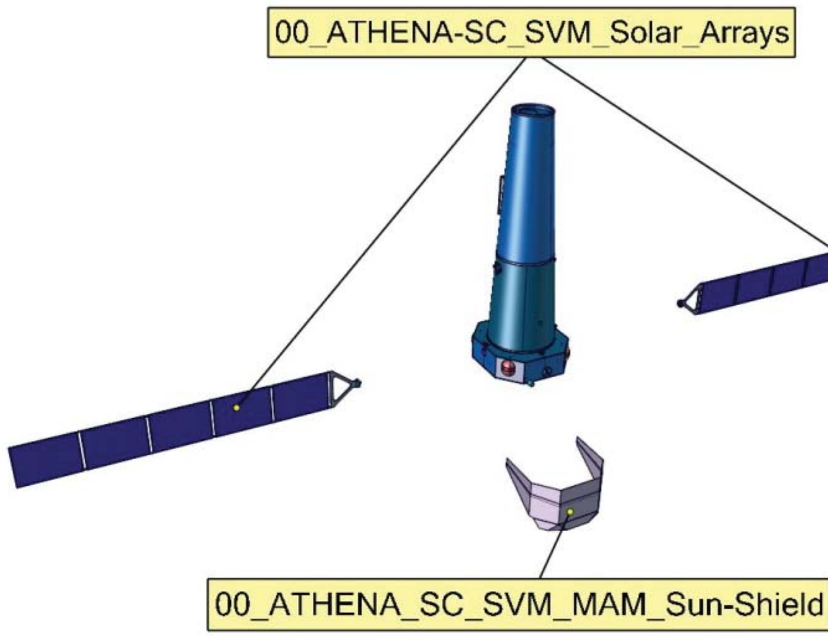

Figure 8-6: SVM deployable sub-systems

Figure 8-6 shows the Solar Arrays and the deployable sun shield on the SVM. These parts are stowed during launch.

The SVM has a main body, which includes the 2624 launcher adapter ring, on top of which the lower and middle parts of the FMS are positioned. Since the FMS is a large volume, it needs to be vacated in a controlled manner. For that purpose a Venting baffle together with a small mechanism opening venting doors is included. The heritage of this sub-system can be found on the XMM SC. Figure 8-7 shows these SVM elements.

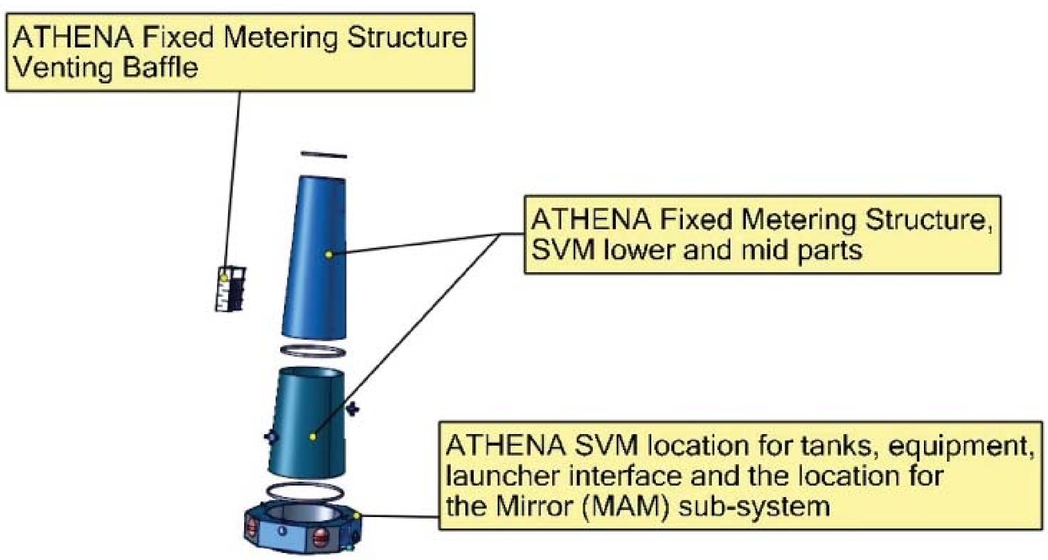

Figure 8-7: SVM elements

In Figure 8-8 the main body of the SVM is shown. It consists of a more classic layout also comparable to the XMM SC. A central cylinder is the back-bone of the whole SC to which panels are connected carrying all relevant electronics and sub-systems.

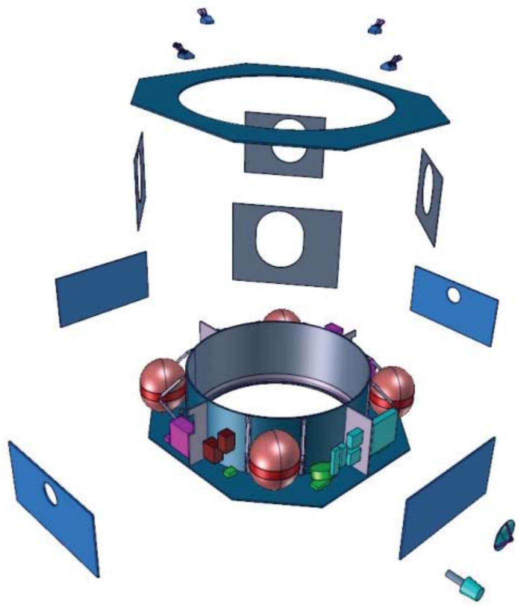

Figure 8-8: SVM main body design

Inside the central cylinder of the SVM the MAM (mirror sub-system) is suspended with a Hexapod type of mechanism. Integration of the MAM is done via the top part of the SVM cylinder, see Figure 8-9.

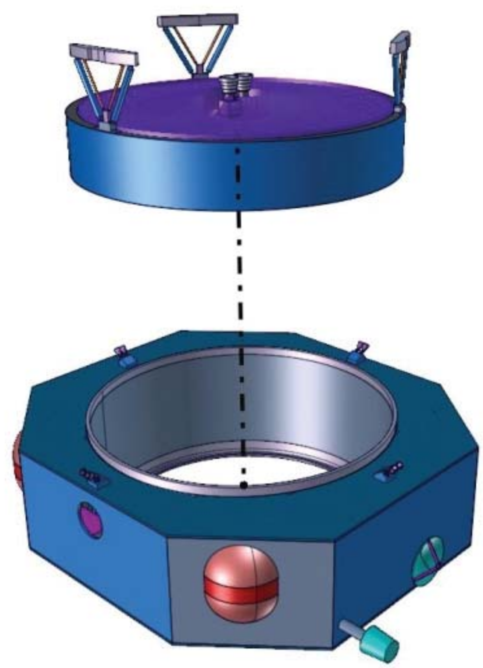

Figure 8-9: Integration sequence for the Mirror sub-system

The reason for this comes from the requirement to have as large a MAM as possible. This results in a diameter that will closely fit the SVM central cylinder. The 2624 launcher adapter has a Launcher Authority pre-defined geometry, which includes a flange for stiffness and ejection purposes. Figure 8-10 shows that the adapter ring has an inner diameter of around 2489 mm, and the mirror is larger with more than 2570 mm. Hence the integration cannot come from below, but from the top, before the FMS is assembled onto the SVM main body.

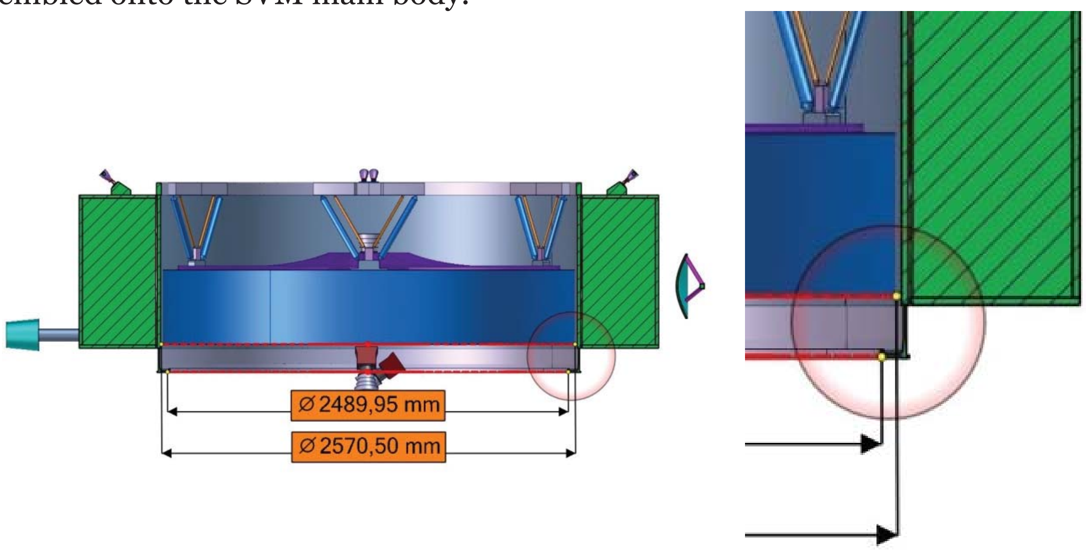

Figure 8-10: Mirror sub-system spacing inside the SVM

Figure 8-11 shows the major elements of the MAM design. The Hexapod shown is a conceptual visualisation. The details of this design shall be completed in the next phases, when more details of all relevant sub-systems become available. This also holds true for the Pore-Optics Mirror Modules layout and detailing of the support structure, which require close cooperation between different discipline specialists for achieving an optimal design.

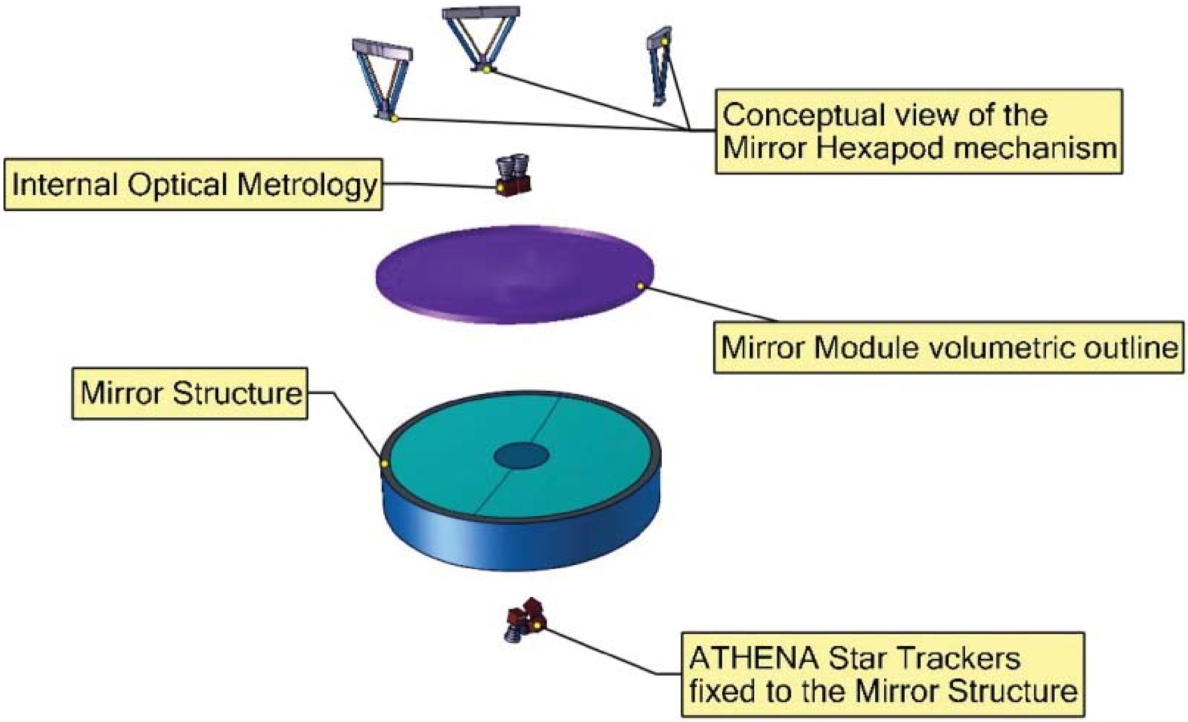

Figure 8-11: Mirror Sub-system elements

The FPM is shown in Figure 8-12. Behind the Sun Shield, MLI and radiators, the instruments and their electronic units are attached to a main instrument platform.

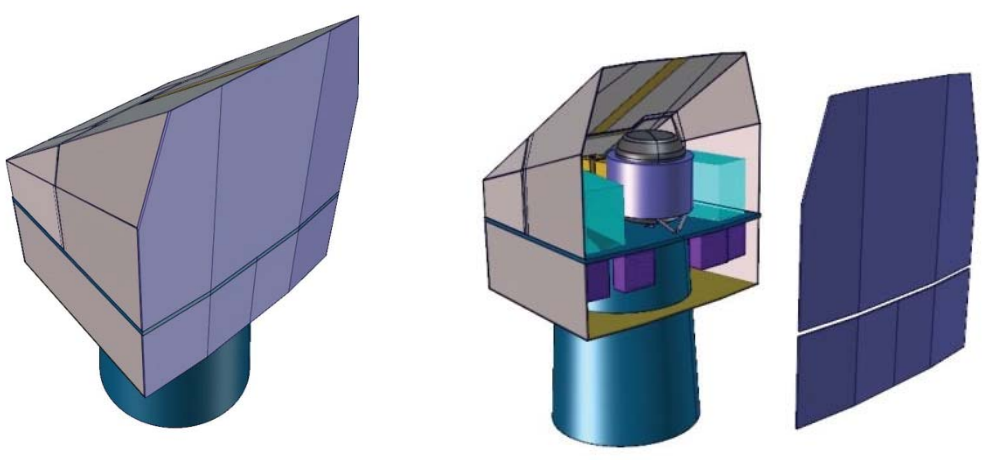

Figure 8-12: Focal Plane Module

Also clearly visible is the upper part of the FMS, a large conical support for the actual focal plane platform, interfacing with the middle part of the FMS on the side of the SVM (as shown in Figure 8-7). Figure 8-13, shows an exploded view of the external Sun Shield, Radiators and MLI closure, and the FMS below.

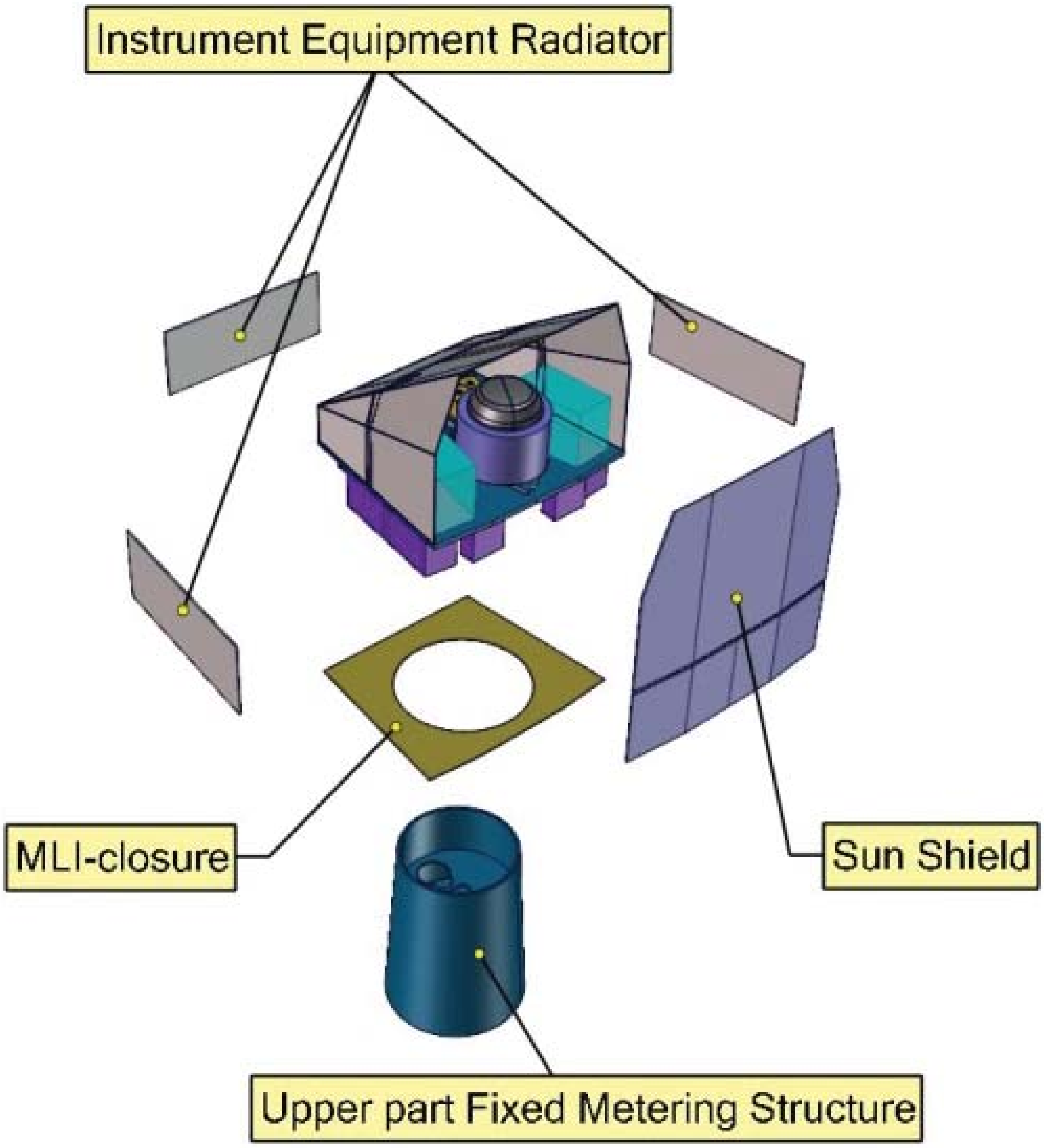

Figure 8-13: FPM exploded view

Figure 8-14 shows the electronic units of the instruments located on the bottom side of the structural platform of the FPM. This was done to keep these units separated from the instruments (WFI and X-IFU) providing a better and controlled thermal environment.

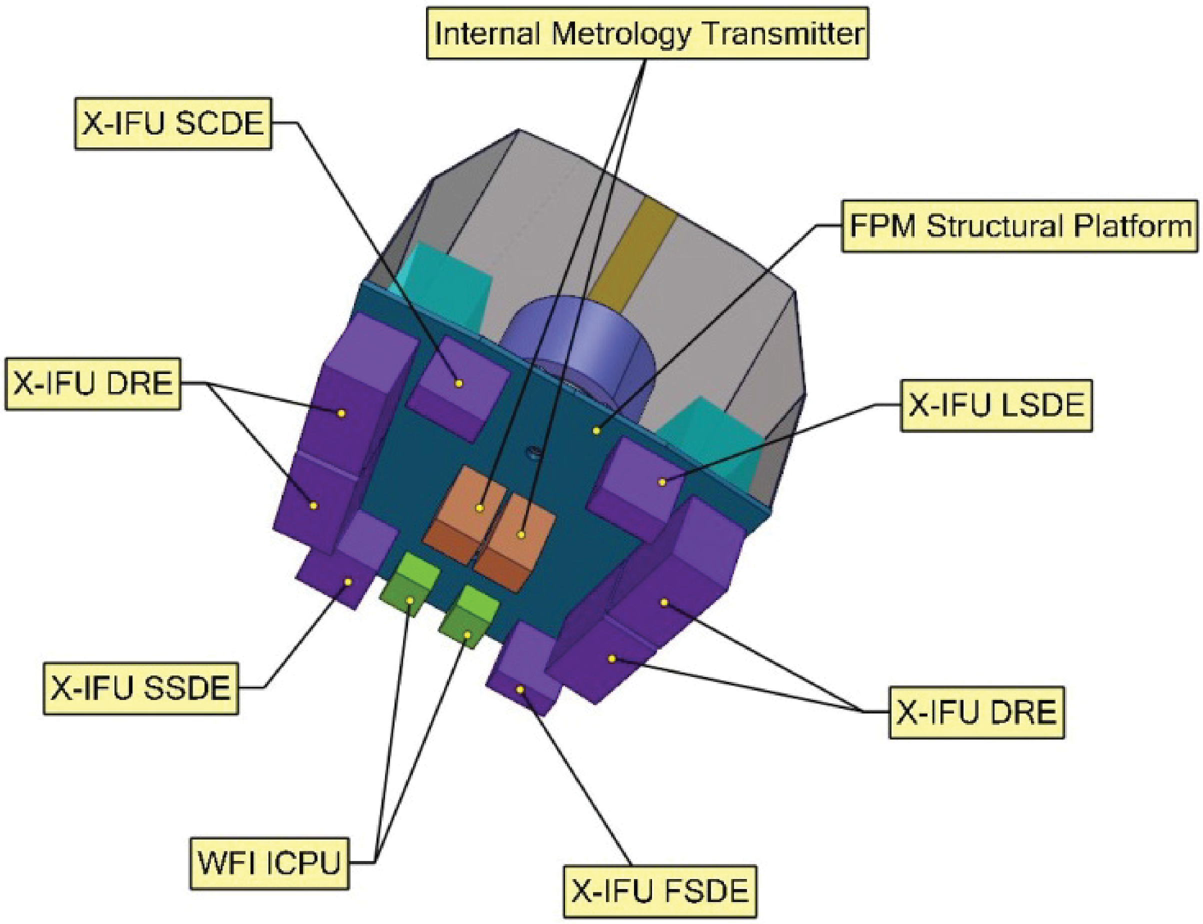

Figure 8-14: FPM electronic units

Figure 8-15 shows the conceptual layout of the ATHENA instruments WFI and X-IFU. The WFI is a completely integrated sub-system, including the radiators. In this way it can be tuned and tested separately, after which it can be integrated onto the FPM platform.

For the X-IFU instrument the Dewar is indicated in between two volumes. These volumes are allocated for the various cooling stage equipment that will interface with the Dewar. The concept is to have these cooling stages integrated on the FPM platform, such that only at the end the Dewar needs to be integrated. Before that the Dewar can be tuned and tested separately.

A detailed description and design of the instruments is given in chapter 5. In this chapter only a conceptual design outline is shown.

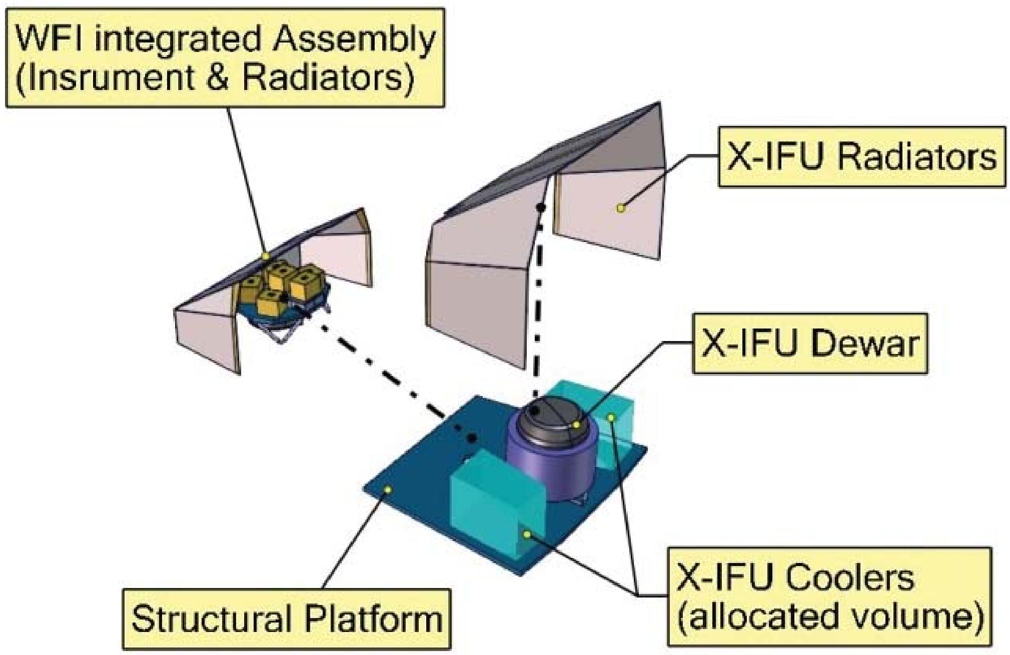

Figure 8-15: Instruments on the FPM

In Figure 8-16 several views are shown for the FMS. To the left a general view shows the overall external design. In the middle image, a cut view shows the baffles internally as well as the Venting baffle. The image to the right shows a view from the bottom of the SC up (from SVM towards FPM). In this way the baffling concept is shown.

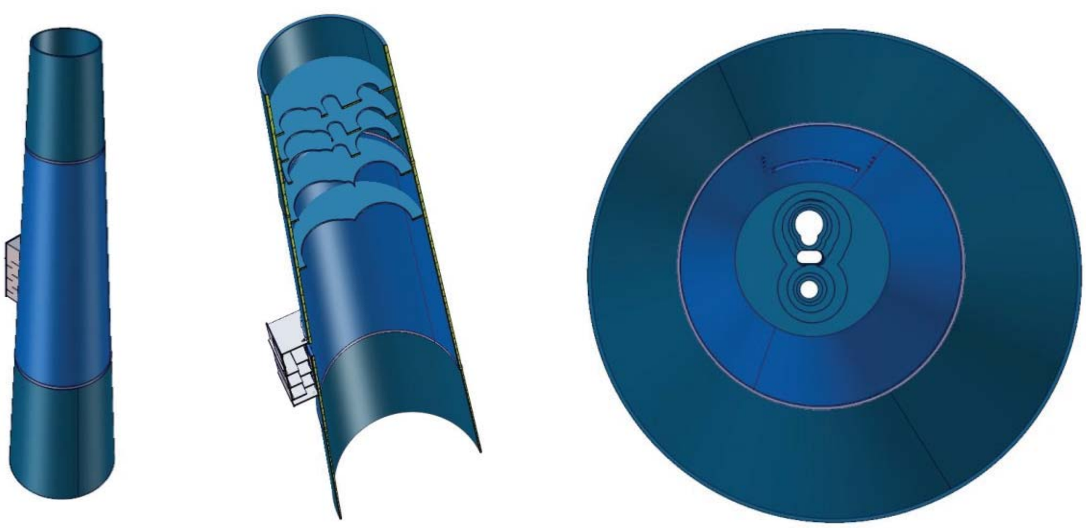

Figure 8-16: Fixed Metering Structure with internal baffles

The Field of View [FoV] that the instruments have on the MAM (mirror) is shown in Figure 8-17.

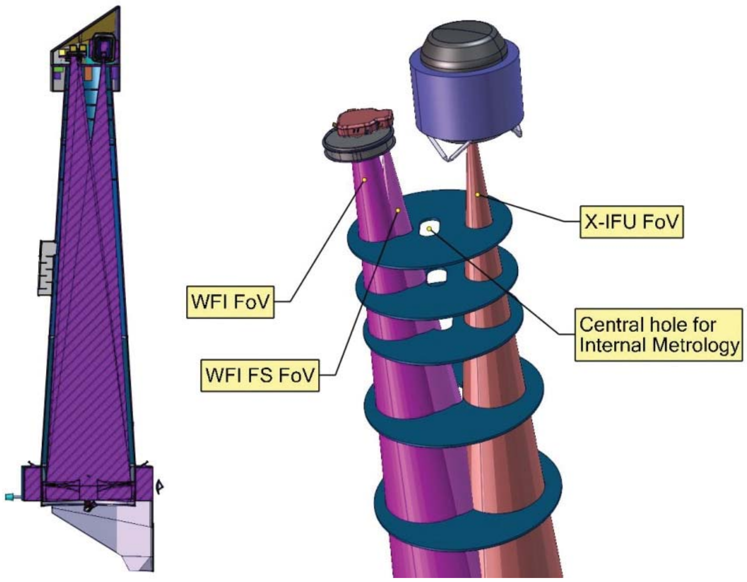

Figure 8-17: Instruments Field of View on the Mirror

A more detailed side "cross-section" view of these FoV at the instruments is given in Figure 8-18. From left to right the WFI Large Sensor, WFI Fast Sensor and the X-IFU.

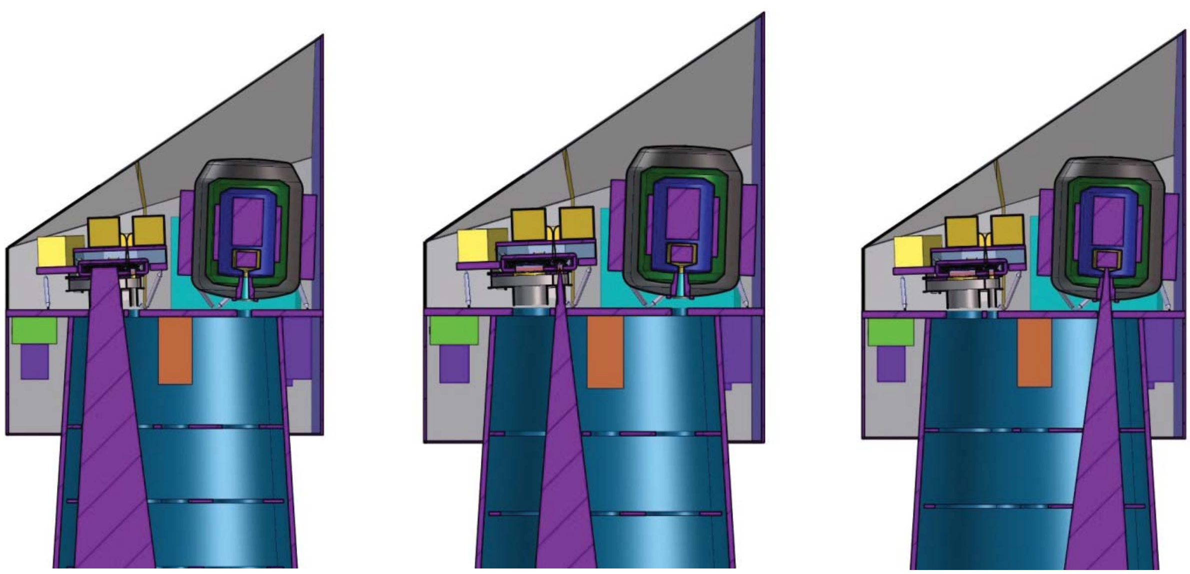

Figure 8-18: Field of view detail at the Instruments

In this feasibility phase for the ATHENA SC and mission, the instruments are not yet sufficiently detailed to make an optimisation for the maximum rotation needed but the MAM hexapod mechanism. In the next development phases this can be optimised and the rotation angles for the MAM can be achieved.

8.4 Overall Dimensions

Figure 8-19 shows the main dimensions of the ATHENA SC in stowed configuration.

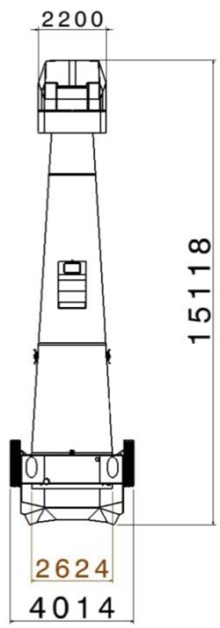

Figure 8-19: Main dimensions in stowed configuration

The overall dimensions of the deployed SC are depicted in Figure 8-20

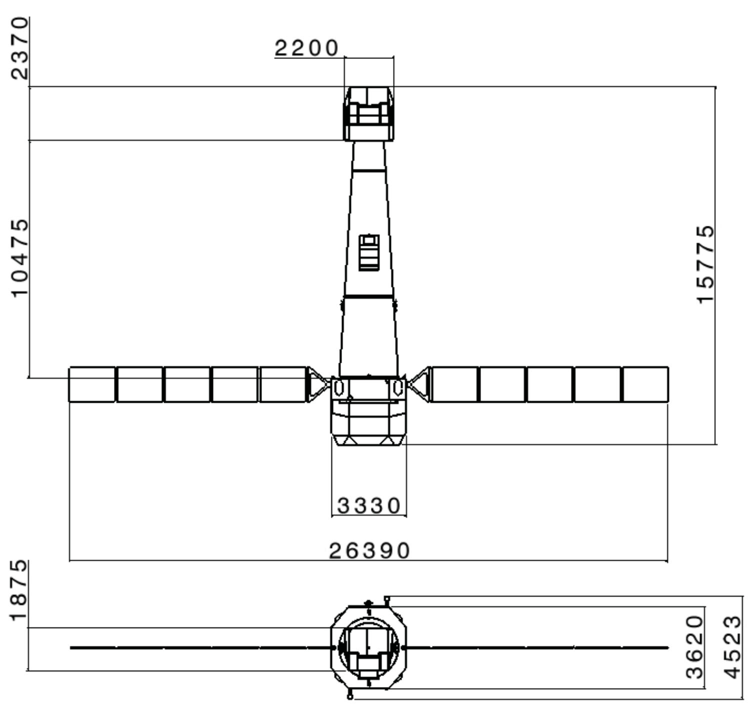

Figure 8-20: Main dimensions in deployed configuration

This Page Intentionally Blank

9 STRUCTURES

9.1 Requirements and Design Drivers

The requirements reported in Table 9-1 were identified for the ATHENA SC structural sub-system.

Subsystem requirements		
Req. ID	**STATEMENT**	**Parent ID**
STR-010	2624 VS PLA static moment $S_{max} \leq 24500$ kgm	
STR-020	The SC main lateral mode frequencies shall satisfy the following frequency requirement: f ≥ 8 Hz [4500kg ≤ SC mass ≤ 6500kg]	
STR-030	The SC main axial mode frequencies shall satisfy the following frequency requirement: f ≥ 27 Hz [SC mass ≥ 4500 kg]	
STR-040	The main lateral modes of the MMA installed into the SC shall satisfy the following frequency requirement: 12 Hz ≤ f ≤ 16 Hz	
STR-050	The main axial mode of the MMA installed into the SC shall satisfy the following frequency requirement: 28 Hz ≤ f ≤ 34 Hz	
STR-060	The modal effective mass of the main lateral and axial MMA modes in hard mounted condition shall be ≥ 95%	
STR-070	The main modes of the MMA installed into the SC shall satisfy the following frequency requirement: 1 Hz ≤ f ≤ 3 Hz	
STR-080	The MM misalignment due to on orbit thermo-elastic distortion of the mirror structure shall not exceed: a. dx + dy ≤ 20 μm b. dz ≤ 500 μm c. rx ≤ 30 arcsec (outer MMs) d. ry ≤ 18 arcsec (outer MMs) e. rz ≤ 1.7 arcsec (outer MMs)	
STR-090	The SC moment of inertia with respect to the SC separation plane $I_{max} \leq 90000$ kgm^2 [4500kg ≤ SC mass ≤ 6500kg]	

Table 9-1: Requirements identified for structural subsystem

Requirement STR-010 limits the product of SC mass times CoG height and is a main design driver for the structural subsystem given the large focal length of ATHENA and the associated height of the SC. Requirements STR-020 up to and including STR-050 are originating from the SC frequency requirements imposed by the Ariane-5 launcher (RD[17]) and by its booster pressure oscillation loading environment. Requirement STR-060 follows from earlier trade-offs made for the ATHENA mirror structure with regards to shock attenuation. Requirement STR-070 is related to the off-loading of the actuators of the hexapod pointing mechanism. Requirement STR-080 defines the mirror module misalignment limits, where the misalignment is induced by thermo-elastic distortion of the mirror structure. Requirement STR-090 limits the moment of inertia defined with respect to the separation plane of the SC.

All requirements will be further explained in the following sections of this chapter.

9.2 Assumptions and Trade-Offs

9.2.1 SC – LV Interface

For the design of the ATHENA SC it was assumed that the Ariane-5 2624 payload adaptor (PLA) would be used. An adaptor with a larger diameter, such as the one used for ATV (3936 mm) was ruled out for reasons of mission cost. The adaptor details are presented in Figure 9-1. The one selected for the ATHENA mission has a height of 175 mm and can sustain a max static moment of 7000 kg at a CoG height of 3.5 m (24500 kgm, STR-010). Details on the payload adaptor can be found in RD[17].

9.2.2 MMA versus MIP

From a structural point of view it was already anticipated in the early phase of the design project that a Movable Instrument Platform (MIP) would lead to an increased Focal Plane Module (FPM) mass which could lead to a violation of the STR-010 static moment requirement. For this reason, the MIP option could be excluded already early in the design process and design work was focused on the Movable Mirror Assembly (MMA).

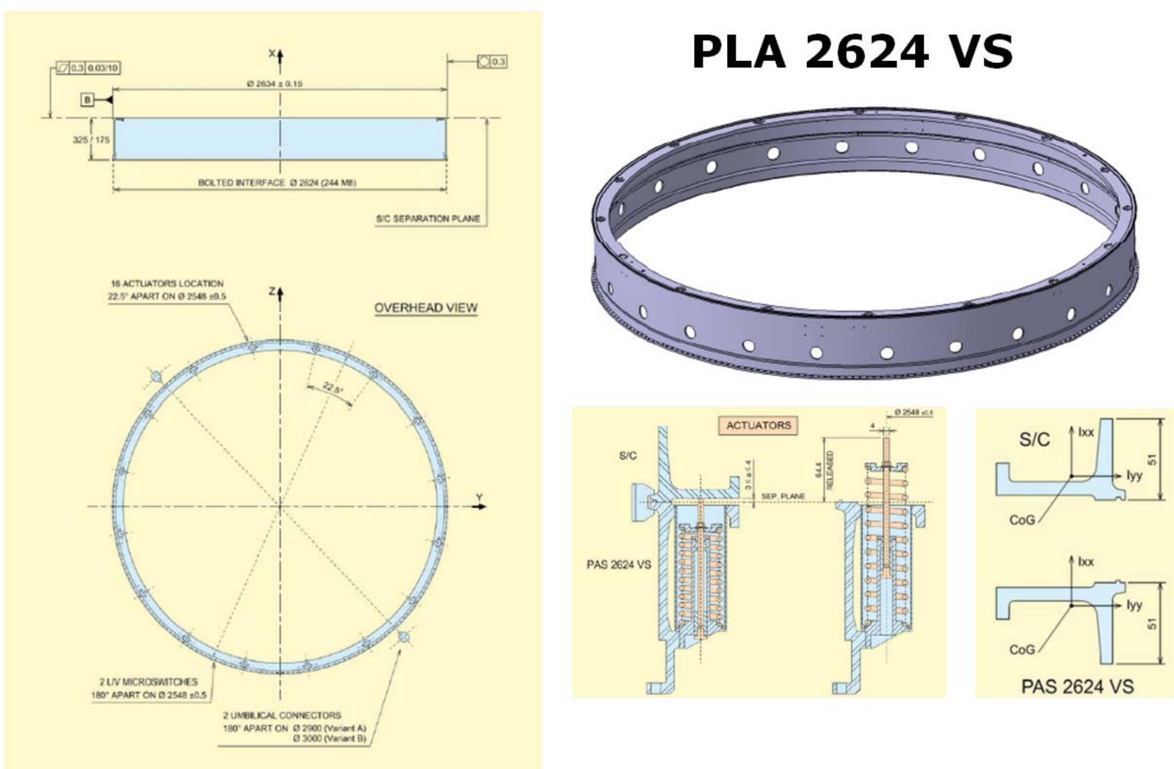

Figure 9-1: 2624 VS Payload Adaptor

9.2.3 MMA Mirror Structure Material Trade-Off

In order to select a suitable material for the MMA mirror structure (MS) several design parameters for material selection were explored and compared. The specific stiffness E/ρ, CTE and ΔCTE with respect to INVAR (the material of the brackets of the mirror modules) are all important to come to a material choice. The parameter E/ρ should be as high as possible to maximise natural frequencies for minimal structure mass. The material CTE should be as low as possible to reduce thermo-elastic distortion of the MS and associated MM misalignments. The ΔCTE should be minimised to reduce MM interior deformations and misalignments of the SPO elements. Besides those design parameters, also the manufacturability plays a major role in choosing the MS material. In terms of potential MS materials only titanium and CFRP were considered. Ceramic materials were a priory ruled out for reasons of too high sensitivity to shock loads, i.e. too low fracture toughness. Since the MMA is positioned nearby the SC interface the shock loads due to clamp band release will be high and might be detrimental for a ceramic MS.

Material	E [GPa]	ρ [kg/m³]	CTE [ppm/K]	E/ρ [MPa·m³/kg]	ΔCTE [ppm/K]	manufacturability
INVAR (Mirror Module Brackets)	***140***	***8100***	***1.4***	***n.a.***	***n.a.***	***n.a.***
Ti	**110**	**4400**	**8.8**	**25**	**7.4**	+ +
CFRP	**170**	**1600**	**1.5**	**106**	**0.1**	– –

Table 9-2: Mirror structure material trade-off

Although titanium is inferior to CFRP for what concerns specific stiffness, CTE and ΔCTE, titanium was still chosen as the baseline material for the mirror structure. The main reason was the easier, cheaper and more precise manufacturing procedure. A titanium MS could be manufactured by milling of a monolithic forging or a set of identical forged segments. Large titanium forgings have been manufactured in the US for the F22 raptor, see Figure 9-2a. Another viable option would be to manufacture it using Additive Layer Manufacturing (ALM), also referred to as 3D printing, see Figure 9-2b. The drilling of holes required to fit the dowel pins of the mirror modules is much more straight-forward for a titanium structure than for a CFRP structure. In fact for a CFRP structure radial ribs would have to be laminated around a pin mould to create the dowel holes. In addition an expensive assembly jig would be required to glue together the concentric circumferential ribs produced by filament winding and the radial ribs. The precision of such an assembly procedure is questionable and is probably insufficient to satisfy the strict misalignment tolerances of the mirror modules. Another problem with CFRP lies in the potential distortions due to moisture release. Such problems do not exist for titanium structures.

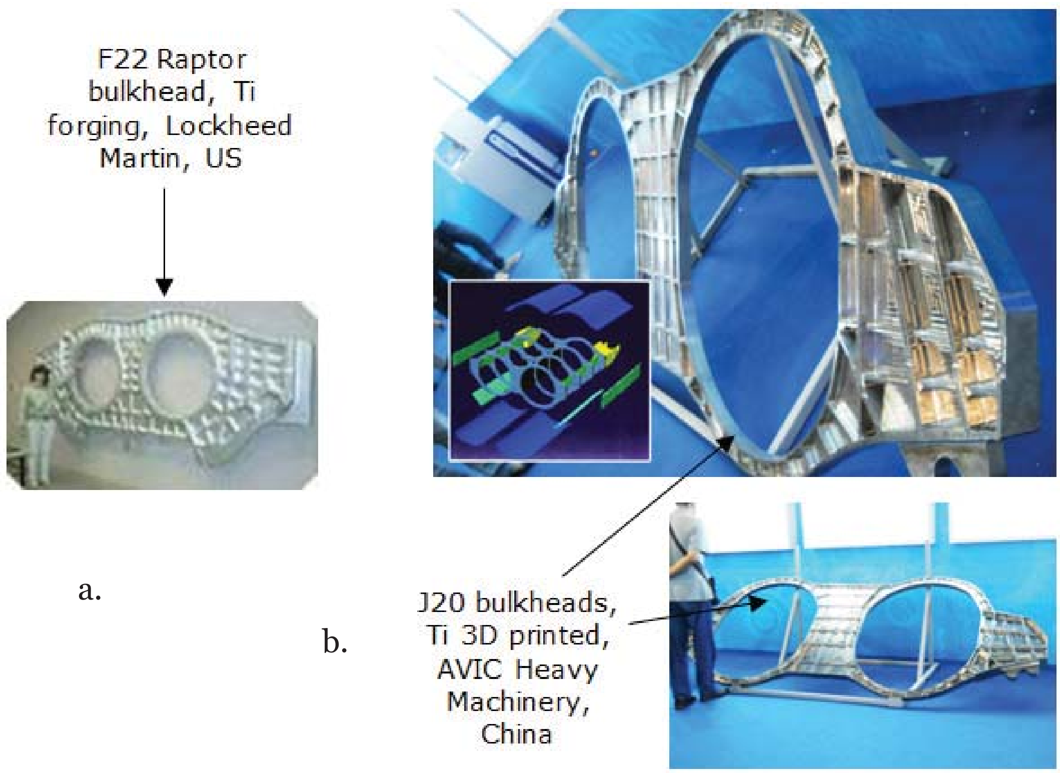

Figure 9-2: Large forging and 3D printed bulkheads for fighter planes

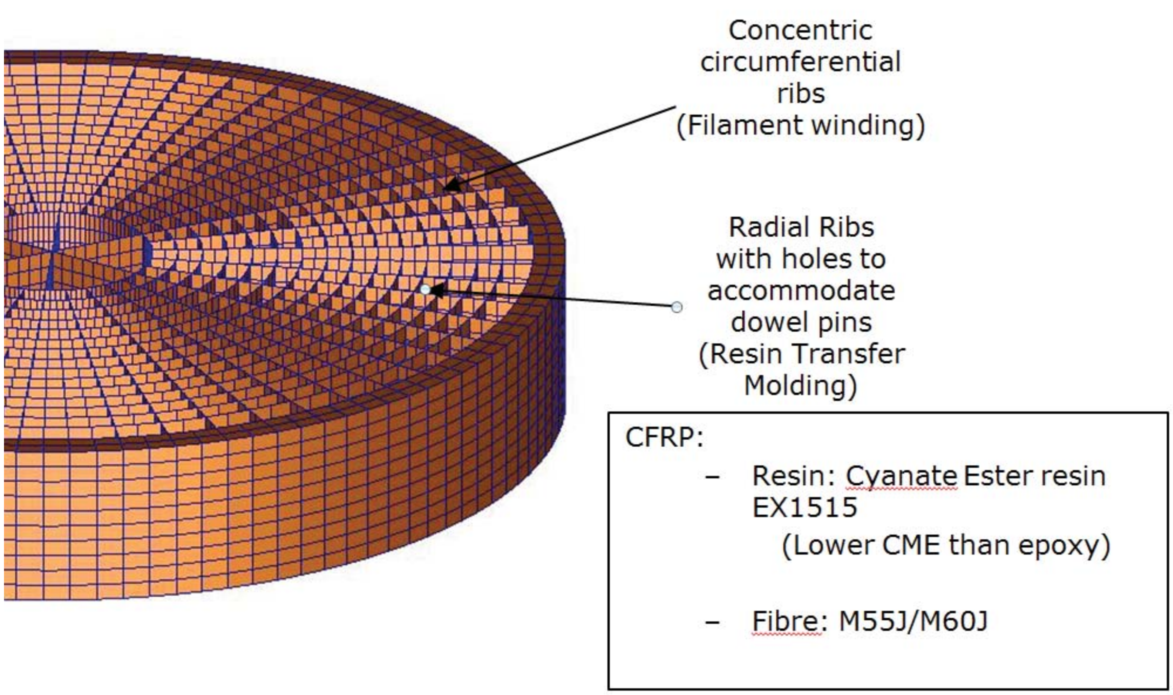

Figure 9-3: CFRP manufacturing concepts

9.2.4 Fixed Metering Structure

The fixed metering structure (FMS) has to be optimised for high stiffness, low mass, small thermo-elastic deflections and high stability against buckling. The SCSC main mode frequency requirements imposed by the Ariane-5 launcher (RD[17]) demand the main lateral modes to be higher than 8 Hz and the first axial mode to be higher than 27 Hz (see STR-020 and STR-030 for the details). Thermo-elastic deflections of the FMS shall be minimised to avoid large off-pointing errors of the X-Ray mirror with respect to the focal position on the detectors. To obtain high stiffness, low mass and small thermo-elastic deflections, CFRP is considered the best material choice, refer also to Table 9-2.

Concerning the stability against buckling, several design options exist such as a sandwich structure or a monolithic CFRP structure with stiffening members. Here the classical sandwich structure with CFRP faces and aluminium honeycomb core was chosen, which from a manufacturing point of view seems simpler and hence cheaper. Related to this choice, a simple conical shape was selected. Circular aluminium frames are envisaged on those axial stations where an interface or internal baffle is foreseen. In order to reduce distortion effects due to moisture release Cyanate Ester resin EX1515 (low CME) is selected in conjunction with the M55J fibre. An orthotropic lay-up is foreseen to increase the bending stiffness of the FMS.

9.2.5 Focal Plane Module

No trade-offs were made for the FPM for what concerns the structural design. CFRP / aluminium honeycomb sandwich was selected for all panels of the FPM. The material choice is the same as for the FMS.

9.2.6 Service Module

No trade-offs were made for the SVM for what concerns the structural design. CFRP / aluminium honeycomb sandwich was selected for all panels of the SVM. The material choice is the same as for the FMS.

9.3 Baseline Design

9.3.1 Movable Mirror Assembly

In this section the structural design of the Movable Mirror Assembly (MMA) is discussed.

9.3.1.1 MMA Architecture & Requirements

The architecture of the MMA is depicted in Figure 9-4. The mirror structure (MS) is made of titanium and is either milled out of a monolithic titanium forging or is manufactured by 3D-printing (Additive Layer Manufacturing, ALM). The MS is populated with 15 rows of MMs and is attached to the SVM drum by means of HDRMs. During launch all loads will pass through the HDRM bipods while in orbit the bipods are disconnected by 6 Non-Explosive Actuators (NEA). From that moment onwards the MS will be kept in position by a hexapod mechanism which consists of 6 actuators mounted parallel to the bipod struts.

The struts of the bipods are thin-walled titanium tubes with flexible necks at each end of the strut to avoid transfer of bending moments. The cross-sectional area of the struts is sized such that the frequency requirements at SC level (STR-020 & STR-030) are met. In addition, other frequency requirements associated with the avoidance of excitation by the Ariane-5 booster pressure oscillations shall be satisfied (STR-040 & STR-050). On top of that, the main modes of the hard-mounted MMA, i.e. clamped at the ends of the bipods, shall have a high effective modal mass to act as a low pass filter for high frequency shock loads (STR-060). Accordingly the main modes will exhibit low modal strain energy in the MS structure and high modal strain energy in the bipods. In order to stiffen the MS, spars are incorporated at n x 60° in azimuthal direction (n=1:6). In addition the height of the structure was increased with respect to previous designs and now amounts to a value of 400 mm.

The actuator struts shall have very low stiffness compared to the struts of the bipods to avoid the transfer of launch loads through the actuators. Accordingly the main axial and lateral mode natural frequencies for the on orbit MMA configuration shall lie within a band of 1-3 Hz (STR-070).

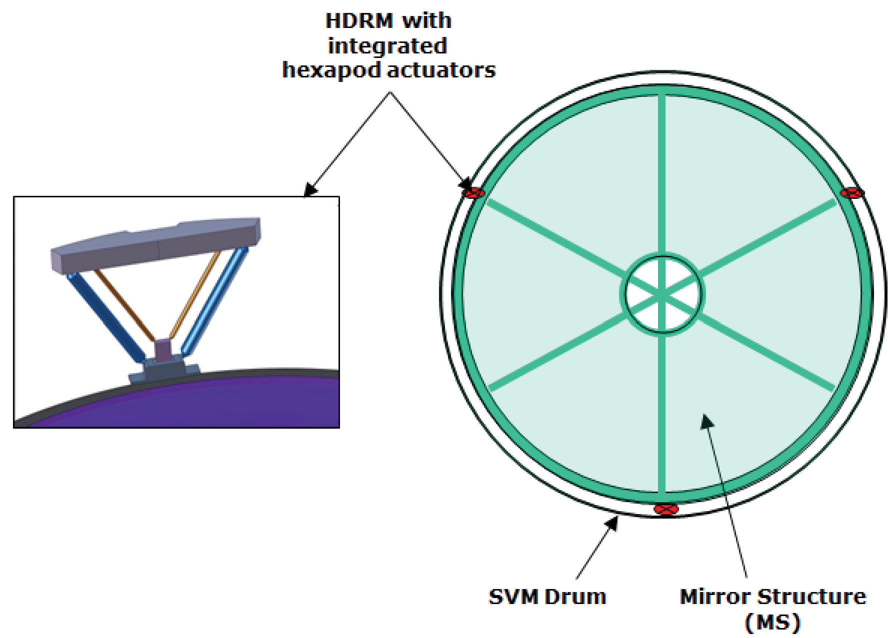

Figure 9-4: MMA architecture

9.3.1.2 MMA FEM

The full MMA FEM is depicted in Figure 9-5. The MS titanium structure has a height of 400 mm, the wall thickness amounts to 2.5 mm globally and the structure is surrounded by a closed ring which provides high torsional rigidity. The ring has a rectangular cross-section with dimensions 400 mm x 80 mm, and a wall thickness of 2.5 mm. The interior of the MS is a web structure which supports the mirror modules. Six spokes are incorporated which meet in the centre. These spars have shear webs of 2.5 mm thickness and girders with a 60 mm x 60 mm square cross-section with again a wall thickness of 2.5 mm. The titanium tubes of the bipods have a circular cross-section with a diameter of 20 mm and a wall thickness of 0.8 mm to obtain the desired stiffness for natural frequency positioning. In reality, the bipods will have struts with a thicker wall thickness and the desired flexibility will be obtained by sizing the necks of the struts. In the detailed design of the struts attention shall be paid to the fracture control requirements of the struts as they are safe life items. The end points of the struts are pinned joints meaning no bending moments can be transferred. Not visible in the FEM, though modelled, are the actuators of the hexapod mechanism that control the position of the MS. The actuators are modelled in the same way as the bipods though the stiffness of the actuators is tuned such that the on orbit frequency requirements are met.

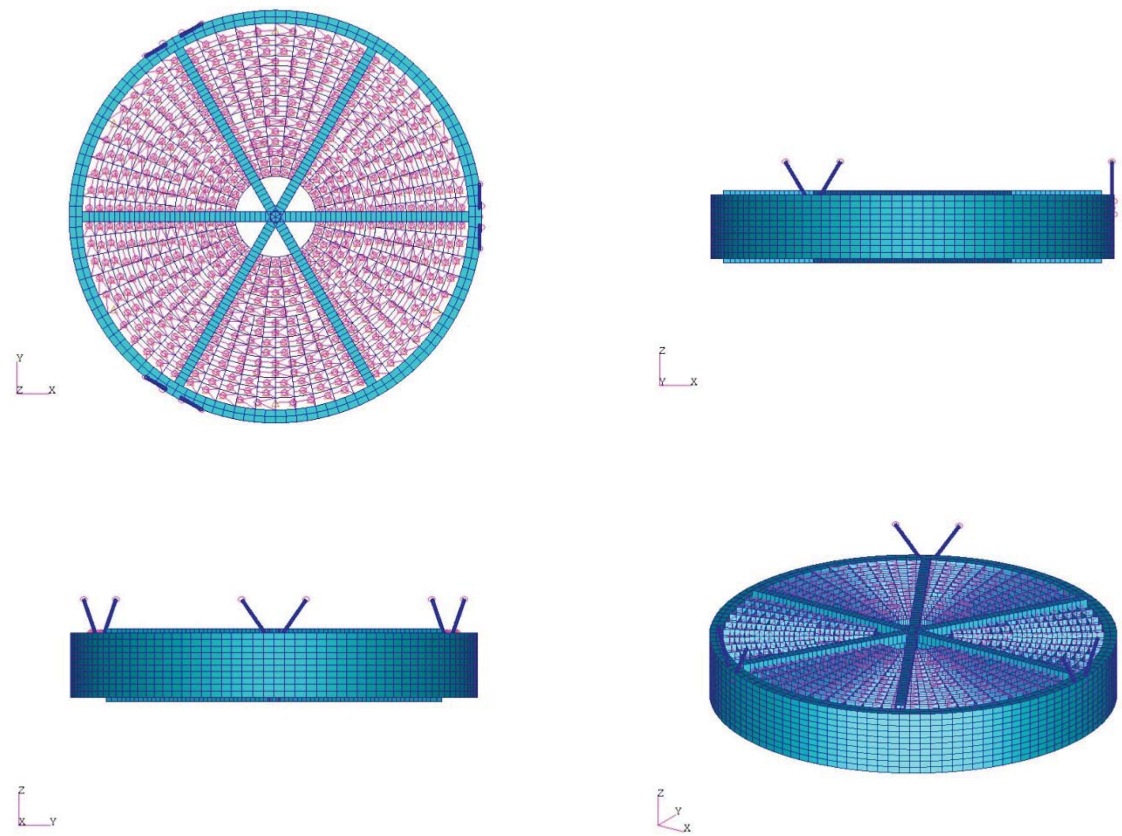

Figure 9-5: MMA FEM

The MS accommodates 15 rows of mirror modules with a total mass of 300 kg. The MS weighs 650 kg including the bipods and a non-structural mass of 100 kg has been added to account for heaters and hexapod mechanism, star tracker and OBM. The MMA total mass with neither equipment nor system mass margins therefore adds up to 1050 kg. The mass properties are summarised in Table 9-3 and do not include the equipment mass margin nor the system mass margin.

MMA Mass Properties	
mass	1050 kg
CoG w.r.t mid plane mirror modules	-0.136 m
$I_{xx} = I_{yy}$	730 kgm²
I_{zz}	780 kgm²

Table 9-3: MMA mass properties without any mass margins

9.3.1.3 MMA Natural Frequency Positioning

In order to design the MMA to meet the natural frequency and modal effective mass requirements (STR-020 up to and including STR-070) the MMA was first hard-mounted at the end points of the bipods before employing it at SC level. First the stiffness of the hexapod actuators was tuned in order to meet the on orbit natural frequency requirements (STR-070). Subsequently the stiffness of the bipods was tuned to meet the natural frequency and effective modal mass requirements (STR-040, STR-050, STR-060). As can be observed from Figure 9-6 all aforementioned requirements are met.

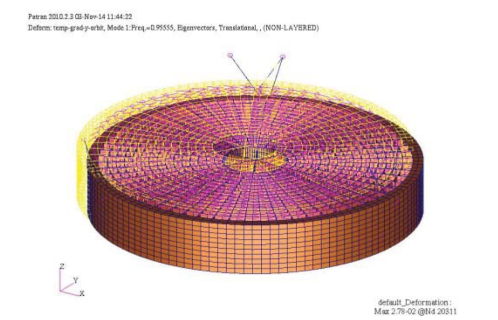 1.0 Hz, lateral	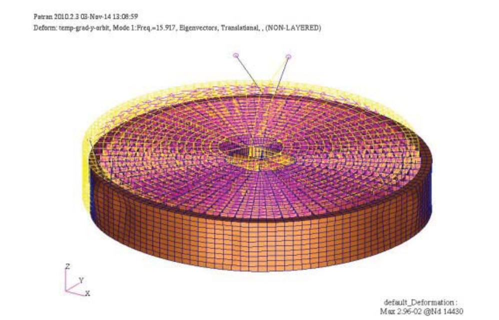 15.9 Hz, lateral, m_eff_lat = 99.6%
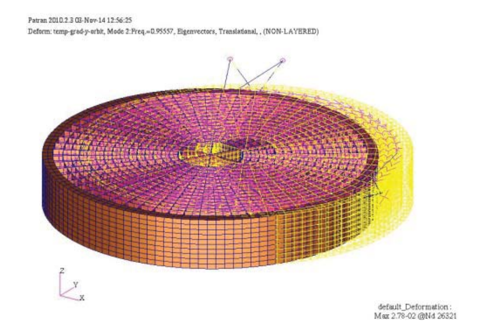 1.0 Hz, lateral	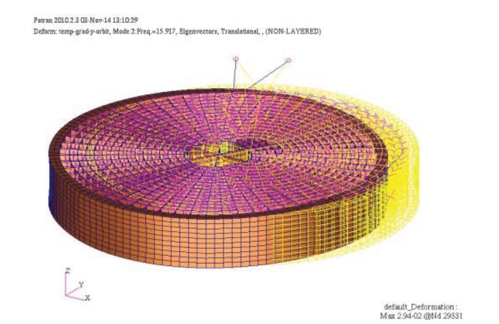 15.9 Hz, lateral, m_eff_lat = 99.6%
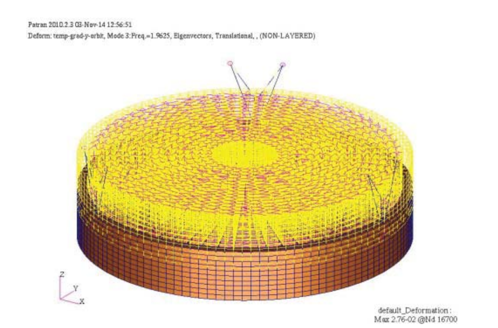 2.0 Hz, axial	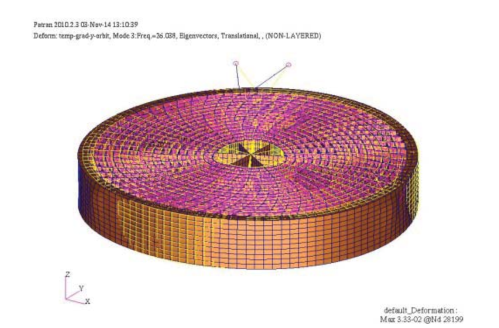 26.0 Hz, torsional, m_eff_tor = 87.1%

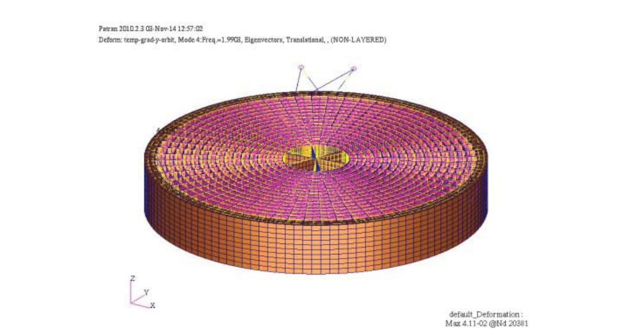

2.0 Hz, torsional

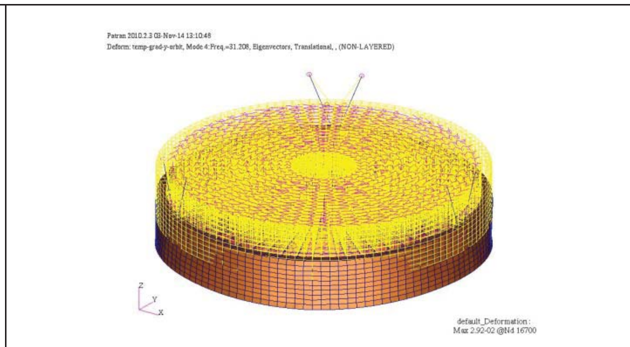

31.2Hz axial, m_eff_ax = 99.7%

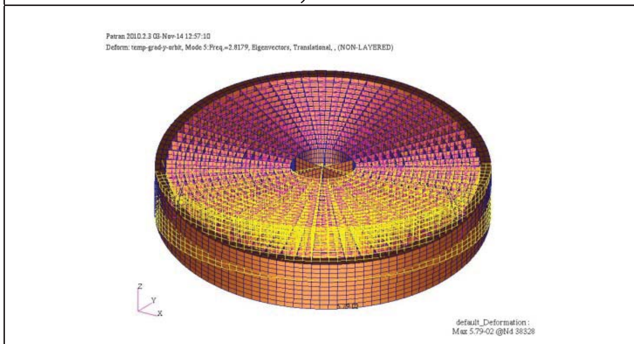

2.8 Hz, gimballing

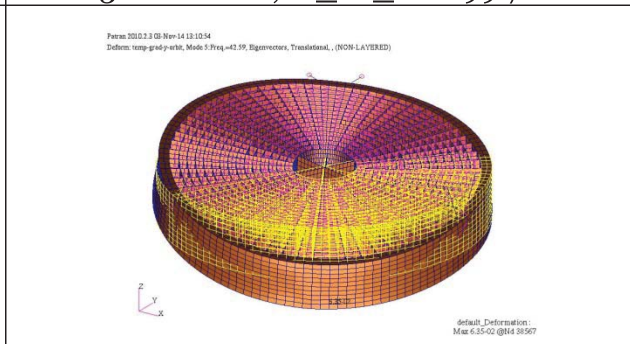

42.6 Hz, gimballing, m_eff_gim = 91.4%

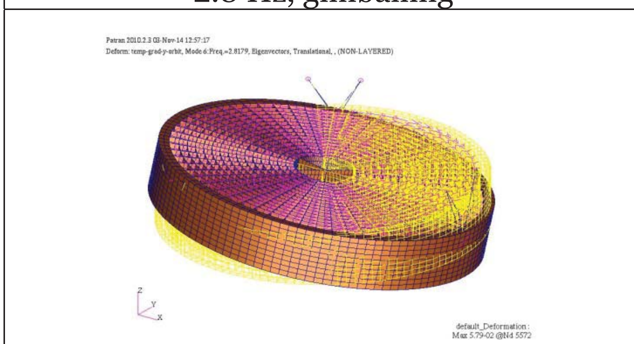

2.8 Hz, gimballing

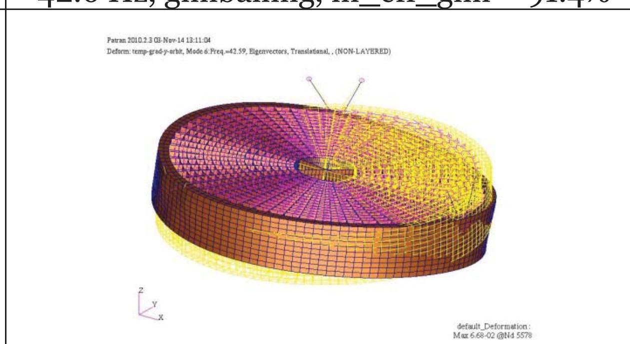

42.6 Hz, gimballing, m_eff_gim = 91.4%

Figure 9-6: Mode shapes – On orbit (left) and launch configuration (right)

The natural frequency positioning is further illustrated in Figure 9-7 in which the launch vehicle related frequency requirements and the "forbidden" frequency ranges associated with the booster pressure oscillations of the Ariane-5 launcher are indicated. The abscissa indicates the SC natural frequency and the ordinate the effective modal mass. The green zones correspond to the frequency ranges dictated by requirements STR-040 and STR-050. The bold vertical grey lines indicated the SC main frequency requirements STR-020 and STR-030. As can be seen, the main lateral and axial modes are nicely positioned in the green zones satisfying all aforementioned requirements. In addition, the modal effective mass requirement (STR-060) is met with sufficient margin. It should be noted that the natural frequencies of the MMA main modes are foreseen to drop slightly when the MMA is installed in the SC SVM drum structure. In section 9.3.2.3 the MMA frequency requirements will be verified again at SC level.

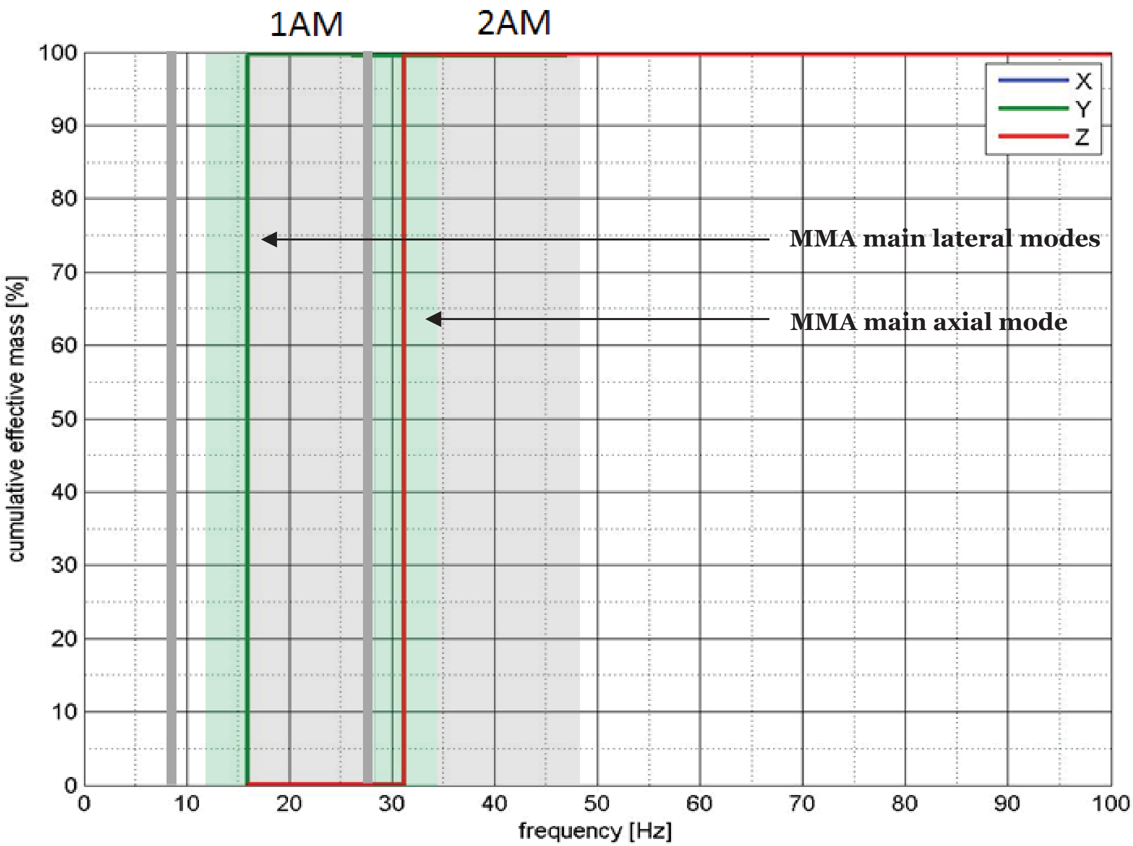

Figure 9-7: MMA natural frequency positioning

9.3.1.4 MMA Shock Attenuation

Now the natural frequency positioning of the MMA has been established, and the modal effective mass of the main modes was assured to be greater than 95% of the MMA rigid body mass, it is worthwhile to compute the transfer functions of some selected points on the MS with respect to the MMA interface points (end of bipod struts). The roll-off of the transfer functions - introduced by excitation of the MMA main modes - is a measure for the attenuation of the shock loads at higher frequencies. The steeper the roll-off, the better the filtering of the high frequency loads. As can be seen from the graphs in Figure 9-8 the roll-off reaches values of the order of 4 to 5 dB/octave. The modes excited at frequencies higher than 100Hz can be moved towards higher frequencies once the simplified modelling approach of the mirror modules is replaced with a more sophisticated one. In the current modelling approach, the mirror modules are modelled as lumped masses and connected to the MS by means of RBE3 elements which do not induce any additional stiffness. In a follow-up approach, the RBE3 elements could be replaced with RBE2 elements and elastic connections to the MS by means of spring elements.

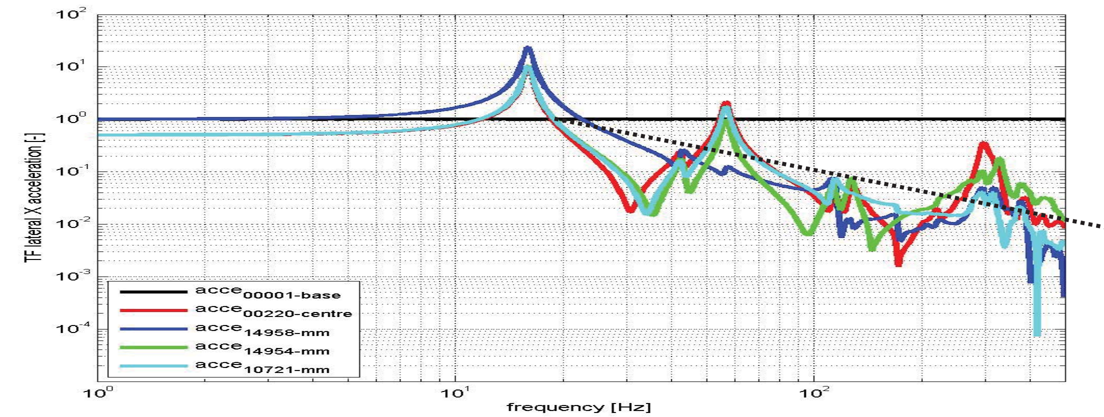

Excitation in X-direction

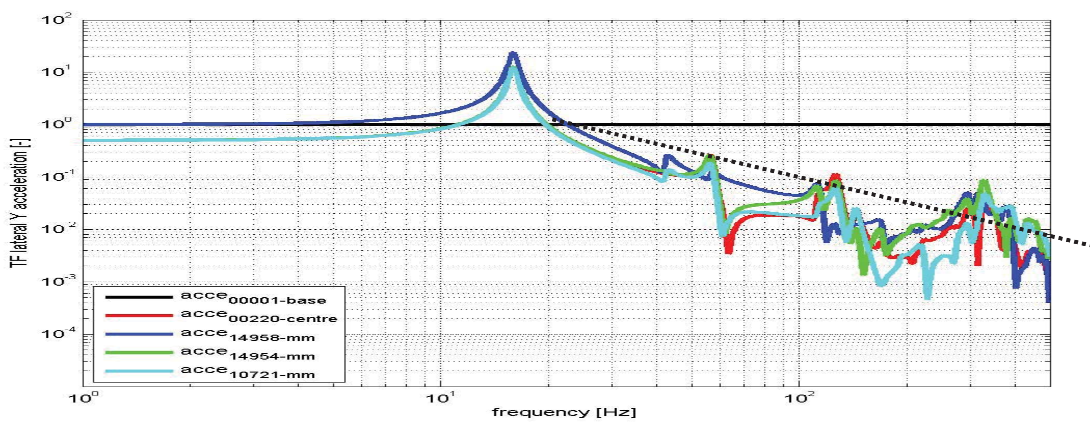

Excitation in Y-direction

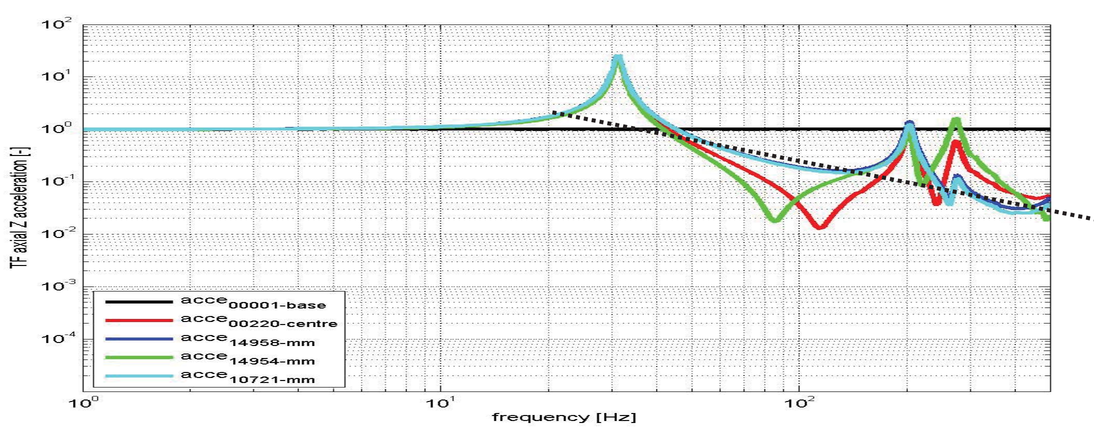

Excitation in Z-direction

Figure 9-8: Transfer functions of some MM positions w.r.t MMA base

9.3.1.5 MMA Thermo-elastic Displacements

A key functionality of the MS is to provide thermo-elastic stability in terms of mirror module pointing and hence to minimise mirror module misalignment. In order to define sizing requirements for the thermal control of the MS, 3 thermo-elastic load-cases were defined:

1. A global delta T of 1 K with respect to room temperature (RT)
2. A 1 K gradient along the mirror lateral direction with respect to RT
3. A 1 K gradient along the mirror axial direction with respect to RT.

The temperature distribution for load-cases 2 and 3 is depicted in Figure 9-9.

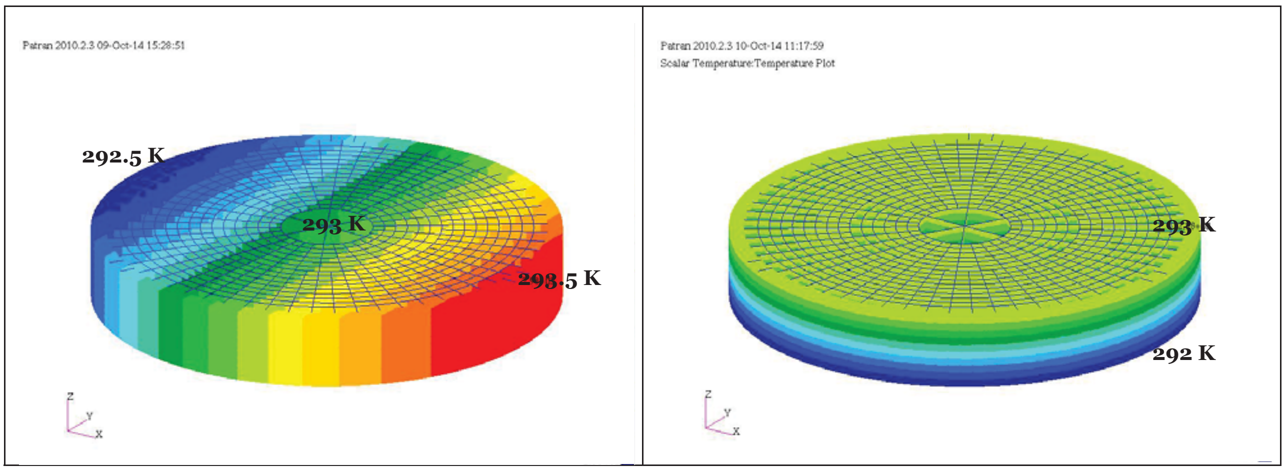

Figure 9-9: Thermal gradients for load-cases 2 (left) and 3 (right)

For the aforementioned thermo-elastic load-cases, the on orbit MM misalignment requirements (STR-080) will be verified. The displacement directions expressed in the MM co-ordinate system are depicted in Figure 9-10.

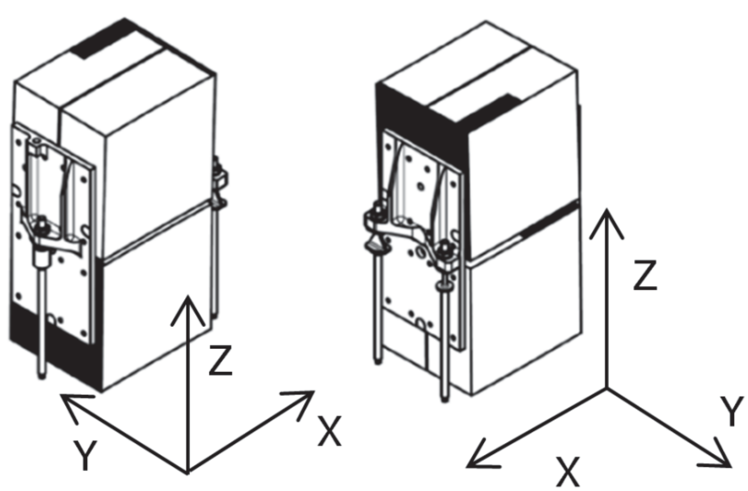

Figure 9-10: MM local co-ordinate system

9.3.1.5.1 Load-case 1

The MS distortion due to a global dT of 1 K is depicted in Figure 9-11. The maximal radial displacement occurs for the most outer mirror modules and amounts to 10.9 µm. By linear scaling it can be seen that a global dT of 1.8 K should occur to reach the misalignment limit of 20 µm in lateral direction, as formulated by the STR-080-a requirement.

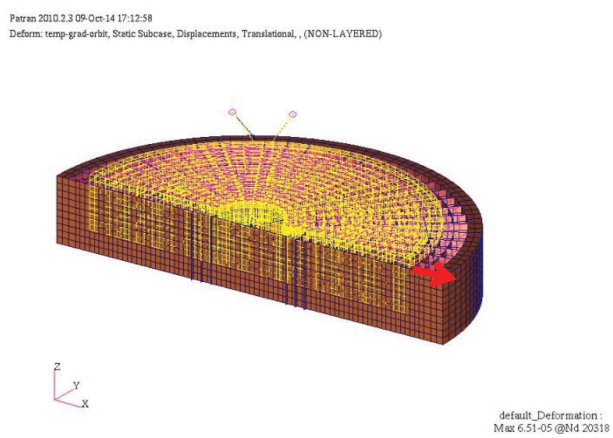

Figure 9-11: MS distortion load-case 1

9.3.1.5.2 Load-case 2

The MS distortion due to a 1 K gradient along the mirror lateral direction is depicted in Figure 9-12.

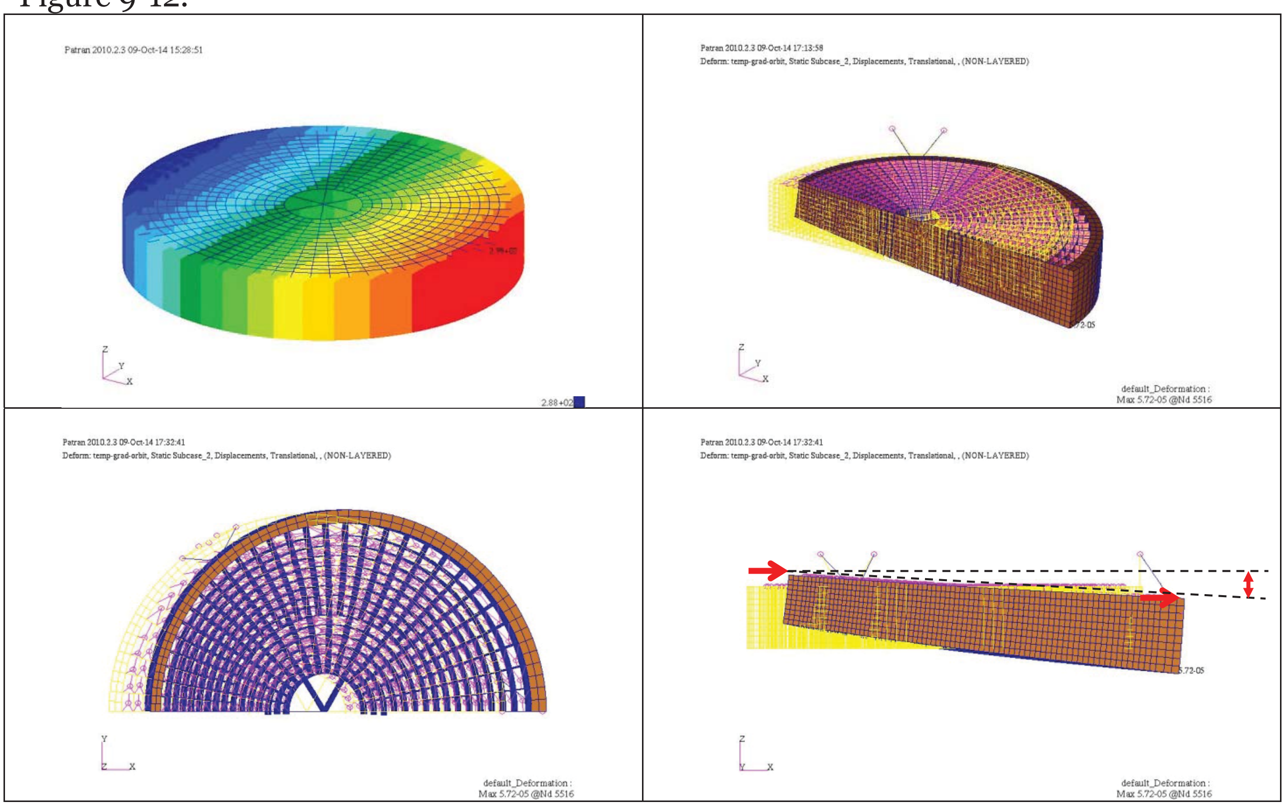

Figure 9-12: MS distortion load-case 2

The global rotation of the MS/MM mounting surface could be cancelled out by the hexapod mechanism. The lateral displacement induced by shrinking of the MS on the –X side of the MS and expansion on the other side (+X) leads to misalignment. The maximum displacement is seen by the outer mirror modules in the vicinity of either the -X or +X axis and amounts to 5.4 µm. By linear scaling it can be seen that a thermal gradient of 3.7 K should occur to reach the misalignment limit of 20 µm in lateral direction as formulated in STR-080-a. This translates to a thermal gradient per unit length of 1.4 K/m. This load-case was also run for a thermal gradient in Y-direction which leads to the same result.

9.3.1.5.3 Load-case 3

The MS distortion due to a 1 K gradient along the mirror axial direction is depicted in Figure 9-13.

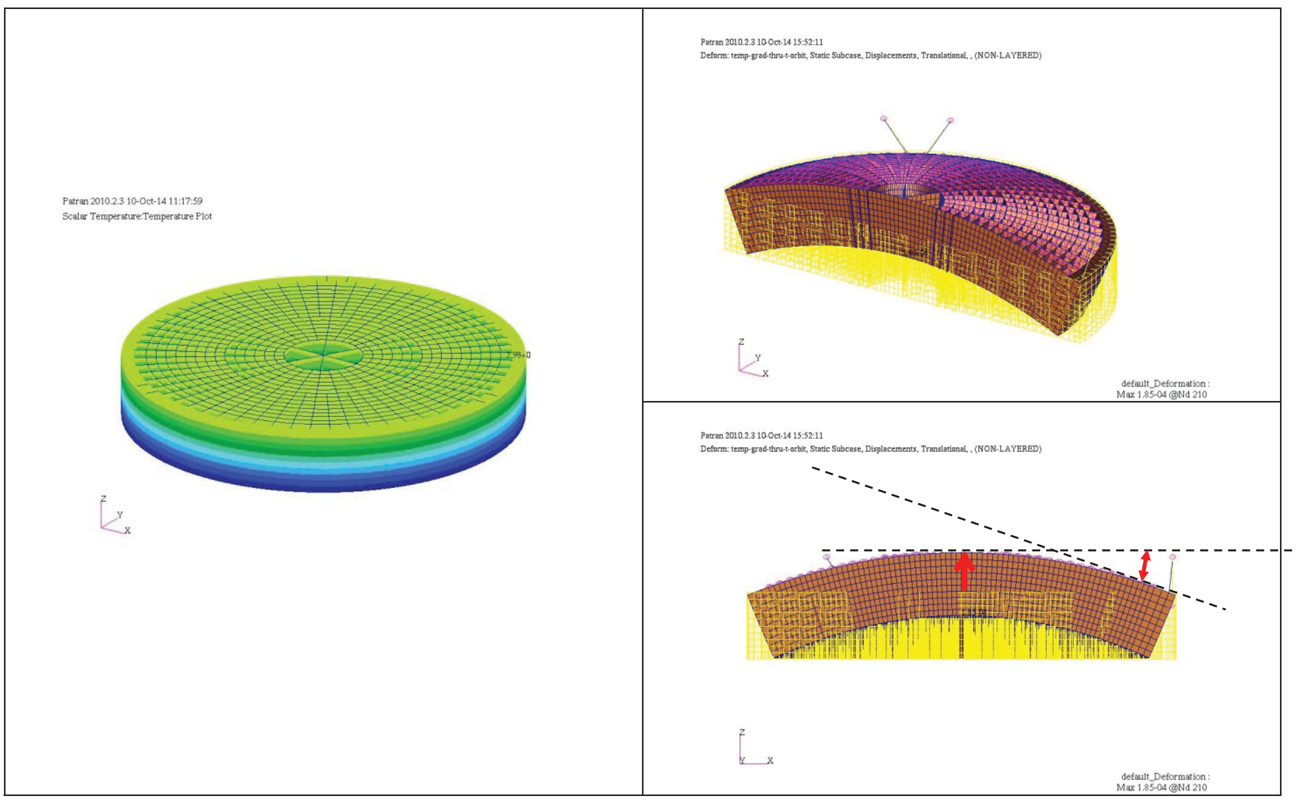

Figure 9-13: MS distortion load-case 3

The rotation of the mirror modules is a function of the radius. For that reason it cannot be cancelled out by the hexapod mechanism. The maximal rotation is seen by the outer mirror modules and amounts to 5.6 arcsec. By linear scaling, it can be seen that a thermal gradient of 3.2 K should occur to reach the misalignment limit of 18 arcsec formulated in STR-080 for rotations about the Y-axis (ry). This translates to a thermal gradient per unit length of 8 K/m. The rotations about the X-axis (rx) are less stringent and therefore do not drive the thermal gradient limitation. The maximum displacement in Z-direction is seen by the most inner mirror modules and amounts to 17 µm for a unit gradient. Again, this displacement does not drive the thermal gradient limitation.

9.3.1.5.4 Requirements derived for the sizing of the MS thermal control

In Table 9-4 the results of the above analyses are translated into requirements for the sizing of the MS thermal control system.

Global dT shall be less than :	±1.8 K
Gradient in XY plane shall be less than :	1.4 K/m
Gradient in Z-direction shall be less than :	8.0 K/m

Table 9-4: Requirements for MS thermal control

9.3.2 SC Assembly

In this section the structural design of the SCSC load carrying structure is presented.

9.3.2.1 SC FEM

The full SC FEM is depicted in Figure 9-14 and consists of the SVM, MMA, FMS and FPM substructure elements.

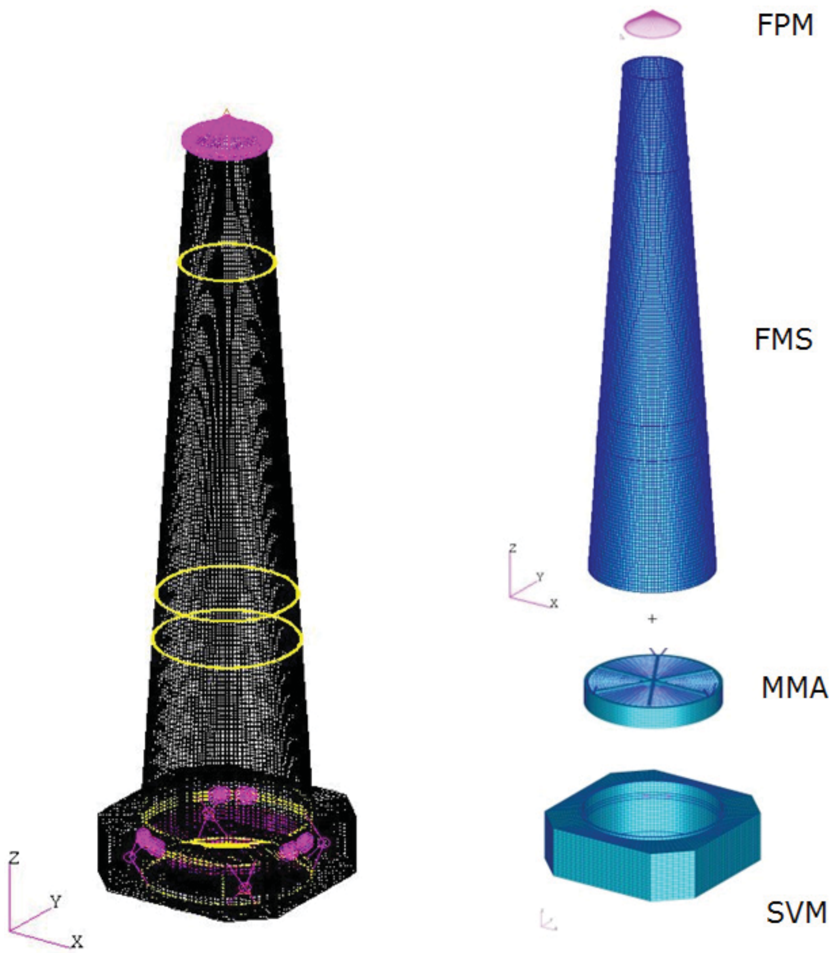

Figure 9-14: SC FEM

The mass-breakdown of the SC FEM into the aforementioned main substructure elements is given in Table 9-5.

Substructure Name	Mass [kg]	Structural Mass Percentage [%]
SVM	978	22%
MMA	1050	62%
FMS	887	53%
FPM	1028	23%
SC Grand Total	3943	n/a

Table 9-5: SC Mass Breakdown without propellant and mass margins

Including the averaged equipment mass margin (1.17), system mass margin (1.20) and propellant mass (392 kg), the overall SC mass adds up to:

M_{SC} = 3943 x 1.17 x 1.20 + 392 = 5928 kg

The CoG height and moment of inertia of the SC at the SC base amounts to:

H_{CoG} = 4.64 m

I_{SC} = 208000 kgm^2

The main structural properties of the SC FEM are summarised in Table 9-6.

Substructure	**Material / modelling description**
SVM cylinder	20 mm sandwich, 2 mm CFRP face sheets, aluminium honeycomb core
SVM octagonal structure	20 mm sandwich, 1 mm CFRP face sheets, aluminium honeycomb core
MMA	Titanium mirror structure, wall thickness 2.5 mm, 15 rows of SPO mirror modules
FMS	20 mm sandwich, 2 mm CFRP face sheets, aluminium honeycomb core
FPM	lumped mass connected to FMS top ring by RBE2 element
Sandwich	CFRP: M55J / EX1515 cynate ester Core: Hexcel aluminium honeycomb flex core F5052/F80

Table 9-6: SC structural properties

9.3.2.2 SC Bending Moment & Moment of Inertia

It is foreseen to launch the ATHENA SC on Ariane-5 on the 2624VS payload adapter. Because of its large axial dimension the bending moment induced at the base of the SC was considered an issue already at the start of the design studies. For this reason, the bending moment capacity of the 2624 payload adapter was continuously monitored and a best estimate was made at the end of the studies on the basis of the SC FEM and the OCDT tool in the CDF.

The maximum static moment that can be sustained by the 2426 adapter is given by STR-010. With the SC mass and CoG height mentioned in 9.3.2.1 this yields a bending moment equal to:

$S_{SC} = M_{SC} \times H_{CoG} = 5928 \times 4.64 = 27800$ kgm > S_{max} (13.5% over the limit)

Hence the current ATHENA SC design is not compatible with the 2624VS bending moment capability. Compatibility might be achieved from a combination of the following measures:

- Optimisation of the FMS sandwich structure for minimum mass
- Down-scaling of the instruments
- Reduction of FMS height
- Increased stroke of hexapod mechanism to provide piston movement of mirror in the direction away from the instruments, to compensate the reduction of FMS height per previous point.

In addition it can be seen that the SC moment of inertia with respect to the SC separation plane (208000 kgm^2) exceeds the limit prescribed by requirement STR-090 (90000 kgm^2). This exceedance is most likely tolerable as long as the overflux of the running load at the SC interface is kept under control, i.e. is kept below 10%. Arianespace should be contacted to discuss this point which is related to the proper functioning of the SC clamp-band release system.

9.3.2.3 SC Natural Frequency Positioning

In Figure 9-15 the main modes of the SC are plotted. The SC main modes are compliant with the frequency positioning requirements STR-020, STR-030, STR-040 and STR-050. It is recalled here that requirements STR-020 and STR-030 are imposed by the Ariane-5 UM (RD[17]) and demand the main SC lateral modes to be higher than 8 Hz and the first axial mode to be higher than 27 Hz. Requirements STR-040 and STR-050 are associated with the avoidance of excitation of the MMA by the Ariane-5 booster pressure oscillations.

 Mode #1: 8.2 Hz SC Bending Y-direction **STR-020**: f ≥ 8 Hz	 Mode #2: 8.2 Hz SC Bending X-direction **STR-020**: f ≥ 8 Hz	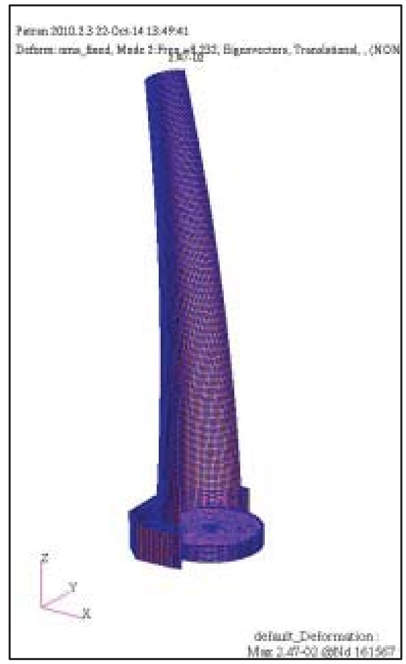 Mode #3: 14.6 Hz MMA Y-direction **STR-040**: 12 Hz ≤ f ≤ 16 Hz
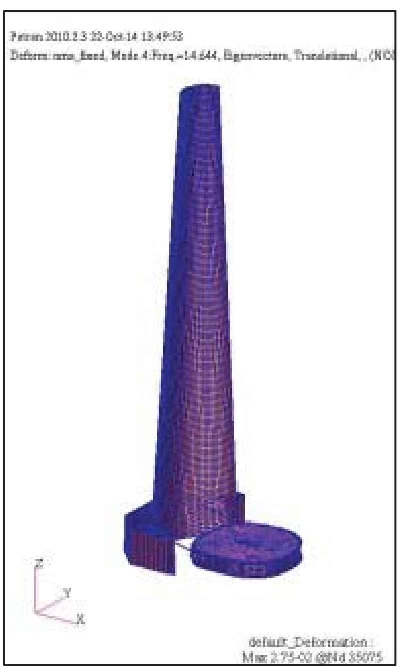 Mode #4: 14.6 Hz MMA X-direction **STR-040**: 12 Hz ≤ f ≤ 16 Hz	 Mode #5: 28.9 Hz MMA Z-direction **STR-050**: 28 Hz ≤ f ≤ 34 Hz	 Mode #7: 68.6 Hz SC axial Z-direction **STR-030**: f ≥ 27 Hz

Figure 9-15: Main modes at SC level

9.3.2.4 SC FMS thermo-elastic distortion

In order to verify the need for on-board metrology (OBM) for pointing the mirror to one of the instruments detectors, a thermo-elastic analysis was run at SC level. A temperature gradient of 1K over 2.624m distance was defined in the X-direction, see Figure 9-16. The resulting thermo-elastic displacements are plotted in Figure 9-16 as well. The displacement results for the FPM interface plane are collected in Table 9-7. On orbit a gradient of 4 K across the FMS diameter is expected which would lead to a relative displacement between mirror and FPM interface of the order of 168 μm.

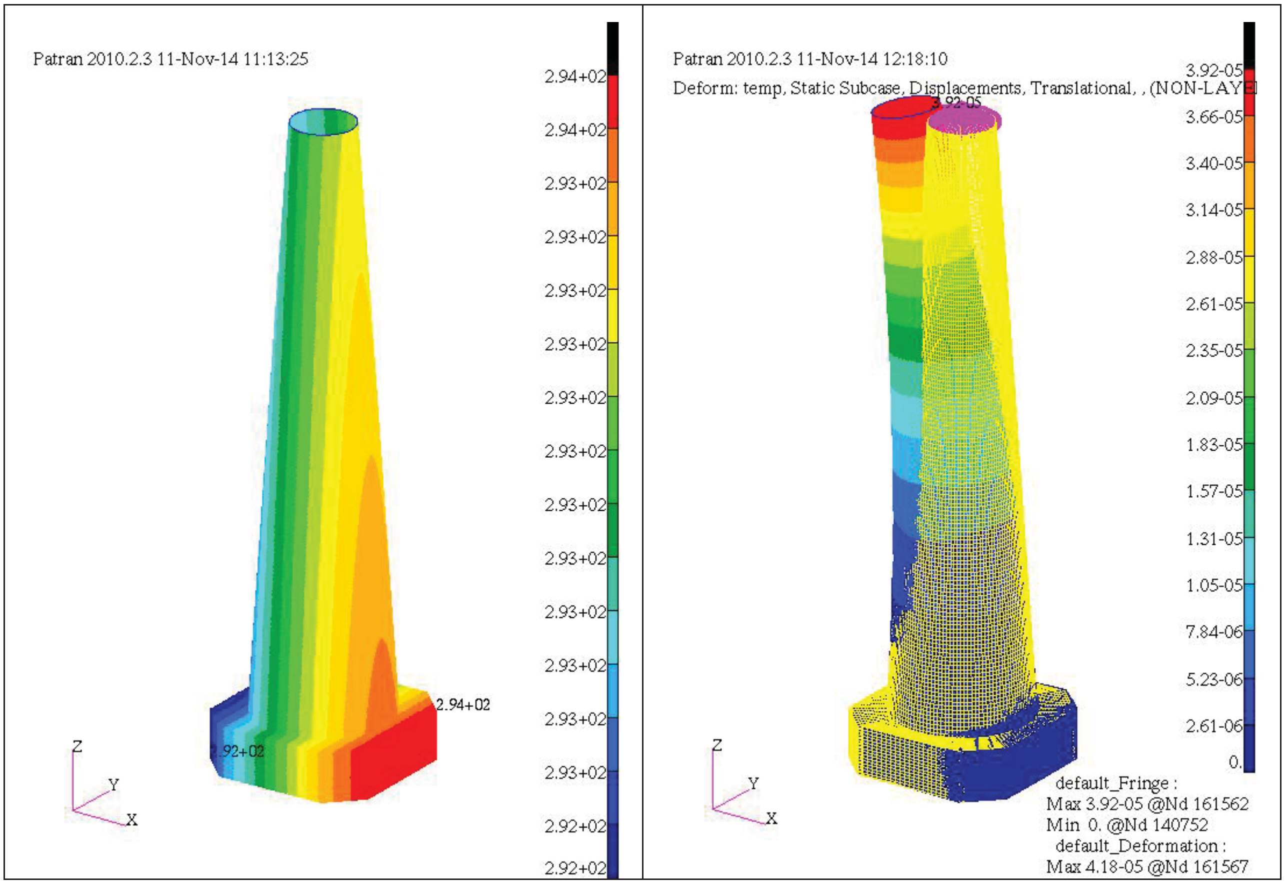

Figure 9-16: Temperature gradient (left) and thermo-elastic displacements (right)

	Gradient 1 K / 2.624 m	Gradient 4 K / 2.624 m
dθ FPM [arcsec]	1.4	5.6
dx FPM [μm]	42	168

Table 9-7: FPM displacements due to SC thermo-elastic deformation

It should be noted that the MIP displacement in lateral direction can be compensated by the MMA hexapod pointing mechanism in case OBM is used.

9.4 List of Equipment

	mass (kg)	mass margin (%)	mass incl. margin (kg)
FMS	468.50	20.00	562.20
FPM	240.00	20.00	288.00
FPM_Str	240.00	20.00	288.00
MAM	650.00	20.00	780.00
MirStr	650.00	20.00	780.00
SVM	190.80	20.00	228.96
SVM_Str	190.80	20.00	228.96
Grand Total	1549.30	20.00	1859.16

9.5 Technology Requirements

The following technologies are required or would be beneficial to this domain:

Included in this table are:

- Technologies to be (further) developed
- Technologies available within European non-space sector(s)
- Technologies identified as coming from outside ESA member states.

Equipment and Text Reference	Technology	Suppliers and TRL Level	Technology from Non-Space Sectors	Additional Information
FMS cone sections	Fibre placement or filament winding to minimise mass	AIRBUS DS CASA Espacio, Madrid, Spain, TRL 8-9		Helps to reduce SC bending moment
Mirror Structure	Titanium 3D printing	AVIC Heavy Machinery, China, TRL 6		
Mirror Structure	Titanium forging	MT Aerospace, TRL 8-9	US (Lockheed Martin) / European Military Aircraft Industry	
MMA HDRM	HDRM with titanium bipods, NEAs, and embedded hexapod mechanism	AIRBUS DS Toulouse, France, TRL 2		Some heritage from GAIA

10 MECHANISMS

10.1 Requirements and Design Drivers

Subsystem requirements		
Req. ID	**STATEMENT**	**Parent ID**
MEC-010	Angular range: 3.6 deg / Translation range: 750 mm.	
MEC-020	Actuation Resolution: <10 arcsec.	
MEC-030	Line of Sight Stability during image acquisition: <10 arcsec.	
MEC-040	Launch Locking devices: via HDRMs.	
MEC-050	Low shock HDRM shall be used for the launch-lock of the Mirror, <500 g SRS (TBC).	
MEC-060	The Launch-locked position shall allow the observation with one instrument, in case a failure of the HDRMs occurs.	
MEC-070	Dwelling focal locations: 3x total, 2x about 750 mm apart on the Focal Plane, 1x intermediate.	
MEC-080	Number of full strokes: >5000.	
MEC-090	First natural frequency: >1 Hz.	
MEC-100	Motion control bandwidth: >1 Hz.	
MEC-110	Time for full stroke repositioning: <400 s.	
MEC-120	Max exported torque: <100 Nm during repositioning, <1 Nm during science operations.	

10.2 Assumptions and Trade-Offs

10.2.1 Assumptions

For the preliminary studies of the MMA and MIP mechanisms, the following main assumptions have been used:

- Mirror Inertia and Mass: ~420 kg*m2 and ~1200 kg
- Instrument Platform (IP) Mass: ~1300 kg.

The following two important assumptions involve selection criteria belonging to system-level design considerations. They are greatly affecting the design of the MMA or MIP mechanism, as it will be recalled later in the preliminary design descriptions.

The use of an On Board Metrology System to accurately measure the actual position and orientation of the mirror, and provide corrective motion is assumed. This implies that the mechanism position sensors do not need to reach optical-level global accuracy.

It is assumed that a Mechanical Ground Support Equipment (MGSE) is used to support and move the heavy Mirror during possible testing and calibration operations on ground. This implies that the mechanism will not need to support the Mirror mass on ground.

Finally, assumptions related to accuracy and misalignments are addressed. Misalignments are intended as differences between the actual position/orientation of the mirror or the Instrument Platform (IP), and the reference one obtained during the ground calibration. Only deviations related to the mechanism are here considered, that is, deviations measured with the respect to the I/F of the mechanism on the structure and the movable mirror or IP. Misalignments occurring in the metering structure, or within the mirror or IP are therefore out of the scope of this section.

Mirror and IP, supported in orbit by the mechanisms and here considered as a rigid body, can be subject to misalignments in 3 rotational and 3 translational directions.

For the MMA, at least one of the rotations is actuated by the mechanism itself (1-DoF solutions), and therefore shall be corrected with the required accuracy of 10 arcsec. It is understood that the main optical effect which limits the tilt is vignetting. The rotation misalignment around the optical axis of the mirror does not have stringent limitations, since the mirror is axial-symmetric. For 1-DoF solutions, the rotation around the third axis cannot be corrected. Therefore the misalignment has to be kept within the accuracy requirement of 10 arcsec throughout the whole life. For the misalignments along translational directions, the decentring errors will shift the image on the focal plane, while piston motions will create a degradation of the image quality. For the angular accuracy, a requirement for the translation accuracy can also be derived:

$$\Delta x = \Delta\alpha\ f = 48.5 * 10^{-6}\ 12000 = \ 0.581\ mm$$

Where f= 12000 mm is the focal length. The value is also considered for piston (TBC).

In the MIP case, the 3 translation DoF undergo the same requirements as the mirror translations. Rotational misalignments are understood not to be critical, and will not be dealt with.

Multiple DoF solutions will be able to adjust the position of the mirror, or the IP, in different directions, therefore they are more robust with respect to misalignment induced by the structure, mirror or IP deformation.

It is recalled that with an On-Board Metrology system, the actual relative position of the Mirror w.r.t the Instrument Platform (IP) is known with a sufficient accuracy. Corrections are possible by rotating the mirror (MMA case), translating the Instruments (MIP case), and in-general by re-pointing the SC. The purpose is mainly to reduce vignetting, that is, to maintain the X-Ray incoming beam as much as possible orthogonal to the mirror principal plane.

In Figure 10-1, a schematic of the effect of a thin-lens decentring and tilt on the image position is shown, from RD[25]. For first-order accuracy evaluations, the X-Ray mirror can indeed be considered as a thin lens from the optical point of view.

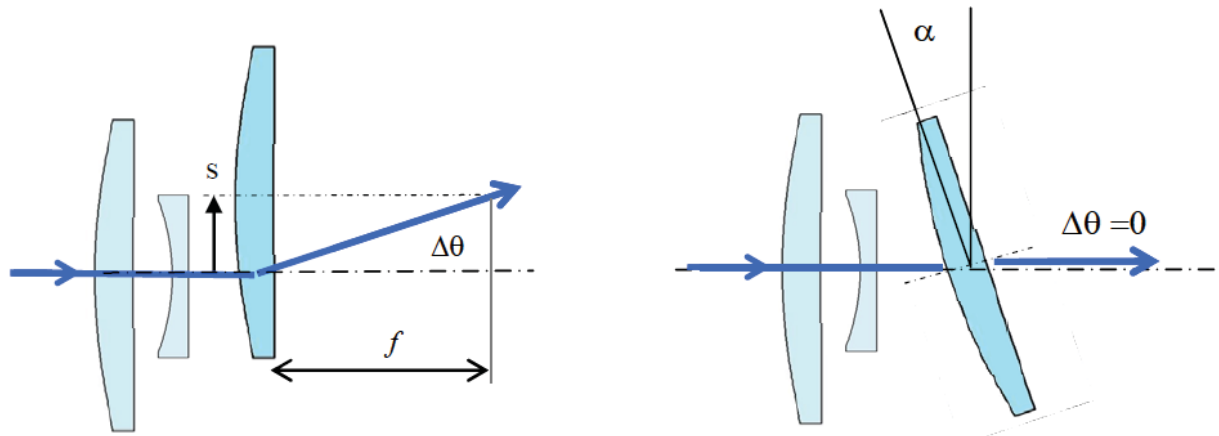

Figure 10-1: Lateral translation of a thin lens by an amount s causes the transmitted light to be deviated by an angle Δθs. Tilt of the thin lens has no significant effect. From RD[25]

Typical sources of misalignments, possibly ordered from the most critical to the least one are:

- Residual difference of bearing loads between ground calibration (with 0-g MGSE) and orbit conditions
- Pre-load relaxation and relative deflections or micro-slippage due to the action of the HDRM, launch vibration, thermal cycles etc.
- Thermo-elastic deformations
- Wear of the balls and bearings races
- Micro-debris coming from the wear of the bearings.

As noted before, manufacturing and assembling errors can be reduced by on-ground calibration and therefore they are not accounted for above.

10.2.2 Proposed Designs and Trade-Offs Summary

The study has followed a bottom-up design approach, in which, several design solutions have been studied and proposed for the mechanisms, and carefully evaluated at system level for the baseline selection of the SC configuration.

The block diagram in Figure 10-2 shows the Trade-off logic. For the main design aspects, different solutions have been studied. The chosen solutions have a red-line connector.

Trade-offs on the left side are performed at sub-system (mechanism) level, while the trade-offs on the right involve selection criteria at system level.

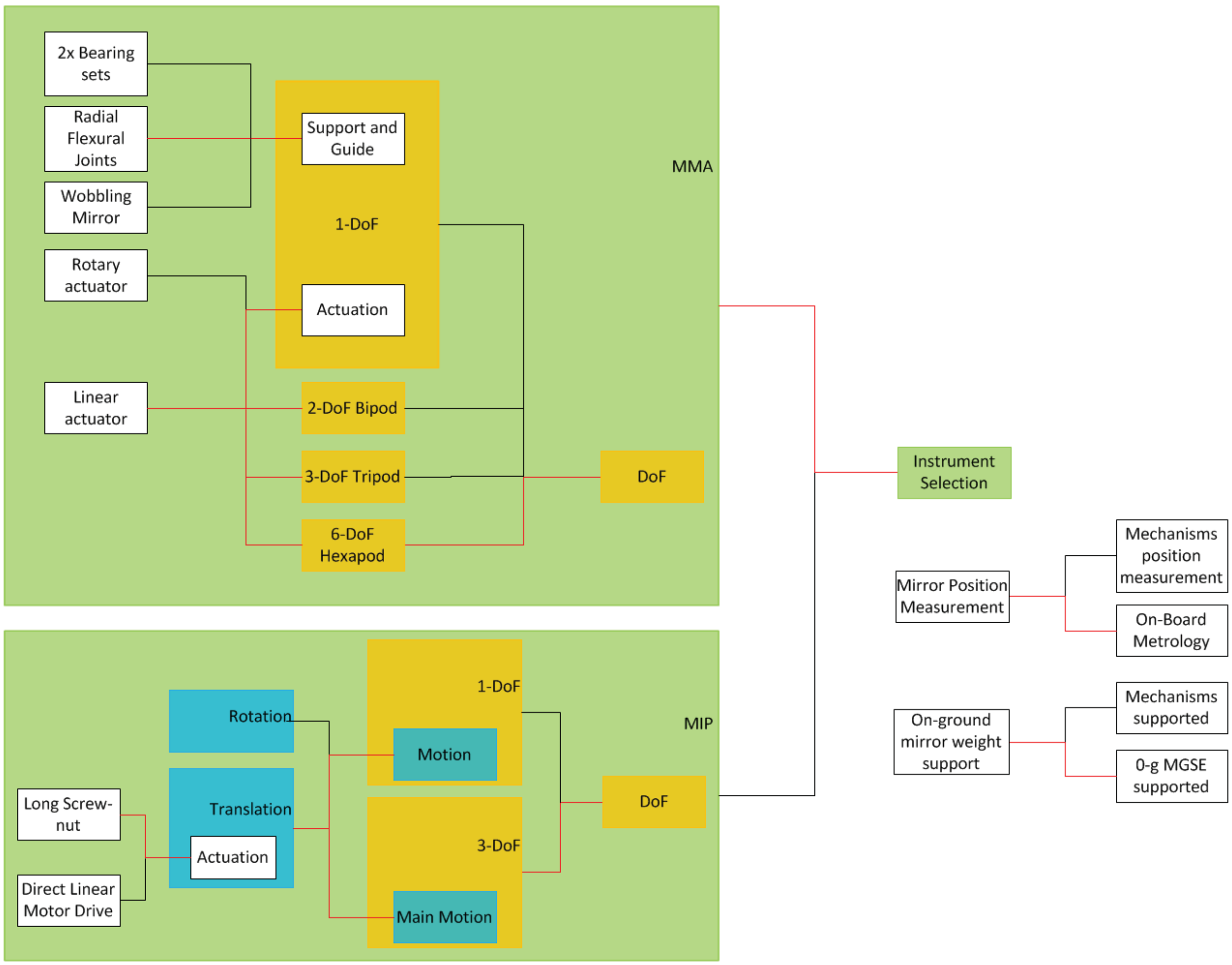

Figure 10-2: Trade-off tree. Each block represents a design solution for various aspects. The red lines represent the selected solutions, black the discarded ones

On the ATHENA SC the following other mechanisms are used:

- Mirror Low Shock Hold Down and Release Mechanism (HDRM)
- Deployable Sun Shield
- Antenna Deployment and Pointing Mechanism (ADPM)
- Solar Array Deployment Mechanism (SADM)
- Outer Mirror Cover
- Venting Mechanism.

These are less critical compared to the MIP or MMA mechanism for the following reasons:

- They have been already evaluated in previous similar studies
- The solutions have a higher heritage and TRL level
- The impact at system level of different design choices is lower.

No trade-offs have been performed for these items.

10.2.3 MMA Mechanism Trade-Off

This section describes the design studies done for the MMA solution. Both 1-DoF and multi-DoF solutions are shown. For the 1-DoF solutions, different options are shown for supporting and actuating (rotating) the mirror. Several design considerations for the 1-DoF solution are also applicable to the multi-DoF ones, like the linear actuator or the flexure joints.

10.2.3.1 Support Design Assessments

10.2.3.1.1 Commonalities

Two design-driving particularities of this application are the large mass of the mirror (more than 1 ton), and its size (about 2.6 m in diameter). Accurate guidance is also needed: an accuracy of 10 arcsec is assumed allocated on the axis orthogonal to the rotational axis, and 500 µm on decentring and piston translation direction. These values do not include the SC metering structure misalignments, and the contribution of the distortions occurring in the mirror itself. The misalignment has to be interpreted as the different between the worst orientation/position of the axis in orbit and the reference orientation/position reached during ground calibration.

For the mechanism to survive launch loads, Hold-Down and Release Mechanisms (HDRMs) need to be used.

The large mass makes the sizing difficult if during ground operations the mirror needs to be supported by the mechanism. As addressed before, it has been assumed possible to use 0-g offloading MGSEs during ground operations. It is believed that this condition could make more complex several AIT operations, or limit the possibilities of some tests. For instance, only testing at subsystem level (modules) could become possible. Anyway at the moment there are not enough details to make a reliable assessment. It is recommended to review this hypothesis in the future phases.

The use of 0-g suspension MGSE for the mirror makes however the requirements for the supporting mechanisms less critical. The sizing requirement becomes mainly the stiffness in orbit. In any case, a comparison with a design for 1-g load support is also presented for some of the solutions.

10.2.3.1.2 2-Bearing Sets

Bearing assembly configuration

A solution made of 2-Bearing Sets is here presented. It is one of the simplest and most widely used configurations to support and guide the rotation of an optical mirror. Such a solution is common in similar type of mechanisms like in scanner applications. It uses commercial off the shelf elements (ball bearings and related parts), and design, development, assembling and testing methods which are found in almost all the mechanisms which need to guide the rotation of an element.

The design foresees the use of 2 pairs of angular contact ball bearings in "X" configuration. The bearing pairs are located at opposite points on the mirror structure, and external to the mirror rim in order to limit the reduction of the optical effective area. Each bearing set supports a short shaft, which is rigidly connected to the mirror structure. The external housing of the bearings is mounted on the telescope tube structure. A conceptual scheme of the solution is shown in Figure 10-3 below.

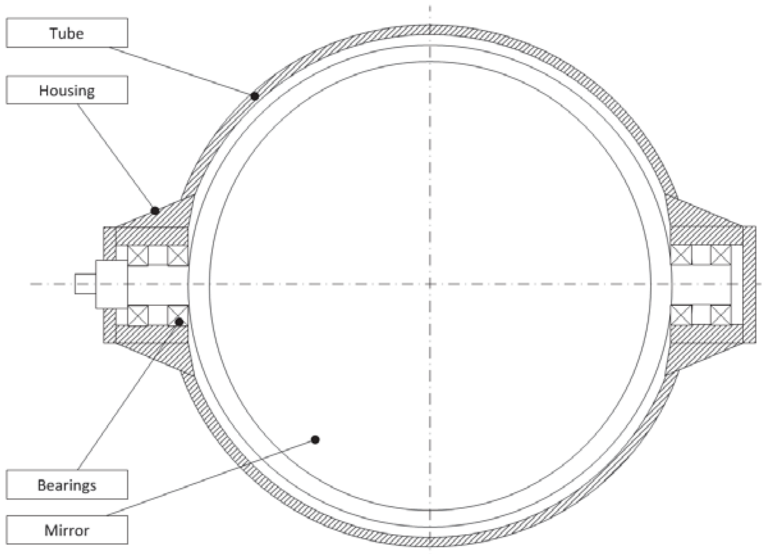

Figure 10-3: Scheme of the 2x Bearing sets Support. Mirror and bearings are not in scale with respect to each other

The Face-to-Face configuration allows any rotational hyperstaticity to be avoided. Each bearing pair is axially preloaded to avoid gapping and hammering during launch vibrations, and to remove any axial or radial play in orbit conditions. One of the pair must be free to axially translate, or shall be mounted on an intermediate housing structure which has a relatively low stiffness along the mirror axis. A conceptual scheme of the bearing assembly is shown in Figure 10-4.

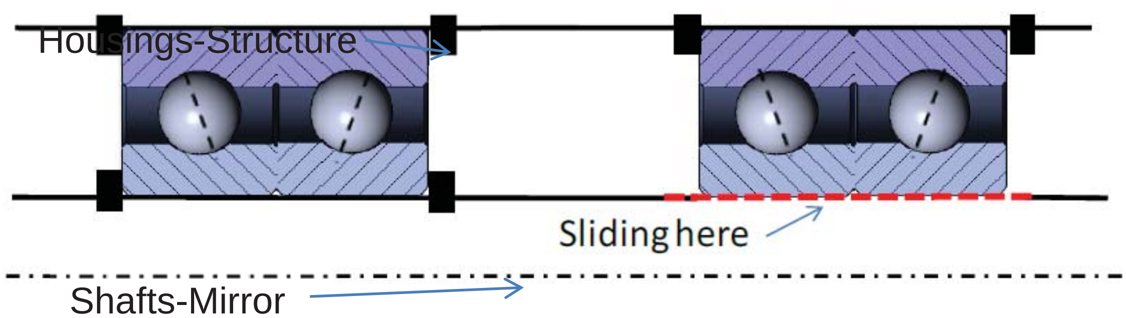

Figure 10-4: Schematic of 2 pairs of angular contact ball bearings assembly, from RD[18]. Each pair is in the Face-to-Face configuration. In this example, the indicated sliding surface will allow to isostatically locate the shaft-mirror structure

Accuracy and misalignments

From the accuracy requirement, the supports have to keep the rotation axis within an angle of 10 arcsec (4.85 μrad). This angle, at a distance of 2.6 m (mirror diameter), corresponds to a radial displacement of 0.126 mm. Each of the two bearing assemblies should therefore have a total misalignment (w.r.t the calibration), including run-out of less than 63 μm. More detailed investigations are out of the scope of this study, but the accuracy requirement does appear to be within the capabilities of typical precision mechanisms.

Lateral decentring and piston error, for what concerns the mechanism contribution, must be kept within 500 μm (focal length × angular accuracy), for both (TBC). Such value is also believed to be in the capacity of the proposed mechanism.

Loads and stiffness

For a preliminary sizing of the bearings, loads and stiffness requirements must be stated. In the assumption that the weight of the mirror is supported by suitable MGSE during ground operations, or else the mirror is fastened to the structure when there is no need to move it, the sizing requirement becomes the stiffness in orbit.

Taking a mirror piston mode as reference for this evaluation, and looking for a first eigenfrequency above 1 Hz, the minimum radial total stiffness for the whole 2x Bearing set assembly is:

$$K_{tot} = (2\pi f)^2 m = 42\ kN/m$$

As for the bearings, each one of the 4 bearings can easily provide a stiffness in the order of 100 MN/m. The total stiffness should not be too high anyway, otherwise the bearings will suffer from excessive loading when the HDRM are active, and the assembly becomes over-constrained. Suitable compliance on the system must therefore be allocated to compensate for possible misalignments in the HDRM interfaces. This can be obtained with a proper structural design of the housings. Assuming a total stiffness of the order of 1 MN/m, and 1 mm of residual (not adjustable) gap in piston for all the HDRM interfaces, the radial load change will be in the order of 1 kN. The size class of the bearing for this application can have radial preloads in the order of 10 kN, which is a value compatible with the load changes assumed above. Another factor contributing to overloading is the effect of thermo-elastic deformation. Again, the order of magnitude of the displacement, considering a piston motion direction, can be assumed as 1 mm, and the same change of load on the bearing mentioned above can be expected.

This is only a first evaluation, since other deformations than in piston shall be accounted as well. Anyway for the scope of this study, the approach gives enough insight about the feasibility and possible implication for other subsystems.

Lubrication, cleanliness, lifetime and friction

A high level of cleanliness is required, since dirt on mirror surfaces can affect its optical performance. In this preliminary study, the use of dry (solid) lubrication can be assumed in the baseline.

This lubrication technology does not ensure the same lifetime as wet (liquid) lubrication, but the number of cycles required (~5000) is limited and therefore not critical. Lead and MoS2 coatings on ball bearings have been already qualified for more than 1 million revolutions, when a moderate to high pre-load is applied. Note that the bearing will have to travel 4 deg. A cycle in this case will comprise a go and back motion of 8 deg, which has to be compared with a full revolution of the tests reported in the literature. Balls and races will experience local wear for the segments of arcs covered by the small rotations.

Liquid lubrication, together with labyrinth seals and a bake-out process, could be allowed if demonstrated that the potential realised quantity of vapour is small enough to be negligible for the vast surface area of the mirror.

A dry lubricated bearing will produce a higher friction torque than a liquid lubricated one. It has however to be noted than as the rotation speed is very low, the lubrication regime will be in the boundary region of the Stribeck curve, and friction coefficient can be close to those experienced for wet lubrication.

Sizing

A basic sizing is here presented to have an estimation of the mass and dimensions.

The bearing ADR 6010H has the characteristics reported in Table 10-1.

Basic designation	6010H
Inner diameter [mm]	50
Outer diameter [mm]	80
Contact angle [deg]	15
Width [mm]	13
Static load, radial [N]	16300
Static load, axial [N]	31400
Mass [kg]	0.252

Table 10-1: Dimension and load capacity of the bearing chosen in the design example

Four of these bearings have to be used, two per each side.

Without going into details with the calculations, it can be said that such a bearing will be able to sustain an axial preload of up to 1000 N if needed, and therefore can even support the weight of the mirror on ground in the radial direction. Mass and size are very limited: the bearings can be easily accommodated into a suitable housing. The bearing preload must be verified against gapping with launch loads. If gapping occurs, the ball and races can undergo high contact stress for local impact loads (hammering), and be damaged by small permanent indentations (brinelling effect). Even if the HDRMs will block the main mass of the mirror, local modes can anyway involve the mass distributed between the closest HDRM and the bearing housing, and, depending on the effective mass involved, it can generate dynamic contact loads on the balls that overcome the preload (gapping) or directly produce plastic deformations due to their intensity. The structural design and the level of preload have to be properly optimised.

10.2.3.1.3 Radial Flexure Joints

A second alternative for the supporting function is to use a series of radial flexural joints to hold the two mirror shafts. Flexure joints or hinges are widely used to support and guide movable parts of high precision mechanisms applications for optics, where small rotation or translation strokes are typically needed.

In this solution, fewer parts are needed compared to the previous one and there is no rolling contact. The latter aspect eliminates the problem of lubrication, wear and friction. The natural linearity of the elastic behaviour of the material improves the accuracy and repeatability of the motion.

Sizing of the Flexure joints has to consider:

- Maximising the stiffness of the constrained DoF, to ensure a suitable high eigenfrequency when in orbit
- Minimising the stiffness of the free DoF, the mirror rotation, to reduce the elastic torque required for the actuator
- Allowing suitable compliance to compensate HDRM I/F misalignments and thermo-elastic distortions without too high internal force being generated.

It is noted that the first and the third requirements are conflicting. A preliminary design has been done in order to demonstrate the feasibility of the solution for this application.

The flexure joint support structure is constituted by 4 flexure joints placed in two sides of the mirror (Figure 10-5) that point in the centre of each side. In Figure 10-6 is shown a detail with two Flexure joints.

Figure 10-5: Schematic flexure joint modelled through lumped parameters. The tubular shape is not representative

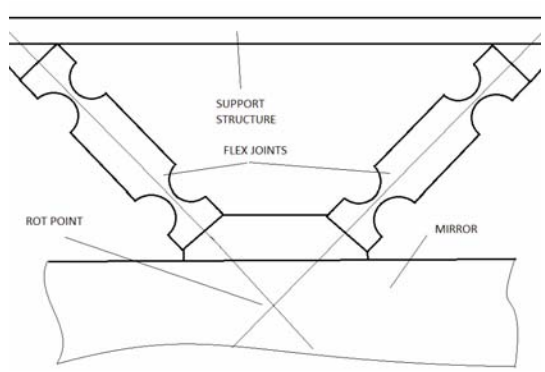

Figure 10-6: Detail of flexure joint support structure

Is this study a solution to obtain a Flexure Joint Support Structure able also to support the mirror during ground operations was sought. This would be a great advantage in simplifying the needed MGSE and reducing the risk of complex AIT operations.

A first study has been conducted modelling the flexure joint through lumped parameters in order to evaluate its dimensions. The flexible characteristics of the joints have been evaluated considering the equivalent stiffness (reported in Table 10-2) of a clamped beam made of titanium alloy. In Table 10-3, the resulting dimensions are given, while Figure 10-7 shows a scheme of the beam model.

Stiffness	Formula
k_x (longitudinal)	$\dfrac{1}{\left(\dfrac{l_m}{2EA_m}+\dfrac{l_b}{2EA_b}\right)}$ = 7.65e7 (N/m)
k_y (lateral bending)	$\dfrac{3EI_2}{l_b^{\,3}}$ = 2.28e8 (N/m)
k_z (piston bending)	$\dfrac{3EI_1}{l_b^{\,3}}$ = 1.38e5 (N/m)
$k_{\theta x}$	$\dfrac{Gbh^3c}{l_b}$ = 4.864e1 (Nm/rad)
$k_{\theta y}$	$\dfrac{3EI_1}{l_b}$ = 5.50e1 (Nm/rad)
$k_{\theta z}$	$\dfrac{3EI_2}{l_b}$ = 8.80e4 (Nm/rad)

Table 10-2: Stiffness formula for a clamped beam modelled with lumped parameters

Configuration	45 deg with respect to the horizontal plane
Length	Total: l_{tot}=300 mm Necks: l_b=20 mm Middle beam: l_m=260 mm
Thickness	Necks: h_b= 1 mm Middle beam: h_m= 4 mm
Width	b= 40
Distance from the center	100 mm

Table 10-3: Final configuration of the flexure joints

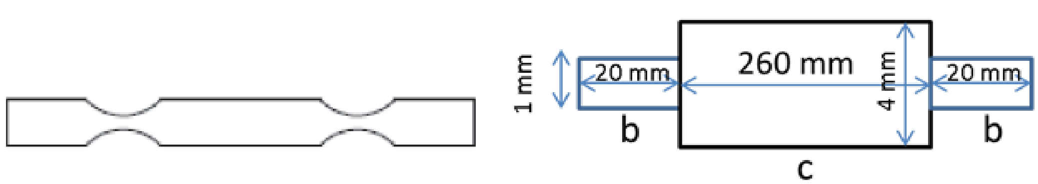

Figure 10-7: Schematic view of the flexure joint: on the left its real shape, on the right, the model made of three beam of different section (not in scale)

In Table 10-4 the first calculated eigenfrequencies for the constrained motions, like lateral, piston and torsion are greater than 1 Hz. The eigenfrequency for the mirror tiling motion, first row, has to be as low as possible, to allow the rotation without producing a high elastic reaction torque.

Frequency	Mode shape
0.14 Hz	tilting
9.3 Hz	lateral
64.2 Hz	piston
91.9 Hz	torsion

Table 10-4: First 4 frequencies of the system constituted by the mirror and by the lumped flexure joints

The torque, that the mechanism motor has to provide to tilt the mirror 2 deg, is about 126 Nm. At this deformation, the stress on the beam is in the range of 40 MPa, which is compatible with the strength of the widely used titanium alloy Ti 6Al-4V.

The simulation shows that the maximum displacements of the centre of mass of the mirror are 0.1 mm and 3 mm respectively in vertical and horizontal ground-configurations of the SC. Therefore, already this preliminary design of the flexure joint assembly can avoid the use of off-loading MGSE.

The flexure joints can be, if necessary, preloaded in traction to further increase their stiffness. To properly balance the pre-loads, they shall be provided with strain-gauges. Adjustment of the flexure joints along their longitudinal direction will allow the rotation centre to be accurately regulated. As for the compliance with respect to HDRM I/F misalignments and thermo-elastic distortions, the stiffness shall be optimised, and if the case reduced, to avoid unnecessary overloading. The modal analysis discussed above shows that there are sufficient margins to spend some of the stiffness in favour of an improved behaviour with respect to these effects.

10.2.3.1.4 Wobbling mirror

A completely different solution from the previous ones foresees the use of a wobbling mechanism, with the main rotation axis the SC vertical axis. The schematic view in Figure 10-8 shows the concept.

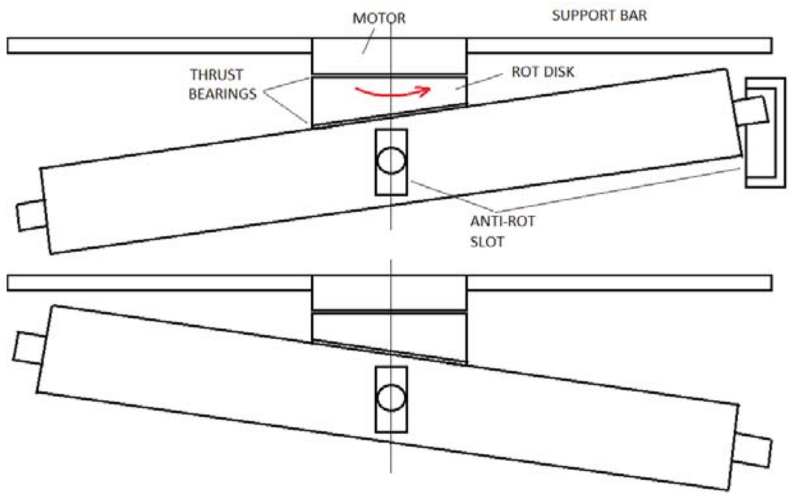

Figure 10-8: Schematic view of the wobbling mirror concept

It consists of a supporting structure (support bars), which holds the motor-bearing assembly located at the centre of the mirror. One bearing set holds the rotation disk in the motor housing. At the other end of the rotation disk, another bearing set holds the mirror. A tilt angle exist between the two bearing sets, therefore as the disk rotates, the mirror wobbles. This wobble produces the desired oscillation of the mirror. In this configuration the mirror needs to be guided by anti-rotation slots.

This solution has the advantage that the large mirror is supported directly at its centre. This would potentially allow a higher stiffness, and a more direct way to support the ground loads in case no 0-g devices are used.

Some disadvantages are:

- Partial cover of the mirror due to the supporting bars
- Need for a central support in the mirror.

During the study, especially the second disadvantage has been considered particularly critical. No further investigations have been done for this solution.

10.2.3.2 Actuator Design Assessments

Two design solutions are presented for the 1-DoF actuation functionality: a rotary and a linear actuator.

10.2.3.2.1 Rotary Actuator

The simplest and most widely used method to perform a rotational motion is by using a rotary actuator. Many solutions exists in space, from scanner mirrors to antenna pointing mechanism, thruster vectoring mechanisms, SADM etc.

Sizing

The main sizing requirements are the accuracy and the rotational stiffness.

From the positioning accuracy of 10 arcsec, intended as stability during the acquisition time, the sensor resolution, and the motion resolution are derived.

An absolute optical encoder with 18 bits, directly mounted on the mirror shaft, can provide a measurement resolution of $2\pi/2^{18}$= 24.0 μrad= 4.9 arcsec.

The drive system is composed of a stepper motor, permanent magnet type with 24 full steps per revolution, a 3-stage planetary gearbox with reduction ratio of 150, and a Harmonic Drive with reduction ratio of 100.

The total reduction ratio is 15000. In this way a step for the motor (input) will correspond to 2π/24/15000= 17.4 μrad= 3.6 arcsec of motion resolution, enough to control a positioning with 10 arcsec accuracy.

The Harmonic Drive such as the Size 50 CSG can provide up to 600 Nm continuous torque (when liquid lubricated), and a minimum stiffness of 250 kNm/rad. Note that with a dry lubricated HD, the output torque can be lower. Specific R&D activities are currently going on about this topic, and data will be available soon. With a mirror having a moment of inertia around the rotation axis of 400 kgm^2, the resulting natural frequency is:

$$f_n = \frac{1}{2\pi}\sqrt{\frac{k_{HD}}{J_{mirror}}} = 3.9\ Hz$$

This value is enough to allow the required controllability, since the motion control bandwidth is in the order of 1 Hz.

The Permanent Magnet stepper motor needs a torque of only 0.05 Nm to generate an output torque of 225 Nm. Here a total efficiency of 0.3 for the transmission has been assumed, considering the dry lubrication requirement. These types of stepper motors have a lower number of steps per revolution than the hybrid ones, but can provide a much higher and repeatable detent torque when switched-off, a characteristic which can be used to save power. As an alternative, a brake can act on the motor shaft during image acquisition (exposure). The use of the detent torque or the brake has to be considered further on, comparing the torque disturbances generated by the AOCS during the steering of the SC, reliability etc. To perform a smooth motion of the heavy mirror, the motor can be controlled in micro-steps.

If the full steps are commanded at a frequency of 10 Hz (corresponding to 25 rpm), the full stroke of 4 deg can be accomplished in about 360 s. Such a low speed has the main advantage to reduce the power consumption. A higher speed can be used if the repositioning time needs to be reduced.

The angular acceleration required for repositioning is very low, the most of the resistive torque will come from the gears and bearing friction, the harness and the anti-backlash device (or the elastic reaction of the Flexure Joints). Therefore the rotational stiffness, rather than the max torque, will be the sizing requirement, as stated in the beginning.

In the case that the mirror is not off-loaded during ground testing operation, the motor has to react to the possible static unbalance of the mirror. For a mirror with the mass of 1200 kg, 10 mm of static unbalance will generate 120 Nm of torque. To reduce this torque to an acceptable level, it can be useful to seek for an adjustment that, adding small ballast mass, orients the eccentricity vector (from CoG to the rotation axis) to be vertical, and the keeps CoG under the rotation axis. It can be argued that the elastic displacement of the structure under gravity load will already act in favour of these conditions.

The motor, planetary gearbox, harmonic drive, sensor, housing and brake can have a total mass of 20 kg.

Accuracy and Backlash

The planetary gearbox can have a backlash of 18 arcmin (see Phytron VSS Extreme Environment Stepper Motors RD[20]). This corresponds at the output shaft to 10.8 arcsec. Hence, an anti-backlash device is needed to comply with the needed accuracy. The support solution which uses the flexure joints has an intrinsic anti-backlash functionality due to the elastic reaction provided. Otherwise the anti-backlash can be obtained via a rotational spring. The HD has no significant backlash, but a smaller stiffness when the torque is low, which is the minimum stiffness used before.

Lifetime

About 5000 go-and-back cycles, and therefore 4*2*5000 = 40000 deg = 111 output revolutions are required as objective. The input shaft of the gearbox has to accomplish 1.7 Mrev. This value is close to the actual limit of dry-lubricated gearbox lifecycles. About the HD, the small rotation means that always the same teeth are working, therefore 5000 go-and-back cycles have to be compared with 10000 full revolutions. Also this value is close to the actual limit of lifecycles for dry lubricated gearboxes.

Other components

The rotary actuator must be completed with the following elements:

- Brake
- Preloading / play recovery device
- 2x “soft” mechanical end stops: due to the high inertia of the mirror, the action of the mechanical end stop must be gradual, to avoid high forces. These end-stops cannot be used for accurate referencing
- 2x limit switches
- Position sensor
- Coupling joint: Oldham or other flexible joint, which transmit the rotation to the shaft, while allowing small relative translations and rotations.

10.2.3.2.2 Linear Actuator

A linear actuator can be used in combination with one of the supporting solutions illustrated before. Mounted at a certain offset with respect to the rotation axis, it will provide with its elongation, the necessary tilt range to the mirror.

The linear actuator presented here is made of a Permanent Magnet Stepper Motor, a Planetary Gearbox, and a Ball-Screw spindle-nut.

It must be mounted in an assembly (Linear Actuator Assembly) which includes suitable flexure joints at the ends. The flexure joints are needed to allow the small relative rotation of the linear actuator with respect to the structure and the mirror. They provide a decoupling without sliding and contact friction, therefore high reliability and precision is ensured. Another function is to be compliant enough to avoid that HDRM I/F misalignments and that thermo-elastic distortions would generate dangerous loads on the bearings. Their axial stiffness needs anyway to be high enough to obtain an eigenfrequency higher than 1 Hz (indicative), when in operation in orbit.

As for the case of the rotational actuator, the stiffness, axial in this case, will be the driving sizing requirement, together with accuracy and motion resolution.

Assuming the actuator assembly placed at the rim of the mirror, about r= 1.3 m from the axis of rotation, a rotational stiffness of 250 kNm/rad will allow to reach 3.9 Hz for the first eigenfrequency, as seen for the case of the rotational actuator. The axial stiffness for the actuator assembly is:

$$k_a = \frac{k_r}{r^2} = 150\ kN/m$$

Therefore, the axial stiffness of the actuator and the two flexure joints, when combined in-series, shall be higher than this value.

To avoid hyperstaticity in the axial direction, one of the two flexure joints shall have a lower stiffness than the other. A combination that can be assumed for the stiffness is shown in Table 10-5, with the calculated actuator natural frequency and the axial load it undergoes when a 1 mm offset in the HDRM interface occurs. It has been assumed a mass of 10 kg for the whole assembly (probably conservative). To perform an angular stroke of 4 deg (+/- 2 deg), the linear actuator needs to extend about 90 mm.

Actuator mass	m_{act}	10	kg	
Actuator stiffness	K_{act}	3000	kN/m	
Compliant Flex joints stiffness	$K_{flex,c}$	200	kN/m	
Stiff Flex joints stiffness	$K_{flex,s}$	1000	kN/m	
Total stiffness	K_{tot}	157.9	kN/m	$\frac{1}{\frac{1}{K_{act}} + \frac{1}{K_{flex,c}} + \frac{1}{K_{flex,r}}}$
Flex parallel stiffness	K_{par}	1200	kN/m	$K_{flex,c} + K_{flex,r}$
Actuator eigenfrequency	$\omega_{n,ac}$	346.4	rad/s	$\sqrt{\frac{K_{par}}{m_{act}}}$
Actuator eigenfrequency	$f_{n,ac}$	55.1	Hz	$\frac{\omega_{n,ac}}{2\pi}$
HDRM I/F offset	h_{hd}	1	mm	
Force from the HDRM offset	F_{hd}	157.9	N	$h_{hd} K_{tot}$

Table 10-5: Linear actuator and flexure joints axial stiffness

There are very few space applications of linear actuators, and no significant data has been found for the size needed. In order to have a partial assessment of the characteristics and specifications for such a component, similar actuators used in industrial applications have been assessed. For example the SKF series CASM 32 BS, has a screw diameter of 10 mm and a pitch of 3 mm. The manufacturer specifies a max static force of 700 N on the spindle, which could be compatible with the load requirements, considering space-environment related factors for dry-lubrication and pre-load. The following table shows the assumptions and results for the calculation of the resolution and output force, which depends also on the assumed motor (input torque).

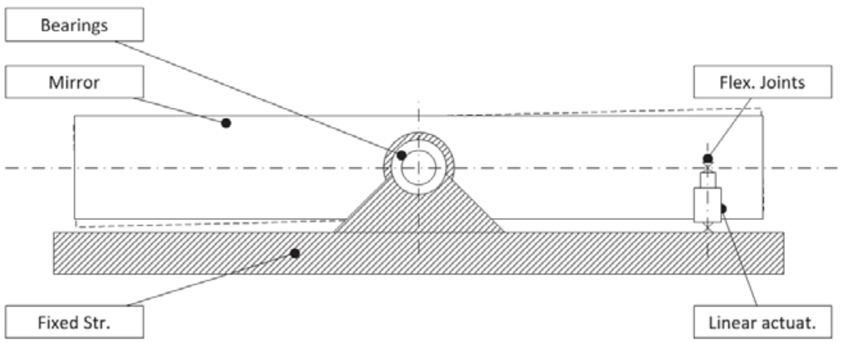

Figure 10-9: Scheme showing the conceptual design of a mirror tilting mechanisms motorized by a linear actuator

Figure 10-10: Example of industrial linear actuators, SKF (left) and ISP System (right), RD[22]

Arm	b_{arm}	1.3	m	
Stroke required	h_{la}	90.7	mm	$b_{arm} r_{range}$
Pitch	p_{la}	3	mm	
Revolutions per stroke	n_{rev}	30.2	rev	$\frac{h_{la}}{p_{la}}$
Reduction ratio	$r_{red,la}$	5	-	
Steps per stroke	$n_{st,la}$	3627	steps/ stroke	$r_{la} n_{rev} n_{strd}$
Resolution, translation	r_{res}	25	µm	
Resolution, rotation	$r_{res,rot}$	19	µrad	
Resolution, rotation	r_{rot}	3.97	arcsec	

Input torque	T_{in}	0.16	Nm	
Gearbox+spindle efficiency	$\eta_{gb,sp}$	0.5	-	
Force, output	F_{out}	133	N	$T_{in} a_{gb_{sp}} \frac{r_{red,la}}{p_{la}}$
Torque, output	T_{out}	173	Nm	$F_{out} b_{arm}$

Table 10-6: Linear resolution assessment

The efficiency assumes all the bearings and gears are dry-lubricated. The motion resolution is compliant with the accuracy requirement.

No data about the axial stiffness is available for this size of actuator. Comparisons with other applications and sizes, and assumptions on scaling factors, show that the assumed stiffness should be reachable with the proposed size. Otherwise a bigger actuator must be adopted.

The spindle nut needs to be preloaded in order that the vibration loads during launch do not damage the bearings and the races. The same shall be done for the ball bearings supporting the screw.

A stepper motor of the Permanent Magnet type is chosen, with 24 steps per revolution. The same criteria described for the rotational actuator apply also here. The needed reduction ratio can be realized with a single-stage planetary gearbox.

Lifetime and lubrication

The most critical element for wear resistance and life is the spindle nut, due to the dry-lubrication required by the high cleanliness standard. The choice to use recirculating balls screws is done to limit as much as possible the sliding. By comparison, roller and plain screws are more stiff and load capable, but the contact points undergoes higher level of sliding. No sufficient data is available in the literature to make a comparison to past space-applications and estimate a possible life. It can be calculated that with about 30 revolutions per stroke, and 10000 strokes required, the needed revolutions are in the range of 300000.

Other components

The same additional elements shown for the rotary joint are needed:

- Brake
- Preloading / play recovery device
- 2x “soft” mechanical end stops: due to the high inertia of the mirror, the action of the mechanical end stop must be gradual, to avoid high forces. These end-stops cannot be used for accurate referencing
- 2x limit switches
- Position sensor
- Flexure joints: they shall provide from a kinematic point of view, the same functionality as the universal joint. See next section for further details.

10.2.3.3 Bipod and Tripod Design Assessments

Bipod and Tripod solution use 2 or 3 linear actuators respectively to produce the desired motions, in tip/tilt for the Bipod, tip/tilt/piston from the Tripod.

Bipod

The Bipod uses two linear actuators and one passive support to obtain a 2 DoF tip/tilt motion of the mirror. By locating the support at the rim of the mirror, it follows that one of the rotation axis is not passing through the mirror centre. It is therefore convenient to position the actuators in order that the axis of the main rotation will pass through the mirror centre, and the other axis for minor adjustments can be offset.

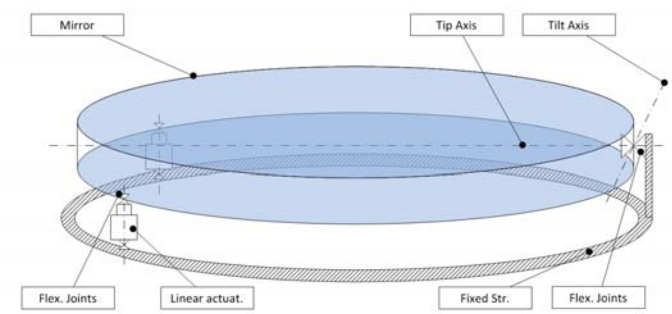

Figure 10-11: Schematic of the Bipod concept, for tip/tilt motions of the Mirror

The linear actuators follow the same design criteria discussed in the previous section. The flexure joint shall allow two rotations, around the axis shown in Figure 10-11. The rotation around the vertical axis must be constrained. From the kinematic point of view, its function shall be similar to the universal joint (or Cardanic joint). Figure 10-12 shows an example of implementation using cross-sections shapes. It has to be noted that the machining of such shapes can be a critical process.

Flexure joints are also to be used as end-joint of the linear actuator. On one side, it shall be the universal joint type, while on the other a spherical joint type (3 DoF rotations allowed). Together with the first flexure joint on the mirror, a kinematic (isostatic) constraint is realized.

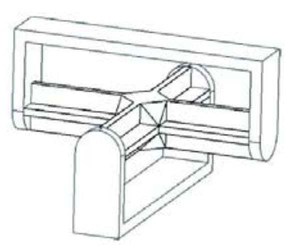

Figure 10-12: Example of a Universal Joint type of flexure joint, made by two cruciform hinges RD[23]

Tripod

In the Tripod solution, the support function is accomplished by the 3 linear actuators. At one end of each linear actuator, a flexure joint of the type of spherical hinges shall be used. At the opposite end, a flexure joint of the type of a universal joint is needed. In this way the mechanism is kinematically determined.

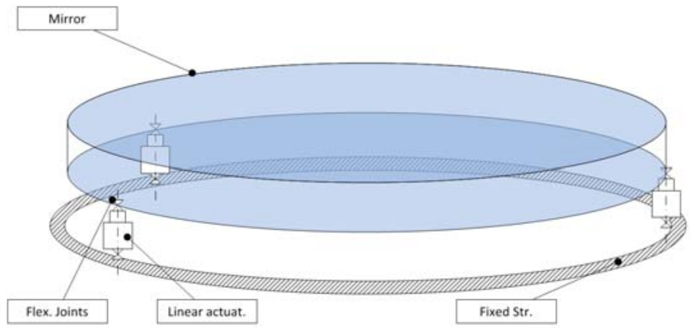

Figure 10-13: Schematic view of Bipod concept, for tip/tilt motions of the Mirror

10.2.3.4 Hexapod Design Assessments

The Hexapod or Steward Platform mechanism is a design solution which allows the motion of the mirror along 6 DoF: tilt around two axes, piston, decentring along two lateral directions, and rotation around the mirror axis. The motion is realised by the axial extension of 6 linear actuators (legs or pods).

Since the mirror has an axial symmetric geometry, only 5 DoF are actually needed. The possibility to rotate around the mirror axis partially allows \ one degree of redundancy, in the event that a linear actuator could fail. It is noted that the rotation needed for one of the tilt is about 4 deg. On all the other DoF, the displacements are of the order of 1 mm, since they are only needed to adjust the misalignments occurring in orbit between the instruments and the mirror.

In Figure 10-14, a scheme of a possible Hexapod configuration is shown. The main rotation which sends the X-ray beam on the different instrument detectors is realized by rotating the mirror around the highlighted axis. If the actuators are placed symmetrically with respect to this axis, it can be seen that the stroke needed for the two located close to the axis (actuators 1 and 2) is smaller than for the other 4. For the same reason, also the required resolution must be smaller. This can be accomplished by a higher reduction ratio on the planetary gearbox, a factor of 8 could be necessary.

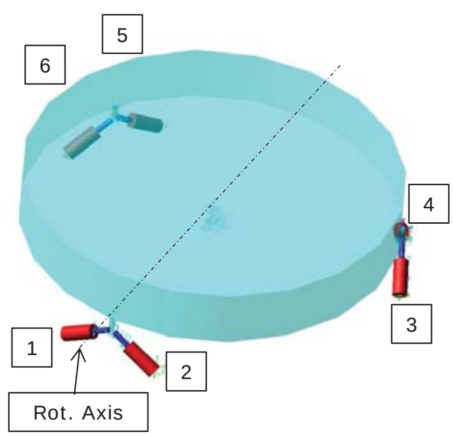

Figure 10-14: Schematic view of Hexapod concept. Main rotation axis is highlighted

They geometrical configuration (legs orientation and location of the attachment points) allows the optimisation of the stiffness (and eigenfrequency) with respect to different modes, and range of travel.

These two properties can be studied using the kinetostatic analysis, from the inverse kinematic of the mechanism. Being as the hexapod is a closed mechanism, the inverse kinematic is a particularly simple expression.

In this tentative design, a first configuration has been assessed. Some of the chosen parameters are shown in Table 10-7.

Angular distance for each bipod	120 deg
Distance of the flexure joint node close to the mirror	100 mm
Distance of the flexure joint node far from the mirror	275 mm
Angle between each element of the bipod	60 deg
Stroke on actuators 1 and 2	6 mm
Stroke on actuators 3 to 4	40 mm

Table 10-7: Main parameters for the geometrical configuration presented in this study

To minimise the envelope of the actuators in the radial direction of the mirror, which would shadow some areas, the ends of the legs are located at the same radius.

With this configuration, the stroke on the actuators have been calculated with the inverse kinematic functions, and reported also in Table 10-7.

As for the assessment of the modal behaviour, a stiffness for each actuator assembly of 100 kN/m has been assumed. This stiffness is the combination of the one of the actuator itself and of the flexure joints mounted at its ends. The same criteria described in the section about the linear actuator are applicable. The resulting eigenfrequencies and mode shapes are shown in Table 10-8. The values estimated in this preliminary design are compatible with the requirement to have the lower natural frequency higher than 1 Hz. The angles of the linear actuators axes w.r.t the vertical axis could be reduced, in this way the Piston mode will increase its natural frequency, while the other eingenfrequencies will decrease.

Frequency	**Mode shape**
1.8 Hz	Piston
2.1 Hz	Lateral X
2.1 Hz	Lateral Y

Frequency	Mode shape
2.8 Hz	Tilting X
2.8 Hz	Tilting Y
5.0 Hz	Torsional

Table 10-8: Eingenfrequencies and mode shape for the hexapod.

The joints connecting the linear actuators to the mirror on one side and to the structure on the other can be made of flexible elements, in the same way described for the previous solutions about the linear actuator, bipod and tripod. One end of the linear actuator shall be of the spherical joint type. The other end shall be a flexure joint of the universal joint type.

10.2.3.5 MMA Mechanism Selection

For the selection criteria of the MMA mechanism, see the System Engineering section (chapter 7). The trade-off driving criteria are coming from system level considerations.

A high importance has been given to the possibility to adjust possible misalignments between the mirror and the instruments occurring from the assembly/calibration on ground throughout the whole life in orbit. In this respect, the 6-DoF Hexapod mechanism has the greatest advantage, and therefore has been selected as the baseline solution for this study.

Anyway, by employing criteria belonging to the mechanisms domain, a selection of the support and actuation solutions described above can be made and discussed.

Among the various support solutions, the one using flexure joint is preferred for its simplicity (few elements), and the absence of point-contact, friction and lubrication. On the other hand, many more applications use the 2x bearing sets type of solution, but this advantage in heritage is not considered sufficient to overcome the advantages of the flexure joints in this case, especially for the high mass of the mirror and the small motion range.

The selection of the actuation system is more difficult, since both the linear and the rotary actuators can apparently satisfy the requirements of accuracy and stiffness. Probably the linear actuator can easily reach a higher stiffness and load capacity, but heritage and availability of the components are in favour of the rotary actuator solution.

Of course, the linear actuator is the only possible actuator solution for the multi-DoF configurations. In these cases, the actuator also accomplishes the support function.

10.2.4 MIP Mechanism Trade-Off

An alternative solution to the problem of focusing the X-Ray beam on different detectors is to shift the position of the instruments, while keeping the beam with the same orientation with respect to the SC.

In this case, the proposed mechanisms are divided in two groups, according to the number of DoF they are allowed to move. The 3-DoF solution actually contains the 1-DoF one as a separate stage.

10.2.4.1 1-DoF MIP Mechanism Assessments

For the 1-DoF case, 2 solutions are proposed. One consists of rotating the MIP around a vertical axis, the second in translating it. The 3 detectors are in line and separated by a distance of 750 mm.

10.2.4.1.1 MIP Rotation Mechanism

The MIP rotation mechanisms has not been deeply investigated during the study, but is only mentioned here in order that it can be reconsidered, if necessary, in the future.

It consists of a main thrust bearing set, made of two angular contact ball bearings, in back-to-back configuration, an actuation stage made of a stepper motor, a gearbox and a pinion-spur gear. The bearings hold the IP and allow its rotation around the main axis of the SC. The motor actuates the spur gear, which is mounted on the IP, thus producing its rotation.

A big advantage of this solution from a mechanical point of view is that the supporting thrust bearing is simpler than linear guides, and the cable wrap would also be simplified.

10.2.4.1.2 MIP Translation Mechanism

The MIP translation mechanism has the function to actuate and guide the translation.

The actuation function can be realized with a spindle-nut ball screws. As highlighted in the description of the linear actuator for the MMA solutions, the main advantages compared to plain screws or roller screws are:

- The low friction
- Limited micro-sliding and hence, better wear resistance.

They present lower load stiffness and load capabilities, but this drawback is less critical than the advantages for this kind of mechanism.

The long stroke of 750 mm necessitates the adoption of a screw of a comparable length. The requirement of keeping the MIP during launch in a location which can be useful for the science observation prevents fixing the MIP at the middle of the length (this is in any case needed to comply with the launcher fairing envelope). Holding the MIP at the extremes of the strokes increases the screw overhang, decreases its first eigenfrequency, and therefore poses some criticality for the survival of launch loads. It has to be noted that the screw has to be held by the balls on the screw-nut.

For cleanliness reasons, the lubrication shall be realized by a solid coating. The constraint is more stringent than for the case of the other actuators described before due to the big length, hence area, and for the fact that there is not a simple solution to provide a seal along the full length. The screw needs to be kept clean as well, and if coated with MoS_2, it needs special protection (N_2 purging) from air oxygen and moisture during storage and ground operations.

The rotation of the screw can be accomplished by a stepper motor, PM type. There is no need for a reduction gearbox, since the resolution requirement can be met thanks to the long stroke and the selection of a suitable screw-pitch.

An alternative for the actuator can be the use of a linear motor. It features the big advantages of removing point-contact elements and critical lubrication needs, and the issue of the launch-locking for the long screw. It needs a more complex control electronic, and care to residual magnetic field which can affect sensitive instruments. Many solutions exist in industrial applications, an example is shown in Figure 10-15.

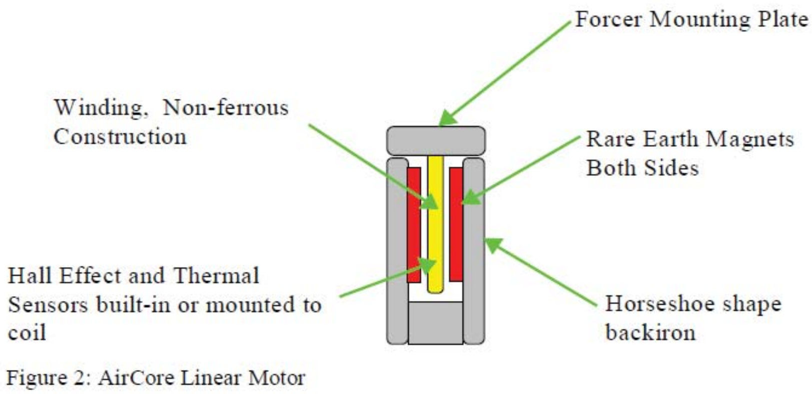

Figure 10-15: Example of a linear motor AirCore type (Parker Hannifin Corp.)

A linear position sensor is needed to measure the location and check the correct functioning of the actuation chain. As for the other cases, the position with respect to the SC reference system is given anyway by the On Board Metrology system.

Limit switches, mechanical end-stops, and an emergency brake complete the set of main components.

As for the guiding functionality, 2 linear guides need to be used. They can be of the type of pre-loaded, recirculating ball guides, or cam-rollers.

As for the case of the screw, a wide area need to be dry lubricated, and kept clean and protected during ground operations. This increases the complexity of the solution.

Care must be taken during the design to avoid hyperstatic configurations of the assembly. The screw-nut together with the carriages on the rails shall have the suitable number of allocated degrees of freedom, or compliances, to avoid that assembly misalignments or thermo-elastic distortions result in excessive loads on the rolling elements. It can be particularly challenging to meet this need, and at the same time guarantee a sufficient stiffness, for such a long linear stage.

Few applications of linear guides have been found in space, and none documented with the size needed for this case. In Figure 10-16, a solution for industrial use is shown.

Figure 10-16: Example of a linear stage for industrial use, with ball-screw and linear guides (from SKF)

Assuming a mass of the MIP of about 1300 kg, the guides could provide enough strength to support the weight during ground operations, especially when the SC is in vertical position (therefore no loads on the screw); otherwise the implementation of off-loading devices appears quite complex. Along the direction of the actuator, the MIP shall be in any case constrained with a brake, since the actuator will be back-drivable.

10.2.4.2 3-DoF MIP Mechanism Assessments

A 3-DoF mechanism, providing the 3 translations along orthogonal axes, has been evaluated. One translation motion, the base has to locate the detectors on the focal point, and its motion range is 750 mm. This stage is assumed the same as the one already described for the 1-DoF MIP. In principle, also the solution with the rotating IP can be applied.

On top of the base stage, fine-adjustment motions of the order of 1 mm and resolution better than 0.05 mm can be accomplished by dedicated stages.

The actuation can be performed by a stepper motor connected with a planetary gearbox which rotates a plain screw-nut. At the interface nut/movable structure, flexure hinges must be placed to compensate with their compliance the small relative motions and to avoid overloading the screw.

Two orthogonally-placed actuation stages are needed. In Figure 10-17, a conceptual scheme of the design is shown. Fine-motion linear actuators are represented with thick arrows. The green actuator performs the vertical displacement. The blue arrows represent the second actuator structure, which provides the same displacement at two points, separated vertically by a certain distance. In this way the actuator structure provides the constraint of the rotation along Z axis. The parallel motion of the two contact points can be realized in a number of ways. One solution is to hinge the actuator structure in order to allow only the rotation around the Y axis. Figure 10-18 shows an implementation of this solution.

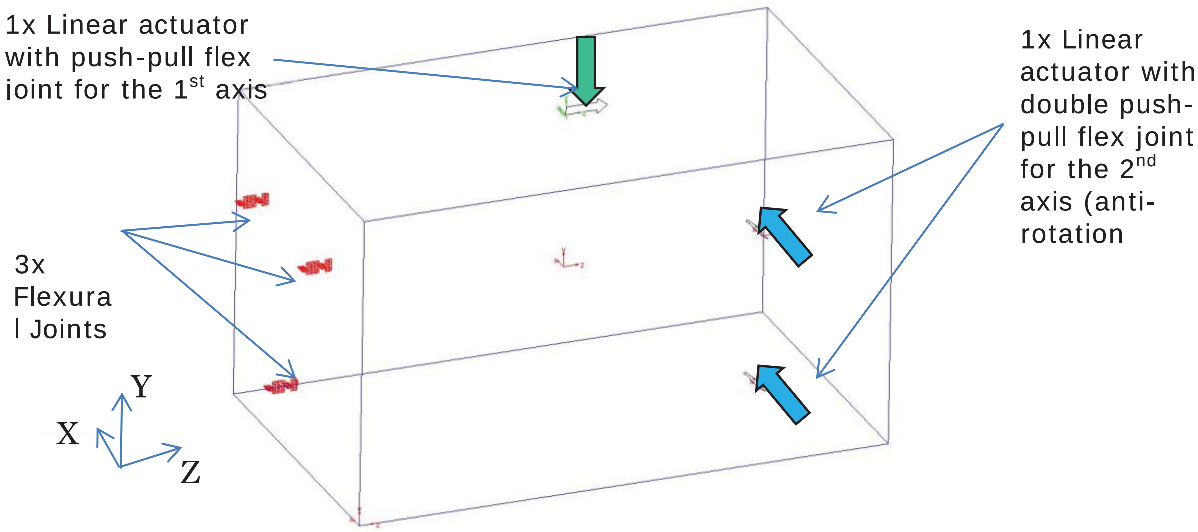

Figure 10-17: Schematic representation of the fine-motion translational stages of the MIP. The green arrow represents the vertical linear actuator, the blue one the displacement provided by the other actuator structure

The guidance function can be performed by suitable sets of flexure joints. They remove any sliding contact, friction and problems of concentrated hertzian stress, therefore they are suitable for a reliable and high accuracy application like this. A critical issue, as mentioned also for the flexure joints described in the previous sections, is the need to provide sufficiently high stiffness, while providing a reduced elastic resistant force to the actuator action. Another requirement is to limit as much as possible the parasitic motion (or cross-talking) between different axes.

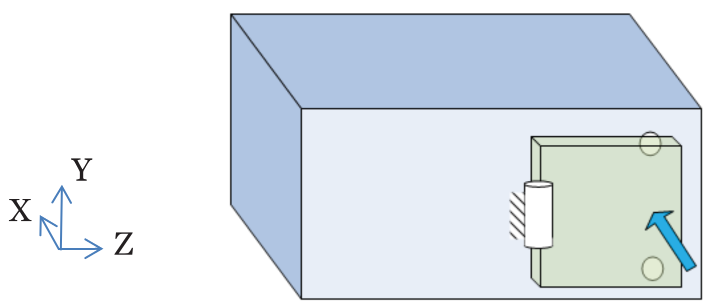

Figure 10-18: Conceptual scheme of the actuator structure which allows the motion along the arrow direction of the moving mass, while constraining the rotation around Z axis thanks to the vertical hinge

A possible solution for the guidance is the one using 3 cross-notched flexure joints, as shown in Figure 10-19. This allows 5 DoF and provides only one constraint, along their axial direction. Three of them, mounted on the same plane, will therefore block the translation along Z, and the rotations around Y and X. The rotation around Z is blocked by the structure of the second actuator, therefore the only remaining DoF is the translation along X and Y, properly defined by the actuators. In this way, a kinematic mount (isostatic) of the instrument panel is realized.

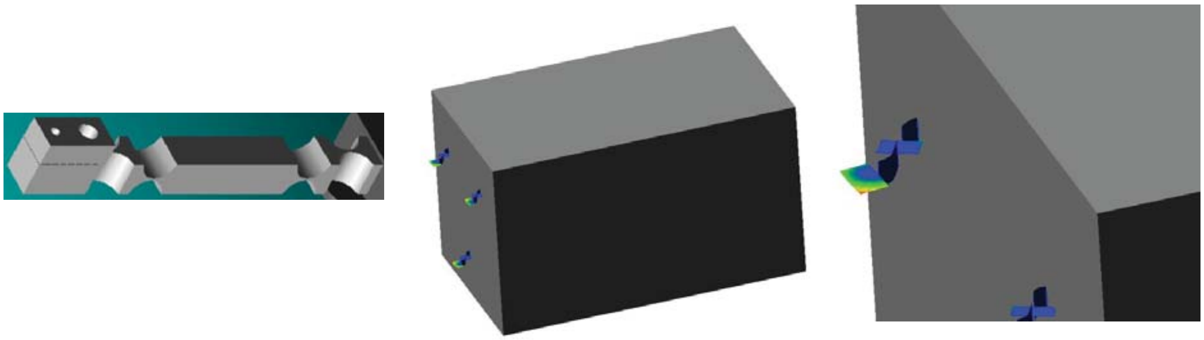

Figure 10-19: On the left image, a Cross-Notched Flexure Joint. In the middle, the model mace of the movable box and the 3 flex. Joints. On the right, a detail view of the deformation of the flexure joints (not in scale). In the FEM model, they have been represented by shell elements

A preliminary sizing of the flexure joints has been performed to assess the stiffness and the natural frequency. The modal analysis gave the lowest eigenfrequency at 16 Hz (rotation), while the max elastic reaction was 30 N. This is the elastic force an actuator has to withstand. The preliminary feasibility is therefore demonstrated.

10.2.4.3 MIP Mechanism Selection

For the selection criteria of the MIP mechanisms, the trade-off driving criteria are coming from system level consideration.

As for the MMA case, the main consideration is that the multiple DoF solution will allow more capability to correct possible misalignments along different directions occurring after ground calibration.

10.2.5 MMA-MIP Mechanism Trade-Off

Apart from selection criteria belonging to system level considerations, from a mechanical perspective the MIP solution appears to be more complex, heavy, and employing elements with less heritage than most of the solutions evaluated for the MMA. At this stage therefore, the MMA solution appears more feasible.

10.3 Baseline Design

10.3.1 MMA Hexapod

The Hexapod preliminary design has been described in a previous section.

10.3.2 Hexapod HDRM

Special attention is given to the HDRM units for the Hexapod. They likely need a preload capability higher than 30 kN, due to the heavy mass of the Mirror. They also need to provide a low level of induced shock, to mitigate as much as possible the risk of damaging the sensitive mirror.

A reference HDRM can be the Low-Shock Release Unit from Ruag Austria. The actual model provides 30 kN of preload, and an induced shock of 500 g. In Figure 10-20, a cut-section of the LSRU is show, from RD[24].

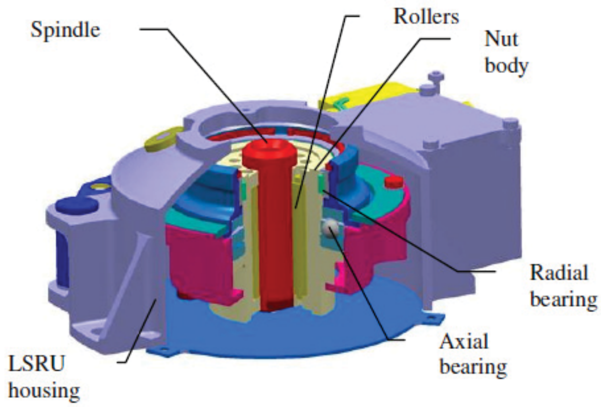

Technical Properties

- Nominal preload:	30 kN
- Max. preload (proof load):	33 kN
- Min. preload (over full stroke):	100 N
- Typical release time at ambient:	< 1 s
- Misalignment capability (half cone):	1.4 °
- Shock output (typically):	500 g's @ 4 kHz
- Qualification temperature range (op.):	- 95 °C / + 120 °C
- No. of actuations before flight:	10
- Mass:	900 g ± 5 %

Figure 10-20: Cross-sectional view of LSRU and main specifications

10.3.3 Deployable Sun Shield

A Deployable Sun-Shield for the mirror, similar to the one used for XMM is here considered. Main characteristics:

- Allows pitch 34 deg
- Sun-Shield mass assumed 90 kg
- Actuated by springs (electrically passive).

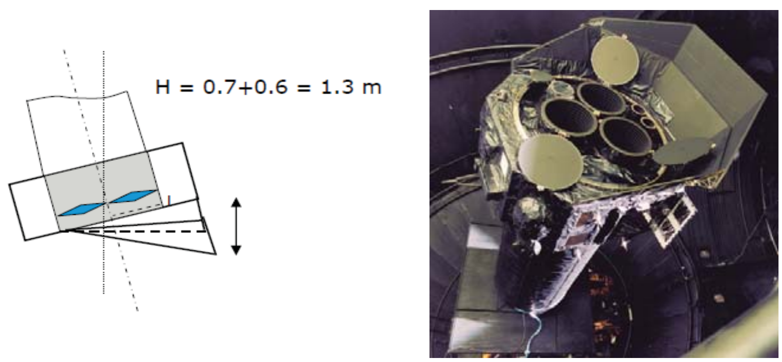

Figure 10-21: Deployable mirror sunshield for XMM

10.3.4 Antenna Deployment and Pointing Mechanism (ADPM)

The ADPM steers the High Gain Antenna (HGA) toward the Earth. The required pointing accuracy is 0.5 deg, and rotations need to be realized in directions (2 DoF).

The HGA is assumed to have a diameter of 40 cm and about 1 kg of mass.

The following main components are assumed:

- Motors: 2x stepper motors (HGAMA APM Rosetta heritage)
- Power consumption (<6 W/DoF)
- 1x HDRM.

The solution adopted for Rosetta is shown in Figure 10-22.

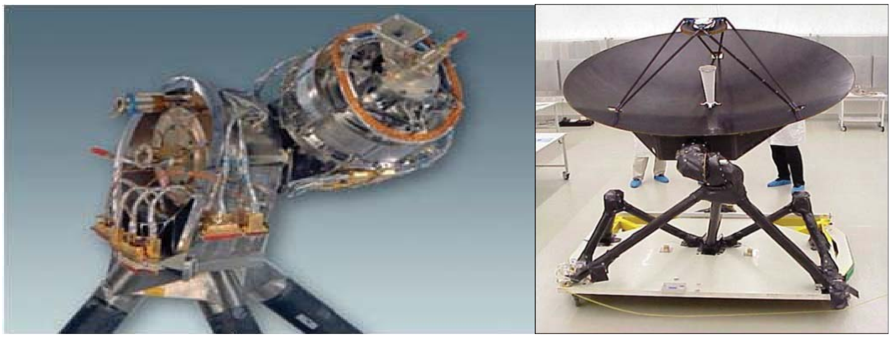

Figure 10-22: Antenna pointing mechanism used for Rosetta

10.3.5 Solar Array Deployment Mechanism (SADM)

The Solar Array is made of 2 deployable solar wings, which remain in fixed orientation after deployment. Each wing has 5 panels, reaching about 30 m² total surface area. A total SA mass of 140 kg, including the yoke, has been roughly estimated.

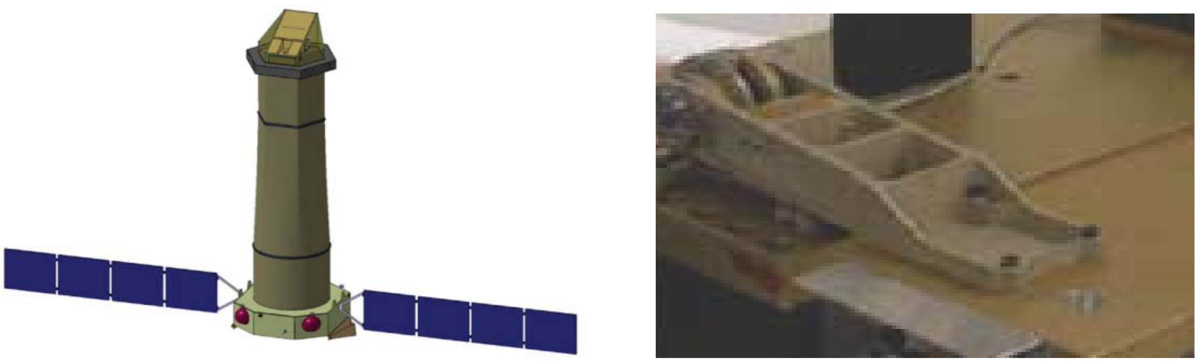

Figure 10-23: Solar Array for ATHENA. On the Right, a detail of a deployment hinge

Also the HDRM unit can be COTS, Dutch Space model for instance. One HDRM takes 60 s to release. The sequence will be 2 HDRM at a time per panel, hence a required power of about 60 W during the deployment time (15Wx2 HDRMx2panels).

The Deployment mechanisms can consist of COTS hinges with redundant deployment springs (5000 Nm/rad) manufactured by Sener, Dutch Space or EADS Ottobrun. It is provided with synchronisation mechanisms (hinges and pulleys) to control the motion of the SA in deployment, see Figure 10-24. Viscous fluid deployment dampers are dedicated to the control of the deployment speed, a purely passive system. Finally, the latching mechanisms embedded in the hinges will ensure a stiff deployed configuration.

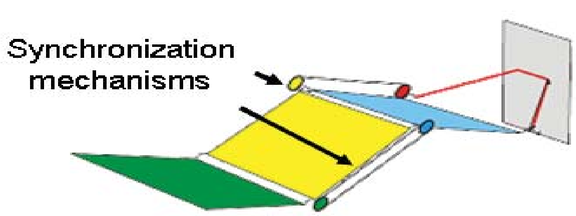

Figure 10-24: Schematic view of synchronisation mechanisms for Solar Array Deployment

10.3.6 Outer Mirror Cover

To mitigate the risk of contamination or accidental damage, the mirror will be protected by an ejectable cover. Main specifications are;

- Separation velocity of 0.5 m/s
- Cover mass 120 kg
- Cover thickness 7mm.

In this study, the cover was assumed made of a flat disc of aluminium alloy and the sizing of the thickness considers the strength need to withstand launcher acoustic loads. Since the mass is remarkable due to the diameter of the mirror, mass saving can be easily performed if an aluminium honeycomb or stiffening ribs, are applied, without significant increase of complexity and costs.

The ejection mechanisms is made of 8 NEA 9101A "extremely low shock" non-explosive actuators and complemented with 8 ejection springs.

It is assumed that the mirror cover can be ejected in compliance with the space debris regulations.

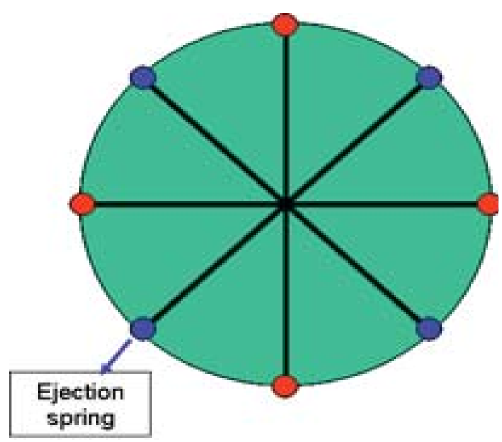

Figure 10-25: Conceptual design of the spring eject-able Mirror Cover, and hold down and release points

10.3.7 Venting Mechanism

The Venting System allows:

- The SC to be sealed against contamination during AIV
- The air to escape during launch
- The prevention of incoming contamination from the CFRP during out-gassing, and the eventual out-gassing of the inside of the SC.

The solution consists of 2x Venting and Outgassing Doors (VODs) and 1x Outgassing Baffle (OGB). Both come from XMM heritage.

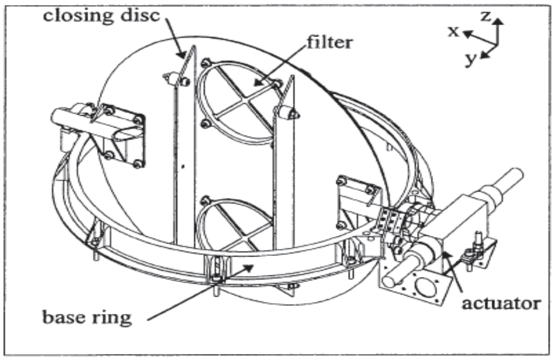

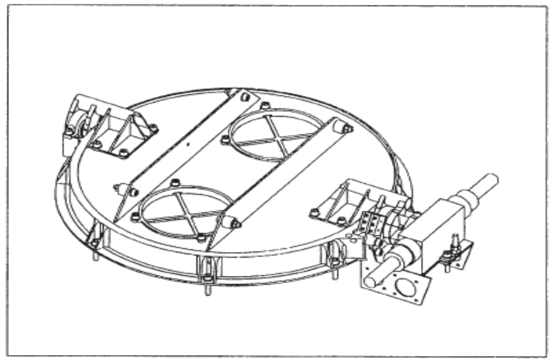

Figure 10-26: Venting mechanism from XMM

10.4 List of Equipment

The following table reports the mass budget for the baseline.

	mass (kg)	mass margin (%)	mass incl. margin (kg)
FMS	**16.22**	**10.00**	**17.84**
Venting_Mech	**16.22**	**10.00**	**17.84**
Hexapod	**36.00**	**18.33**	**42.60**
HDRS_0	**1.00**	**10.00**	**1.10**
HDRS_1	**1.00**	**10.00**	**1.10**
HDRS_2	**1.00**	**10.00**	**1.10**
HDRS_3	**1.00**	**10.00**	**1.10**
HDRS_4	**1.00**	**10.00**	**1.10**
HDRS_5	**1.00**	**10.00**	**1.10**
Lin_Act_0	**5.00**	**20.00**	**6.00**
Lin_Act_1	**5.00**	**20.00**	**6.00**
Lin_Act_2	**5.00**	**20.00**	**6.00**
Lin_Act_3	**5.00**	**20.00**	**6.00**
Lin_Act_4	**5.00**	**20.00**	**6.00**
Lin_Act_5	**5.00**	**20.00**	**6.00**
SVM	**235.30**	**16.27**	**273.58**
ADPM	**4.50**	**17.78**	**5.30**
HDRS	1.00	10.00	1.10
(blank)	3.50	20.00	4.20
Mirror_Cover	**137.00**	**20.00**	**164.40**
HDRS_0	1.50	20.00	1.80
HDRS_1	1.50	20.00	1.80
HDRS_2	1.50	20.00	1.80
HDRS_3	1.50	20.00	1.80

	mass (kg)	mass margin (%)	mass incl. margin (kg)
HDRS_4	1.50	20.00	1.80
HDRS_5	1.50	20.00	1.80
HDRS_6	1.50	20.00	1.80
HDRS_7	1.50	20.00	1.80
(blank)	125.00	20.00	150.00
SADS	**21.80**	**10.00**	**23.98**
HDRS_0	1.50	10.00	1.65
HDRS_1	1.50	10.00	1.65
HDRS_2	1.50	10.00	1.65
HDRS_3	1.50	10.00	1.65
HDRS_4	1.50	10.00	1.65
HDRS_5	1.50	10.00	1.65
HDRS_6	1.50	10.00	1.65
HDRS_7	1.50	10.00	1.65
HDRS_8	1.50	10.00	1.65
HDRS_9	1.50	10.00	1.65
SA_Damper_0	0.40	10.00	0.44
SA_Damper_1	0.40	10.00	0.44
SA_Hinge_0	0.75	10.00	0.83
SA_Hinge_1	0.75	10.00	0.83
SA_Hinge_2	0.75	10.00	0.83
SA_Hinge_3	0.75	10.00	0.83
SA_Hinge_4	0.75	10.00	0.83
SA_Hinge_5	0.75	10.00	0.83
SA_Hinge_6	0.75	10.00	0.83
SA_Hinge_7	0.75	10.00	0.83
Sun_Shield	**72.00**	**10.97**	**79.90**
HDRS_0	1.00	20.00	1.20
HDRS_1	1.00	20.00	1.20
HDRS_2	1.00	20.00	1.20
HDRS_3	1.00	20.00	1.20
SSDM	3.00	20.00	3.60
(blank)	65.00	10.00	71.50
Grand Total	**287.52**	**16.17**	**334.02**

Table 10-9: Mass budget for mechanism subsystem

The following table shows the power budget for the baseline.

Power (W)	P_on	P_stby
FMS	**20.00**	**0.00**
Venting_Mech	**20.00**	**0.00**
Hexapod	**420.00**	**0.00**
HDRS_0	**40.00**	**0.00**
HDRS_1	**40.00**	**0.00**
HDRS_2	**40.00**	**0.00**
HDRS_3	**40.00**	**0.00**
HDRS_4	**40.00**	**0.00**
HDRS_5	**40.00**	**0.00**
Lin_Act_0	**30.00**	**0.00**
Lin_Act_1	**30.00**	**0.00**
Lin_Act_2	**30.00**	**0.00**
Lin_Act_3	**30.00**	**0.00**
Lin_Act_4	**30.00**	**0.00**
Lin_Act_5	**30.00**	**0.00**
SVM	**980.00**	**2.00**
ADPM	**55.00**	**0.00**
HDRS	40.00	0.00
(blank)	15.00	0.00
Mirror_Cover	**320.00**	**0.00**
HDRS_0	40.00	0.00
HDRS_1	40.00	0.00
HDRS_2	40.00	0.00
HDRS_3	40.00	0.00
HDRS_4	40.00	0.00
HDRS_5	40.00	0.00
HDRS_6	40.00	0.00
HDRS_7	40.00	0.00
(blank)	0.00	0.00
SADS	**405.00**	**2.00**
HDRS_0	40.00	0.00
HDRS_1	40.00	0.00
HDRS_2	40.00	0.00
HDRS_3	40.00	0.00
HDRS_4	40.00	0.00
HDRS_5	40.00	0.00
HDRS_6	40.00	0.00
HDRS_7	40.00	0.00

Power (W)		
	P_on	P_stby
HDRS_8	40.00	0.00
HDRS_9	40.00	0.00
(blank)	5.00	2.00
Sun_Shield	**200.00**	**0.00**
HDRS_0	40.00	0.00
HDRS_1	40.00	0.00
HDRS_2	40.00	0.00
HDRS_3	40.00	0.00
SSDM	0.00	0.00
(blank)	40.00	0.00
Grand Total	**1420.00**	**2.00**

Table 10-10: Installed power for mechanisms equipment

Note that the word (blank) in the tables denotes the mass or power that is not accounted for in the lower level elements.

It is noted that most of the power is needed for the command of the HDRM. The reported power is for peak values, only acting when the release is commanded. Only few HDRM are commanded each time, therefore the actual power consumption is not the algebraic sum of all the single HDRM power, this is taken into account with reduced duty cycles in the power budget.

10.5 Options

The various options available in the design are treated in the trade-off section.

10.6 Technology Requirements

The following technologies are required or would be beneficial to this domain:

Included in this table are:

- Technologies to be (further) developed
- Technologies available within European non-space sector(s)
- Technologies identified as coming from outside ESA member states.

Equipment and Text Reference	Technology	Suppliers and TRL Level	Technology from Non-Space Sectors	Additional Information
MMA Hexapod	Linear actuators	TRL 3	Consolidated	Flight solutions to be scaled up, and adoption of dry-lubrication (TBC).
MMA Hexapod assembly	Flexure joints: Universal Joints and	TRL 2	In development for high precision mechanisms.	Shape optimisation, manufacturability,

Equipment and Text Reference	Technology	Suppliers and TRL Level	Technology from Non-Space Sectors	Additional Information
	Spherical Joints types.			possible opportunities from additive manufacturing technologies, compatibility with launch-locks.
Mirror HDRM	Low shock HDRM	Ruag Austria, TRL 4	N/A	Flight solution to be scaled up.
MIP (not in baseline)	Ball-screw, dry-lubricated	TRL2	Consolidated	Long length, launch lock, lubrication and protection.
MIP (not in baseline)	Linear guides, dry-lubricated	TRL2	Consolidated	Long length, launch lock, lubrication and protection.
MIP (not in baseline)	Flexural joints for small motions	TRL4	Consolidated	Flight solutions to be scaled up, compatibility with launch-locks.
MIP (not in baseline)	Linear motor	TRL3	Consolidated	Space environment, residual magnetic field.

11 THERMAL

The thermal subsystem is described in three distinct parts, the Focal Plane Module, the Service Module and the Mirror Assembly Module. Each part is described separately including their unique requirements and assumptions.

11.1 Focal Plane Module

11.1.1 Requirements and Design Drivers

11.1.1.1 Requirements

Concerning the Payload Module, no specific thermal requirement was explicitly stated. Consequently the requirements that were used to drive the design are either classical, or derived from other subsystems:

Subsystem requirements		
Req. ID	**STATEMENT**	**Parent ID**
R1	Maintain the units (including instrument focal planes) in their Operational and Non-operational temperature range during the mission lifetime.	
R2	Guarantee the Thermo-elastic Stability of the Focal Plane Module.	

11.1.2 Assumptions and Trade-Offs

11.1.2.1 Uncertainties and Margins

The temperature uncertainties applied are the following:

- Hot Case:
    - +10K on computed temperature
- Cold Case:
    - -5K on computed temperature (active thermal control)

The following TCS design margin was agreed during the course of the CDF:

- To demonstrate the possibility to accommodate > +15% surface for room temperature radiators
- To demonstrate the possibility to accommodate > +20% surface for Camera Head radiators.

11.1.2.2 Attitude and Orbit

The following orbit and attitude characteristics are of interest for the thermal control subsystem of the FPA:

- L2 Halo orbit without eclipses: has an impact on the external fluxes
- Pitch with respect to the Sun: +/- 34 degrees
- Roll around the axis of the telescope +/-10 degrees maximum, +/- 5 degrees considered during operation.

As a design rule in order to avoid transient effects and problems linked to the thermal stabilisation of the FPA, all the external surfaces of the FPM were designed to avoid Sun impingement in Operational Mode.

11.1.2.3 Design Temperatures and dissipation

11.1.2.3.1 Focal Plane Assembly Platform

The classical way to fulfil requirement R2 is to maintain the whole FPM platform at a constant temperature (+/- TBD°C) during all operational phases of the mission. In order to simplify the integration and verification of the FPA, it is decided to maintain it around ambient temperature in operational mode.

$$\boxed{T_{FPA,OP}=20°C}$$

11.1.2.3.2 WFI Instrument

The information concerning the temperature limits and dissipations to be considered for the instruments are coming from RD[6]:

Parameter Type	Scale	WFI total	CH	DE	FW	ICPU
Equipment Generic Parameters						
Temperature Range						
maximum non-operational temperature	[K]		313	313	313	313
maximum operational temperature	[K]		200	300	300	300
minimum operational temperature	[K]		190	250	273	250
minimum non-operational temperature	[K]		185	240	253	240
Power Parameters						
mean consumed power	[W]	569.5	72.2	6x 72.5	1.0	61.3
power duty cycle	[1]	1	1	1	0.01	1
power margin	[%]	20	20	20	20	20

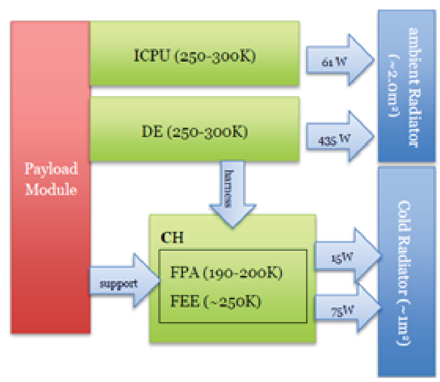

Figure 11-1: WFI Instrument Thermal Constraints

The dissipations of the camera head can be rejected at different temperatures, as described in the sketch on the right.

The first remark that can be drawn when looking at this table is that the camera head requires that a fairly high dissipation has to be rejected at low temperature. This will have an impact on the radiator sizing and the thermal links to be used.

11.1.2.3.3 X-IFU Instrument

The information concerning the temperature limits and the dissipations were collected from RD[6]. The accommodation constraints were transmitted by the System team at the beginning of the project.

		Number of boxes	Minimum Non-operational Temperature (K)	Minimum Operational Temperature (K)	Maximum Operational Temperature (K)	Maximum non-operational Temperature (K)	Number of boxes simultaneously active	Power On (per box) (W)	Possible to move to SVM	Constraints
X-IFU	Dewar	1	200	200	293	303	1	0	No	
	2K JT Compressor	2	223	273	303	343	2	50	No	
	Shield Coolers (compressors)	2	223	253	303	343	2	60	No	Close to the Dewar
	Shield Coolers (Cold Fingers)	2	223	253	293	343	2	90	No	On the Dewar
	JT-Precoolers (compressors)	3	223	253	303	343	3	60	No	
	JT-Precoolers (cold finger)	3	223	253	293	343	3	90	No	
	Filter Wheel	1	243	253	323	333	1	2	No	
	Power Supply Unit	2	243	253	323	343	1	21	No	
	Total Dissipation							**873**		
	CryoAC Warm Front Electronics	1	243	253	323	333	1	5	Yes	Max distance of 2 m from Dewar
	Warm Front Electronics	1	243	253	323	343	1	25	Yes	Max distance of 2 m from Dewar
	Digital Readout Electronics	4	243	253	323	333	4	93.25	Yes	Max distance of 2 m from Warm Front Electronics
	Total Dissipation							**403**		
	CryoAC Back End Electronics	1	243	253	323	333	1	15	Yes	
	First Stage Drive Electronics	1	243	253	323	333	1	79	Yes	
	Filter Wheel Electronics	1	243	253	323	343	1	9	Yes	
	Last Stage Drive Electronics	1	243	253	323	343	1	27	Yes	
	Power Distribution Unit	2	243	253	323	343	1	5	Yes	
	Shield Cooler Drive Electronics	1	243	253	323	343	1	53	Yes	
	Second Stage Drive Electronics	1	243	253	323	343	1	60	Yes	
	ICU	1	243	253	323	343	1	20	Yes	
	Total Dissipation							**268**		

Table 11-1: X-IFU Thermal Constraints

Concerning the temperature limits, some units (e.g. Dewar, JT Precooler) need to be maintained below 20 degC, but others could sustain higher operational temperature.

Nevertheless, in order to simplify the thermal control of the FPM enclosure and be compatible with the requirement of maintaining the FPM platform around 20 degree C, it has been decided to maintain the whole FPM+X-IFU thermal enclosure (Platform, Dewar, Coolers, FEEs, Filter Wheel, PSUs) at 20 degC.

Apart from that the 2 following points can be mentioned:

- The instrument has a high power density (points toward thermo-hydraulic solutions)
- The fact that the dissipative DREs need to be accommodated close to the dewar is a design driver for the thermal control of the FPM baseline design.

11.1.3 Baseline Design

11.1.3.1 Thermal Enclosures

Due to accommodation constraints (size of the radiators, exclusion angles and fairing clearance), it has been decided to separate the instruments between 2 thermal enclosures: the top of the FPM platform that will accommodate mainly the non-electronics part of the instrument and an enclosure below the FPM platform that will accommodate the electronics that need to be close to the Focal Plane Assembly.

- Top of the FPM thermal enclosure:
  - WFI:
    - Camera Head
    - Detector Electronics
    - Support Structure and Thermal Control System associated
  - X-IFU
    - Dewar
    - Coolers
    - Filter Wheel
    - PSU
    - CryoAC Warm Front Electronics
    - Warm Front Electronics
- Electronics Enclosure:
  - WFI:
    - ICPU (2)
  - X-IFU:
    - DRE (4)
    - First Stage Drive Electronics
    - Second Stage Drive Electronics
    - Shield Cooler Electronics
    - Last Stage Drive Electronics.

Note: The X-IFU ICU is considered to be accommodated in the SVM but could be accommodated under the FPM platform if its volume permits it.

For both thermal enclosures, an ESATAN TMS Radiative model was created to compute the radiative links, tune and verify the accommodation. A ThermXL model was then used to calculate the temperatures in order to verify that the predictions (including 10 degree C uncertainties) were compatible with the requirements or design drivers described previously.

11.1.3.2 Top of the FPM Platform

Figure 11-2 describes the accommodation of the radiators around the top of the FPM Platform for both WFI and X-IFU.

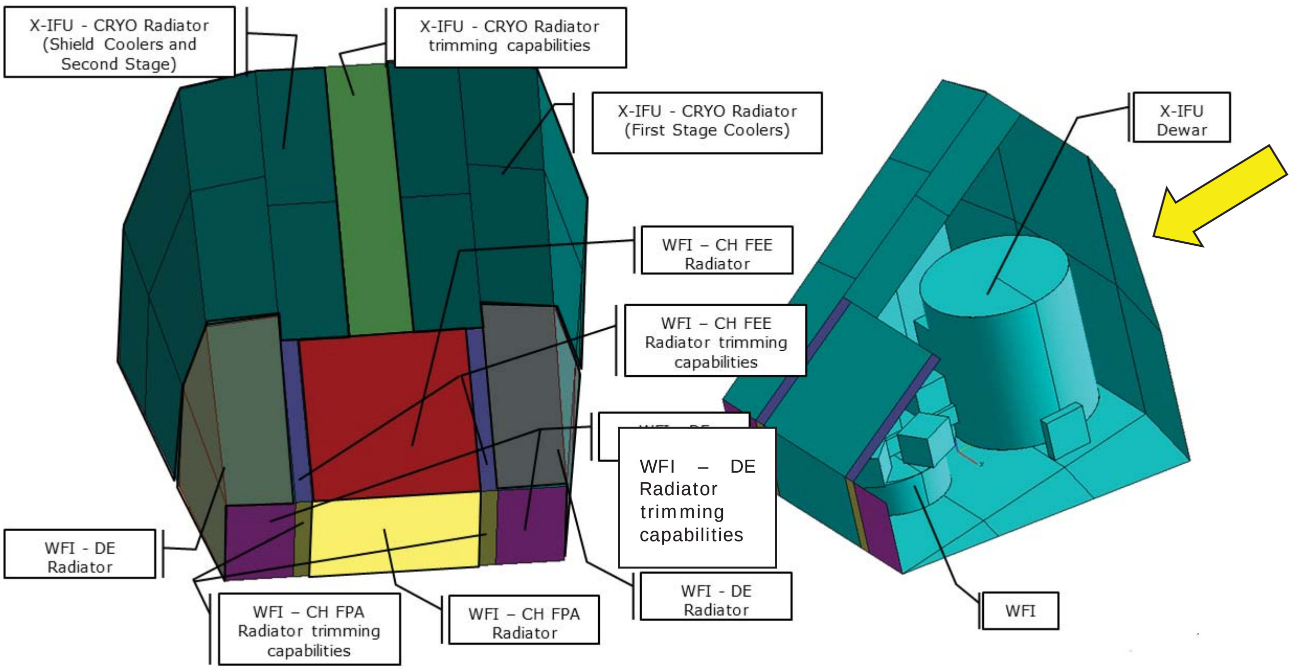

Figure 11-2: Accommodation of the Radiators of the FPA platform

11.1.3.2.1 WFI Radiator Sizing and Thermal Links

Table 11-2 summarises the characteristics of the radiators and trimming capabilities for the WFI. The temperatures reported below include the 10 degrees C of uncertainties:

Instrument	Dissipation	Maximum Operational Temperature (K)	Thermal Link	Temperature of the Radiator (including +10K uncertainties)	Temperature of the element (including +10K uncertainties)	Size of the radiator in the GMM in m2	Trimming area in the GMM in m2 (%)
WFI-CH-FPA	15.00	200.00	Ethane HP (PRISMA, Sentinel 5 p)	193K	196K	0.36	0.072 (20%)
WFI-CH-FEE	75.00	250.00	CNES Low temperature LHP	242K	252K	0.643	0.128 (20%)
WFI-DE	435.00	300.00	1 Double HP per DE	282K	297K	1.92	0.43 (22%)

Table 11-2: WFI Radiators

Note: The slight NC for the temperature of the FEE is due to a lack of time to optimise the surfaces but it seems that the accommodation proposed seems compatible with WFI requirements

The following hypotheses were assumed for the radiators:

- OSR Coated (ε=0.8)
- Radiator efficiency of 85%.

Note: a radiator efficiency of 85% is realistic for big radiators (>0.2 m²) with embedded heat pipes every 15-20 cm, but can be increased at the expense of the mass budget.

The following thermal links were assumed for the different elements of the WFI.

- WFI – DE: 1 ammonia double heat pipe per DE (6 in total).
  - **Heritage**: commonly used in space programs.
  - **Performances assumed**: 1500W/m2K (saddle contact surface) between elements and fluid (both ends) in series with 30W/K conductance for the adiabatic part.

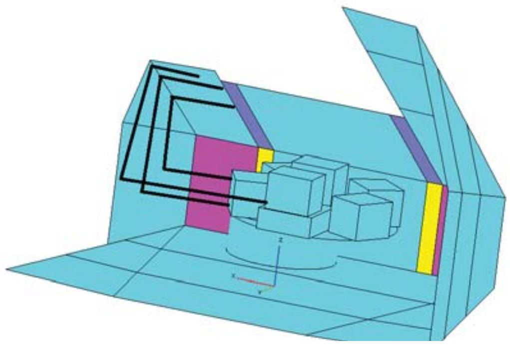

Figure 11-3: Sketch of the Ammonia HPs routing for the DEs

- WFI – CH FPA: 1 Ethane Heat Pipe.
  - **Heritage**: Qualified for Prisma, being qualified for Tropomi.
  - **Performances assumed**: roughly 3 times less conductivity than an equivalent ammonia heat pipe.

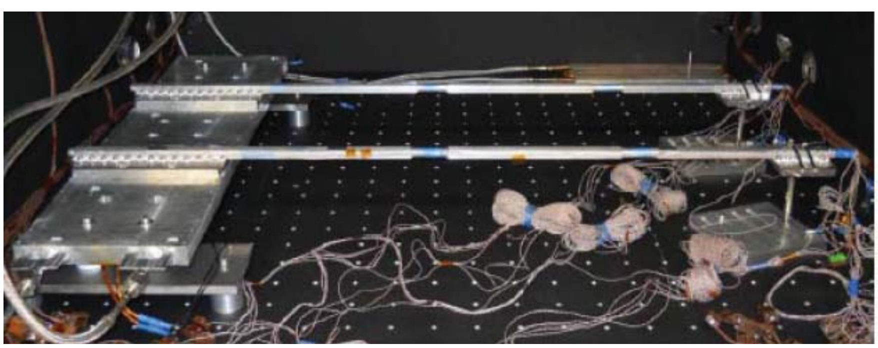

Figure 11-4: Ethane Heat Pipes under test for Tropomi (courtesy ADS)

- WFI – CH FEE: 1 Ethane Loop Heat Pipe.
  - **Heritage**: Characterized by Airbus DS and Iberespacio under a CNES contract.
  - **Performances assumed**: ~7.5W/K.

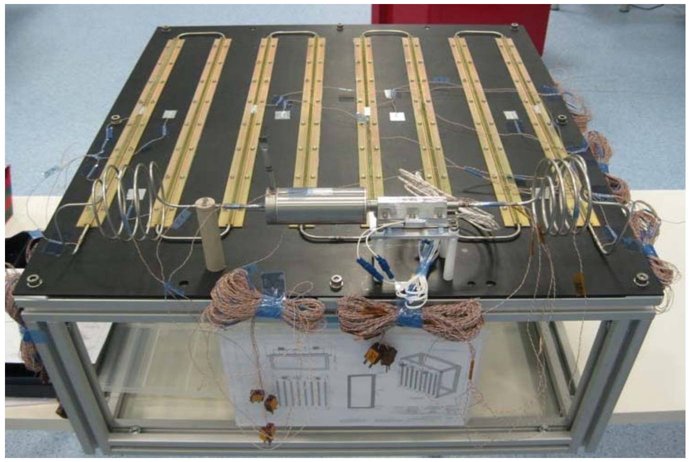

Figure 11-5: Ethane Loop Heat Pipe (Courtesy CNES)

The active heating power of WFI in all modes being included in the power budget provided by the instrument, It has not been evaluated in the frame of this CDF.

11.1.3.2.2 X-IFU Radiator Sizing and Thermal Links

Table 11-3 summarises the characteristics of the radiators and trimming capabilities for the X-IFU. The temperatures reported below include the 10 degrees C of uncertainties:

	Dissipation	Maximum Operational Temperature (K)	Thermal Link	Temperature of the Radiator (including +10K uncertainties)	Temperature of the element (including +10K uncertainties)	Size of the radiator in the GMM in m2	Trimming area in the GMM in m2 (%)
JT Compressors (2 units)	100	293	HPs (2HP per cooler)	274K	285K	2.1	0.4 (19%)
Shield Coolers (2 units)	300	293	HPs (2HP per cooler)				
JT Precoolers (3 units)	450	293	HPs (2HP per cooler)	276K	287K	2.1	0.4 (19%)
CRYO AC WFEE	5	323	Radiative	NA	286	NA	NA
WFEE	25	323	Radiative	NA	286	NA	NA

Table 11-3: X-IFU Radiators

The following hypotheses were assumed for the radiators:

- OSR Coated (ε=0.8)
- Radiator efficiency of 85%.

Note: a radiator efficiency of 85% is realistic for big radiators (>0.2 m²) with embedded heat pipes every 15-20 cm, but can be increased at the expense of the mass budget.

The following thermal links were assumed for the different elements of the WFI.

- X-IFU Coolers: 2 ammonia heat pipe per cooler (14 in total).
  - o **Heritage**: commonly used in space programs.

- **Performances assumed**: 1500W/m2K (saddle contact surface) between elements and fluid (both ends) in series with 30W/K conductance for the adiabatic part.

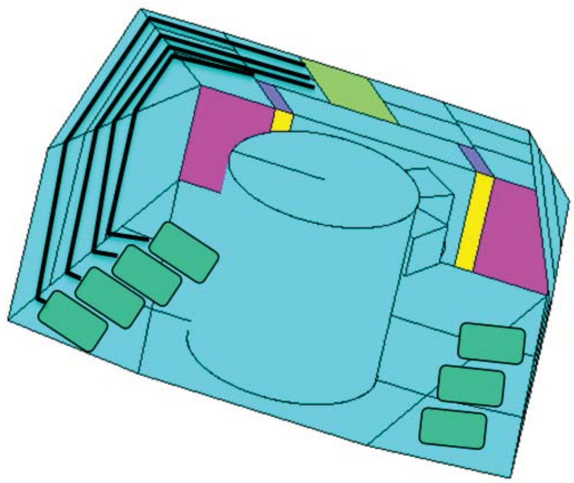

Figure 11-6: Sketch of the Ammonia HPs routing for the Des

Considering the number of heat pipes, the fact that their routing is not trivial and the fact that Pulse Tubes add constraints, a special care needs to be paid for ensuring the on-ground testability of the FPM Thermal Control System. With the configuration presented, the FPM is testable on ground with +Z pointed up (anti- gravity).

The heating power necessary to maintain the FPA Thermal enclosure at -25degC (Non Operational limit +5 degC) is 592W, which corresponds to an installed power of 789W with 75% duty cycle.

11.1.3.3 Electronics Enclosure

The following Instrument electronics are accommodated in a dedicated thermal enclosure located just below the FPA platform:

- WFI:
  - ICPU (2) in Green
- X-IFU:
  - DRE (4) in Red
  - Cooler Drive Electronics in Yellow
    1. First Stage Drive Electronics
    2. Second Stage Drive Electronics
    3. Shield Cooler Electronics
    4. Last Stage Drive Electronics

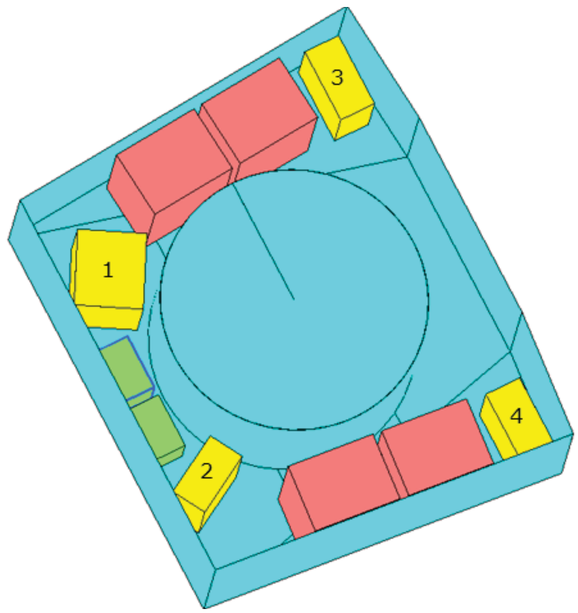

Figure 11-7: Accommodation in the Electronics Enclosure

The walls are considered coupled to the platform but do not need to be structural (as they are not carrying the electronics).

The following tables summarise the Thermal results obtained by simulation with the Electronics Enclosure:

	Dissipation	Maximum Operational Temperature (K)	Thermal Link	Temperature of the Radiator (including +10K uncertainties)	Temperature of the element (including +10K uncertainties)	Size of the radiator in the GMM in m2	Trimming area in the GMM in m2 (%)
DRE (4 units)	373	293	Radiative	230-240	294K	3.75	Depends on the allowable height
CDE First Stage	79	293	Radiative		290K		
CDE Second Stage	60	293	Radiative		283K		
CDE Last Stage	32	293	Radiative		293K		
CDE Shield Coolers	58	293	Radiative		293K		
ICU (2 units)	61	293	Radiative		289K		

Table 11-4: Electronics Enclosure Radiators Sizing

In this calculation, the radiator is assumed to be 0.7m high, but more height will permit to gain some trimming capabilities.

The heating power necessary to maintain the Electronics Enclosure at -25degC (Non Operational limit +5 degC) is 428W, which corresponds to an installed power of 571W with 75% duty cycle.

11.2 Thermal SVM

11.2.1 Requirements and Design Drivers

11.2.1.1 Requirements

Concerning the Service Module, no specific thermal requirement was explicitly stated. Consequently the requirements that were used to drive the design are either classical, or derived from other subsystems:

Subsystem requirements		
Req. ID	**STATEMENT**	**Parent ID**
R3	Maintain the units of the SVM in their operational and non-operational temperature range during the mission lifetime.	

11.2.2 Assumptions and Trade-Offs

11.2.2.1 Uncertainties and Margins

The temperature uncertainties applied are the following:

- Hot Case:
  - +10K on computed temperature
- Cold Case:
  - -5K on computed temperature (active thermal control).

The following TCS design margin was agreed during the course of the CDF:

- To demonstrate the possibility to accommodate > +15% surface for room temperature radiators.

11.2.2.2 Attitude and Orbit

The following Orbit and Attitude characteristics are of interest for the thermal control subsystem of the SVM:

- L2 Halo orbit without eclipses: has an impact on the external fluxes
- Pitch with respect to the Sun: +/- 34 degrees
- Roll around the axis of the telescope +/-10 degrees maximum, +/- 5 degrees considered during operation.

It has been assumed for this rough evaluation of the SVM TCS, that it was possible to accommodate all the radiators in Anti-Sun direction.

11.2.2.3 Design Temperatures and dissipation

For the evaluation of the budget of the TCS of the SVM, it has been assumed that all elements (electronic boxes, propulsion module) shall be maintained around ambient temperature. This assumption is somehow a sizing case but could be realistic if the SVM has some thermo-elastic stability requirements.

$$\boxed{T_{SVM,OP}=20°C}$$

For the dissipation, a rough estimate of 500W has been considered:

$$\boxed{P_{SVM,OP}=500W}$$

11.2.3 Baseline Design

The Thermal Control of the Service Module will rely only on classical solutions: MLI, heating lines, Black Paint, SSM, insulating Stand-Offs. If some units are more dissipative than expected, thermo-hydraulic solutions can be foreseen (heat pipes).

The basic principle is to cover the whole SVM with MLI except dedicated areas which will be covered with radiator coatings (OSR tiles).

Heating lines (composed with Kapton foil heaters, thermistors and thermostat) will guarantee the thermal stability in operational modes and the minimum operational/non-operational temperatures in Safe Mode.

With the assumptions listed previously and considering 20% of trimming capabilities, the necessary radiator surface is the following:

Sradiators =2.4m2

The heating power necessary to maintain the SVM at -25degC (Non Operational limit +5 degC) is 411W, which corresponds to an installed power of 549W with 75% duty cycle.

11.3 Mirror Assembly Module

11.3.1 Driving Requirements

The thermal control strategy of the Mirror Assembly Module (MAM<) is determined by two driving requirements:

Subsystem requirements		
Req. ID	**STATEMENT**	**Parent ID**
R4	The temperature of each mirror module (MM) must be maintained at 20 ±1˚C.	
R5	The thermo-elastic deformations of the mirror structure must be limited such that the scientific requirements are met.	
Based on simulations on the thermo-elastic deformation, the structural engineer has derived the allowable temperature gradients within the mirror structure.		
R5a)	The temperature difference ΔT in axial z-direction through the mirror structure shall remain <3˚C.	
R5b)	The one-directional temperature difference ΔT across the mirror structure shall remain <3.5˚C.	
R5c)	The global temperature variation of the mirror structure shall not exceed ±1.5˚C.	

These preliminary requirements are used as an input for the thermal analysis.

11.3.2 Thermal Model

11.3.2.1 Geometrical Mathematical Model description

The geometrical mathematical model is intended to focus on the mirror structure and the MMs. The remaining parts of the SC are modelled in a very simple way.

<u>SC:</u>

The metering structure is modelled as a cylinder shell (named “tube”) with a length of 12m and a diameter of 2624mm, which is defined by the 2624-launch adapter. The MAM structure has the same outer diameter and is directly attached to one end of the metering tube, which is a simplification of the real configuration. The interface between both defines the x-y-plane of the model. The z-axis is aligned with the focal length, with the <u>negative</u> z-direction pointing towards the instruments.

It should be noted that this coordinate frame definition differs from the SC coordinate frame, in which the x-y-plane lies within the launch adapter plane and the <u>positive</u> z-axis points towards the instruments.

The tube is closed with a radiatively inactive disc (shell name: “top”) on the instrument side.

The whole assembly is surrounded by MLI, which is represented by another cylinder shell, “MLI”, with a slightly larger diameter (2428mm) to allow radiative coupling with the metering structure and the MAM.

The service module is omitted in the model. Hence, the outside of the MAM structure is only insulated from space through MLI in this model. In reality the mirror structure will be surrounded by the service module, which will be maintained at around 20 ˚C. As a consequence the most outer row of MMs and the outer structure part are exposed to harsher conditions in the simulations than there will actually be in reality.

The sun shield is represented by a cylinder, which is diagonally truncated at an angle of 34 degrees. It is attached to the mirror structure at 6 points by user defined conductors. The sun-facing side is covered with black MLI, the anti-sun surface is covered with Single-Layer-Insulation (SLI). The sun shield’s through-conductance value is mainly dominated by the used MLI and therefore set equal to MLI.

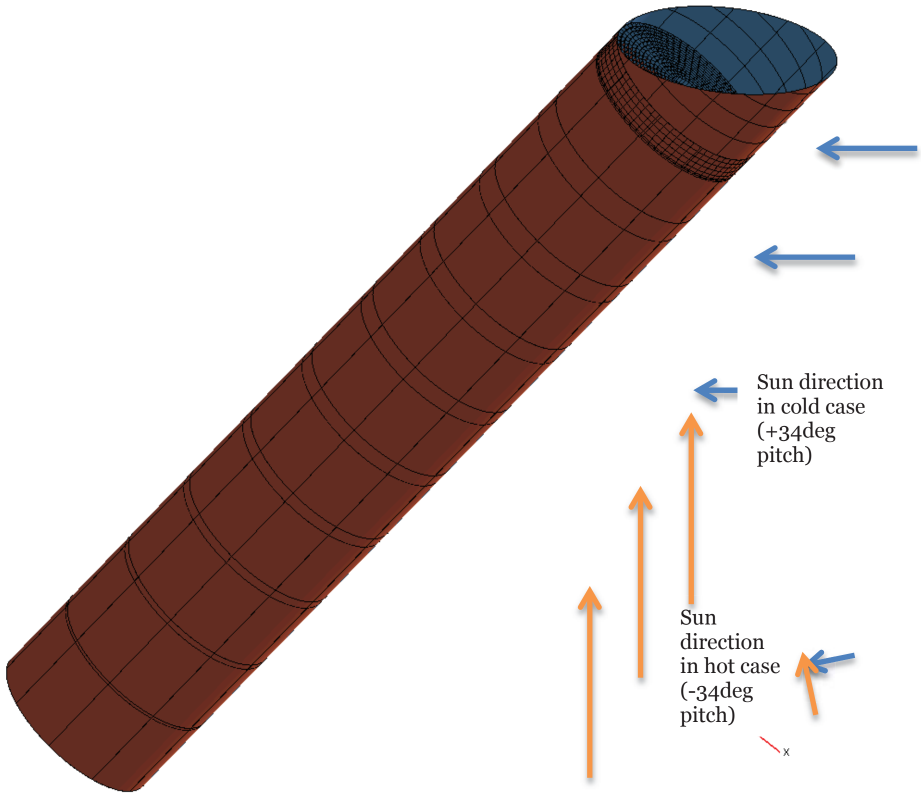

Figure 11-8: Complete Geometrical Mathematical Model for MAM thermal analysis; sun directions for hot and cold case

MMs:

The MAM contains 678 MMs, arranged in 15 rows. The MMs come in pairs of one parabolic MM and one hyperbolic MM stacked together. However, in this model both MMs are combined to only one single node, represented by one box-shell with the dimensions of the stack. The centre of every MM box is located within the x-y-plane.

The bracket, which is used to attach the MM to the mirror structure, is modelled as a user-defined conductor. Its value of 0.03775 W/K is derived from previous ATHENA-studies.

Mirror structure:

Since the mirror structure is a very large and complex shape, the thermal model is built in a way that easily allows the use of automation features. ESATAN-TMS provides a tool, which is able to auto-generate conductive interfaces between two or more shells, given that those shells share a common edge.

This evolves directly to a major guideline for the thermal model of the mirror structure: In order to use the available automation capabilities in the most effective way, every MM is enclosed by four single shells with four common edges. The main drawback of this modelling philosophy is the quite large number of shells/thermal nodes, requiring higher computation time.

Starting point for the mirror structure are concentric rings, which separate the MM-rows from each other. In addition, rectangular shells are arranged perpendicular to these rings, connecting not more than two rings. Their purpose is to separate MMs within the same row from each other.

The concentric rings are set up of many small cylinder segments, each consisting of one single shell. Theoretically, the amount of shells per ring is chosen to be equal to the amount of MMs in the same row.

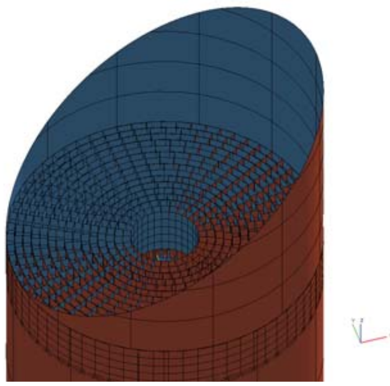

Figure 11-9 Close-up view of the mirror structure and sun shield

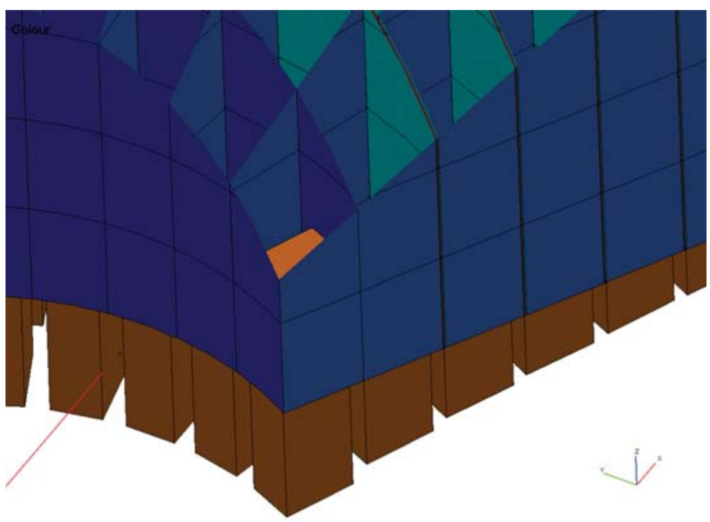

Figure 11-10: Set-up of the GMM: MMs (orange), combined cylinders (dark blue), rectangles (lighter blue), inner and outer cylinders (cyan) with auxiliary cylinders in between (red)

In practice, the amount of MMs per row varies from one row to another. As a consequence, the rings are facing a different number of MMs on the inside than they are facing on the outside.

Each affected ring is now broken down into three separated concentric cylinders with slightly different diameter (±1 mm). This is resulting in one “inner cylinder” (facing only the inside row of MMs), one “outer cylinder” (facing only the outside row of MMs) and one “auxiliary cylinder” in between. Now it is possible to divide the inner ring and the outer ring independently into the desired number of shells.

The thermal links between inner cylinder, auxiliary cylinder and outer cylinder are established by contact zones with a very high conductance value (10000 W $K^{-1}m^{-2}$), while the material of the mirror structure is titanium with low thermal conductivity. The single thicknesses of these three shells sum up to the actual physical thickness of the mirror structure, which is 2.3 mm, according to inputs from the structural engineer. Due to the chosen high conductance of the contact zone, the total through-thickness-conductance is practically only driven by the through-thickness-conductance within the material, but not by the conductive links between the three shells. In this way the through-thickness-conductance of the assembly is in fact equivalent to one single shell with a bulk thickness of 2.3 mm.

In fact there are rings, which separate two rows with the same amount of MMs. For those rings it is sufficient to use only 1 shell with a bulk thickness of 2.3mm. The shells of these rings are then named “combined cylinders”.

The resulting mirror structure can now be easily conductively fused at their edges using auto-generated conductive interfaces.

<u>Material and optical properties:</u>

The assumed material and optical properties assumed for this model are summarised in the tables below.

Component	Material	Conductivity in W/(m K)
Mirror Structure	Titanium	7.8
MM	Silicon	148.9
Tube	CFRP	20

Table 11-5: Material properties

The MLI was assumed to be 20 layer black MLI with an effective conductance of 0.0095 W/K and an effective emittance of 0.0075.

Component	Optical properties	IR emissivity	UV absorptivity
Mirror Structure, tube inside	Black paint (Aeroglaze Z306, EOL)	0.87	0.92
MM	Iridium & B4C Multilayer	0.40	0.40
Tube outside	CFRP	0.80	0.92
Black MLI, Sun shield outside	MLI (black Kapton)	0.82	0.96
Sun shield inside	SLI (VDA coated Kapton)	0.05	0.10

Table 11-6: Optical properties

11.3.2.2 Model hierarchy

The MAM consists of six identical petals or segments. Only one petal was modelled and then copied and moved to the right positions five more times, before being conductively fused. Each segment is a separate sub-model, named from “S1” to “S6”. All other components (MLI, tube, top, sun shield) are assigned to one sub-model “SC” (SC for “SC”).

Each segment S1 to S6 contains MMs, rectangle shells and cylinder shells. The cylinder shells are distinguished by combined, inner, outer and auxiliary cylinders.

Node numbering

The node numbering logic should enable the thermal engineer to immediately identify the node’s position within the model. The position within the model is basically determined by the structural segment, the row of the corresponding MM and its position within the row.

Each node number consists of the sub-model identifier and 8 digits:

Submodel : X XX XX X XX

Digit	Description	Value
Submodel	submodel identifier	S1, S2, … S6, SC
1st digit	indicates shell type	1 MM
		2 aux cylinder
		3 inner cylinder
		4 outer cylinder
		5 combined cylinder
		6 rectangle
		7 tube
		8 MLI
		9 sun shield
2nd and 3rd digits	indicate the position (row number)	00…15
4th and 6th digits	indicate position within row, starting from the right	00…99
7th digit	defines shell side	1 outside
		2 inside
8th and 9th digit	node number increment	00…99

Table 11-7: Node numbering logic

Example: **S3:40803104** (Sub-model S3, outer cylinder, 8th row, 3rd position from right, outside, node 04)

11.3.2.3 Orbit

ATHENA is placed in a L2 halo orbit. The orbit is modelled as a sun-centred circular orbit without taking into account any albedo or infrared heat fluxes from Earth. ATHENA’s attitude is maintained such that the y-axis is aligned with the velocity vector and that Sun is always kept within the x-z-plane. The pitch angle (angle between x-axis and sun direction within x-z-plane) is varied for different cases, as well as the orbit radius, which is determining the solar constant for each case.

- Cold case:

  The cold case is driving the maximum required heater power to maintain the MMs and the mirror structure within the specified temperature range. Also the largest temperature gradients on the structure between sun side and anti-sun side are expected in this case. The MAM is pointing away from the sun at a pitch angle of 34 degrees.
  Distance to Sun: 153,406,090 km
  Solar constant: 1293 W/(m K)

- Hot case:

  The hot case is used to verify that the maximum temperatures are not exceeded. The MAM is pointing towards the sun at a pitch angle of -34 degrees.
  Distance to Sun: 148,063,200 km
  Solar constant: 1388 W/(m K)

11.3.2.4 Heater philosophy

Since the MMs and mirror structure have to maintain strict temperature requirements while facing open space, an active thermal control strategy is applied. Electrical heaters are glued on the mirror structure. The applied heat is mainly radiated to the MMs and conductively distributed across the mirror structure.

Two heater strings are dedicated to each MM, facing two opposing sides of the MM: one glued to the outside of the next inner structure ring and one glued to the inside of the next outer structure ring. Redundancy will be obtained by using double layers Kapton heaters. In the model, it is simply assumed that both strings are connected in series and thus always operate together.

The structure with a length of 400mm in z-direction acts as a thermal baffle, which minimises the view factor of the MMs to cold space. On the other hand, due to the its low thermal conductivity, the titanium mirror structure itself will be exposed to thermal gradients in longitudinal direction.

In order to minimise these temperature gradients in z-direction, each heater string consists of three single electrical heaters, which are placed along the length of the structure. The heaters are serially connected, but may have different electrical resistance, and thus different power dissipation. The top heater (layer A) is driving the MM’s temperature, while the centre and bottom heaters (layers B and C) are supposed to equalize the temperature gradients in z-direction. The following picture is visualising this concept of three heater layers.

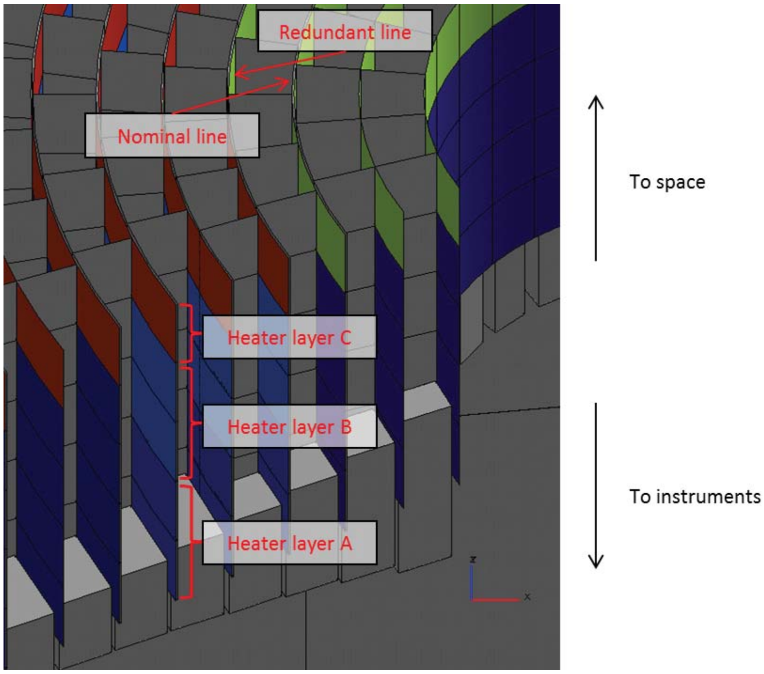

Figure 11-11: Heater philosophy: every MM is heated by two heater strings (nominal & redundant) with three heater layers (A,B and C). All heaters are attached to the mirror structure

Heater layer A and layer B are modelled of 2 nodes each, layer C contains only one node.

The temperature gradients through the structure between the sun side and the shadow side of the SC are encountered by defining several heater zones. These zones can be controlled separately from each other, while all heaters within one zone are connected. The temperature control logic of the heaters will follow an on-off modulated approach.

11.3.3 Thermal Analysis

11.3.3.1 Objectives

The thermal analysis is performed with steady state simulations. Heater powers are applied as internal heat sources on the corresponding thermal nodes.

The thermal analysis aims on the following objectives:

- Maintain all MMs at 20±1°C
- Minimise temperature gradients within the mirror structure to meet the specified requirements
- Determine the required heater power
- Identify optimal heater control zones, while minimising the number of independent heater lines.

11.3.3.2 Results

As a first approach, the cold case has been run assuming a completely passive TCS, i.e. without applying any power to the heaters. The simulation results for the cold case are shown in the two figures below, the first figure shows the temperature distribution of the MMs, the second figure shows the temperature distribution within the structure. All temperature values are in [°C], the Sun's direction is from the right.

11.3.3.2.1 Completely Passive TCS

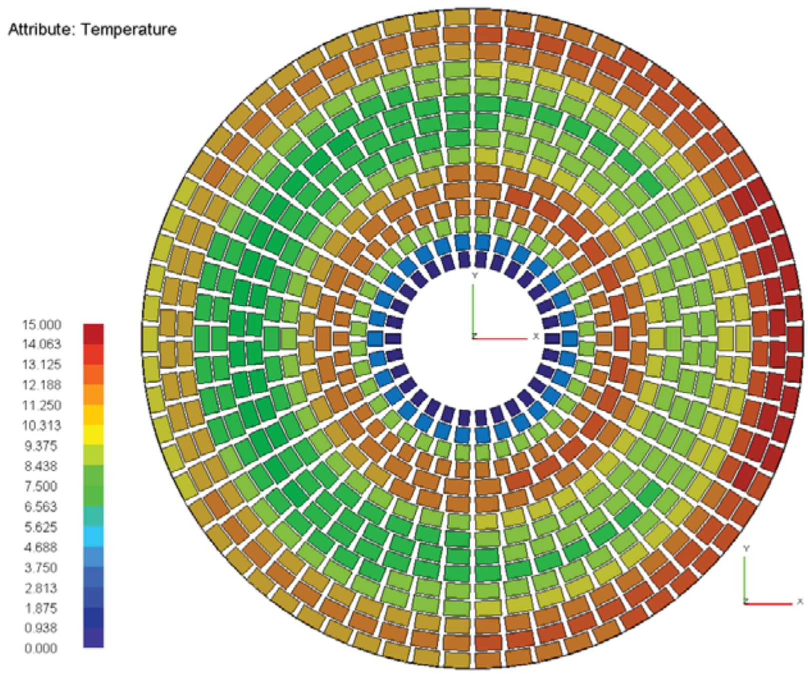

Figure 11-12: Temperature distribution of MMs in cold case, without any active thermal control

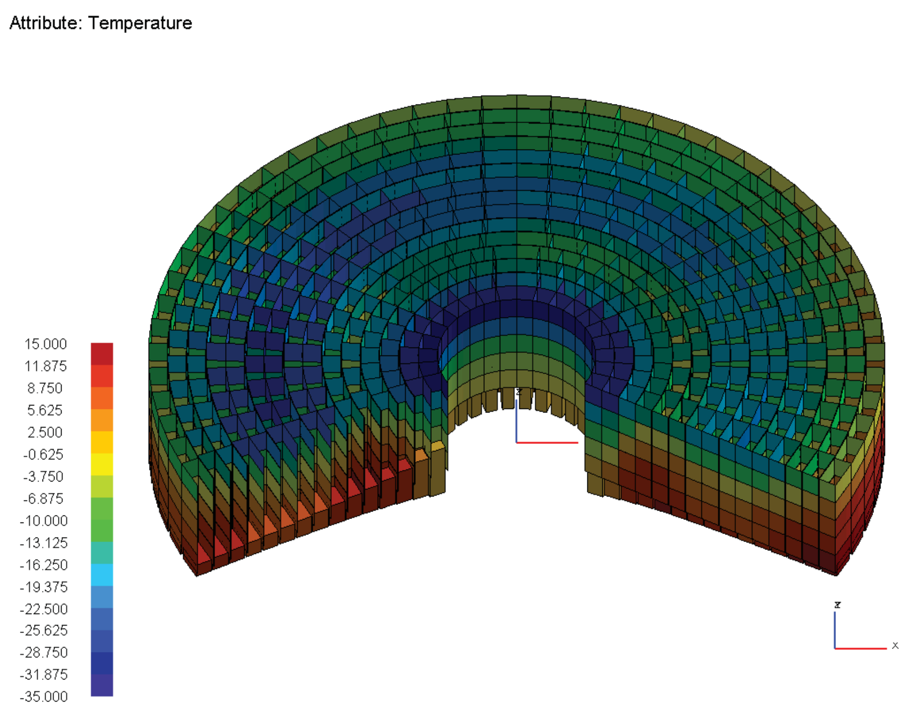

Figure 11-13: Temperature distribution of mirror structure in cold case, without any active thermal control

Without only passive TCS, all MMs have temperatures is between 0˚C and 15˚C. The structure reaches temperatures from -35˚C to +15˚C. The temperature differences in z-direction reach up to 40˚C. The largest temperature differences in radial direction can be found between the inner ring and the most outer ring, reaching 23˚C.

11.3.3.3 Definition of heater zones and power dissipation

The next step is to find a heater zoning scheme, which maintains all MMs within the limit of 20˚C±1˚C, while using as few heater lines as possible.

One possible solution is presented below. The whole MAM is divided in two halves, the sun side (right) and the shadow side (left). One zone contains several MM rings. The black lines in the next figure indicate 12 individually controllable heater zones. The dashed lines optionally increase the number of zones from 12 to 16. All simulations presented in the following are only using 12 zones.

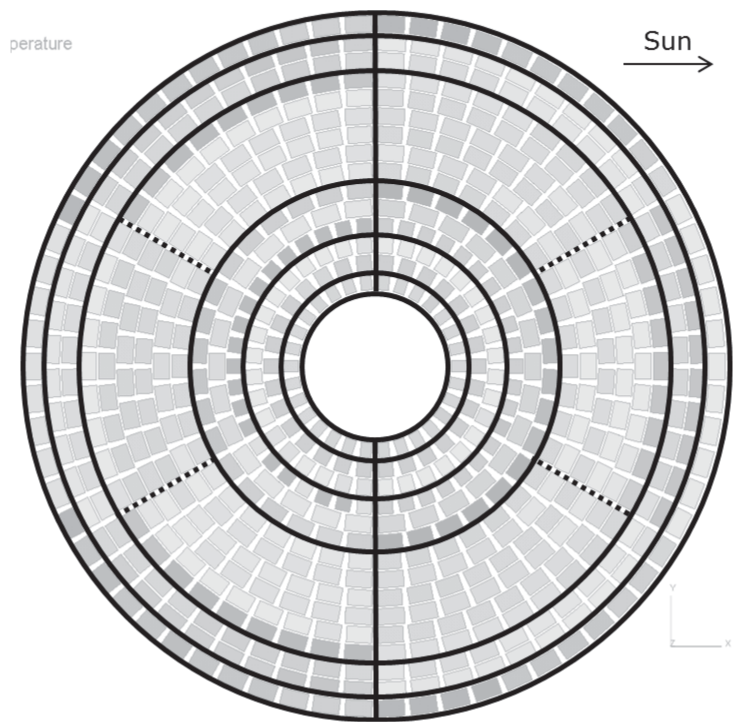

Figure 11-14: Heater zones, independently controllable

In the next step, electrical power is applied to the heaters according to the previously defined zones. The dissipated electrical power, which is applied on each heater, can be seen in the following figure and table. (Note: the colour scale is visualizing heat per node (not heat per heater!), since heaters of layer A and B consist of 2 nodes each.)

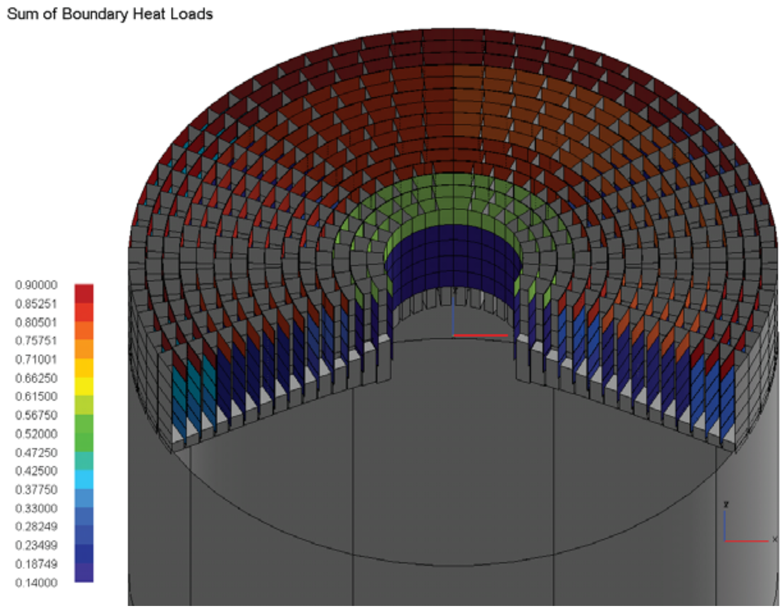

Figure 11-15: Dissipated heater power in cold case in Watt (sun side on the right, shadow side on the left)

MM Rows	Layer A (MM side)		Layer B		Layer C (space side)
	Node 0	Node 1	Node 2	Node 3	Node 4
Sun side:					
0…1	0.16 W	0.16 W	0.17 W	0.17 W	0.58 W
2, 3	0.14 W	0.14 W	0.17 W	0.17 W	0.58 W
4…6	0.26 W	0.26 W	0.31 W	0.31 W	0.81 W
7…12	0.19 W	0.19 W	0.20 W	0.20 W	0.78 W
13, 14	0.32 W	0.32 W	0.30 W	0.30 W	0.88 W
15	0.32 W	0.32 W	0.30 W	0.30 W	0.88 W
Shadow side:					
0…1	0.16 W	0.16 W	0.15 W	0.15 W	0.60 W
2, 3	0.14 W	0.14 W	0.14 W	0.14 W	0.60 W
4…6	0.28 W	0.28 W	0.30 W	0.30 W	0.85 W
7…12	0.20 W	0.20 W	0.22 W	0.22 W	0.81 W
13, 14	0.33 W	0.33 W	0.38 W	0.38 W	0.90 W
15	0.36 W	0.36 W	0.39 W	0.39 W	0.90 W
Total heating power for all 678 MMs: **2449.74 W**					

Table 11-8: Applied heater powers per node in each heater control zone

11.3.3.4 Cold Case

The first important result of this analysis is that the MMs' temperature requirement can be achieved with the found zoning scheme. The temperature of the MMs is shown in the next figure.

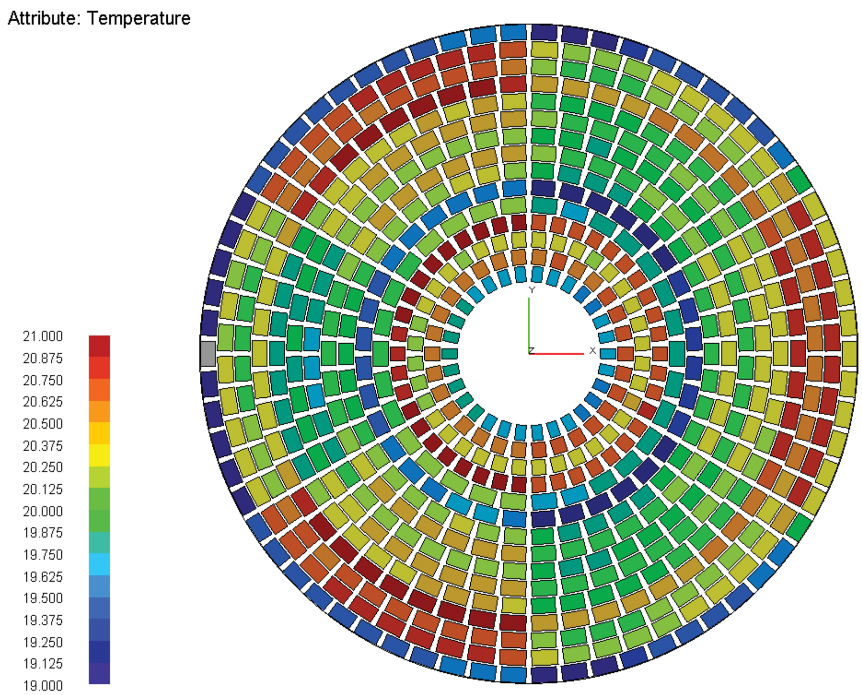

Figure 11-16: Temperature distribution of MMs in cold case

In the thermal model the outside of the MAM structure is insulated from space only by MLI. In reality the mirror structure will be surrounded by the service module, which is maintained at around 20 ˚C. As a consequence this simulation assumes harsher conditions for the most outer row of MMs and the outer structure part than it will be the case in reality.

In this simulation one of the MMs (left side, most outer row, on minus-x-axis) is found to be below the required temperature of 19˚C. Its temperature is 18.97 ˚C, which can still be considered acceptable.

The heater zoning does not only ensure a homogenous temperature distribution for the MMs, but it also limits the thermal gradient in radial direction. This corresponds to the requirement of a maximum one-directional temperature difference of ΔT < 3.5K, which can be achieved by further optimisation of the applied heater powers. The resulting temperature distribution in the structure is shown in the next figure.

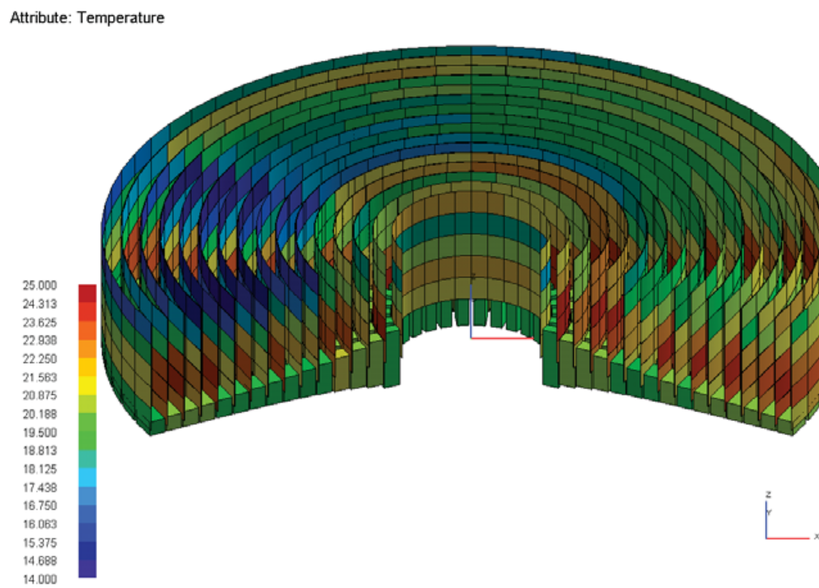

Figure 11-17: Temperature distribution within mirror structure in cold case

The amount of heater power has been determined in an iterative process, in which the applied heat boundary conditions have been manually modified from one step to another. The iteration steps and their impact on the driving parameters (temperature range of the MMs, maximum temperature difference in z-direction and required heater power) are shown in the following table. The most relevant iteration steps are highlighted in red (hot case) and blue (cold case).

Case Name	Temp.-range of MMs	Temp.-range of mirror structure	Maximum ΔT in z-direction	Required heater power	Comment
Cold_NoBC	7.5±7.5°C	-8.5±22.5°C	27°C	0 W	Cold case, passive TCS
Cold_03	20±1.6°C	20±6°C	3°C	2025 W	As proposed in power budget; based on obsolete structure thickness values and without sun shield!
	6±2°C	9±6°C	6°C		repeated with new shell thickness (2.3mm) & sun shield
Cold_02	20±1.5°C	20±10°C	6°C	2187 W	As presented in final presentation; based on obsolete structure thickness values!
	11±4°C	15±9°C	10°C		repeated with new shell thickness (2.3mm)
Cold_04	20±4°C	22.5±8.5°C	11°C	2473 W	
Cold_05	20±3°C	21.5±6.5°C	5°C	2463 W	Additional heater zone for rows 4..6
Cold_06	20±2°C	18±6°C	10°C	2435 W	Different zones for sun side and shade side

Case Name	Temp.-range of MMs	Temp.-range of mirror structure	Maximum ΔT in z-direction	Required heater power	Comment
Cold_07	18.5±2.5˚C	18±6˚C	7˚C	2394W	new heater lines for rows 0..4 and 5..6
Cold_08	20±1.1˚C	19.5±5.5˚C	8˚C	2448 W	Introduce new heater lines
Cold_09	20±1˚C	19.5±5.5˚C	8˚C	2449 W	Baseline for cold case
Hot_09	20.2±1.2˚C	19.5±5.5˚C	9˚C	2449 W	Baseline for hot case

Table 11-9: Iteration steps and their impact on driving parameters

The required heater power in this case is 2449.74 W. This value is higher than was expected in earlier stages of the analysis. The cases Cold_02 and Cold_03, which were used to generate the inputs for the power budget and for the final presentation, were initially assuming a thickness of 6mm for some of the structure rings, due to a modelling error in the GMM. The error has been corrected later and the simulations repeated with the correct values.

The main driver for the required heater power is the thermal gradient requirement in z-direction of the structure: While one end of the structure is controlled around 20˚C, the other side is facing cold space. The material used for the structure is titanium, which has low thermal conductivity and a thickness of only 2.3mm. The largest amount of heat is required on the open side of the structure, in heater layer C. Most of that heat is radiated to space, while a smaller amount is conducted through the structure. This results in an inhomogeneous temperature distribution within the structure and requires a high amount of heating power.

11.3.3.5 Hot case

The last requirement states that the global temperature variation shall be less than ±1.5˚C. In order to verify this requirement, the cold case and hot case are compared to each other.

The next figures show again the temperature distributions of the MMs and the mirror structure, this time for the hot case. The applied heater power in hot case is still the same as in cold case.

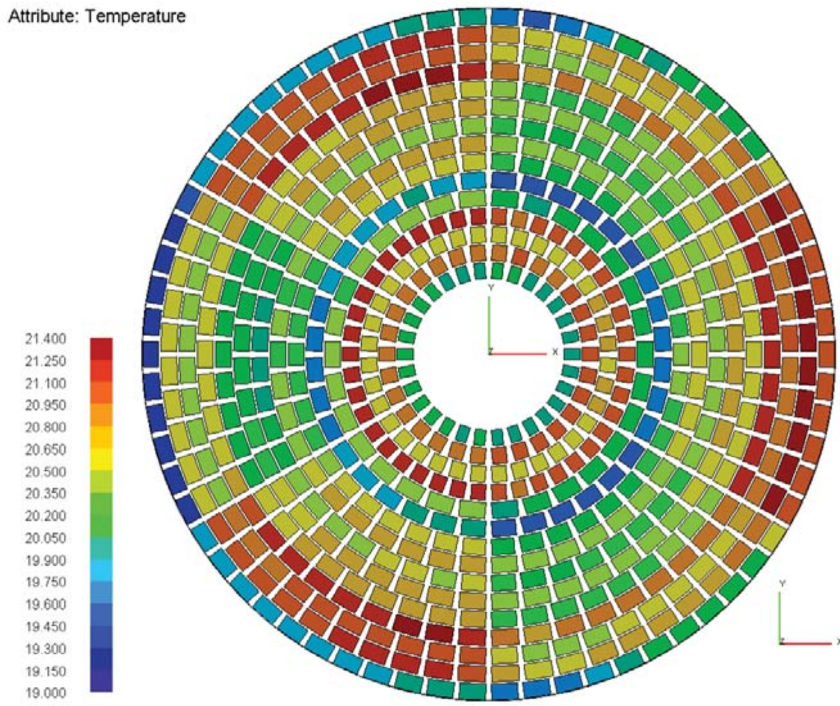

Figure 11-18: Temperature distribution of MMs in hot case

The MMs have slightly higher temperatures than in the cold case, between 19˚C and 21.4˚C. This is only 0.4˚C warmer than required, so it can easily be regulated by the heater controller.

Also the temperature distribution within the mirror structure is not very different from the cold case. The most affected regions are some outer rings of the Sun side (on the right in the picture). These areas have become warmer by less than 1 ˚C compared to the cold case. The temperature of the shadow side regions is mainly determined by the applied heater power and cold space, less by the amount of heat flux by the Sun.

The requirement of global temperature variations within ±1.5˚C is fulfilled, according to the performed simulations.

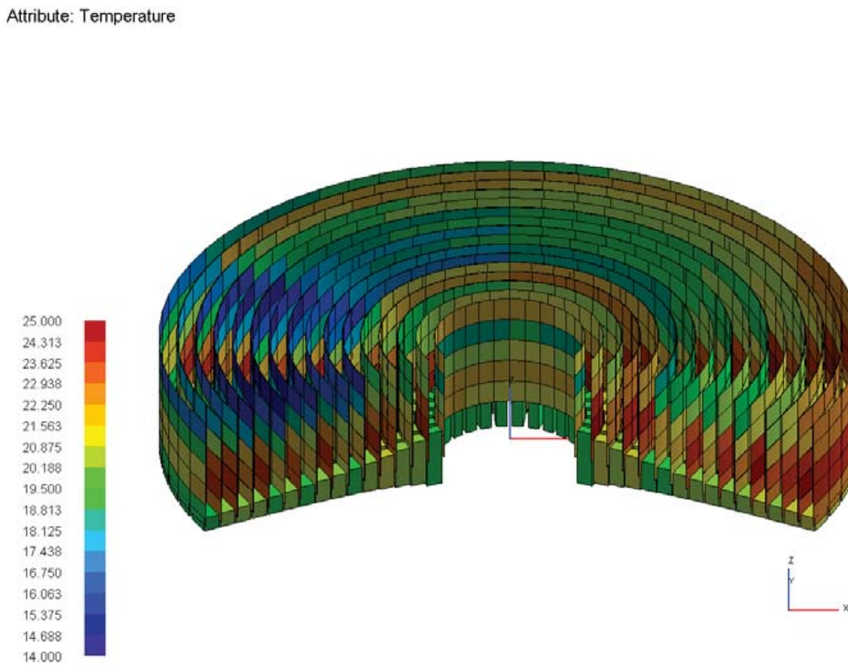

Figure 11-19: Temperature distribution within mirror structure in hot case

11.3.3.6 Sensitivity analysis: Mirror structure shell thickness

Until now all simulations were assuming a thickness of 2.3mm for the mirror structure shells. In order to characterise the influence of the mirror structure's thickness, the nominal cold case is now performed with adjusted conductivity values for the titanium structure. The conductivity value is scaled such that it corresponds to a shell thickness of 3 mm or 1 mm respectively. The results are summarised in the following table:

Case Name	Thickness of mirror structure shells	Temp.-range of MMs	Temp.-range of structure	Maximum ΔT in z-direction only	Comment
Cold_09	2.3 mm	20±1˚C	19.5±5.5˚C	8˚C	Reference case
Cold_10	3 mm	13±1.5˚C	13.5±4.5˚C	4˚C	
Cold_11	1 mm	40±4˚C	37±11˚C	15˚C	

Table 11-10: Sensitivity analysis results for different mirror structure thicknesses

The thicker mirror structure (3 mm) has better conductance and leads to a more uniform heat distribution within the structure, which helps to decrease temperature gradients.

On the other hand, the thicker structure conducts more power from the MMs to the open side of the structure, where the heat is mainly radiated to cold space. Therefore the heat losses are higher and the mean temperatures of both, MMs and structure, decrease.

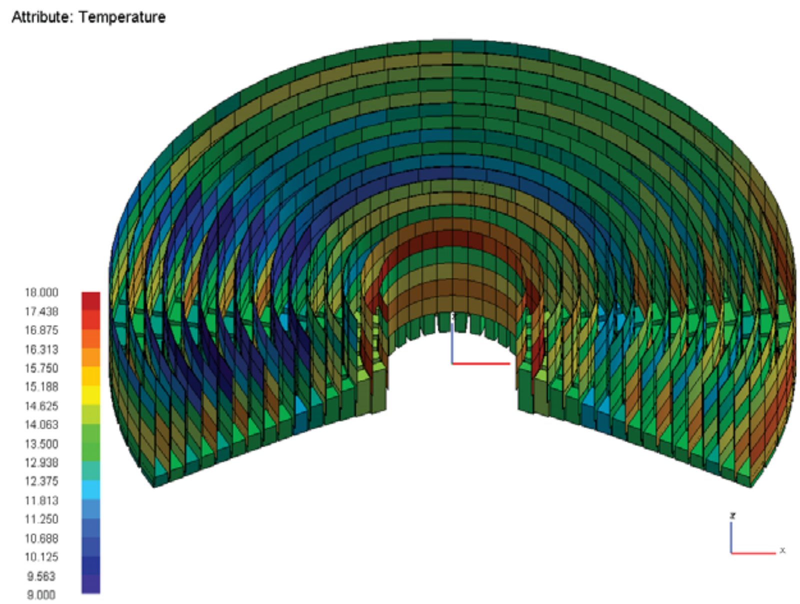

Figure 11-20: Temperature distribution with mirror structure thickness increased to 3 mm

The thinner structure (1 mm) shows just the opposite behaviour: Since the applied power is poorly conducted away from the heaters, a higher amount of heating power is immediately radiated by the heater close to the MMs. This results in a more efficient use of the applied electrical power, and also in a higher mean temperature for MMs and structure. As a major drawback, the low conductance leads to local hot and cold spots and high thermal gradients within the structure.

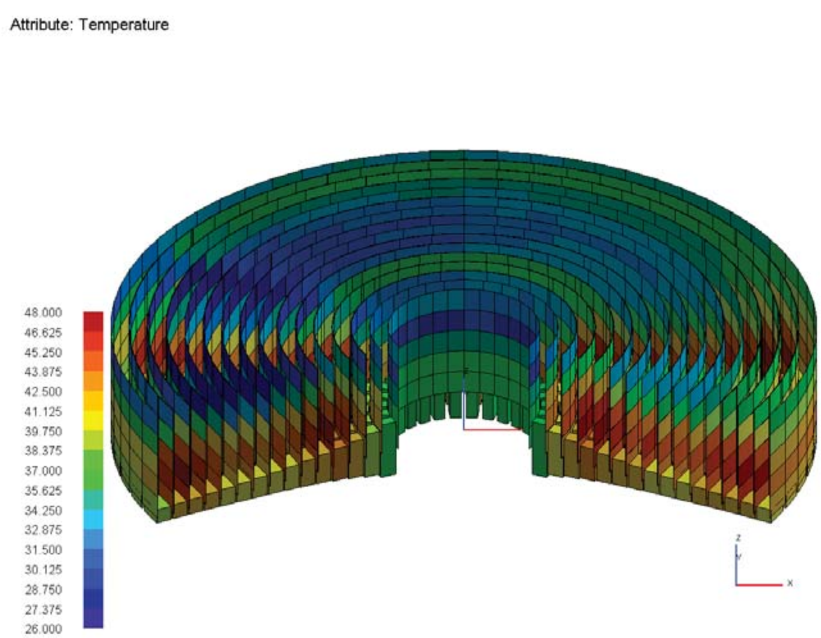

Figure 11-21: Temperature distribution with mirror structure thickness decreased to 1 mm

The driving requirement for the required heating power is mainly the temperature gradient in z-direction, not the overall temperature. This means that maintaining the required temperature range for the MMs is less costly in terms of heating power than meeting the requirements of temperature gradients within the structure.

Therefore it is suggested that the mirror structure should be manufactured with increased thickness or using a material with higher thermal conductivity. This will result in a decrease of the temperature gradients, especially in z-direction. Although locally higher amounts of heater power have to be applied to counteract the lower MM temperature, the savings of overall required electrical power will still be dominant.

11.3.4 Conclusions and Outlook

With the proposed 12 heater zones, it is possible to maintain the MMs within the required temperature range of 20±1 ˚C with a Active Thermal Control consumption of ~2500W. The requirement to keep the temperature differences in radial direction within the requirement of $\Delta T < 3K$ can be achieved by tuning the dissipated heater power for each zone. This gradient can also be decreased by further optimising the heater zoning, as suggested by the dashed lines in the zoning scheme described above.

The most difficult requirement to meet is the maximum temperature difference in z-direction $\Delta T < 3.5K$. In order to meet this requirement, a suitable power dissipation ratio between the heater layers A, B and C still needs to be found and optimised.

This requirement is directly driving the required heater power. Relaxing this requirement would result in a large decrease in required heater power.

The required heating power is also sensitive to the structure's conductivity. Increasing the shell thickness leads to a more uniform temperature distribution within the material. This would decrease the temperature gradient in z-direction and therefore also the required heater power.

A second optimisation would be to increase the number of heaters on the height of the structure, in order to grade more efficiently the dissipation along the Z axis.

Another possibility to decrease the required heater power would be an additional thermal baffle attached to the mirror structure in order to limit the structure's view factor to open space. This has already been proposed in previous ATHENA studies. The compatibility of the accommodation of such a baffle with the mounting solution with the launcher has not been addressed in the frame of this CDF. A rough estimation of the mass and the gain of power (scaled from previous studies) is presented hereafter:

- Mass of the Thermal Baffle: 55kg without margin.
- Gain of Heating Power: ~ -650W (necessary heating power down to ~1850W).

11.3.5 Consideration on Chosen Equipment for the MAM

The TCS of the MAM are composed of heaters (glued on the mirror structure, as described in paragraph 11.3.2.4 Heater Philosophy) and MLI wrapped around the Cylinder and the Mirror Modules Assembly.

A very simple and 'brutal' assumption of harness was taken for the Active Thermal Control of the MAM. Considering the mass of the harness, but also the cost and planning impact that integrating such a harness could induce, it is recommended to look into advanced Active Thermal Control architecture for the MAM (e.g. Heater bus, RIU).

11.4 List of Equipment

	mass (kg)	mass margin (%)	mass incl. margin (kg)
MAM_Heat	65.80	20.00	78.96
MLI_Tele	39.30	20.00	47.16
SVM_TCS	14.40	20.00	17.28
TheBaf	0.00	0.00	0.00
XIFU_Cool_Rad	40.46	20.00	48.55
XIFU_Ebox_Rad	17.16	20.00	20.59
X-IFU_Th_Link	12.60	20.00	15.12
Grand Total	189.72	20.00	227.66

Table 11-11: Mass budget for thermal subsystem

Power (W)		
	P_on	P_stby
MAM_Heat	2025.00	0.00
SVM_TCS	549.00	0.00
TheBaf	0.00	0.00
XIFU_Cool_Rad	789.40	0.00
XIFU_Ebox_Rad	570.70	0.00
Grand Total	3934.10	0.00

Table 11-12: Installed power for thermal subsystem

Note that under the baseline design, the Thermal baffle function is provided by mirror structure itself, this is the reason why no mass is allocated to it.

11.5 Technology Requirements

The following technologies are required or would be beneficial to this domain:

Included in this table are:

- Technologies to be (further) developed
- Technologies available within European non-space sector(s)

- Technologies identified as coming from outside ESA member states.

Equipment and Text Reference	Technology	Suppliers and TRL Level	Technology from Non-Space Sectors	Additional Information
Ethane Loop Heat Pipe		Iberespacio TRL4 ADS TRL4		Characterisation study has been performed under a CNES contract
Ethane Heat Pipe		TBD		Used in the PRISMA program (S), under qualification for TROPOMI

12 POWER

12.1 Requirements and Design Drivers

12.1.1 Solar Illumination Environment

The operational environment is a halo orbit at the Sun-Earth L2 point. This provides steady illumination conditions with no eclipses.

The SC axis will point approximately 90° to sun direction/ecliptic plane, with deviation to cover the field-of-regard (FoR):

- ±30° for a 50% FoR (minimum requirement)
- ±34° for a 60% FoR (preferred goal)
- No rotation about the SC axis is required (or only very small/temporary rolls).

No eclipses are foreseen during the LEOP and transfer to L2. However, during the TCM#1 manoeuvre, the SC axis will be aligned approximately in the ecliptic plane, i.e. orthogonal to the operational attitude. This could cause a temporary loss of solar power, depending on the solar array configuration.

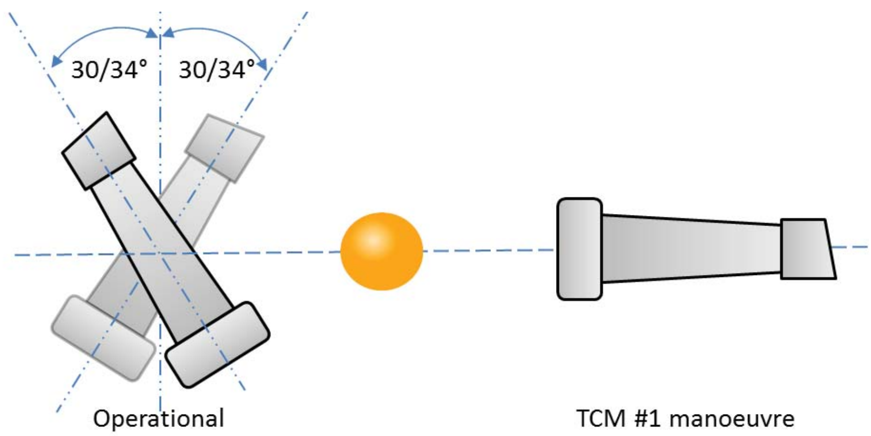

Figure 12-1: Attitude with respect to Sun

12.1.2 Power Budget

The power requirements of the SC platform and payload are derived from the power consumption data of the individual equipment element definitions in the OCDT ATHENA model.

The “ON” power, “STANDBY” power, and the system mode-specific duty cycles of the equipment elements are used to derive mode-average power consumptions. These are shown in Table 12-1. A maximum power consumption (per system mode as defined in chapter 7.3.3) can also be determined by simple addition of the equipment “ON” power values, but of course this is a crude worst case, and so should be used carefully.

NOTE – Some increases to the power budget were identified after the study – see Section 12.1.3.

Row Labels	Com	FSlew	Lau	Man	ObsWFI	ObsXIFU	Safe	SlSlew	SwIn
FPM	**1215**	**926**	**1020**	**1035**	**1610**	**1602**	**1241**	**926**	**1035**
WFI	285	0	0	0	570	570	0	0	0
XIFU	930	926	0	1035	1041	1033	221	926	1035
XIFU_Cool_Rad	0	0	592	0	0	0	592	0	0
XIFU_Ebox_Rad	0	0	428	0	0	0	428	0	0
SVM	**465**	**490**	**496**	**527**	**300**	**300**	**543**	**260**	**155**
CDMU	29	29	0	29	29	29	29	29	29
PDHU	30	10	0	10	30	30	0	10	10
RTU	8	8	3	8	8	8	8	8	8
EPC1	3	0	0	0	0	0	0	0	0
EPC2	3	0	0	0	0	0	0	0	0
GYRO_Sireus1	0	0	2	0	0	0	6	0	0
GYRO_Sireus2	0	0	2	0	0	0	6	0	0
RW_RDR68_3_1	11	11	0	11	11	11	0	11	0
RW_RDR68_3_2	11	11	0	11	11	11	0	11	0
RW_RDR68_3_3	11	11	0	11	11	11	0	11	0
RW_RDR68_3_4	11	11	0	11	11	11	0	11	0
RW_WDE8_45_1	15	15	0	15	15	15	5	15	0
RW_WDE8_45_2	15	15	0	15	15	15	5	15	0
RW_WDE8_45_3	15	15	0	15	15	15	5	15	0
RW_WDE8_45_4	15	15	0	15	15	15	5	15	0
STR_HydraEU_2	11	11	0	11	11	11	0	11	11
STR_HydraEU1	11	11	0	11	11	11	0	11	11
TRASP_Tx_MOD_Rx_DED1	40	20	0	20	23	23	21	20	20
TRASP_Tx_MOD_Rx_DED2	40	20	0	20	23	23	21	20	20
TWT1	58	0	0	0	7	7	3	0	0
TWT2	58	0	0	0	7	7	3	0	0
Mirror_Cover	3.2	0	0	0	0	0	0	0	0
Fill_Dr_Val_0	0	0	0	0	0	0	0	0	0
Fill_Dr_Val_1	0	0	0	0	0	0	0	0	0
Latch_Valve_0	0	30	10	30	0	0	0	0	0
Latch_Valve_1	0	30	10	30	0	0	0	0	0
Press_Transd_0	0	0	0	0	0	0	0	0	0
Press_Transd_1	0	0	0	0	0	0	0	0	0
Thr_Pair_22N_0	6	0	0	19	0	0	0	0	0
Thr_Pair_22N_1	6	0	0	19	0	0	0	0	0
Sun_Shield	1.2	0.4	0	0.4	0	0	0	0.4	0.4
ADPM	1	0	0	0	0	0	0	0	0
SADS	6	0	0	0	0	0	0	0	0
Venting_Mech	0	0	0	0	0	0	0	0	0
Fill_Dr_Val_2	0	0.2	0.066	0.2	0	0	0	0	0
Fill_Dr_Val_3	0	0.2	0.066	0.2	0	0	0	0	0
Fill_Dr_Val_4	0	0.2	0.066	0.2	0	0	0	0	0
Fill_Dr_Val_5	0	0.2	0.066	0.2	0	0	0	0	0
Fill_Dr_Val_6	0	0.2	0.066	0.2	0	0	0	0	0
int_metrology_transmitt1	3.8	3.8	0	3.8	3.8	3.8	0	3.8	3.8
int_metrology_transmitt2	3.8	3.8	0	3.8	3.8	3.8	0	3.8	3.8
RIU	8	8	2.64	8	8	8	8	8	8
SVM_TCS	0	0	411.75	0	0	0	411.75	0	0
Thr_Pair_1N_00	0	14	4.62	14	0	0	0	0	0
Thr_Pair_1N_01	0	14	4.62	14	0	0	0	0	0
Thr_Pair_1N_02	0	14	4.62	14	0	0	0	0	0
Thr_Pair_1N_03	0	14	4.62	14	0	0	0	0	0
Thr_Pair_1N_04	0	14	4.62	14	0	0	0	0	0
Thr_Pair_1N_05	0	14	4.62	14	0	0	0	0	0
Thr_Pair_1N_06	0	14	4.62	14	0	0	0	0	0
Thr_Pair_1N_07	0	14	4.62	14	0	0	0	0	0
Thr_Pair_1N_08	0	14	4.62	14	0	0	0	0	0
Thr_Pair_1N_09	0	14	4.62	14	0	0	0	0	0
Thr_Pair_1N_10	0	14	4.62	14	0	0	0	0	0
Thr_Pair_1N_11	0	14	4.62	14	0	0	0	0	0
int_metrology_transmitt_elec1	3.8	3.8	0	3.8	3.8	3.8	3.8	3.8	3.8
int_metrology_transmitt_elec2	3.8	3.8	0	3.8	3.8	3.8	3.8	3.8	3.8
STR_HydraEU3	11	11	0	11	11	11	0	11	11
STR_HydraEU4	11	11	0	11	11	11	0	11	11
MMA	**1827**	**1823**	**203**	**1823**	**1823**	**1823**	**891**	**1823**	**2003**
Hexapod	4	0	0	0	0	0	0	0	180
MAM_Heat	1823	1823	203	1823	1823	1823	891	1823	1823
Grand Total	3506	3238	1719	3385	3732	3724	2676	3008	3192
Total inc. 20% margin	4208	3885	**2063**	4062	**4478**	4469	**3211**	3609	3830

Table 12-1: Power budget. Values are in Watts, and are averaged per mode

12.1.3 Post-Study Power Budget Update

Subsequent to the end of the ATHENA study, some increases to the power budget were identified. These would have negligible impact on the battery sizing calculations, but a 15% increase in the sizing-case ObsWFI average power demand is significant (but still falls within the 20% power margin that was applied to the budget values for system sizing purposes).

Therefore, the solar array sizing presented below can be regarded as being a “low-margin” or non-conservative case as compared to usual CDF standards.

The updated power budget is presented in Table 12-2 for information. It was NOT used for the power system sizing.

Sum of Value	Column Labels								
Row Labels	Com	FSlew	Lau	Man	ObsWFI	ObsXIFU	Safe	SlSlew	SwIn
⊟FPM	1338	1021	1020	1175	1780	1729	1200	1021	1175
WFI	285	0	0	0	570	570	0	0	0
XIFU	1053	1021	0	1175	1211	1160	180	1021	1175
XIFU_Cool_Rad	0	0	592	0	0	0	592	0	0
XIFU_Ebox_Rad	0	0	428	0	0	0	428	0	0
⊟SVM	488	490	496	527	302	302	545	260	155
ADPM	1	0	0	0	0	0	0	0	0
CDMU	29	29	0	29	29	29	29	29	29
EPC1	3	0	0	0	0	0	0	0	0
EPC2	3	0	0	0	0	0	0	0	0
Fill_Dr_Val_0	0	0	0	0	0	0	0	0	0
Fill_Dr_Val_1	0	0	0	0	0	0	0	0	0
Fill_Dr_Val_2	0	0	0	0	0	0	0	0	0
Fill_Dr_Val_3	0	0	0	0	0	0	0	0	0
Fill_Dr_Val_4	0	0	0	0	0	0	0	0	0
Fill_Dr_Val_5	0	0	0	0	0	0	0	0	0
Fill_Dr_Val_6	0	0	0	0	0	0	0	0	0
GYRO_Sireus1	0	0	2	0	0	0	6	0	0
GYRO_Sireus2	0	0	2	0	0	0	6	0	0
HGA_ATHL	0	0	0	0	0	0	0	0	0
int_metrology_transmitt1	4	4	0	4	4	4	0	4	4
int_metrology_transmitt2	4	4	0	4	4	4	0	4	4
Latch_Valve_0	0	30	10	30	0	0	0	0	0
Latch_Valve_1	0	30	10	30	0	0	0	0	0
LGA1	0	0	0	0	0	0	0	0	0
LGA2	0	0	0	0	0	0	0	0	0
Mirror_Cover	3	0	0	0	0	0	0	0	0
PDHU	30	10	0	10	30	30	0	10	10
Press_Transd_0	0	0	0	0	0	0	0	0	0
Press_Transd_1	0	0	0	0	0	0	0	0	0
RFDU	0	0	0	0	0	0	0	0	0
RIU	8	8	3	8	8	8	8	8	8
RTU	8	8	3	8	8	8	8	8	8
RW_RDR68_3_1	11	11	0	11	11	11	0	11	0
RW_RDR68_3_2	11	11	0	11	11	11	0	11	0
RW_RDR68_3_3	11	11	0	11	11	11	0	11	0
RW_RDR68_3_4	11	11	0	11	11	11	0	11	0
RW_WDE8_45_1	15	15	0	15	15	15	5	15	0
RW_WDE8_45_2	15	15	0	15	15	15	5	15	0
RW_WDE8_45_3	15	15	0	15	15	15	5	15	0
RW_WDE8_45_4	15	15	0	15	15	15	5	15	0
SADS	6	0	0	0	0	0	0	0	0
STR_HydraEU_2	11	11	0	11	11	11	0	11	11
STR_HydraEU1	11	11	0	11	11	11	0	11	11
STR_HydraOH1	0	0	0	0	0	0	0	0	0
STR_HydraOH2	0	0	0	0	0	0	0	0	0
STR_HydraOH3	0	0	0	0	0	0	0	0	0
Stry_Baffles_Div	0	0	0	0	0	0	0	0	0
SUN_MoogBrad_CSS1	0	0	0	0	0	0	0	0	0
SUN_MoogBrad_CSS2	0	0	0	0	0	0	0	0	0
SUN_MoogBrad_CSS3	0	0	0	0	0	0	0	0	0
Sun_Shield	2	0	0	0	0	0	0	0	0
SVM_TCS	0	0	412	0	0	0	412	0	0
Thr_Pair_22N_0	6	0	0	19	0	0	0	0	0
Thr_Pair_22N_1	6	0	0	19	0	0	0	0	0
TRASP_Tx_MOD_Rx_DED1	51	20	0	20	24	24	22	20	20
TRASP_Tx_MOD_Rx_DED2	51	20	0	20	24	24	22	20	20
TWT1	58	0	0	0	7	7	3	0	0
TWT2	58	0	0	0	7	7	3	0	0
Thr_Pair_1N_00	0	14	5	14	0	0	0	0	0
Thr_Pair_1N_01	0	14	5	14	0	0	0	0	0
Thr_Pair_1N_02	0	14	5	14	0	0	0	0	0
Thr_Pair_1N_03	0	14	5	14	0	0	0	0	0
Thr_Pair_1N_04	0	14	5	14	0	0	0	0	0
Thr_Pair_1N_05	0	14	5	14	0	0	0	0	0
Thr_Pair_1N_06	0	14	5	14	0	0	0	0	0
Thr_Pair_1N_07	0	14	5	14	0	0	0	0	0
Thr_Pair_1N_08	0	14	5	14	0	0	0	0	0
Thr_Pair_1N_09	0	14	5	14	0	0	0	0	0
Thr_Pair_1N_10	0	14	5	14	0	0	0	0	0
Thr_Pair_1N_11	0	14	5	14	0	0	0	0	0
int_metrology_transmitt_elec1	4	4	0	4	4	4	4	4	4
int_metrology_transmitt_elec2	4	4	0	4	4	4	4	4	4
STR_HydraEU3	11	11	0	11	11	11	0	11	11
STR_HydraEU4	11	11	0	11	11	11	0	11	11
STR_HydraOH4	0	0	0	0	0	0	0	0	0
STR_HydraOH5	0	0	0	0	0	0	0	0	0
⊟MAM	2205	2205	245	2205	2205	2205	1078	2205	2205
MAM_Heat	2205	2205	245	2205	2205	2205	1078	2205	2205
TheBaf	0	0	0	0	0	0	0	0	0
⊟FMS	0	0	0	0	0	0	0	0	0
Venting_Mech	0	0	0	0	0	0	0	0	0
⊟ISM	4	0	0	0	0	0	0	0	180
Hexapod	4	0	0	0	0	0	0	0	180
Grand Total	4035	3715	1762	3907	4288	4236	2823	3485	3715
Total inc. 20% margin	4843	4458	2114	4689	5145	5084	3387	4182	4458

Table 12-2: Updated power budget NOT used for sizing. Values are in Watts, and are averaged per mode

12.1.4 Battery Requirements

Because there will be no eclipses during the mission, the sizing of the battery will depend on either:

- The energy requirements in launch phase prior to solar array deployment, or
- The energy requirements during the TCM#1 manoeuvre, **if** fixed solar arrays are used.

The timeline and energy requirements for the launch phase case are shown in Table 12-3. This covers the worst-case scenario of a loss-of-attitude anomaly occurring immediately after solar array deployment.

The timeline and energy requirements for the TCM#1 case are shown in Table 12-4. The total energy requirement is less than that of the launch phase case. Therefore, the launch phase is the sizing case for the battery.

It is not necessary to size the battery for the launch phase plus TCM#1 in series, because the intervening time period (min. 24 hours) will be long enough to fully recharge the battery.

Time period	Minutes	Seconds	Seconds cumulative	Source for time assumption	SC mode	Mode av. power, W	Time period energy req., Wh
On pad from UPS disconnect	15	900	900	Solar Orbiter	Launch	1719	430
Launch ascent	25	1500	2400	ATHENA (A5) value from ESOC CDF engr.	Launch	1719	716
CPS initialisation	10	600	3000	Solar Orbiter	Launch	1719	287
Rate reduction period	5	300	3300	Solar Orbiter	Launch	1719	143
Sun acquisition period	20	1200	4500	Solar Orbiter	Launch	1719	573
Solar array deployment	15	900	5400	Solar Orbiter	Launch	1719	430
Contingency	60	3600	9000	Solar Orbiter	Launch	1719	1719
ANOMOLY: Detumble & sunpoint in safe mode	15	900	9900	Assessment by ATHENA CDF AOGNC engineer	Safe	2676	669
				Total energy, Wh.			4967
				Total energy incl. 20% margin, Wh.			**5960**

Table 12-3: Pre-sun energy requirement

Time period	Minutes	Seconds	Seconds cumulative	Source for time assumption	SC mode	Mode av. power, W	Time period energy req., Wh
Slew to burn attitude	20	1200	1200	ATHENA CDF AOGNC engineer	Launch	1719	573
Engine burn	120	7200	8400	ATHENA CDF propul. engineer	Launch	1719	3438
Slew back to cruise attitude	20	1200	9600	ATHENA CDF AOGNC engineer	Launch	1719	573
				Total energy, Wh.			4584
				Total energy incl. 20% margin, Wh.			**5501**

Table 12-4: TCM #1 manoeuvre energy requirement

12.2 Assumptions and Trade-Offs

12.2.1 Solar Array Configuration

	Advantages	Disadvantages	Verdict
Fixed body-mounted array	Maximum simplicity, reliability.	Required array area is likely to be too large to practicably implement as body-mounted. Could present an operational difficulty during AIT. Could introduce thermoelastic loads to the telescope during manoeuvres. Must be sized to accommodate off-pointing up to cos34°=0.83	Discard
Deployable wings, fixed	Simple, reliable	Must be sized to accommodate off-pointing up to cos34°=0.83	Baseline
Deployable wings, rotating	Can have (almost) 17% fewer strings than the fixed array. (The advantage is slightly less in terms of area and mass: ≈ 13% less array area ≈ 10% less mass).	2 x cable-wrap SADM ≈ 12 kg. 1 x SADE ≈ 6 kg Increased complexity, reduced reliability. Mechanical disturbances of the SADM may affect telescope performance.	Retain as an option.

Table 12-5: Solar array configuration trade-off

12.2.2 Power Bus Configuration

The power budget indicates that a 4.5kW EPS is required. This power level leads to the consideration of a higher voltage bus (e.g. 50V), because:

- At 28V, the large current leads to large ohmic losses and/or heavy harness
- Regulated bus stability standards cannot be achieved in practice under 28V in multi-kW conditions (the bus impedance cannot be made low enough).

However, a large fraction of the required power is for heaters. Heaters, being essentially simple ohmic resistors, do not require to be fed from a high quality regulated bus.

Therefore, a primary/secondary bus configuration should be optimum:

- Primary bus - 50V unregulated battery bus. Heaters (and maybe other loads in a detailed design iteration) can run directly from it. This means there is no need for BCR and BDR that would be used only once or twice in LEOP, and would thereafter be nothing but unused mass and complexity.
- Secondary bus - 28V regulated bus. This is the solution likely to give simplest interfaces for science payload and avionics etc.

12.3 Baseline Design

The assumptions, trade-offs and requirements detailed above have been used as inputs to create a power system model (saved as RD[26]) in the ESA power system modelling tool *PEPS*. The configuration, with some explanatory notes, is shown in Figure 12-2.

The battery is 12s 114p with 10 strings (10%) assumed failed (but no fading/degradation, because the battery is only required in LEOP, except for anomalies).

The solar array is 28s 280p with 20 strings (or one MPPT regulator) assumed failed. Degradation factors are set to the PEPS option of 15 years GEO (this is conservative for the ATHENA case, because the radiation environment at Sun-Earth L2 is less severe than GEO, and the ATHENA lifetime is 10 years).

Figure 12-3 shows the results of the sizing case model run in PEPS. The model scenario represents a 4.4 hour timeline, starting with the launch-phase pre-sun power requirement defined in Table 12-3, followed immediately by the worst-case average power consumption of the OBS-WFI mode, including 20% margin. From zero to 9900 seconds, no sunlight is present. From 9900s onwards, the illumination conditions are those of L2, with a 34° off-pointing of the solar array.

The lower plot area shows the load profile applied on the 50V bus (red), and the 28V bus (blue). Also shown is the power extracted from the solar array (green).

The upper plot area shows battery status, both in terms of cell voltage (blue) and state-of-charge (red). Battery current is shown in green, with a positive gradient indicating charging, and a negative gradient indicating discharge.

The battery SoC falls to 14% (2.7V per cell) before sunlight arrives at 9900s. This is an extreme discharge, but the battery sizing already includes ample margin/conservatism in terms of the 10 failed strings assumed failed (at BOL), and the 60 minutes of launch-mode “contingency” in the timeline.

The battery is just barely charging in the sunlight period after 9900s, showing that the power budget is only narrowly positive. However, the solar array sizing already includes ample margin/conservatism from the 20% power budget addition, the assumption of 20 failed strings, and the use of GEO 15-years degradation parameters.

Note that in LEOP, the charging of the battery after first sun acquisition will be very fast, because the 34° array off-pointing and EOL solar cell degradation assumed here will not apply. The battery will be fully charged in less than 5 hours even with the conservative assumption of the high-power ObsWFI system mode.

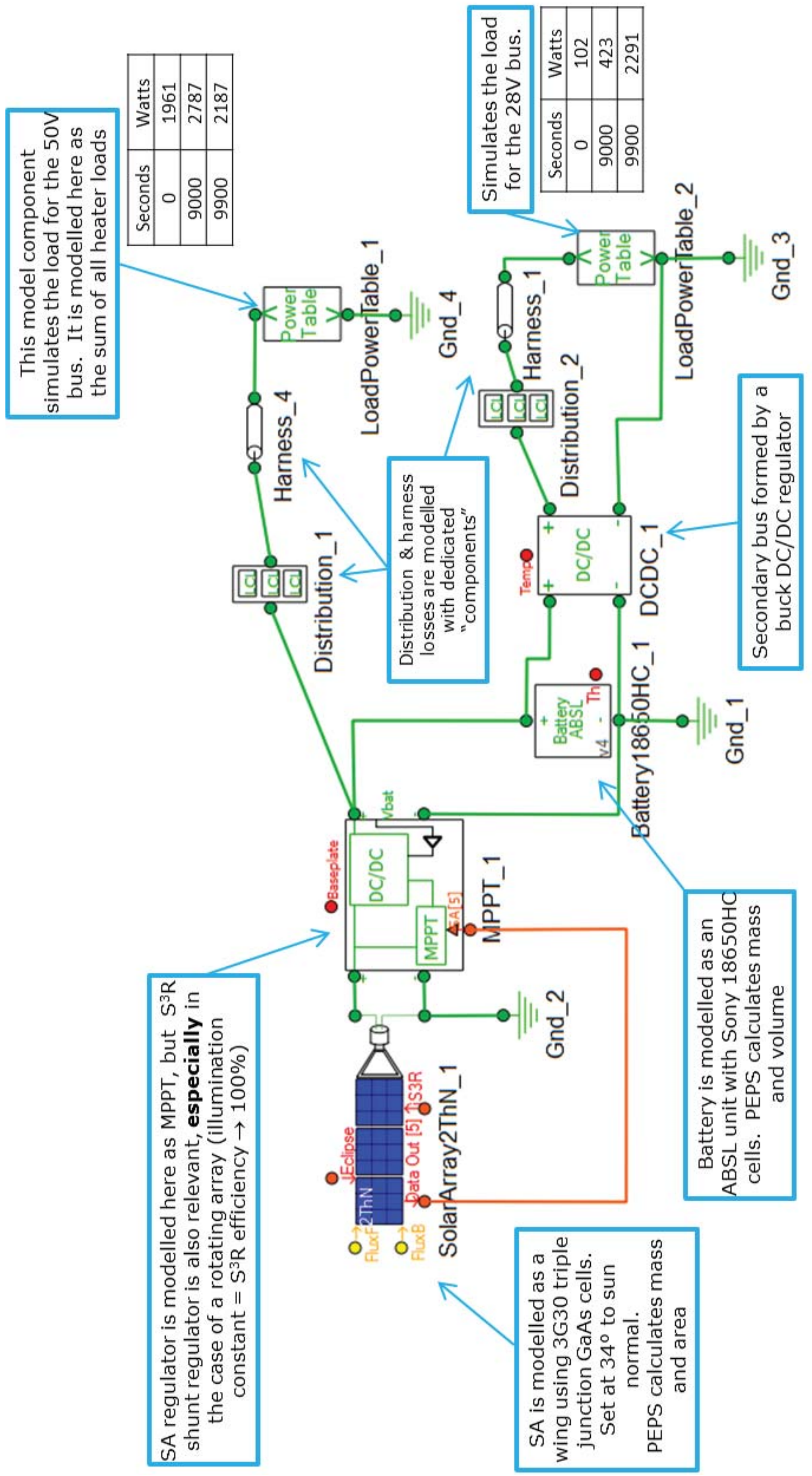

Figure 12-2: Power system baseline design, represented in the PEPS modelling tool

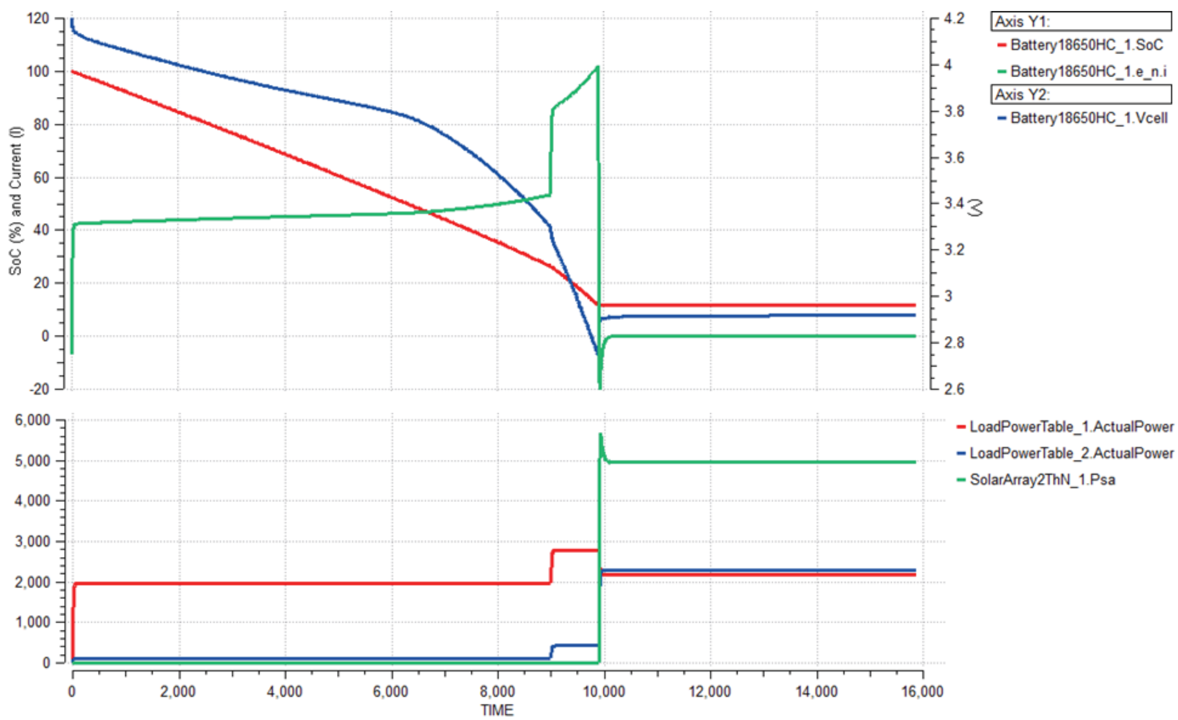

Figure 12-3: Results from sizing case model of the power system in PEPS

12.4 List of Equipment

12.4.1 Solar Array

Triple-junction GaAs 3G-30% cells are assumed, as is now standard.

The mass and area calculation is direct from the PEPS model (based on deployable wings), using 28 cells per string, and 280 strings in total on the SC.

This results in a total of 30m² array area, 154 kg total mass. This is assumed to be implemented as **2 fixed deployable wings, each 15m², 77 kg.**

12.4.2 Battery

A Li-ion battery of 7.4 kWh energy (nameplate) is required.

The sizing is based on the PEPS model representation of an ABSL battery using Sony 18650HC Li-ion cells. (Other Li-ion space batteries e.g. from SAFT are also fully applicable).

The ABSL/Sony 18650HC assumption leads to a requirement of 1368 cells, configured as 12s, 114p.

This is assumed to be implemented as **2 batteries**, **each with a "12s, 57p" configuration**, **mass of 37 kg and volume of 37 litres**.

12.4.3 PCDU

PEPS does not provide mass/volume sizing calculations for PCDUs in the same way as it does for batteries and solar arrays. Therefore, the mass and volume of the ATHENA PCDU have been estimated by reference to SC with similar topologies:

	SA nominal power, kW.	PCDU total mass, kg
Galileo - 50V primary and 29V secondary bus	2	18
Alphasat - 100V primary and 50V secondary bus	13	44

Linear interpolation between these two data points, for the ATHENA case of a 5kW solar array, gives a PCDU mass of **25 kg**.

Applying a typical PDCU density of 0.7kg/l gives a volume of **36 litres.**

12.4.4 Equipment Summary

	mass (kg)	mass margin (%)	mass incl. margin (kg)
Bat18650HC	37	20	44.4
Bat18650HC2	37	20	44.4
PCDU	25	20	30.0
SA1	77	20	92.4
SA2	77	20	92.4
Grand Total	253	20	303.6

Table 12-6: Mass budget for power subsystem

12.5 Options

As mentioned in Section 12.2.1, a realistic option is to implement the solar array as rotating wings. 360° rotation would not be required, so cable-wrap or twist capsule SADMs could be used rather than slip-ring units.

The decision whether to implement this is likely to be driven by cost, balancing the savings on solar cells against the expense of rotating SADMs and the associated SADE. The question of mechanical vibration from the SADM affecting the payload performance would also have to be addressed.

12.6 Technology Requirements

All required power system technologies are already available.

13 AOGNC and RELATIVE METROLOGY

13.1 Requirements Iteration and Design Drivers

The main driving requirements for the AOCS are:

- ToO slew duration allocation - leading to selection of thruster-based ToO slews
- LoS pointing AKE – leading to need for demanding on-board relative metrology and potentially a high performance gyroscope or next generation star tracker
- LoS pointing RPE (allocation from HEW) – potentially requiring a high performance gyroscope.

This section describes how the requirements were iterated during the course of the study.

13.1.1 Iterated Science Requirements

Several requirements were added or modified during the study and the AOGNC baseline was derived using the updated requirements.

Modified/Created Science requirements		
Req. ID	**STATEMENT**	**Comment**
SCI-AST-R-01 *(to be deleted)*	ATHENA shall achieve an initial Astrometric error of 3'' to 99.7% confidence level for all observations.	The only important AKE is the ground-reconstructed AKE.
SCI-AST-R-02 *(modified)*	ATHENA shall achieve a reconstructed Astrometric error of 3'' to 99.7% confidence level.	This was relaxed by the scientists since 1'' AKE is difficult to achieve, particularly with the X-IFU where the improvement from ground-based processing is less (than the factor 3-4 realised by XMM Newton) due to the lack of multiple stars in the image. Taking the centroid of the primary stellar source may allow some improvements to the AKE, but this is yet to be quantified. Flows to SC pointing AKE requirement

13.1.2 Iterated Mission Requirements

Several mission requirements were added or modified during the study and the AOGNC baseline was derived using the updated requirements. These should be included in the MRD upon agreement with the scientists.

Modified/Created Mission requirements		
Req. ID	**STATEMENT**	**Comment**
R-SC-___ *(created)*	95% of the PSF energy @ 10keV shall remain within the selected window (36" x 36") of the WFI detector in window mode.	Flows to line-of-sight pointing APE. Uncertain of parent.
R-SC-___ *(created)*	The SC shall restrict Effective Area loss due to vignetting to 2% at 99.7% confidence with temporal statistical interpretation	There is a separate requirement to restrict to 10% below 3keV at end of mission, but during this study a new requirement of <1% effective area loss (vignetting) was proposed. However, since the raster scan involves off-pointing to levels associated with >1% vignetting, a 1% limit is not considered a hard number, and therefore subject to iteration by the scientists. 10" LoS pointing APE (existing allocation) contributes to 1% vignetting, and we allocate an additional 10" (~1%) to mirror optical axis offset from LoS, bringing the total level to ~2% using a bottom up approach. Flows to LoS pointing APE and mirror alignment APE.
R-SC-___ *(created)*	The Absolute Knowledge Error of the effective area at the centre of the detector shall be <1% at 99.7% confidence with temporal statistical interpretation	The effective area varies across the detector, but is greatest at the detector centre. It is a function of the angle between the mirror optical axis and the line between the detector pixel and stellar source. The scientists require that the vignetting pattern across the detector be known accurately. 1% is a rough order of magnitude desire, but at the edges of the detector 1% may result in very stringent pointing knowledge requirements since the vignetting curve is steeper. Therefore the requirement is written as only being applicable at the centre of the detector. Flows to mirror alignment AKE. LoS pointing AKE is driven instead by 3" astrometry requirement.
R-SC-___ *(created)*	During a raster-scan-point attitude hold, the total detector area exposed with the HEW (0.1 - 7keV) shall not overlap with that from a previous scan point.	If there is overlap then there is no guarantee that the pointing drift doesn't concentrate the exposure at a single point on the detector for two successive scan points. Flows to LoS pointing PDE.

13.1.3 Iterated SC Requirements

13.1.3.1 Pointing

Modified/Created SC pointing requirements		
Req. ID	**STATEMENT**	**Comment**
R-SC-370 *(modified)*	For observations, the SC telescope LoS reconstructed Absolute Knowledge Error (AKE), over all frequencies up to the Nyquist limit of the SC attitude metrology, shall be <3" to 99.7% confidence level with temporal statistical interpretation.	Requirement is on reconstructed AKE, not on-board AKE. Statistical confidence level should match that of parent. There has been an implicit interpretation of the AKE that it only applies up to the Nyquist frequency, since corrections to instrument image will only be made up to this frequency. All frequencies above this contribute towards degradation of the HEW. There seems to be no explicit requirement on the metrology measurement frequency, but any lowering of that frequency will also lengthen the time window for the RPE requirement. **Scientists should check that there is really no requirement on the pointing metrology frequency and whether the AKE truly only applies up to this frequency.**
R-SC-380 *(modified)*	During observations, the SC telescope LoS Absolute Performance Error (APE) shall be <10" (goal <3") to 99.7% confidence level with temporal statistical interpretation.	Derives from need to keep PSF within selected window (18" half-width) of WFI detector in windowed mode. 95% PSF energy @ 10keV = 7" half-width, leaving ~11" for off-pointing (rounded down to 10"). 3" goal is an ATHENA L2 update from the scientists based on simulations, but has no parent requirement. 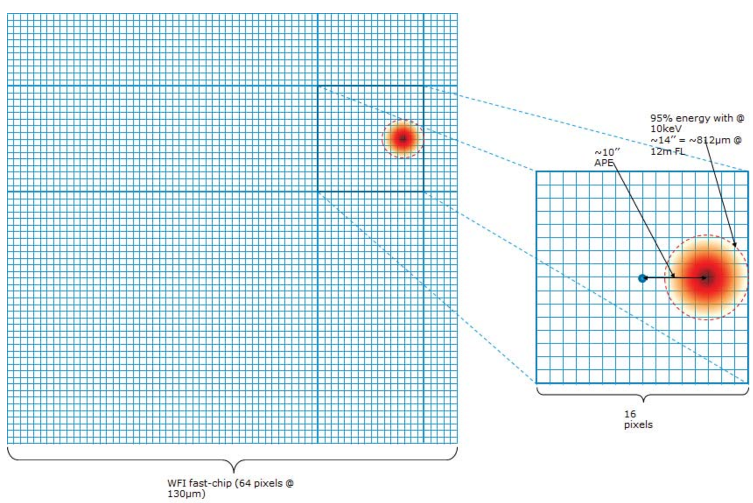
R-SC-380 *(modified)* *Note duplicate numbering.*	APE roll requirement and RPE requirements should include: "with temporal statistical interpretation".	Compliance with ECSS-E-ST-60-10C – Control Performance standard.
R-SC-360 *(modified)*	*Raster scan parameters…* (Typical values are	Scan point separation distance directly drives the PDE requirement. However, 3 pixels is arbitrary and must be refined by Scientists.

Modified/Created SC pointing requirements		
	M=N=3, d=13” (3 pixels).)	
R-SC-380 *(modified)* *Note duplicate numbering.*	During an observation of duration 2.5ks, the SC telescope LoS Performance Drift Error (PDE) shall be <4” to 99.7% confidence level with temporal statistical interpretation over a time window corresponding to the Nyquist frequency of the SC attitude metrology.	It was necessary to introduce a time window over which the mean pointing is computed. The Nyquist frequency is apparently above which all contributions are allocated to the HEW therefore this seems a reasonable choice. Flows from 3 pixel spacing number above. If a previous raster-point hold encountered a 4” drift to the left, and the current raster point also drifts 4” to the right, there is still no overlap in the 5” diameter HEW due to 3 pixels (13”) spacing of points (4+4+5=13). 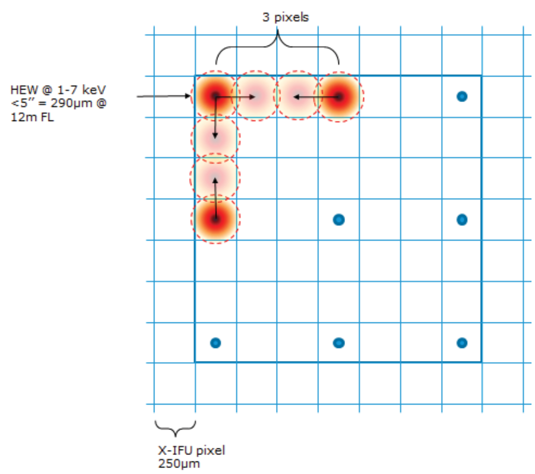

13.1.3.2 Mirror alignment

These mirror alignment requirements apply directly to design of the instrument switch-out mechanism and selection of on-board metrology.

Modified/Created SC mirror alignment requirements		
Req. ID	**STATEMENT**	**Comment**
R-SC-____ *(new)*	During observations, the APE of the half cone angle between the mirror optical axis and the line between the detector center and the stellar source shall be <10” to 99.7% confidence level with temporal statistical interpretation.	Derives from allocation of the new maximum effective area reduction requirement.
R-SC-____ *(new)*	For observations, the reconstructed AKE of the half cone angle between the mirror optical axis and the line between the detector center and the stellar source, over all frequencies up to the Nyquist limit of the SC attitude metrology, shall be <7” at 99.7% confidence with temporal statistical interpretation.	Derives from allocation of the new knowledge requirement on maximum effective area reduction.

13.1.3.3 Attitude manoeuvres

Modified/Created SC attitude maneuver requirements		
Req. ID	**STATEMENT**	**Comment**
R-SC-290 *(modified)*	The SC shall, in the event of receiving a GRB-afterglow ToO-alert (new MTL), slew to the ToO with the X-IFU instrument in the focal plane within 60 minutes for a 180 degree slew case.	Systems engineer modified the allocation to the SC for the ToO response time.

13.2 Assumptions

13.2.1 Reference Frames

See RD[2], Figure 14-1 and 14-3 for definitions of relevant frames. The SC body frame is defined in RD[5], Figure 2, copied below.

Figure 13-1: SC body frame definition

It is important also to define the instrument line of sight, which is the line passing through the centre of the detector and the mirror node (the centre of the mirror assembly).

13.2.2 Physical Properties

The following assumptions have been considered for the design of the AOCS.

	X	Y	Z
Mass (kg)	4533		
Deployed Inertia (kg.m^2)	81000	81000	4700
Deployed Cross-section area (m^2)	39.2	39.2	
Deployed CoP – CoM offset (m)	0.05	0.05	1.1
Surface reflectivity	0.5		

Table 13-1: Physical property assumptions for AOGNC design

These values derive from a combination of ATHENA_L1 study data (inertias) and early estimates for ATHENA L2.

13.2.3 Perturbation Torques

The disturbance torques are entirely dominated by solar pressure. With the assumed values, the torque is 0.29 mNm consistent with the CoG-CoP distance in the chosen configuration (see RD[2] 14.1.3.1 for formula), resulting in a momentum accumulation of 25 Nms/day about the body Y-axis and 1 Nms/day about the body Z-axis.

13.3 Baseline Design

This section describes the functional needs of the mission in terms of AOCS modes as well as the actuator and sensor selection trades. Attitude propellant and pointing budgets are also presented.

13.3.1 AOCS Modes

Based on the needs of the mission, the following modes have been defined. Two slew sub-modes are included to distinguish between ToO slews and slews between targets in the nominal science plan, since the requirements are different.

- Acquisition and safe hold mode (ASH)
    - De-tumble
    - Slew to Sun
    - Hold rough Sun pointing attitude
- Fine Pointing Slew Mode (FPS)
    - Fast Slew
    - Nominal Slew
    - Inertial pointing
        - Normal observations
        - Dither
        - Raster scan
        - Lissajous pattern
- Thruster Control Manoeuvre (TCM).

13.3.2 Actuator Selection

Actuator selection is conducted by examining the needs of the different modes.

13.3.2.1 Nominal Slew

The nominal slew should be conducted with wheels to save thruster propellant. The maximum duration of the slew can be computed from the science availability budget. Assumptions were: 3 days of safe mode per year, 2.8 hrs for orbit maintenance (burn time corresponding to 1.1 m/s delta-V with 100% margin and 1N of thrust), 53 hrs wheel offloading (computed using maximum wheel torques and dumping every 3 days). Given these assumptions, nominal slews (mean angle ~35 deg) plus instrument switch out must occur within 2.5 hrs (300 per year) to achieve 90% SC availability (R-SC-390).

			% annual time	
Safe mode duration per year	hrs	72.0	0.8	
Orbit maintenance per year	hrs	2.8	0.0	
No-science communications periods per year	hrs	0.0	0.0	
Target occultation, % of time	%	0.0	0.0	Depends on orbit and instrument target
Wheel off-loading	hrs	53.1	0.6	
Number of slews per year	-	300.0		
Average slew duration	min	150.0		
Slew time per year	hrs	750.0	8.6	
Time available for observations	%		90.6	

Table 13-2: Science availability budget

This requires ~16 Nms wheels (4-wheel pyramid considering 1 failure) with a bang-coast-bang slew profile. The wheel spin axes are assumed to be offset 75 deg from Z-axis to place most of the capacity in X and Y axes (see 13.3.2.2).

Note if the wheels are near saturation prior to a slew then the speed of the slew will be significantly constrained by the large gyroscopic torques and limited momentum. It is therefore recommended the wheel momentum be dumped prior to a large slew to avoid significant penalties to the science availability budget.

13.3.2.2 Inertial Pointing

The science observations can be serviced by reaction wheels. Wheel torque noise levels are satisfactory given the requirements. Micro-vibrations are not expected to be critical due to the high lateral inertias of ATHENA, therefore isolators are probably not required. Unbalance effects were computed to be negligible even using only the inertia of the MMA as the reaction mass. A micro-vibration allocation has been made in the pointing budget based on past industrial studies.

Raster scan, dithering and lissajous patterns are associated with relatively slow motion requirements, hence wheels are perfectly adequate.

Momentum dumps cannot occur more frequently than every 100 000 sec (1.2 days) to avoid interrupting observations (R-SC-320). This requires ~30 Nms wheels (4-wheel 75deg elevation pyramid considering 1 failure) to store the momentum.

The momentum dump needs are therefore more demanding than the nominal slew. To allow sizing margin, and the potential to go several days between momentum dumps, RCD 4 x 68 Nms wheels are baselined. This is subject to trade with systems/science teams, to decide whether the ConOps could accommodate momentum dumping every ~1.5 days and thereby permit embarkation of smaller wheels (perhaps a total 0.2 Meuro, 3.2 kg, 20 W saving – relatively small amounts). However, the larger wheels provide greater improved science availability. The momentum budgets are presented below.

	X	Y	Z
Available (Nms)	183.6	183.6	68.0
Disturbances (after 3 days) (Nms)	0.0	75.0	3.4

Slew (Nms)	100.0	50.0	5.0
Margin (Nms)	83.6	58.6	59.6
Margin (%)	45.5	31.9	87.6

Table 13-3: Reaction wheel momentum budget, nominal case

	X	Y	Z
Available (Nms)	136.0	136.0	54.4
Disturbances (after 3 days) (Nms)	0.0	75.0	3.4
Slew (Nms)	100.0	20.0	5.0
Margin (Nms)	36.0	41.0	46.0
Margin (%)	26.5	30.1	84.5

Table 13-4: Reaction wheel momentum budget, 1 wheel failure case

A tetrahedral pyramid elevation angle of 75 deg has been selected to place most of the actuation authority on the lateral axes, where it is needed. The per-axis slew allocations allow for ~95% science availability with adequate margins and consider the needs from the field of regard constraint.

The thruster minimum impulse bit requirement derives from the transition from thruster control (slew or momentum dump) to inertial pointing wheel control. Assuming the wheels should absorb no more than 5 Nms per axis due to cancelling residual rates from thruster-based control, the minimum force impulse is 1.1 Ns (assuming 2 thrusters at 2.2 m mean moment arm).

13.3.2.3 Fast Slew

R-SC-290 drives the AOCS design for the ToO fast slew. To allocate budgets to slew time, settle time, instrument swap out, etc., the following was decided:

1. Simultaneous operation of a heavy mechanism (MIP or MMA) introduces significant complexity into the analysis (e.g. coupled modes analysis) and test of the SC. To reduce costs and complexity it is decided not to engage attitude control during instrument switch out, as is the case during appendage deployments.
2. It is recommended that the instrument swap out occur prior to the slew, such that the slew can clean up any additional attitude changes introduced by the swap out.
3. A brief (e.g. 1 min) MIP/MMA fine tuning may be necessary after the slew, to allow for correction of thermal deformations to the LoS. This may require the AOCS to return to free drift.
4. The flexible modes that may have a non-negligible effect on pointing include those associated with the solar panels and instrument switch-out mechanism. These modes will be excited by the slew actuations, but will be below the Nyquist

frequency (e.g. 5-8 Hz) of the attitude metrology. The MMA has a lateral mode at ω_n = 2.1 Hz, and the solar panels are likely to be significantly less than this. Therefore, they will not affect the AKE or the RPE. There will be some effect on the APE, but this is thought to be small.

For these reasons, and preliminary estimates of MMA move times, it was decided to allocate:

- 45 min – SC slew (over 180 deg) and settle
- 15 min – instrument swap out and fine tune

13.3.2.3.1 Post-slew Settle Time

The settle time of the SC modes is estimated below, assuming ζ = 0.005 damping ratio for flexible modes and a rough estimate for the solar panel modal frequency and AOCS control parameters.

Mode Description	Mode Frequency (Hz)	Damping ratio	Settling time, within 1% of goal (min)
Closed Loop Rigid System	0.01	1	1.2
Solar Panel	0.1	0.005	24.4
MMA longitudinal	1.8	0.005	1.4
MMA lateral	2.1	0.005	1.2

Table 13-5: SC modes – settle time

Clearly some flexible modes may still be actively oscillating during the observation, but the amplitude is thought to be small. A very rough estimate for the lateral MMA mode (thought to be the most significant contributor in terms of amplitude) can be obtained by computing the stiffness of the lateral MMA mode using the known frequency and mass (m = 1200 kg), and assuming the main structure is much more massive than mirror mass.

The transfer function from force to translational displacement is:

$$G(s) = \frac{1/m}{{\omega_n}^2 + 2\zeta\omega_n s + s^2}$$

The equivalent step load at the MMA resulting from switch-on of a 1N thruster at the service module can be calculated using c.g. lever arm distance ratios. Assuming (rough order of magnitude) a c.g. 4.5 m from the most distant thruster and 7.5 m from the MMA:

$$\text{Force} = 1 * (4.5 / 7.5) = 0.6 \text{ N}$$

Translational displacement can be converted to a worst case LoS angle error using the telescope focal length of 12 m. The step pointing error step response is therefore:

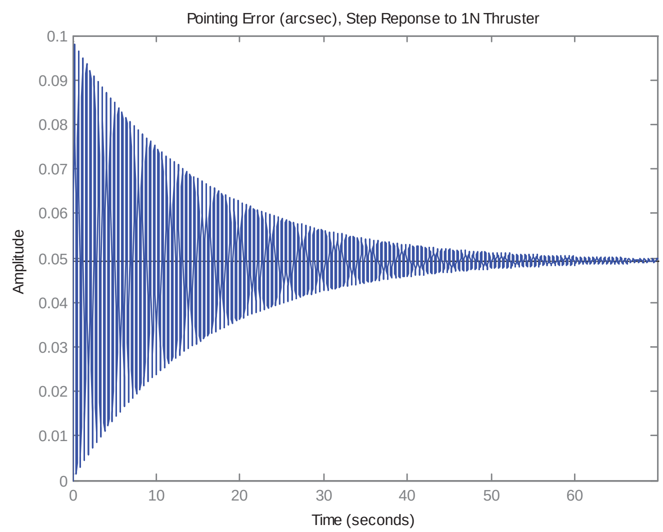

Figure 13-2: Estimated pointing Error (arcsec) due to 1N thruster at service module

The oscillations of 0.1" are negligible compared to the APE budget. Solar panel oscillations are likely to persist for much longer but will probably have less effect on the pointing error. The exact amplitude of the modes could not be analysed in the frame of this study because the FEM mode shape data was not yet available. A thruster based slew will excite these modes more than a wheel based slew, but this is not a factor in the actuator trade since the effect on pointing is thought to be small.

The AOCS can employ roll-off or notch filtering and thruster duty cycle ramping to minimise flexible mode excitations. Furthermore, the operation frequency of the AOCS loop should be selected such that it does not coincide with any of the flexible modes, particularly those of the MMA (see mechanisms section), thereby causing resonance.

13.3.2.3.2 Slew Actuator Type

For reasons stated above, it is assumed that settle time is negligible and that the entire 45 min allocation can be consumed by the slew manoeuvre.

<u>Reaction Wheels</u>

A 45 min, 180 deg slew requires 190 Nms momentum capacity (mostly on the X-axis) and 0.14 Nm torque (bang-bang slew) with no margin. The momentum needs could be reduced in a bang-coast-bang slew profile, but the torque required would quickly increase beyond what is realistic.

Allowing for 1 wheel failure, the SC would nominally require a 4 x 92 Nms wheel pyramid or a 5 x 69 Nms pyramid. In both cases the wheel spin axes are assumed to be offset 75 deg from Z-axis to place most of the capacity in X and Y axes (see 13.3.2.2). The 5 wheel design could barely be achieved by Rockwell Collins Deutschland RDR-68 wheels (no margin), whilst the 4 wheel design would require Honeywell (US) HR16 wheels. Presuming a European solution and some margin, the feasible solution is a 6 x RDR-68 pyramid, which represents 2 additional wheels (total 17 kg) compared with the configuration required by the nominal mission.

Control Moment Gyros (CMGs)

CMGs provide orders of magnitude more torque than wheels, but generally less momentum. The largest momentum European CMG is around 30 Nms, which permits a feasible 45 min bang-coast-bang slew with a 6 x CMG assembly (1 failure assumed).

This solution will have increased cost, complexity and mass (90 kg more) compared to wheels, with no reduction in slew time due to the high inertia (hence high required slew angular momentum) of the SC and large required slew angle.

Thrusters

A 45 min slew requires 0.03 N thrusters and 0.8 kg of propellant. Faster slews are possible with bigger thrusters. 1N thrusters can achieve an 8 min slew, costing 4.5 kg of propellant, or can be operated with reduced burn time to achieve the 45 min slew with 0.8 kg. Note that extra propellant will be required for the thrusters to counteract the gyroscopic torques due to stored wheel momentum. This will range between 0 and 0.05 kg per slew (worst case 180 deg, 45 min slew, carrying 100 Nms), hence the final fuel budgets will not be significantly affected. To reduce the gyroscopic-compensation propellant the stored momentum could be dumped during the slew or apriori (adding a maximum of ~20 min to the response time).

Thrusters allow the flexibility to conduct very fast slews and hence better science, with a cost of additional propellant depending on the desired slew duration. Propellant consumption can be linearly decreased by increasing the average moment arm from the CoG, however improvement on the baseline would require thruster placement on deployable booms or above the SC CoG.

Over the 10 yr lifetime, with mean ToO slew angle of 90 deg and 20 slews per year, propellant is 8 kg assuming 45 min per slew (i.e. unchanging time allocation with slew angle) or 16 kg assuming 22.5 min per slew (scaling time allocation with slew angle). For conservatism the latter is assumed.

The financial cost of using thrusters for fast slews is that of adding 2 thrusters at the service module for raising torque capacity on the X-axis.

Trade-off

	Reaction Wheels	CMGs	Thrusters
Additional mission mass for fast slew (kg)	17	90	16
Additional cost for fast slew (Meuros)	0.5	3.5	0.25

Thrusters and wheels have similar massCost. A 1N thruster-based fast slew is selected due to capability to slew even faster than the requirement if desired, for improved science at expense of propellant.

13.3.2.4 Acquisition and safe hold

13.3.2.4.1 De-tumble

De-tumble needs to complete quickly for battery sizing purposes, therefore 5 min is allocated. Initial rate about X and Y axes (largest inertias) is ~0.9 deg/s per axis (scaled up from IXO CDF using ATHENA ATHENA_L1 vs IXO stowed inertias). These figures lead to a requirement of 4.4 Nm torque about X and Y axes. Propulsion design includes approximately 2 thrusters per axis with mean moment arm of ~2.2 m. Therefore, de-tumble requires 1 N thrusters assuming 100% duty cycle.

13.3.2.4.2 Slew to sun

Slew to sun also needs to complete quickly for battery sizing purposes, therefore 10 min is allocated. A 180 deg slew about X or Y would require 2.8 Nm torque about X and Y axes. With above mentioned thruster layout assumptions this requires at least 0.6 N thrusters.

13.3.2.4.3 Hold sun pointing attitude

The sun pointing hold can be achieved purely with thrusters or with wheels accompanied by intermittent thruster-based momentum dumps. Both methods require the same secular-disturbance rejection propellant. A pure thruster-based safe mode may require some additional propellant to counteract cyclic torques and respond to attitude sensor errors. However, if the thruster deadband is set as large as possible (allowing the maximum sun off-pointing permitted by the power system) then these components can be small.

Since it is ESA practice to avoid using the same actuators in normal and safe modes, a pure thruster based attitude hold is baselined.

13.3.2.5 Thruster Control Manoeuvre

13.3.2.5.1 Large burns

The perigee burn of ~15m/s in 2 hrs requires at least 14 N of force. Feasible options are:

- 2 x 10 N or 22 N thrusters (plus redundancy) parallel aligned, on opposing corners of service module base. This is the selected baseline.
- 1 or 2 x 10 N or 22 N thrusters (plus redundancy) mounted close to the CoG on the side of the telescope tube. This option has the advantage that the sun pointing attitude can be maintained even during large burns.

13.3.2.5.2 Station Keeping burns

The science availability budget is already compliant with use of 1N thrusters for station keeping (see 13.3.2.1) hence there is no need to increase size for minimising burn time. Smaller thruster loads also reduces flexible mode excitation and disturbances on the MMA/MIP.

13.3.2.5.3 Reaction wheel momentum dumps

Momentum dump time is limited by maximum wheel torques, hence any size thruster (>0.1N) will suffice.

13.3.2.5.4 Summary

To avoid significant increases to the station keeping delta-v budget from parasitic forces, a pure torque generation capability is crucial for thruster based modes. It is also crucial to maximise the thruster moment arm for propellant efficiency at least on the X and Y axes, where usage is greater.

The selected thruster layout is defined in the Propulsion section, and consists of 4 x 22 N and 24 x 1 N thrusters. Attitude control minimum impulse bit requirement is easily satisfied by the 1N thrusters. Further optimisation of this layout for propellant efficiency and reducing number of thrusters, using smart redundancy planning, is recommended.

13.3.2.6 Actuator Summary

The following equipment has been selected for the baseline:

- 4 x 68 Nms RCD reaction wheels for nominal slews and inertial pointing.
- 1 N thrusters for small orbit manoeuvres, safe mode, momentum dumps, and ToO slews. Thruster layout should support a 3-axis pure-torque capability and maximise lever arm for propellant efficiency.
- 22 N thrusters for large orbit manoeuvres (LEOP/commissioning and decommissioning).

13.3.3 Sensor Selection

13.3.3.1 Need for On-Board Metrology (OBM)

The need for on-board metrology to measure the internal misalignments in the LoS has been the subject of IXO and ATHENA_L1 studies. The XMM Newton ground calibration campaign resulted in an estimated AKE of 5'' 3-sigma confidence without on-board measurement of internal LoS misalignments (RD[28]). However, ATHENA is larger, contains a flexible/movable mirror and the thermal elastic deformation alone is 13'' (FEM estimate for ATHENA). To meet a 3'' 3-sigma AKE without an OBM, the structural misalignments between calibrations must not exceed ~2''. It is considered too challenging to guarantee that 85% of the thermal misalignment is predictable after calibration. Therefore, ATHENA requires an OBM.

To meet the AKE budget, 1'' 3-sigma error is allocated to OBM measurement of LoS pitch/yaw. It is proposed only to update the AOCS on-board knowledge of the internal LoS alignment, using OBM data, between observations for reasons outlined in 14.3.5.

Presence of an OBM also has the advantage that it may reduce cost and time for the ground-based alignment campaign (no need to calibrate/verify a thermal distortion model) and it can be used as a sensor for the MIP or MMA, thus reducing the need for very accurate local sensing.

13.3.3.2 On-Board Metrology Type and Placement

13.3.3.2.1 Fiducial projection

Chandra used a special mirror to project fiducial LED patterns on to the star tracker detector plane. The detected LED positions indicate the telescope LoS deformation. However, the star tracker accuracy was 4.5 arcs (RD[29]). This system could be used for ATHENA with a modern APS star tracker but the star tracker software would need to be modified to track the LED reflections.

13.3.3.2.2 Laser alignment

Astro-H will use a laser alignment system, but the accuracy is 4.5 arcsec (RD[30]), therefore not directly suitable for ATHENA. TAS developed a prototype sensor for formation flying that uses a pattern of laser reflectors, accuracy 1 arcsec. This is potentially viable but was at TRL 5 in 2007 and is most likely now a discontinued research program. Many suitable terrestrial-application single-beam (lateral offset measurement only) laser alignment systems are available but would have to be re-packaged/qualified for space, which requires substantial development and investment.

13.3.3.2.3 Optical alignment

Sodern developed a prototype 1 arcsec accurate sensor for formation flying that uses a pattern of LEDs on a transmitter box, observed by a receiver, based on star tracker hardware and ATV VDM software.

13.3.3.2.4 Interferometry

There are several options with interferometer, optoelectronic unit and corner cubes highlighted in RD[2].

13.3.3.2.5 OBM Selection

The IXO baseline OBM was the Sodern optical sensor due to highest TRL (5 or 6) and relatively lower cost compared with interferometry, for example. The rough cost of completing development of this sensor and qualification is estimated at 6 Meuros. ATHENA retains this baseline but it is recommended to study cost and risk of the viable alternatives:

- Chandra-style solution

  Requires extensive software modifications to existing star tracker software and possible modifications to telescope to include an extra mirror. Advantage is that OBM and star tracker misalignments are measured by OBM. Note that this was the original OBM proposal for IXO from the NASA perspective.

- Terrestrial laser alignment system

  Probably requires an existing ESA supplier to package and space qualify. Cost estimate 4 – 5 Meuros.

Regardless of the selected solution it will require significant development time, cost, and some risk in whether the requirement of 1" can be robustly satisfied under on-orbit conditions.

13.3.3.2.6 OBM Placement

The OBM receiver and transmitter should be placed as close as possible to the mirror node and focal plane centre to minimise thermal distortions and therefore errors in the LoS vector measurement. Stray light from OBM transmitters needs to be investigated in future studies, since LED light could reflect off the telescope baffle discs. If stray light issues cannot easily be solved then single-beam laser metrology may provide a more suitable alternative. The disadvantage is that one transmitter (or receiver) would be required on each instrument in addition to any required redundancy.

13.3.3.3 Sun sensor

A Sun direction measurement is required for safe mode and independent anomalous attitude detection during normal operations. The Moog Bradford coarse sun sensor provides sufficient accuracy for these purposes. It is recommended to embark 2 x sensors for safe mode spherical coverage (simpler than partial coverage and sun search algorithm) and 1 extra sensor on sun-facing hemisphere for independent continuous monitoring of sun off-pointing. Sensors are internally redundant.

13.3.3.4 Rate Measurement Unit

Rate measurement is required for safe mode to stabilise the SC about the sun vector, since such motion is not observable from the sun sensor. 2 x Selex SirEUS MEMS gyros are selected for this purpose. These will shortly be flown on MTG.

A separate high performance rate measurement unit may be required to meet strict AKE/RPE budgets since the baseline has small non-compliances. The additional cost estimate is 2.5 Meuro. However, it is recommended that inclusion of such a unit should wait until the baseline pointing performance is studied in greater detail.

13.3.3.5 Star tracker

The selected star tracker is the Sodern Hydra with 3 Optical Heads to meet the tight AKE requirement.

A next generation high accuracy star tracker (currently in early stages of development) may be required to fully comply with AKE/RPE requirements since the baseline has small non-compliances. The associated additional cost estimate 4 Meuro, including some sharing of development costs. A new development entails risk, and it is recommended that inclusion of such a unit should wait until the baseline pointing performance is studied in greater detail.

The star trackers should be placed as close as possible to the OBM to minimise thermal distortions and hence the unknown misalignments between the relative metrology frame and the star tracker frame (see 13.2.1). The individual star tracker optical heads should have non overlapping fields of view to minimise noise correlations between trackers and reduce possibility that multiple heads view poorly populated star fields.

13.3.4 Attitude Propellant Budget

The attitude propellant budget was computed assuming 1 safe mode event per year plus the initial post-launch attitude acquisition, combined with other assumptions mentioned in 13.3.2. The delta-V equivalent propellant assumes 220 sec specific impulse and that all the attitude propellant is consumed at the beginning of the mission (i.e. BOL SC mass). No margins are included in this budget, as these are applied in the propulsion subsystem budget.

ACS PROPELLANT BUDGET	Events over lifetime	Total time (hrs)	Mean duty cycle (%)	Mean per thruster on time (hrs)	Propellant (kg)
Fast slew	200	75.0	6.0	4.5	15.9
Momentum dump	1359	342.0	5.1	17.6	58.6
Detumble	11	0.9	100.0	0.9	9.1
Sun acquisition slew	11	8.3	64.0	5.3	3.9
Safe hold (delta w.r.t. dump)	11	72.0	1.0	0.7	7.1

ACS PROPELLANT BUDGET	Events over lifetime	Total time (hrs)	Mean duty cycle (%)	Mean per thruster on time (hrs)	Propellant (kg)
Total Propellant (kg)					**94.6**
Dv equivalent (m/s)					32.5

Table 13-6: Attitude control propellant budget

13.3.5 Pointing Budget

Pointing budgets were constructed using assumptions from past industrial studies augmented with some updates for ATHENA.

A pointing budget trade study (Table 13-7) regarding the usage of OBM data on-board by the AOCS showed that OBM data is required to be used on-board. This is because the MIP or MMA errors (aligning the internal LoS with the AOCS-expected direction) contribute directly to the LoS pointing APE, PDE and AKE budgets. Feasible 3-sigma allocations for the mechanism were made based on discussions with the mechanisms team; alignment APE = 5" (0.3 mm), PDE = 2" (0.1 mm), RPE = 0.5" (0.03 mm), AKE = 4" (0.25 mm). With these figures the LoS pointing APE requirement could not be met without using the OBM data on-board. It is proposed to use the OBM data on-board to update the AOCS knowledge of the LoS between observations only. With extra stability analysis, interface/software complexity and testing it would be possible to use the OBM data continuously in the AOCS loop, but this only improves the LoS PDE – which is already compliant under the proposed baseline.

	APE	PDE	RPE	AKE								
MIP/MMA local (not global) positioning requirements	5	2	0.5	4								
OBM accuracy requirement (if OBM present)				1								
AOCS 3-sigma requirements	10	4	1	3								
Number of star tracker optical heads	3											
Mechanism	MIP/MMA				MIP/MMA				MIP/MMA			
OBM	OBM, but not used in AOCS				OBM, used intermittently in AOCS				OBM, used continuously in AOCS			
AOCS sensors	Current generation STR				Current generation STR				Current generation STR			
Error metric	APE	PDE	RPE	AKE	APE	PDE	RPE	AKE	APE	PDE	RPE	AKE
Mechanical Alignment Contributions												
Mirror												
Mirror internal translation distortions between boresightings	0.17			0.17	0.17			0.17	0.17			0.17
Instrument												
Instrument internal translation distortions between boresightings	0.05											
Structural												
LoS TED between boresightings	6.00											
LoS TED during observation	0.01	0.01			0.01	0.01						
LoS jitter due to reaction wheels	0.21		0.21		0.21		0.21		0.21		0.21	
LoS jitter due to cryo coolers	0.21		0.21		0.21		0.21		0.21		0.21	
Flex Modes	0.10				0.10				0.10			
STR												
Mirror optical axis to STR LoS distortion between boresightings	2.30											
Mirror optical axis to STR LoS distortion during observation	0.23	0.23			0.23	0.23						
Mirror optical axis to STR LoS jitter	0.12		0.12		0.12		0.12		0.12		0.12	
OBM to STR LoS distortion between boresightings				0.40	0.40			0.40	0.40			0.40
OBM to STR LoS distortion during observation				0.10	0.10	0.10		0.10	0.10	0.10		0.10
Mechanism												
Total mechanism error orthogonal to LoS	5.00	2.00	0.50		2.06	2.00	0.50		0.50		0.50	
OBM												
LED position (w.r.t. instrument) calibration error				1.00	1.00			1.00	1.00			1.00
OBM accuracy				1.00	1.00			1.00	1.00	1.00		1.00
TOTAL (RSS)	***8.15***	***2.01***	***0.59***	***1.48***	***2.57***	***2.02***	***0.59***	***1.48***	***1.60***	***1.00***	***0.59***	***1.48***
GNC Contributions												
STR pitch/yaw per axis bias	0.49			0.49	0.49			0.49	0.49			0.49
STR lateral due to roll bias at edge of detector (offset 25 arcmin)	0.00			0.00	0.00			0.00	0.00			0.00
STR pitch/yaw per axis post-proc NEA				2.03				2.03				2.03
STR lateral due to roll post-proc NEA at edge of detector (offset 25 arcmin)				0.01				0.01				0.01
Gyro-stellar estimator NEA												
GNC RPE (including controller error)	1.11		1.11		1.11		1.11		1.11		1.11	
TOTAL (RSS)	***1.21***	***0.00***	***1.11***	***2.09***	***1.21***	***0.00***	***1.11***	***2.09***	***1.21***	***0.00***	***1.11***	***2.09***
Lateral per axis total	*8.2*	*2.0*	*1.3*	*2.6*	*2.8*	*2.0*	*1.3*	*2.6*	*2.0*	*1.0*	*1.3*	*2.6*
Radial total	***11.7***	***2.8***	***1.8***	***3.6***	***4.0***	***2.9***	***1.8***	***3.6***	***2.8***	***1.4***	***1.8***	***3.6***

Table 13-7: LoS pointing budget for 3 different OBM usage options. Selected option highlighted in yellow. Non-compliances highlighted in red

The 3-sigma baseline performance from Table 13-7: is:

- APE = 4.0 arcs (meets requirement and goal)
- PDE = 2.9 arcs (meets requirement)
- RPE = 1.8 arcs (non-compliant)

- AKE = 3.6 arcs (non-compliant)

Note that the APE does not include the star tracker NEA because it is assumed that this is entirely filtered out by the relatively low bandwidth attitude control system. The pointing knowledge signal cannot filter this out as easily because science is interested in knowledge up to the star tracker Nyquist frequency, and it cannot easily distinguish between what is noise and what is real motion. These assumptions need to be re-evaluated in future studies, complemented by pointing simulations that include modelling of the ground-based attitude reconstruction process.

If the above non-compliances are deemed unacceptable it is recommended to add either a high performance gyro or replace the star tracker with a next generation tracker. These alternatives are studied in Table 13-8. Note that the baseline assumes that on-board star tracker errors are attenuated by a factor 0.7 during on-ground re-filtering of data. Further improvements could be possible from ground processing of raw star positions (if it can be sent in telemetry) to reveal motion correlations between the heads and help differentiate between noise and truth. Ground processing of the WFI data is expected to improve AKE by a factor 3 – 4 (RD[5]), but this factor is expected to be much smaller for the X-IFU since it is only viewing one stellar source.

	APE	PDE	RPE	AKE
MIP/MMA local (not global) positioning requirements	5	2	0.5	4
OBM accuracy requirement (if OBM present)				1
AOCS 3-sigma requirements	10	4	1	3
Number of star tracker optical heads	3			

Mechanism	MIP/MMA				MIP/MMA				MIP/MMA			
OBM	OBM, used intermittently in AOCS				OBM, used intermittently in AOCS				OBM, used intermittently in AOCS			
AOCS sensors	Current generation STR				Current generation STR + gyro				Next generation STR			
Error metric	APE	PDE	RPE	AKE	APE	PDE	RPE	AKE	APE	PDE	RPE	AKE
Mechanical Alignment Contributions												
Mirror												
Mirror internal translation distortions between boresightings	0.17			0.17	0.17			0.17	0.17			0.17
Instrument												
Instrument internal translation distortions between boresightings												
Structural												
LoS TED between boresightings												
LoS TED during observation	0.01	0.01			0.01	0.01			0.01	0.01		
LoS jitter due to reaction wheels	0.21		0.21		0.21		0.21		0.21		0.21	
LoS jitter due to cryo coolers	0.21		0.21		0.21		0.21		0.21		0.21	
Flex Modes	0.10				0.10				0.10			
STR												
Mirror optical axis to STR LoS distortion between boresightings												
Mirror optical axis to STR LoS distortion during observation	0.23	0.23			0.23	0.23			0.23	0.23		
Mirror optical axis to STR LoS jitter	0.12		0.12		0.12		0.12		0.12		0.12	
OBM to STR LoS distortion between boresightings	0.40			0.40	0.40			0.40	0.40			0.40
OBM to STR LoS distortion during observation	0.10	0.10		0.10	0.10	0.10		0.10	0.10	0.10		0.10
Mechanism												
Total mechanism error orthogonal to LoS	2.06	2.00	0.50		2.06	2.00	0.50		2.06	2.00	0.50	
OBM												
LED position (w.r.t. instrument) calibration error	1.00			1.00	1.00			1.00	1.00			1.00
OBM accuracy	1.00			1.00	1.00			1.00	1.00			1.00
TOTAL (RSS)	***2.57***	***2.02***	***0.59***	***1.48***	***2.57***	***2.02***	***0.59***	***1.48***	***2.57***	***2.02***	***0.59***	***1.48***
GNC Contributions												
STR pitch/yaw per axis bias	0.49			0.49	0.49			0.49	0.42			0.42
STR lateral due to roll bias at edge of detector (offset 25 arcmin)	0.00			0.00	0.00			0.00	0.00			0.00
STR pitch/yaw per axis post-proc NEA				2.03								0.21
STR lateral due to roll post-proc NEA at edge of detector (offset 25 arcmin)				0.01								0.00
Gyro-stellar estimator NEA								0.58				
GNC RPE (including controller error)	1.11		1.11		0.22		0.22		1.11		1.11	
TOTAL (RSS)	***1.21***	***0.00***	***1.11***	***2.09***	***0.54***	***0.00***	***0.22***	***0.76***	***1.19***	***0.00***	***1.11***	***0.47***
Lateral per axis total	*2.8*	*2.0*	*1.3*	*2.6*	*2.6*	*2.0*	*0.6*	*1.7*	*2.8*	*2.0*	*1.3*	*1.6*
Radial total	***4.0***	***2.9***	***1.8***	***3.6***	***3.7***	***2.9***	***0.9***	***2.4***	***4.0***	***2.9***	***1.8***	***2.2***

Table 13-8: LoS pointing budget with alternate AOCS sensor options. Baseline option highlighted in yellow. Non-compliances highlighted in red

The pointing budget was also re-created in the Pointing Error Engineering Tool (PEET), see Figure 13-3, with assumptions on error distribution types and parameters for transfer functions. PEET has the advantage that the pointing error estimates are compliant with ECSS standards and it allows the user to model the true frequency content of errors and how they attenuate due to estimation filters, feedback control, dynamics, etc. The 3-sigma results were:

- APE = 7.4 arcsec
- PDE = 7.4 arcsec
- RPE = 1.2 arcsec
- AKE = 6.4 arcsec

The PDE estimate is similar to the APE because in the case of ATHENA the PDE is defined to include all error sources from 0.4 mHz to 8 Hz (i.e. a very broad band). APE includes this same band, with lower weighting, as well as high frequency errors, negligible due to rigid dynamics attenuation, and constant errors. The higher weighting of the 0.4 mHz – 8 Hz band in the PDE apparently balances the inclusion of constant errors in the APE. The non-compliant PDE could be alleviated by increasing the spacing of the raster scan and hence relaxing the PDE requirement.

The AKE and APE are significantly larger than that computed in Table 13-7 because biases that are constant during an observation have been added linearly in PEET as per RD[27] (temporal statistical interpretation) as opposed to root sum squared. It is important in future study phases to define which pointing analysis method is acceptable to ESA. The ECSS approach is more conservative but valid if the science requirement is that for the worst case bias the performance shall be per the requirements 99.7% of the time.

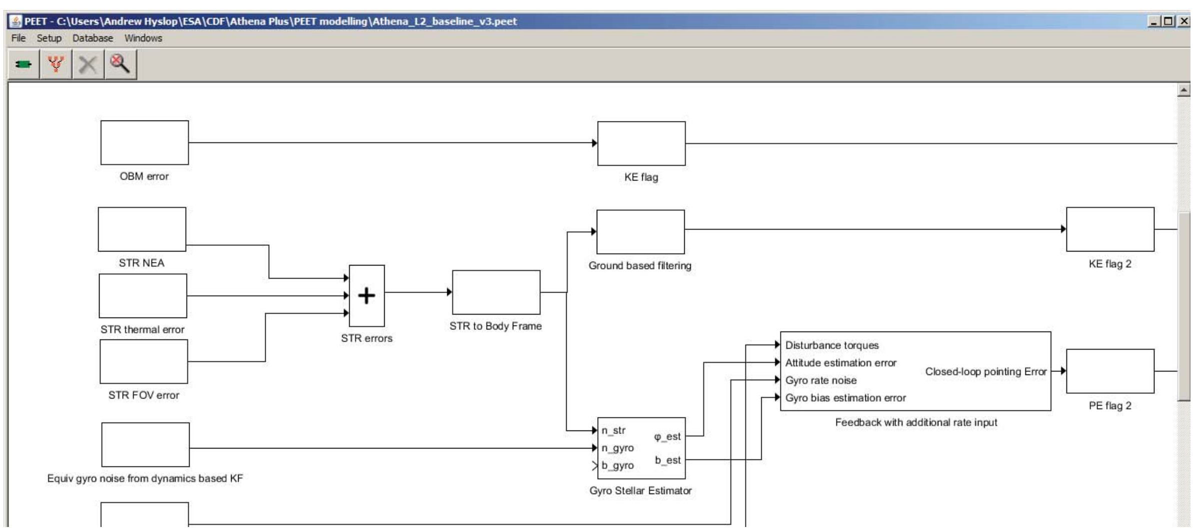

Figure 13-3: Screenshot from PEET analysis of ATHENA L2

13.4 List of Equipment

The AOCS equipment baseline is listed below:

- 3 x Moog Bradford Coarse Sun Sensor, TRL 9
- 2 x Selex Sireus MEMS gyroscope, TRL 6/7
- 3 x Sodern Hydra star tracker optical heads, TRL 9
- 2 x Sodern Hydra star tracker electronics units, TRL 9

- 4 x RDR-68-3 Rockwell Collins Deutschland reaction wheels, TRL 9
- 4 x WDE 8-45 Rockwell Collins Deutschland wheel drive electronics, TRL 9
- 2 x Sodern FFOS (Formation Flying Optical Sensor) receiver optical heads, TRL 5/6
- 2 x Sodern FFOS (Formation Flying Optical Sensor) receiver electronics units, TRL 5/6
- 2 x Sodern FFOS (Formation Flying Optical Sensor) LED transmitter box, TRL 5/6

This usage of this equipment per mode and the recommended transitions between modes is shown in Table 13-9: and Figure 13-1 respectively.

Mode	ASH		FPS		TCM	
Sub-mode definition	Sun acquisition mode	Safe hold mode	Nominal slew	Inertial pointing	Primary orbit control maneuver	Station keeping, fast slew and momentum dump
Sun sensor (safe mode)	X	X				
Sun sensor (monitoring)			X	X	X	X
Gyroscope	X	X				
Star tracker			X	X	X	X
Reaction Wheels			X	X	X	X
On-board metrology			X	X		
22 N thrusters					X	
1 N thrusters	X	X				X

Table 13-9: AOCS equipment usage by mode

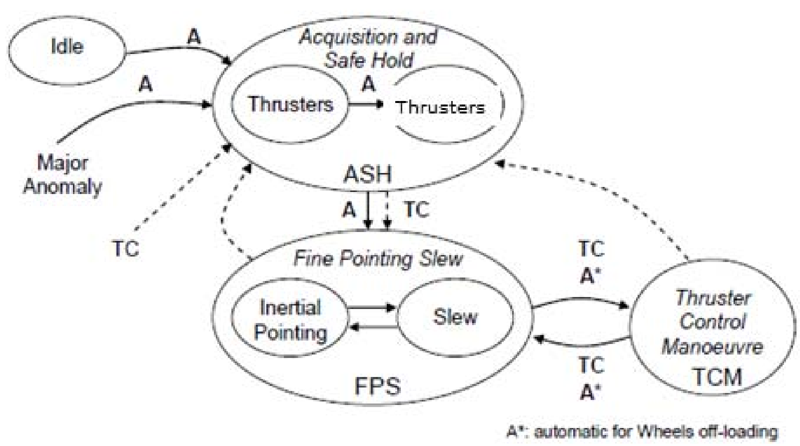

Figure 13-4: AOCS mode transition diagram

The mass and power budgets are summarised below. Note an error in the budget creation tool that included an extra equipment item at the bottom of the list (“blank”).

	mass (kg)	mass margin (%)	mass incl. margin (kg)
GYRO_Sireus1	0.80	10.00	0.88
GYRO_Sireus2	0.80	10.00	0.88
int_metrology_transmitt_elec1	1.38	20.00	1.65
int_metrology_transmitt_elec2	1.38	20.00	1.65
int_metrology_transmitt1	1.38	20.00	1.65
int_metrology_transmitt2	1.38	20.00	1.65
RW_RDR68_3_1	7.60	5.00	7.98
RW_RDR68_3_2	7.60	5.00	7.98
RW_RDR68_3_3	7.60	5.00	7.98
RW_RDR68_3_4	7.60	5.00	7.98
RW_WDE8_45_1	1.25	5.00	1.31
RW_WDE8_45_2	1.25	5.00	1.31
RW_WDE8_45_3	1.25	5.00	1.31
RW_WDE8_45_4	1.25	5.00	1.31
STR_HydraEU_2	1.85	5.00	1.94
STR_HydraEU1	1.85	5.00	1.94
STR_HydraEU3	1.85	5.00	1.94
STR_HydraEU4	1.85	5.00	1.94
STR_HydraOH1	1.37	5.00	1.44
STR_HydraOH2	1.37	5.00	1.44
STR_HydraOH3	1.37	5.00	1.44
STR_HydraOH4	1.37	5.00	1.44

	mass (kg)	mass margin (%)	mass incl. margin (kg)
STR_HydraOH5	1.37	5.00	1.44
SUN_MoogBrad_CSS1	0.22	5.00	0.23
SUN_MoogBrad_CSS2	0.22	5.00	0.23
SUN_MoogBrad_CSS3	0.22	5.00	0.23
(blank)	1.60	10.00	1.76
Grand Total	59.00	6.67	62.93

Table 13-10: Mass budget for the AOGNC subsystem

Power (W)	P_on	P_stby
GYRO_Sireus1	5.50	0.00
GYRO_Sireus2	5.50	0.00
int_metrology_transmitt_elec1	3.80	0.00
int_metrology_transmitt_elec2	3.80	0.00
int_metrology_transmitt1	3.80	0.00
int_metrology_transmitt2	3.80	0.00
RW_RDR68_3_1	45.00	0.00
RW_RDR68_3_2	45.00	0.00
RW_RDR68_3_3	45.00	0.00
RW_RDR68_3_4	45.00	0.00
RW_WDE8_45_1	45.00	5.00
RW_WDE8_45_2	45.00	5.00
RW_WDE8_45_3	45.00	5.00

Power (W)	P_on	P_stby
RW_WDE8_45_4	45.00	5.00
STR_HydraEU_2	11.00	0.00
STR_HydraEU1	11.00	0.00
STR_HydraEU3	11.00	0.00
STR_HydraEU4	11.00	0.00
STR_HydraOH1	0.00	0.00
STR_HydraOH2	0.00	0.00
STR_HydraOH3	0.00	0.00
STR_HydraOH4	0.00	0.00
STR_HydraOH5	0.00	0.00
SUN_MoogBrad_CSS1	0.00	0.00
SUN_MoogBrad_CSS2	0.00	0.00
SUN_MoogBrad_CSS3	0.00	0.00
(blank)	11.00	0.00
Grand Total	441.20	20.00

Table 13-11: Installed power for the AOGNC subsystem equipment

14 PROPULSION

14.1 Requirements and Design Drivers

The overall requirement for the Propulsion system is to provide a ΔV capability for orbital maintenance and attitude control, including repointing capabilities for the telescope to acquire a ToO or in the event of a “safe mode”. Included within this requirement are ΔV requirements for the maintenance of other AOCS actuators for example momentum wheel off-loading.

The primary propulsion during the transfer phases to the operational orbit at L2 is provided by the launch vehicle and upper stage, with a modest on-board ΔV capability for trajectory correction manoeuvres.

The main external drivers for the Propulsion system design come from the following areas:

- Mission - sizing the Propulsion system in terms of ΔV required
- System - overall mass of the SC
- Structure – accommodation envelope available for the propulsion components (in particular propellant tanks, as the largest volume, heaviest mass, and Centre of Gravity position)
- AOCS - Any specific requirements in terms of independent manoeuvres the propulsion system must be compatible with (for example pure torque capabilities, without parasitic translation ΔV), sizing of thrusters for assumed Minimum Impulse Bit (MIB)
- Configuration – Any constraints in terms of thruster plume impingement and line of sight with any optical sensors.

14.2 Assumptions and Trade-Offs

The mission parameters provided for the propulsion system sizing is based on an overall SC mass of 6200 kg and a ΔV budget of 165ms^{-1}. This is derived from a system ΔV budget of roughly 100ms^{-1} for trajectory correction manoeuvres, orbital maintenance, safe mode manoeuvres and an allowance for disposal at the end of life. In addition, 32.5ms^{-1} with 100% contingency making 65ms^{-1} is budgeted for an AOCS assessment of attitude control and repointing manoeuvres over the lifetime of the SC.

The study boundaries requested that all components selected for the propulsion system should be conventional components, requiring little or no additional development, and of European origin wherever practical. The baseline described in section 14.3 below makes maximum use of existing OTS equipment.

Using these initial sizing requirements, an assumed Isp performance for conventional propulsion systems and the rocket equation, a propellant consumption mass to achieve the mission ΔV requirements was calculated. The results indicated that simple four tank monopropellant hydrazine system would meet the sizing criteria in a mass efficient way.

For a nominal Isp of 210s, propellant consumption is 477.21 kg. This Isp is realistic taking into account changes in performance of the thrusters operating in blowdown mode over the life of the SC, ranging from 223s at beginning of life, to 200s at end of life. If a nominal allowance for inefficiencies due to less than ideal thruster alignment to the desired ΔV vector is taken at 92% efficiency, the selected tanks would need to be filled to the maximum 130 kg capacity.

For specific component selection, further trade-offs were investigated, with the priority being given to components of a European origin in the first case, and other non-US sources (such as Japan) in the second case. In the case of propellant tanks, the elastomeric diaphragm technology (Elastomeric diaphragm versus Surface tension PMD type) was the leading trade-off once the appropriate size for the propellant load was selected, and the requirements for pointing stability (low slosh loads) and no constraints in manoeuvre directions to allow for ToO slews in any axes.

14.3 Baseline Design

The baseline design selected is a conventional monopropellant hydrazine system, with four elastomeric (EPDM rubber) diaphragm type propellant tanks operating in 4:1 blowdown mode. This makes use of existing, qualified and flight proven components. A schematic of the system layout is provided in Figure 14-1 below.

There are 2 thruster branches for redundancy so that at each thruster mounting location on the SC there is a pair (prime and redundant units) mounted side by side. The AOCS requirement is to provide pure rotational torques with little or no parasitic translation ΔV. This is achieved with 24 1N class thrusters, (mounted in 12 locations). In addition, 4 22N class (2 prime and 2 redundant) are selected to perform the Trajectory correction manoeuvres #1 and #2 before ejection of the telescope cover.

These higher thrust units are required to be compliant with the requirement to achieve a manoeuvre of $15 ms^{-1}$ within a 2 hour window. The use of 2 x 22N thrusters (operating at nominal 20N each) would allow this manoeuvre to be completed in approximately 37 minutes, whereas the use of smaller thrusters (1N or 5N) would not meet this requirement.

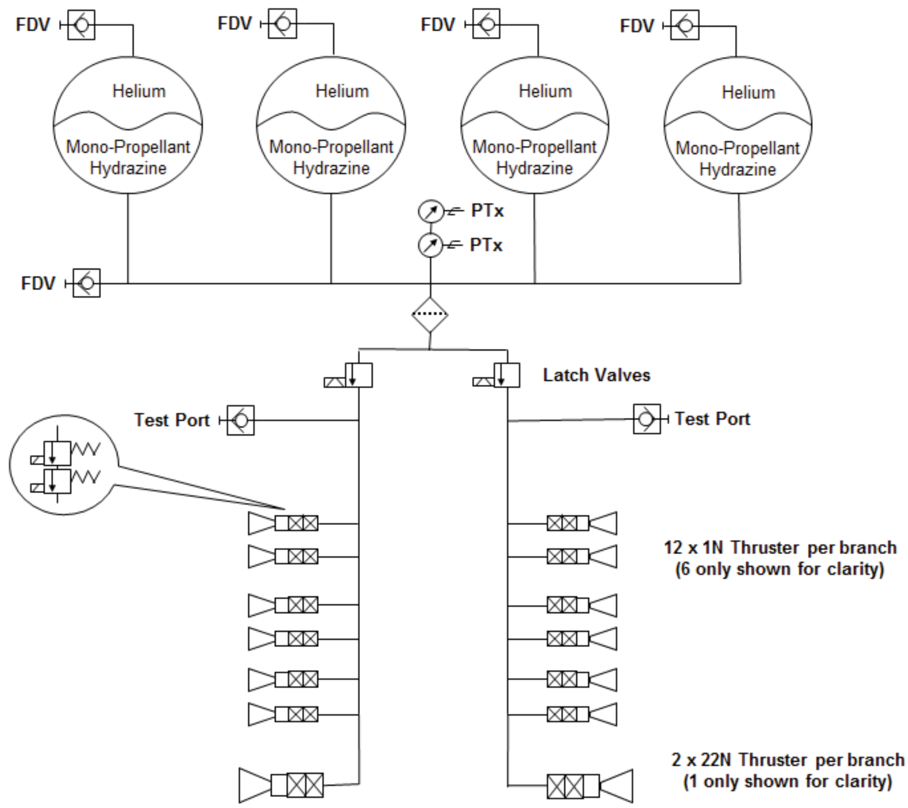

Figure 14-1: Propulsion System Schematic

In order to provide the pure torque manoeuvre capability, Figure 14-2 below illustrates a possible thruster configuration. Further information on the thruster combination to perform the specific manoeuvre is provided in the table on Figure 14-2.

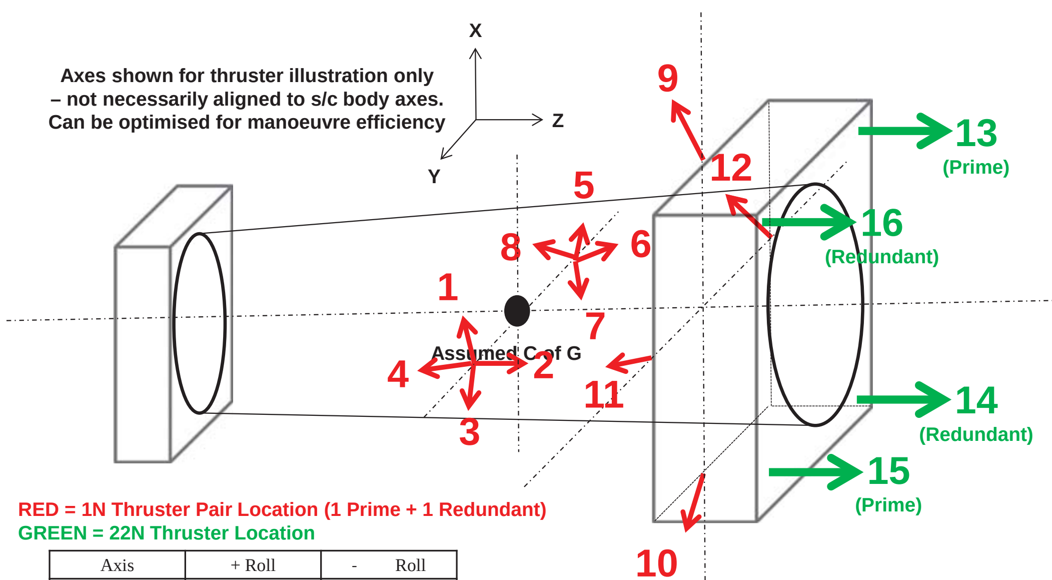

Axis	+ Roll	- Roll
X	4 or 11, 6	2, 8 or 12
Y	10 (1, 5)	9 (3, 7)
Z	1, 7	3, 5

Figure 14-2: Thruster Layout Schematic

Note: In the above, the axes are arbitrary to illustrate the manoeuvre capability. In order to optimise the propellant consumption and reduce the non-observing time, the 2 thruster modules mounted on the fixed metering structure (labelled thruster locations 1 to 8 in the figure above) can be rotated around the fixed metering structure to align with the 28° sun vector.

Thrusters 9 to 12 are mounted on the +Z corners of the SVM away from the telescope aperture, aligned to maximise the X and Y torque capability to allow for fast slews for ToO acquisition.

Thrusters 13 to 16 represent the individual 22N thrusters used to perform the trajectory correction manoeuvres #1 and #2 (before the ejection of the telescope cover) and the disposal manoeuvres at the end of the life.

14.4 List of Equipment

Table 14-1 below lists the equipment selected with quantities and a supplier of a suitable component that would fulfil the requirements of this mission.

Equipment name	Quantity	Potential Supplier
Propellant Tank	4	MT Aerospace, Germany (177 litre Tank – PTD177s)
Propellant Filter	1	Sofrance, France.
Fill and Drain Valve	7	Airbus DS, Germany
Pressure Transducer	2	Moog Bradford, The Netherlands
Latch Valve	2	Airbus DS, Germany
Thruster (1N)	12 pairs (nominal + redundant)	Airbus DS, Germany (CHT 1N)
Thruster (22N)	2 pairs (nominal + redundant)	Airbus DS, Germany (CHT 1N)
Mechanical couplings (Feed line)	2	Parker Stratoflex Dynatube, USA.
Pipework assembly (Feed line)	1	-

Table 14-1: Potential suppliers equipment List

This system has a dry mass of 83.3 kg for the quantities given.

	#	mass (kg)	mass margin (%)	mass incl. margin (kg)
Feed_Line	**1**	**10.00**	**0.00**	**10.00**
Fill_Dr_Val	**7**	**0.07**	**5.00**	**0.07**
Latch_Valve	**2**	**0.55**	**5.00**	**0.58**

	#	mass (kg)	mass margin (%)	mass incl. margin (kg)
Press_Transd	2	0.22	5.00	0.23
Prop_Filter	1	0.77	5.00	0.81
Prop_Tank	4	15.50	5.00	16.28
Thr_Pair_1N	12	0.58	5.00	0.61
Thr_Pair_22N	2	0.79	5.00	0.83
Grand Total		83.34	4.40	87.01

Table 14-2: Mass budget for the propulsion subsystem

Power (W)			
	#	P_on	P_stby
Fill_Dr_Val	7	0.20	0.00
Latch_Valve	2	30.00	0.00
Press_Transd	2	0.20	0.00
Thr_Pair_1N	12	14.00	0.00
Thr_Pair_22N	2	19.00	6.00
Grand Total		267.80	12.00

Table 14-3: Installed power for the propulsion subsystem equipment

Note: The thruster units represent a pair (nominal and redundant). There are a total of 12 x 1N pairs, and 2 x 22N pairs.

14.5 Options

To optimise the propulsion system design, in particular if the required mass of propellant exceeds the capacity of the currently selected tanks, either an additional tank or tanks can be selected, or a new tank with greater propellant capacity can be developed.

14.6 Technology Requirements

No new technologies are required for this solution. All the selected components exist as OTS items. For mass optimisation, an alternative propellant tank might be considered (see 14.5 Options above). For a new tank design, significant cost would be incurred, however this is a low risk, as no new technologies would need to be developed to realise this option.

This Page Intentionally Blank

15 DATA HANDLING

15.1 Requirements and Design Drivers

Subsystem requirements		
Req. ID	**STATEMENT**	**Parent ID**
DH-010	The C&DH subsystem shall provide overall SC control: AOCS, Thermal, Power and FDIR	
DH-020	The C&DH subsystem shall acquire and store platform and payload housekeeping data and payload science data	
DH-030	The C&DH subsystem shall process platform housekeeping data to support on-board autonomous functions	
DH-040	The C&DH shall generate and distribute the SC Elapsed Time	
DH-050	The C&DH shall support data transfer from and to ground.	

15.2 Assumptions and Trade Offs

Apart from the typical tasks of the SC platform avionics, for this mission, the C&DH subsystem is also in charge of sensing the temperature of the instrument mirrors.

The SC shall be able to operate nominally for 4 days with no ground contact. On the nominal scenario, it only communicates with ground on the dedicated transmission windows.

The scientific instruments generate an average science data rate of 863.17 kbps and around 6 kbps of instrument housekeeping. Another 15kbps are reserved for platform housekeeping.

The C&DH subsystem is based on highly recurrent designs with no real need for new technology developments. However, the mission could highly benefit from the use of file based Mass Memory Units and file based operations.

There has been significant work within ESA, with several TRP/GSP activities, in that line. Some ESA missions, such as EUCLID or JUICE, already include CCSDS File Delivery Protocol (CFDP) as baseline for the SC commanding and scientific data transmission to ground

15.3 Baseline Design

The baseline C&DH subsystem is based on the architecture shown in Figure 15-1.

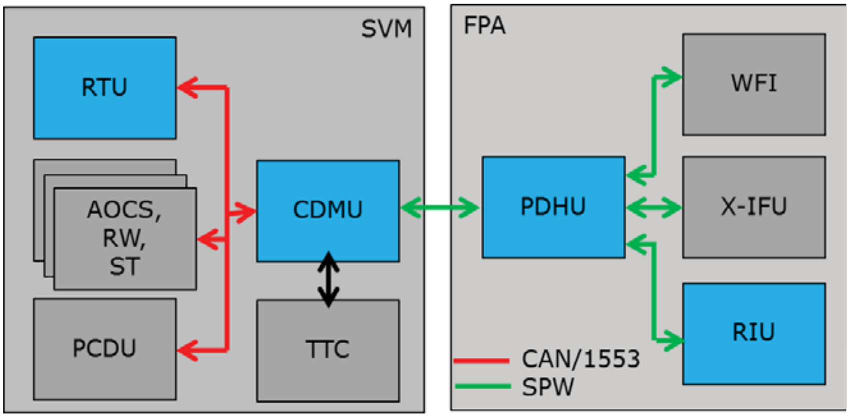

Figure 15-1: C&DH architecture

The CDMU is based on cold redundant processors, MMU and IO boards; and hot redundant power, reconfiguration and TC boards. It contains at least 8 Gbit of file based mass memory, which would be used to store platform housekeeping, OBCPs, SW patches, etc. The SW of the unit implements CFDP class I and class II services for upload and download of data to ground. The protocol is currently under revision and some new extended services are being added, although it is quite unlikely that any of them will be used for this mission. The mass is around 11 kg and the power consumption 29W.

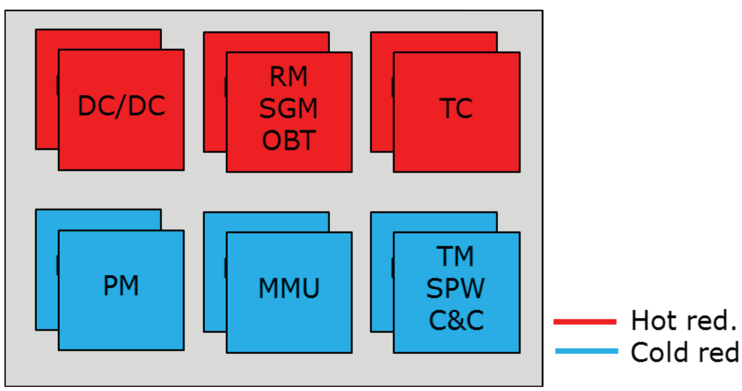

Figure 15-2: CDMU internal architecture

The RTU is in charge of the platform analogue acquisitions, including temperature sensors, as well as interfacing propulsion subsystem, mechanisms, pyros, etc. The RTU is connected to the CDMU via the C&C bus, which can be CAN or 1553. The mass is around 6kg with 8W of power consumption.

The PDHU is in charge of acquiring and storing the scientific instruments data and housekeeping. It contains at least 500 Gbit of non-volatile memory, typically flash based. It interfaces CDMU, instruments and RIU using SPW. The PDHU implements CFDP for data download to ground. The unit is connected directly to the TM board of the CDMU, therefore the unit also formats the data in standard CCSDS packets. The CFDP protocol and CCSDS formatting are implemented, at least partially, in HW which allows the subsystem to achieve higher TM data rates.

The RTU is in charge of acquiring the thermistors from the telescope mirrors. It is connected to the PDHU via SPW.

15.4 List of Equipment

	mass (kg)	mass margin (%)	mass incl. margin (kg)
CDMU	11.00	10.00	12.10
PDHU	15.00	10.00	16.50
RIU	6.00	10.00	6.60
RTU	6.00	10.00	6.60
Grand Total	38.00	10.00	41.80

Table 15-1: C&DH Mass budget

Power (W)	P_on	P_stby
CDMU	29.00	0.00
PDHU	30.00	10.00
RIU	8.00	0.00
RTU	8.00	0.00
Grand Total	75.00	10.00

Table 15-2: C&DH Power budget

15.5 Technology Requirements

The C&DH subsystem uses mostly off-the-shelf units, with minor adaptations to the mission peculiarities. In particular, CDMU and PDHU will, rather likely, follow the SAVOIR standard functional architecture and therefore, will likely be reused from any other mission. RTU and RIU will be largely inspired in similar units, but will probably be new ad-hoc designs

This Page Intentionally Blank

16 TELECOMMS

16.1 Requirements and Design Drivers

Subsystem requirements		
Req. ID	**STATEMENT**	**Parent ID**
COM-010	Shall be able to transmit a gross data volume of 74Gbit/day in 3 hours to Earth	
COM-020	The TT&C subsystem shall implement ranging	
COM-030	Hot redundancy shall be provided for telecommand (uplink) and cold redundancy for telemetry (downlink)	
COM-040	Telecommandability shall be granted at almost all times in order to fulfil the Target of Opportunity requirement	R-MIS-550 / SCI-TOO-R-01
COM-050	The satellite shall orbit around L2 and the nominal distance to Earth shall be 1,770,000 km.	
COM-060	The link budget margins shall be as defined in RD[34] • Nominal > 3dB • RSS worst case > 0dB	

Table 16-1: Communications subsystem requirements

From Table 16-1, the following design drivers were deduced:

- A gross information rate of 7.2Mbit/s during the 3 hours science downlink is needed (1% protocol overhead and 5% margin included)
- An efficient modulation scheme needs to be used to achieve high downlink rates
- Target of Opportunity (ToO) telecommands need to be accepted at any time during the nominal mission
- Antenna repointing should not take place during a scientific observation in order to prevent vibrations that would impair observation
- The maximum communication distance is ~1.77 million km.
- A maximum change in attitude of 3°/day i.e. 0.4°/3hours → no repointing necessary during downlink the antenna gain pattern can tolerate 0.4° off-pointing without substantial gain drop.

16.2 Assumptions and Trade-Offs

16.2.1 Bandwidth Trade-Offs

For frequency coordination, the ATHENA mission is classified as near Earth (category A), space research (SR) mission RD[35]. This restricts the usable frequency bands for telemetry downlink. In the following, a short overview of the different possible frequency bands for both uplink and downlink are reviewed. X- and K-Band are the only viable communications bands for this mission.

16.2.1.1 K-Band (25.5 – 27 GHz)

K-Band could be used to downlink the science telemetry in very little time. This band is meant to be used for high symbol-rate downlink once X-Band cannot provide sufficient bandwidth (limit at 10MHz). For K-Band there are no restrictions on the possibility of using up to the full allocation. The use of such a high frequency carrier poses challenges for on-board spherical coverage and acquisition during LEOP, therefore a dual band (X-Band + K-Band is needed). In conclusion the K-Band option was rejected as it would have made it necessary to have dual-band equipment which requires more mass, space and entails additional unnecessary complexity.

16.2.1.2 X-Band (8.450 - 8.500 GHz)

X-Band has been used extensively for L2 missions in the past and recent missions: Herschel, Planck, Gaia. Transponders, antennae, amplifiers and signal distribution hardware of high TRL and good heritage are available for X-Band. The major drawback of using X-Band is that the bandwidth usage is limited by ECSS to 10MHz RD[34]. This limitation drives the need for a bandwidth efficient modulation and coding in the downlink.

16.2.2 Antenna Trade-Offs

For contingency and LEOP phase, omnidirectional coverage is needed. This can be achieved through the use of at least two low gain antennae (LGA) covering each a hemisphere of the SC. Due to the long range and high information rate required, the use of a high gain antenna (HGA) is mandatory.

16.2.2.1 High Gain Antenna

There is a trade-off between HGA diameter and downlink RF-Power where smaller apertures can be compensated with higher output power. At the same time there is a trade-off between antenna diameter and beam width. This leads to a situation where repointing can be reduced by increasing RF output power which allows for a smaller antenna with wider beam width. In the end, an HGA diameter of 0.4m has been retained as a good trade-off between beam-size, mechanical accommodation and necessary RF power. Its large 3dB-beam-width of 6.2° allows for flexibility in antenna pointing strategy.

16.2.3 Ground Station Trade-Off

Two sets of ground stations were taken into consideration to cover all up and downlink needs.

16.2.3.1 Three 15m ground stations

Using three 15m ground stations it would be possible to provide nearly continuous uplink availability as required by COM-040. Unfortunately the future of the operation of the ESTRACK 15m X-Band capabilities is uncertain. Additionally, the power usage using X-Band to downlink at the required rate would need >300 W for a 40cm HGA and >100W for a 55cm HGA.

16.2.3.2 One 35m & two small stations (~3.5m)

One alternative to the above scenario would be the usage of one 35m G/S augmented by two smaller acquisition aid stations (2.5m and 4.5m) for ToO telecommanding. This scenario leads to lower power usage but is also better from an operational point of view. Only one station needs to be used regularly, while the small stations are just needed occasionally for when a ToO target is to be observed while the 35m station is not in view. An example of such a configuration is shown in Figure 16-1.

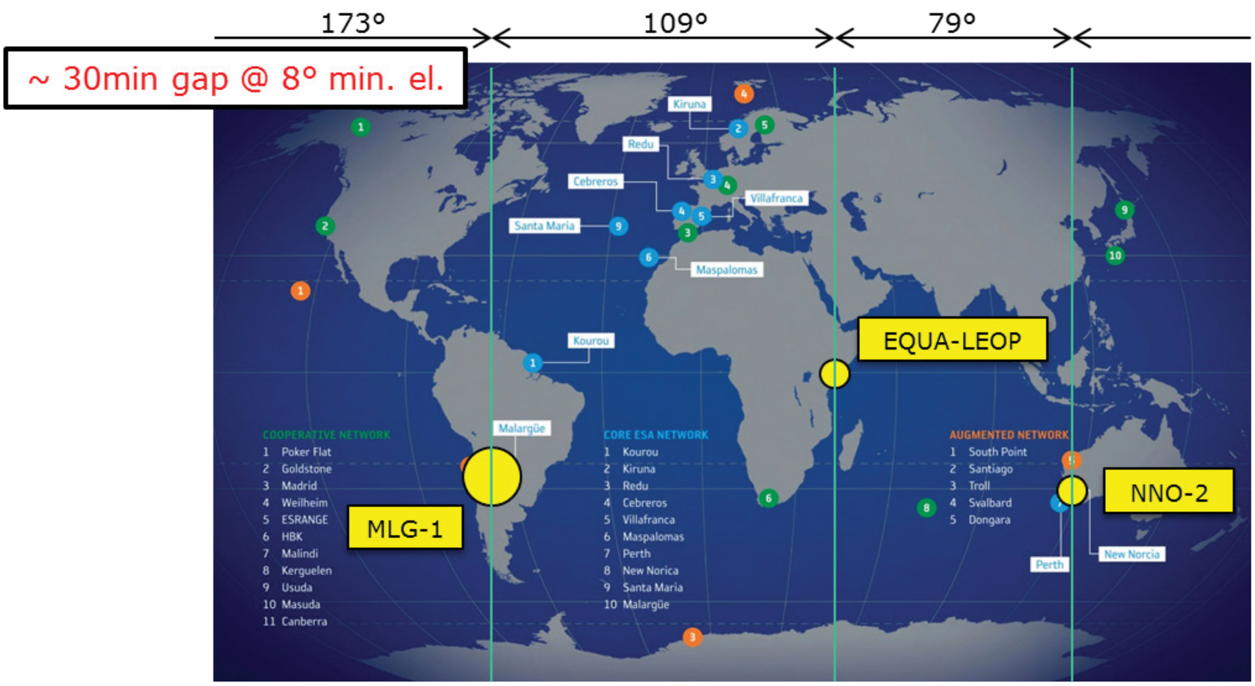

Figure 16-1: Example G/S configuration

16.2.4 Redundancy Trade-Off

The hot redundant LGAs and transponders make it possible to receive telecommands if one of the transponders fails. Receiving is possible in every orientation due to the orientation of the LGAs and their combined radiation pattern.

The failure of one of the TWTAs or one of the transponders also leaves the possibility to continue downlinking via the HGA. Depending on the transponder or TWTA that fails, there is a need to operate an RF-switch. Taking in to consideration RD[37], once inserted on L2 orbit, the activation of the RF-switch is foreseen only as a consequence of a failure of the TRASP/PHA, not as part of the nominal operations, removing therefore the single-point of failure at SC level.

16.3 Baseline Design

16.3.1 Architecture

The baseline architecture of the on-board communication subsystem is illustrated in Figure 16-3. Nominal TT&C operation and scientific telemetry downlink are both performed in X-Band. The overall system includes:

- Two redundant X/X transponders
- Two redundant TWTAs composed of:
  - o A Traveling Wave Tube and
  - o An Electric Power Conditioner
- One steerable X-Band HGA of 40cm diameter
- Two fixed X-Band LGAs
- A Radio Frequency Distribution Unit (RFDU).

The LGAs should be positioned in a way such that continuous coverage is achievable. An example accommodation is illustrated in Figure 16-2.

16.3.2 Modulation, Coding and Ranging

The preliminary selected modulation schemes have been chosen from the ECSS standard RD[34]:

- Telecommand uplink: NRZ/PSK/PM(sine), modulation index: 1.0
- Telecommand coding: None
- Telemetry downlink: GMSK BTb=0.5
- Telemetry coding: Punctured convolutional coding (5/6, 7) (Coding gain: 4.9dB FER=10e-4).

Ranging can be performed parallel to GMSK using regenerative Pseudo-noise (PN) ranging. This technology is not standardised yet at the time of writing but it is expected that this will happen soon and the technology has already been deeply investigated RD[38].

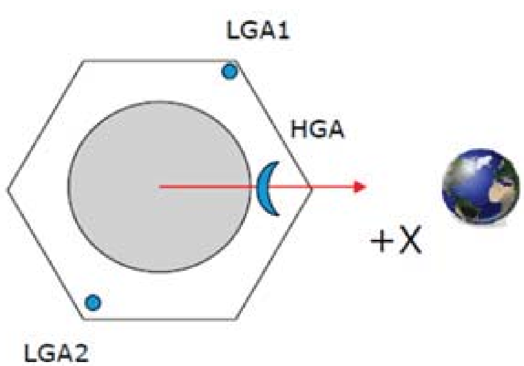

Figure 16-2: Preliminary antenna accommodation

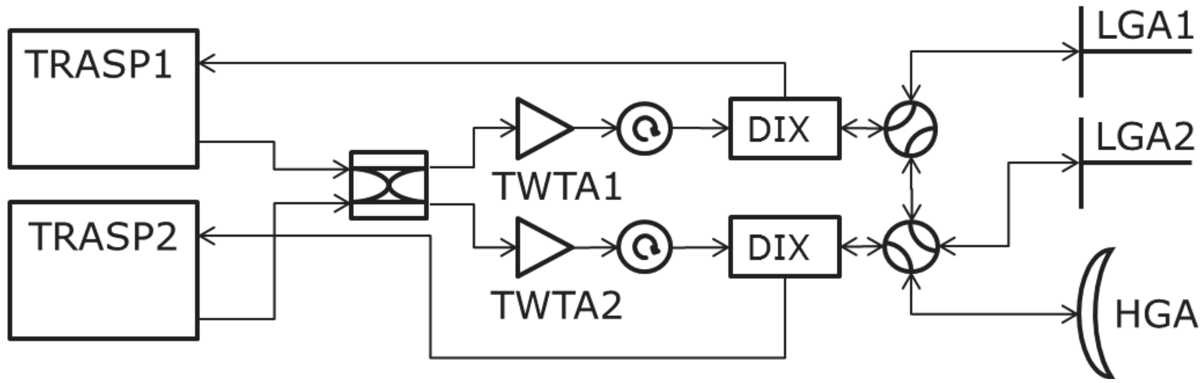

Figure 16-3: Tentative architecture. TRASP: X-Band Transponder, TWTA: X-Band Traveling Wave Tube Amplifier, DIX: Diplexer

16.4 Equipment Details

The following paragraphs describe the chosen equipment in more detail.

16.4.1 High Gain Antenna

A parabolic reflector dish shall be used. The specifications of the HGA are as follows:

- Efficiency: 60%
- Diameter: 40cm
- Mass: 3kg (excl. Pointing mechanism)
- 3dB-beam-width: 6.2°
- Boresight gain: 28.8dBi
- Boresight-0.4° gain: 28.7dBi (c.f. 16.1)

16.4.2 Low Gain Antennae

The two Low Gain Antennae are in charge of receiving and transmitting data during LEOP or potentially in contingency cases.

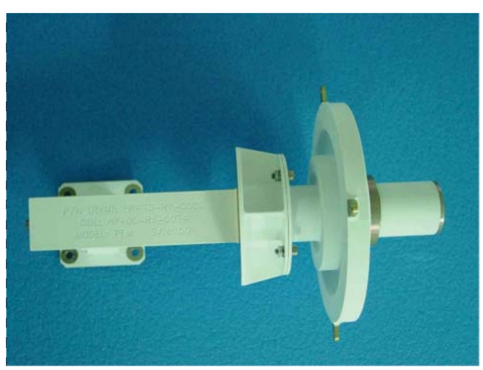

Figure 16-4: Example LGA

Two LGAs are used together to provide an omnidirectional radiation pattern. The gain pattern of a stand-alone antenna is shown in Figure 16-5:

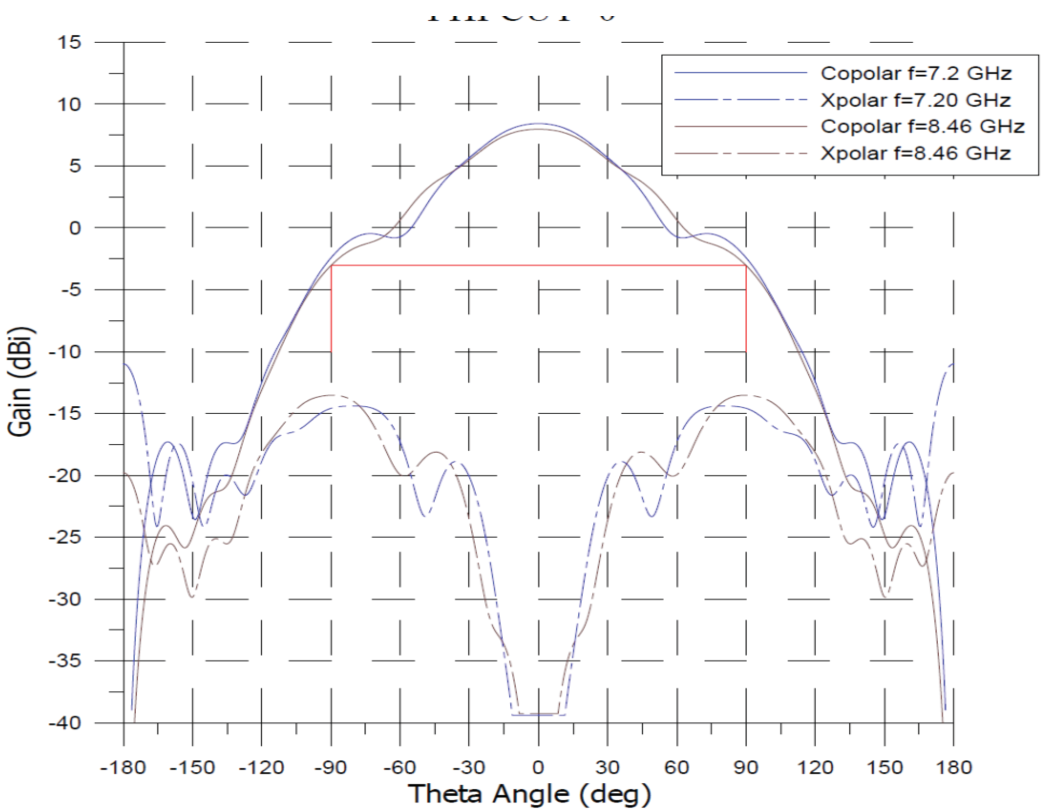

Figure 16-5: LGA radiation pattern

The main performance figures of the LGA are given below (from Table 18-1):

- Antenna type: Choked horn
- Gain: -4 dBi to +6 dBi (in one hemisphere)
- Mass: 0.3 kg (without supporting bracket).

16.4.3 Transponders

The X-Band transponder will demodulate the telecommand signal received from either the LGA or HGA, deliver the demodulated signal to the On Board Computer (OBC),modulate the telemetry data and forward the signal to the amplifier.

The proposed transponder has a TRL of 9 (with the exclusion of possible modification for with rate (GMSK) with parallel ranging (PN). It has been developed by TAS-I and has a heritage from GAIA and Herschel-Planck. The receiving part will work in hot redundancy while the transmitter will work in cold redundancy.

A further development is needed in order to support PN ranging.

The main performance details for this equipment are given below:

- Maximum TC uplink data rate 4 kbps
- Telemetry downlink modulation schemes: BPSK, SP-L and GMSK
- Ranging capability simultaneous with low data rate telemetry
- Total mass considering a 10% margin: 3.2 kg

- Consumed power (transmitter OFF/ receiver ON): 20 W
- Consumed power (transmitter ON / receiver ON): 31 W

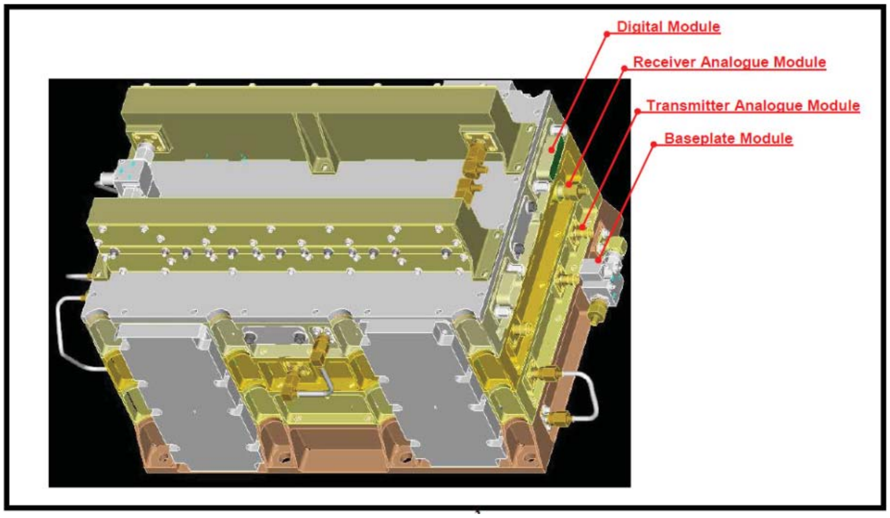

Figure 16-6: X-Band Transponder

16.4.4 Traveling Wave Tube Amplifier

The Travelling Wave Tube Amplifier (TWTA) is in charge of amplifying the downlink signal to the necessary RF output power. It consists of a traveling wave tube (TWT) supplied by an electrical power conditioner (EPC).

The proposed equipment has currently a TRL of 9. The TWTA has been developed by TAS-B and has a heritage on many ESA missions.

Two TWTAs are used to provide equipment redundancy. The operating mode is cold redundancy meaning only one of them is switched on at any time.

The main performance details for this equipment are given below:

- RF output power: 35 W
- Mass: 1 kg (TWT) + 1.4 kg (EPC)
- Consumed power: 58 W (TWT) + 3W (EPC).

Figure 16-7: Travelling Wave Tube Amplifier

16.4.5 Radio Frequency Distribution Unit

The RFDU is composed of all elements needed to interconnect the previously discussed pieces of equipment. It is composed of waveguides guiding the RF-power, RF-switches, diplexers separating the up- and downlink signals, isolators reducing reflections and couplers splitting up RF-signals. The proposed RFDU as shown in Figure 16-3 is only a rough guideline and additional RF-switches could e.g. decrease the impact of a stuck switch as described in 16.2.4.

16.5 List of Equipment

	mass (kg)	mass margin (%)	mass incl. margin (kg)
EPC1	1.40	10.00	1.54
EPC2	1.40	10.00	1.54
HGA_ATHL	3.00	20.00	3.60
LGA1	0.30	5.00	0.32
LGA2	0.30	5.00	0.32
RFDU	5.00	20.00	6.00
TRASP_Tx_MOD_Rx_DED1	3.20	20.00	3.84
TRASP_Tx_MOD_Rx_DED2	3.20	20.00	3.84
TWT1	1.00	10.00	1.10

TWT2	1.00	10.00	1.10
Grand Total	19.80	17.12	23.19

Table 16-2: Mass budget for the communications subsystem

Power (W)	P_on	P_stby
EPC1	2.92	0.00
EPC2	2.92	0.00
HGA_ATHL	0.00	0.00
LGA1	0.00	0.00
LGA2	0.00	0.00
RFDU	0.00	0.00
TRASP_Tx_MOD_Rx_DED1	51.00	0.00
Rx_DED	20.00	0.00
Tx_MOD	31.00	0.00
TRASP_Tx_MOD_Rx_DED2	51.00	0.00
Rx_DED	20.00	0.00
Tx_MOD	31.00	0.00
TWT1	58.33	0.00
TWT2	58.33	0.00
Grand Total	224.50	0.00

Table 16-3: Installed power for communications subsystem equipment (the Grand Total is never achieved due to redundancy, cf. power budget)

16.5.1 Link Budgets

The ATHENA mission has a number of potential bidirectional links to be considered; they are listed in Table 16-4.

The downlink to a 35m station is the sizing case for the HGA since it needs the highest bit-rate. This link can be closed at a distance of 1,770,000km with a telemetry recovery margin of > 5 dB with a gross information rate of 7.2Mbit/s. The downlink has a symbol rate of 7.64Msym/s which leads to an occupied bandwidth of 6.32MHz < 10MHz as required by RD[38].

	HGA		LGA	
	U/L	D/L	U/L	D/L
35m	4kbit/s	7.2Mbit/s	4kbit/s	10kbit/s
4.5m	4kbit/s	15kbit/s	N/A	N/A
2.5m	1kbit/s	8kbit/s	N/A	N/A

Table 16-4: Achievable bitrates in accordance with COM-060

16.6 Technology Requirements

Equipment and Text Reference	Technology	Suppliers and TRL Level	Technology from Non-Space Sectors	Additional Information
Ground segment	GMSK			GMSK needs to be supported for science telemetry downlink
Ground segment	Regenerative PN-ranging			Regenerative PN-Ranging in parallel to
Transponder	GMSK and PN-Ranging			Minor modifications to the transponder are needed.

17 STRAYLIGHT & PARTICLE BACKGROUND

17.1 Instrument Requirements

The sensitivity of the two instruments may be compromised by straylight and particle induced signals. Straylight can be separated into:

- X-rays from directions other than the nominal optical path through the mirror; such photons will contribute directly to the x-ray spectra and images, and cannot be discriminated from photons from sources in the FoV
- IR-UV radiation; these photons will not be detected individually but they will degrade the noise and energy performance of the detectors. Both instruments carry filters which reduce the IR-UV component of the spectrum of the sources in the FoV to an acceptable level.

The requirements for straylight suppression for the two instruments are listed in Table 17-1.

	WFI	X-IFU
Diffuse X-ray background from outside FoV	<0.001 cts/SCm² (0-15keV) [1]	<0.005 cts/SCm²/keV (0-12keV)
UV/Vis stray light ph/SCm² [2]	$< 10^{12}$	$< 1.3\ 10^{10}$ [3]

[1] For illustration purposes a number of <0.0003 cts/SCm²/keV is used in Figure 17-1

[2] Levels refer to the detector surfaces of WFI and to the outer cryostat filter for X-IFU

[3] Assuming a solar spectrum.

Table 17-1: Instrument requirements X-ray and UV/visible stray light baffling

Particle induced signals may also give rise to signals in the energy band of interest of the instruments, which cannot be discriminated from photon signals. The instruments can be well shielded internally against such particles from all directions except from the FoV. In particular, low energy protons and electrons can be collimated by the mirror modules, similar to x-ray photons. Such charged particles can be removed from the FoV by diverting them by means of magnetic fields. The requirements on the magnetic diverters are to deflect only those particles that would give rise to signals in the detectors' energy bands of interest, taking into account energy losses of those particles when they pass through the filters of the instruments. The requirements for particle deflection are listed in Table 17-2.

	WFI	X-IFU
FoV: On sky (arc min) In focal plane (cm)	 40.0 ∅ 19 ∅	 5.0 ∅ 2.2 ∅
Filter stack: Fixed movable	 70 nm Al + 35 nm Si_3N_4 + 35 nm SiO_2 40 nm Al + 320 nm Poly-propylene	 210 nm Al + 280 nm Poly-imide 60 nm Al + 200 nm Poly-imide
spectral range for particle deflection [4]	<30 keV	<20 keV
Max. particle energy to be deflected from focal plane (keV): protons electrons	 75 keV 31 keV	 78/106 keV [1] 21 keV
B_{max} (T)	~1e-3 T	<1e-4 T [2], <1e-3 T [3]

[1] 106 keV is a goal requirement which includes the energy loss in the movable filter, 78 keV does not

[2] During cool down of the superconducting shield through its transition to prevent flux trapping

[3] At any other time during (non)-operation to prevent flux trapping in the superconducting shield when cold

[4] A factor of two in the upper limit is built in as margin.

Table 17-2: Instrument specifications relevant for particle deflection

17.2 The X-Ray Stray Light Baffles

The diffuse x-ray background presents an isotropic illumination of the entire satellite and is characterised by a spectral distribution given by $I(E)=9\cdot E^{-1.42}$ photons/s/steradian/keV (black curve in Figure 17-1).

The fixed metering structure of the ATHENA telescope is only partially opaque for x-ray photons. In Figure 17-1 the purple curve shows the calculated transmission of the fixed metering structure (conservatively modelled as consisting of 2 sheets of 1 mm thick CFRP skins and an effective thickness of 0.27mm Al) under normal incidence and with a total solid angle of 5 ster (representing a hemisphere with the telescope mirror excluded). Clearly, the tube does not provide sufficient shielding at energies E>7 keV. Therefore, the two instruments each need a structure which limits the unobstructed view of the instruments to the mirror assembly and the SVM structure, which is assumed to be opaque and acts as a 'skirt' around the mirror assembly.

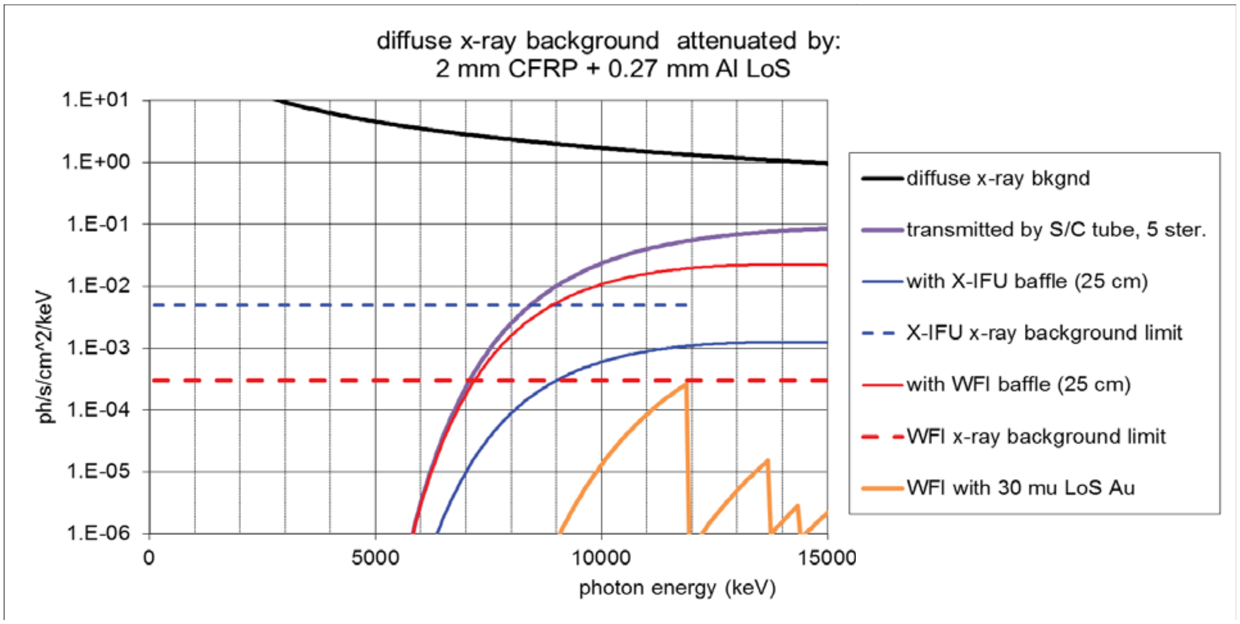

Figure 17-1: Calculated attenuation of the diffuse X-ray back ground spectrum by the fixed metering structure (modelled as effectively 2x1 mm CFRP + 0.27 mm Al). A 30 micron thick Au layer would bring the residual intensity below the required stray light levels

This is partially provided by the instruments' internal structure and baffles. The effect of such instrument baffles with an effective length of 25 cm is also shown in Figure 17-1. For X-IFU, this is already sufficient to bring the residual x-ray background below the requirement. For WFI however, at least another order of magnitude of suppression is needed.

This additional suppression could be provided by various solutions:

- A cylindrical or conical tube of appropriate dimensions and with sufficiently opaque wall; basically this would be an extension of the instrument baffle, but mounted on the instrument platform
- Sufficiently opaque disk-like rings (as in XMM-NEWTON) at appropriate distances from the detector, if needed in combination with a smaller cylindrical/conical baffle, which will be part of the instrument.

Sufficient opacity could be provided by a layer of gold with an effective thickness of 30 micron along the line of sight (orange curve in Figure 17-1), but different materials may be considered to reduce fluorescence.

No in depth trade-off was done between these two solutions, instead the second option with the baffling disks is investigated in more detail.

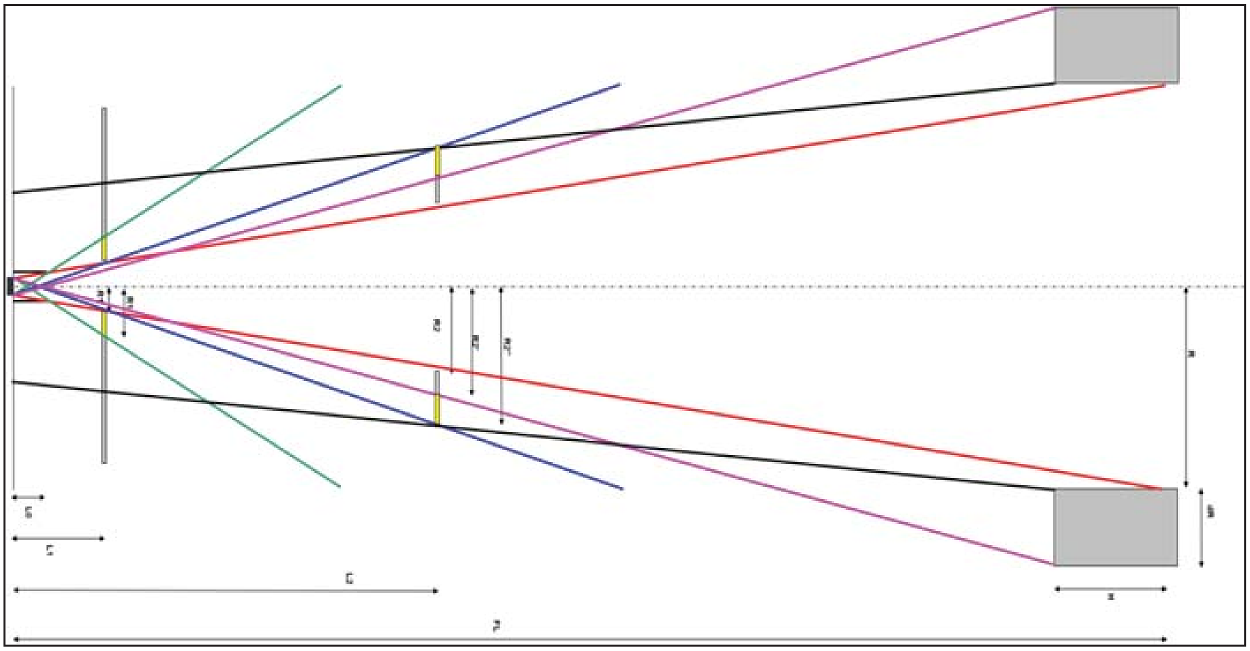

Figure 17-2: Conceptual baffle geometry with gold coated rings to block the view to the metering structure. Detector + small instrument baffle are on the left, mirror and SVM structure on the right, connected by a conical metering structure

Figure 17-3 shows a possible configuration of baffling disks like on XMM-Newton. Small PI provided baffles (~25 cm length) as part of the instruments are assumed. In the current configuration of mirror radius, focal length, SVM dimensions, conical metering structure dimensions, 84cm of instrument separation (X-IFU centre to WFI large imager centre), the baffling system would consist of 5 disks at distances of 1.0, 1.4, 1.8, 2.5 and 3.45 m from the detector planes. These disks would have apertures to prevent obstruction of the FoV, and rings of 50 micron thick (conservative) gold (total mass ~2 kg) at the appropriate positions to obstruct the view to the metering structure. A slightly longer WFI instrument baffle (0.7m) will be needed in combination with these rings. The total mass of the disk system with gold is estimated at ~5 kg (without support structure).

Some complication arises from the requirement not to obstruct the FoV of the fast WFI detector and of X-IFU; this requires additional and/or larger apertures in the disks. Some of these will interrupt the gold-coated rings, at the expense of a larger x-ray background contribution of WFI. Clearly, further optimisation (including graded shielding to reduce secondary emission) will be necessary. Another issue that was not taken into account was the additional hole required in the baffles to allow the use of the OBM in the chosen configuration (with MMA).

17.3 Optical Stray Light Baffling

No stray light analysis has been performed yet for ATHENA, but some similarity with XMM-Newton may exist. The instruments already have internal filtering to suppress directly imaged star light. Scattered light from the mirror assembly may be the main source of residual straylight.

17.4 Charged Particles Diverters

Such diverters could in principle be placed anywhere between the Mirror Assembly and the Focal Plane. However, placing them closer to the Mirror Assembly implies much larger mass (TBC) than placing them close to the FPM. Following the design for IXO, the current baseline is therefore to place these deflectors close to the instrument platform, mounted on the straylight baffling disk at ~1m from the focal plane (see Figure 17-3). The choice of the movable mirror assembly (MMA) as opposed to the movable instrument platform (MIP), complicates the design, as it necessitates separate diverter systems for WFI and X-IFU.

The relevant drivers for the design and accommodation of the diverters are:

- The required deflection efficiency: this is determined by the maximum energy of the particles to be deflected and the area of the sensor from which these particles have to be diverted
- Preventing the obstruction of the X-ray light paths
- Mass optimisation
- Residual magnetic fields at the detectors.

The instruments' requirements with respect to charged particle deflection are listed in Table 17-2. They refer to:

- The maximum energy of the protons and electrons that need to be deflected (with a factor of 2 margin), based on (1) the band pass that needs to be cleared from charge particle signals, and (2) the relevant filter thicknesses to calculate energy loss of these particles in the filters
- The area in the Focal Plane from which the particles have to be deflected
- The maximum residual magnetic field strength that can be tolerated at the position of the detectors.

Particles will lose energy when passing through any filters included in the instrument. This energy loss has been accounted for by using both the proposed fixed filter thickness for each instrument as well as possible additional filters in the filter wheel (see Table 17-2.). The resulting maximum proton and electron energies to be deflected are listed in Table 17-2. It should be noted that the *total* flux of charged particles incident on the detectors may not be reduced significantly, since the low energy particles are only a small fraction of this total flux.

The residual magnetic field induced by the particle diverters at the focal plane is an important constraint, especially for X-IFU, and in particular during the initial cool-down of X-IFU.

For now however, a simple, conservative, scaling of the diverter systems is done from a Hallbach design proposed for IXO. This system consists of a set of permanent magnets in a so-called Hallbach configuration (see Figure 17-3). Such a system provides a very uniform field inside the ring of magnets, and a very low field outside. Such a system could conveniently be accommodated on the lowest baflle disk at ~1m from the focal plane. The fast WFI array is assumed not to require particle deflection (TBC).

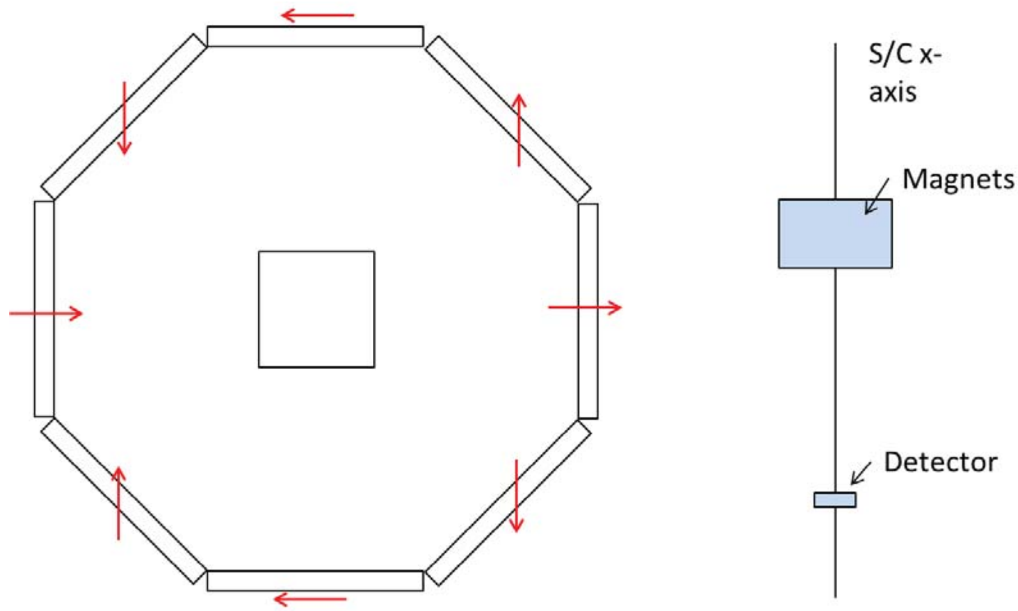

Figure 17-3: Possible configuration of the particle deflecting magnets. The design shown here was for IXO

For the scaling from the IXO to the ATHENA configuration, the following considerations are relevant:

- The focal ratio of the ATHENA telescope (F/5.0) is slightly smaller than for IXO (F/5.3)
- The linear size of the WFI detector on ATHENA is almost twice the linear size of the WFI detector on IXO
- Hence the maximum deflection angle is roughly twice as large, and the Hallbach array needs to be roughly twice as long on ATHENA
- Because the Hallbach array is longer, the sensor area is larger and the F number is smaller, the Hallbach also needs to be wider
- The array should not obstruct the FoV of the fast WFI detector, and hence needs to be wider, at least in one direction
- Therefore the mass of the Hallbach array for WFI on ATHENA is estimated to be 4x the mass of the IXO system (which was 13.7 kg, without support)
- The X-IFU array is estimated conservatively to have the same mass as the IXO diverter system mass.

17.5 Baffling and Particle Diverter Resource Requirements

Table 17-3 lists the resource requirements for baffling (Au layers only) and particle diverters. The mass of the particle diverters is estimated conservatively at 20 kg, similar to the mass of the single, common, particle diverter in the assessment study for IXO. The XMS diverter can probably be significantly reduced in mass.

	mass (kg)	mass margin (%)	mass incl. margin (kg)
Stry_Baffles_Div	**73.70**	**100.00**	**147.40**
x-ray baffle disk system	5	**100.00**	**10**
Particle diverter for WFI	55	**100.00**	**110**
Particle diverter for X-IFU	13.7	**100.00**	**27.4**
Grand Total	**73.70**	**100.00**	**14.40**

Table 17-3: Mass budget for the straylight and non x-ray blocking equipment

Given the very low level of design maturity, a 100% margin on the mass was added.

Clearly, a full optimisation of the particle diverters with respect to accommodation, mass and residual magnetic field is needed. Also the impact of the presence and specific requirements of the fast WFI detectors needs to be assessed.

This Page Intentionally Blank

18 GROUND SEGMENT & OPERATION

18.1 Requirements and Design Drivers

Subsystem requirements		
Req. ID	**STATEMENT**	**Parent ID**
ScIRD R-MIS-550	The ATHENA Mission shall perform Narrow-Field observations of a GRB-ToO within 4 hours of the receipt of an external ToO alert for 80% of validated ToO alerts.	
ScIRD R-MIS-560	The ATHENA Mission should perform all observations of all ToOs within 4 hours of the receipt of an external ToO alert.	
	During LEOP critical operations the SC shall be designed to support a ground response time of up to 2 hours.	Plato (Heritage)
	During LEOP, outside critical operations, the SC shall be able to support a ground response time of up to 12 hours.	Plato (Heritage)
	During any operations of the transfer and commissioning, the SC shall be designed to support a ground response time of up to 48 hours.	Plato (Heritage)
	During nominal science operations, the SC shall be designed to operate nominally, collect and store payload science and housekeeping data for at least 3 days of ground segment outage. Note: No science data shall be lost if two daily communications passes are missed.	Plato (Heritage)
	During nominal science operations, the SC shall be designed to operate nominally, collect and store payload housekeeping data only (i.e. not payload science data) for at least 7 days of ground segment outage. Note: After 3 days without ground contact, the platform will continue to operate nominally and keep the payload in the operational configuration. Payload housekeeping data will be stored, but no new science data will be stored or generated.	Plato (Heritage)
	A minimum operational resource margin of TBD shall be provided for on-board subsystems and payloads that is available at all times during the mission. Note: In order to ensure a simple ToO planning with a minimum number of constraints an operational margin shall be available for TBD types of resources (e.g. momentum storage capability, fuel, power, thermal design, data storage).	
	A margin of 100%, covering uncertainties in mission design and system performance, shall be applied to the propellant required for angular momentum management.	Plato (Heritage)
	The RCS for attitude control and wheel momentum off-loading shall use pure torque thrusters.	Plato (Heritage)
	The propulsion system shall be balanced such to minimise parasitic	Plato (Heritage)

	torques.	
	The propulsion system shall have spherical thrust capability for a prolonged period of time. Note: This shall avoid constraints on the TCM design during the transfer phase.	Plato (Heritage)
	The SC shall provide the capability of performing the transfer phase transfer control manoeuvres (TCMs) without violating the illumination constraints of the telescope. Note: This shall be achieved by a telescope cover.	Plato (Heritage)
	The SC shall provide the capability of performing station keeping manoeuvres without violating the illumination constraints of the telescope. Note: Manoeuvre direction is along an axis 28.6 degrees off the Sun-Earth axis in the Earth orbital plane.	Plato (Heritage)
X-band	Communications with ground shall use X-band (7.2 GHz uplink, 8.4 GHz downlink).	
New ranging standard	SC ranging and Doppler capability shall be available in parallel to the high data rate downlink. Note: This requires ranging modulation in line with RD[40].	
HGA permanently available	During science observations the SC HGA shall always be pointed to Earth with enabled reception capability. Note: This is required to enable the reception of ToO commands.	
	The Mass Memory shall store data in separate files.	EUCLID (Heritage)
	The stored housekeeping data shall be downlinked as files. The real time housekeeping data shall be downlinked with the X band TM link.	EUCLID (Heritage)
	The exchange of files between space and ground shall follow the CFDP protocol specified in RD[42].	EUCLID (Heritage)
	Downlink of files shall use CFDP class 2 and shall be done in “Deferred NAK ARQ” mode.	EUCLID (Heritage)
	Uplink of files shall use CFDP class 1.	EUCLID (Heritage)
	The information distribution service shall provide the capability to distribute any parameter stored in the data pool.	EUCLID (Heritage)
	The capability to compress of stored and real time housekeeping data shall be provided for data downlink.	

With respect to ground segment and operations the ATHENA mission has the following major characteristics and design drivers:

Launch and transfer:

- A5-ECA free-insertion large amplitude Halo orbit around L2 – total mission, Direct ascent scenario without circular parking orbit Δv ~100m/s
- +1 day: Transfer Correction Manoeuvre 1 (TCM#1)
    - Correction of launcher dispersion

  - o Correction of deterministic deviation from stable manifold
  - o Manoeuvre must be executed at day-2 at the latest due to amplification of errors
- +5 days: TCM#2
- +20 days: TCM#3

⇨ Benign launch and transfer scenario, no attitude restrictions due contamination cover, operationally straight forward.

Station keeping:

- Station-keeping manoeuvre every 4 weeks or as required
- No constraints on manoeuvre directions

⇨ Ranging required during every coverage period to track orbit, no particular operational constraints.

Disposal:

- End-of-Life disposal required to avoid Earth-return, 10 m/s currently allocated for disposal via unstable manifold

⇨ Details TBD, 1 month operational efforts assumed for disposal manoeuvres and SC passivation.

SC and instrument complexity:

- Large and complex SC, movable mirror assembly
- Very long structure, large moment of inertia but fast slew capability
- WFI is complex instrument
- X-IFU is a very complex instrument, with 50mK cryogenic cooling

⇨ L-class large operations team required with extensive operations engineering and subsystem knowledge
⇨ On call engineering support for weekends and holydays (quick reaction to anomalies required to bring expensive SC back to nominal and maximise operational product generation.

Operations:

- Classic ESA responsibilities, to be operated by ESOC
- Complex planning for individual pointings (with dithering)
- Switching of instruments
- High data rate, but compatible with 3h daily X-band passes
- Extremely fast ToO-response (<4 hours for 80% of instances) to externally-generated ToO-requests

⇨ New ranging standard compatible with high data rate
⇨ High SC autonomy to minimise ToO complexity and enable for ToO operations by cross trained SPACONs
⇨ Dedicated small stations to support 24h access to SC for ToOs
⇨ 24h availability of Spacons.

Launch date 2028 (enables for advanced developments):

- Possible evolution of operations software, PUS replaced by MO services TBC
- Evolution of common core, enabling for common tools and for commonality of operations and AIV procedures
- Intelligent planning, simplifies ToO handling and replanning, enables for integrated SOC-MOC planning concept based on single tool TBC
- File management
- Streamlined process planning to mission products (e.g. meta data instead of ops effort for auxiliary data)

⇨ Time available to be used for implementing advanced operations tools and methods.

5 years mission duration:

- Long mission duration affects operations cost
- 5 years possible mission extension (with operations hardware replacement)

⇨ Operations required to be cost efficient.

18.2 Assumptions and Trade-Offs

18.2.1 ToO Operations

ATHENA has a stringent Target of Opportunity requirement, that for 80% of instances there shall be a maximum of 4 h between an external alarm and the start of observations (of the γ-ray burst spectrum) (see ScIRD R-MIS-550).

18.2.1.1 Visibility Constraint

The very short reaction time requires a quasi-continuous visibility from Earth, i.e. at least three ground stations distributed around the Earth or satellite based communications. In addition a short setup time of the ground stations is required and those stations need to be available (with a high probability) for ATHENA, i.e. those stations have to be either dedicated to ATHENA, provide priority to ATHENA ToOs, be rarely used by other missions or are co-used only by missions on the Sun side of the Earth.

18.2.1.2 Optical Communications

Because of the far distance from Earth to the satellite of 1.77 million km, optical communications would require a directive telescope on board the satellite which would be rather heavy and costly. A simple system based on optical communications could not be identified. Optical communications are thus not further pursued for the purpose of enabling ToO communications.

18.2.1.3 ToO Communications via Geostationary Satellite: TDRSS

Communications via the geostationary NASA TDRSS (see RD[41]) would allow for 24h/day access to L2. (Note: This requires a respective dedicated link capability with a high gain antenna in S, Ku, or Ka band, i.e. additional antennas and receivers/transponders. This could provide for a guaranteed service with ad-hoc availability independent of ground based communications visibility constraints.

This option is not further pursued here because of the high effort on the satellite for the additional communications channel and the high operational cost for the utilisation of the TDRSS services.

18.2.1.4 ToO Communications via RF ground stations

For ToO communications there are three basic options:

1) Use of large stations on ground and LGA on board
2) Use of HGA on board and small stations on ground
3) Use of HGA on board and mixed network of small dedicated ground stations and scheduling of large stations.

18.2.1.4.1 ToO communications via large ground stations

The use of large ground stations enables for the use of the Low Gain Antenna (LGA) on board.

Large ground station in this context means a diameter of ~15m. (With deep space settings a marginal up and downlink at 10 t0 20 b/s is still feasible with e.g. the 4.5 m diameter New Norcia 2 station, but such a low data-rate is not considered practical for nominal operations.)

The use of the LGA on board for ToO communications has the advantage of minimum constraints for the satellite, but requires a minimum of 3 large ground stations to be always available at short notice on ground. To guarantee coverage in case of a ToO, the stations need to be pre-booked for 21 h per day (i.e. for the duration when there is no science downlink required). By the time of ATHENA, 15m stations will be shut down and thus only deep space stations would be available in the ESTRACK network. Booking these stations would incur costs in the order of magnitude of 5 million €/year which is much more than for the small station option (see 18.2.1.4.2 below).

A variant has been looked at in RD[2] for communications with IXO within 8h. It was assumed that no prior scheduling for ToO passes was made and that a ToO pass would be performed as soon as a gap in the scheduled ground station usage would become available. The estimate for the probability of success of 85% for ToO communications within 8h was based on the 2008 ESTRACK station load (15m + 35 m stations, see RD[2]). (note: 2008 is assumed to be a typical ESTRACK ground station load for the past and present.) For the case of ATHENA, however, the probability of success would be drastically lower, on the one hand because the ESTRACK 15m stations will be shut down by then and there will be only the (heavily booked) ESTRACK deep space stations available. On the other hand the ATHENA pre-warning time is much shorter. In order to perform all steps necessary for the new observation within 4h, the station has to be available within a ~ ½h slot. ½h is much shorter than a typical deep space station pass and thus the chance of availability of the station is in the same order of magnitude as the average deep space station idle time percentage, which is of course much less than 80%. The IXO approach of waiting until a ground station becomes available is thus not considered feasible for ATHENA.

18.2.1.4.2 ToO communications via small ground stations

If the high gain antenna (HGA) on board is permanently pointed to Earth and available for TC reception, uplink and downlink are possible even with a small (and cheap) ground antenna with a diameter as small as ~ 3m.

A permanent active pointing of the HGA could influence the scientific performance because of microvibrations. The HGA of ATHENA, however, has such a wide beam width that a single adjustment of the HGA pointing direction per day is sufficient when the SC is pointing to an inertial target. (For SC pointings shorter than 1 day duration, it is required to adjust the HGA pointing to the new pointing direction, which can be performed during the slew to the new direction.) Table 18-1 shows the beamwidth of a HGA for different diameters. The drift of the centre of the Earth is < 1.5 °/day and the width of the Earth is ~0.5 °, and the width of the dithering pattern is 2 x 20”~0.01°. If the link budget allows a pointing loss of 0.75 dB a beamwidth of: 1.5° + 0.5° + 0.01 = 2.0° is sufficient to keep over a full day the possible ToO antenna locations on Earth within the HGA beamwidth, i.e. this is feasible for all HGA antenna diameters of Table 18-1.

HGA Ø [cm]	**30**	**40** (baseline)	**50**	**60**
Pointing loss - 3 dB	9.8°/8.3°	7.3°/6.2°	5.9°/5.0°	4.9°/4.2°
Pointing loss - 0.75 dB	4.9°/4.1°	3.6°/3.1°	2.8°/2.5°	2.4°/2.1°

Table 18-1 : HGA Beamwidth Up/Downlink

The link budgets for the ToO communications shall be compatible with the reception of Housekeeping and event data to enable for a SC health check prior to the sending of new commands. This requires an order of magnitude of 2 kb/s data rate. Ideally the uplink should support the standard 4 kb/s data rate.

The detailed link budgets are shown in the Telecomms chapter 16. NNO-2 and EQUA – LEOP ground station characteristics are shown in Table 18-2.

	NNO-2 (to be installed at New Norcia)	EQUA-LEOP (to be installed at Malindi)
Diameter	4.5 m	2.5 m
Reception Performance: G/T	26.5 dB/K	18.5 dB/K
RF Power	200 W	150 W
Uplink Performance: EIRP	68 dBW	59 dBW

Table 18-2: Small ESA station characteristics

A ground station of the 4.5m diameter NNO-2 class easily supports the required ToO up and down link budgets.

Smaller stations, e.g. the 2.5m diameter EQUA-LEOP class of stations support only slightly lower data rates. In this case it is recommended to assume housekeeping data compression for the downlink. (HK compression can be assumed to provide a factor 5 compression of the HK downlink data rate and can also be applied for real time data compression). In addition, a content reduction of up to a factor of 2 could be discussed. For the uplink even 0.5 kb/s would still be acceptable (this would still allow to uplink 100 kb of telecommands within 3.3 minutes). The respective reduced rates of 2 kb/s for the downlink and 0.5 kb/s for the uplink data rate of are easily supported by the 2.5m diameter EQUA-LEOP class of stations.

The cost for the NNO-2 and the EQUA-LEOP stations are in the order of magnitude of 4.5 million € for the NNO-2 station and 2.5 million € for the EQUA-LEOP station. Both stations already exist at New Norcia and Malindi respectively, and would be available for ATHENA at no additional investment cost (maintenance of EQUA-LEOP until time of ATHENA launch is TBD). Additional NNO-2 type stations are under discussion for the 2 other ESTRACK deep space station sites (Rank 2 in investment plan, no financial coverage by MOI investment budget). The worst case assumption for ATHENA is that 2 additional small stations are to be paid for by ATHENA. If 2 additional EQUA-LEOP class stations would have to be built for ATHENA, the required investment cost would be in the same order of magnitude as just one year of operations of large ground stations for full ToO coverage. The same is assumed to be true TBC for 2 co-financed NNO-2 class stations. Over the 5 year duration of the mission and in particular for the possible 5 years extension stations the option to use ATHENA dedicated small stations is considerably less costly than the large station option.

It is noted that the concept allows even some room to accept even less performing stations, which could enable to use cheap stations built on the basis of COTS equipment within the available time frame up to the launch in 2018. Because of the long time to launch it is considered very important that the ToO concept provides a high degree of flexibility.

An alternative to ATHENA dedicated small stations could be to rent the respective services from companies or other agencies. Such a service, however, is not readily available because such services are provided only for the Earth observation X-band range. Updates of existing capabilities, however, to the space exploration X-band may be possible at a moderate cost.

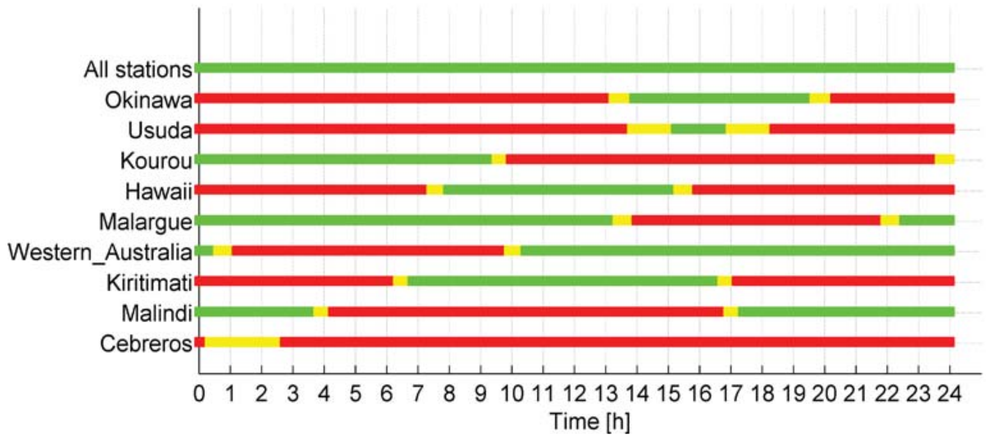

Figure 18-1: ToO station coverage low declination case

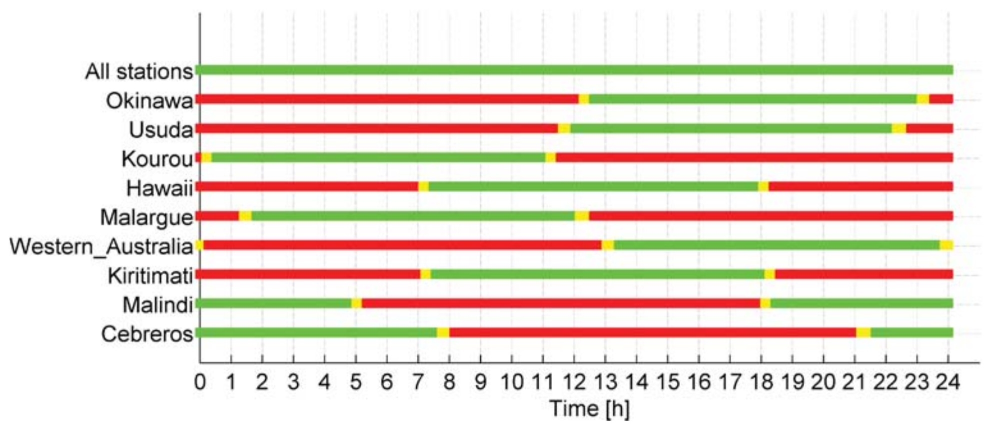

Figure 18-2: ToO station coverage zero declination case

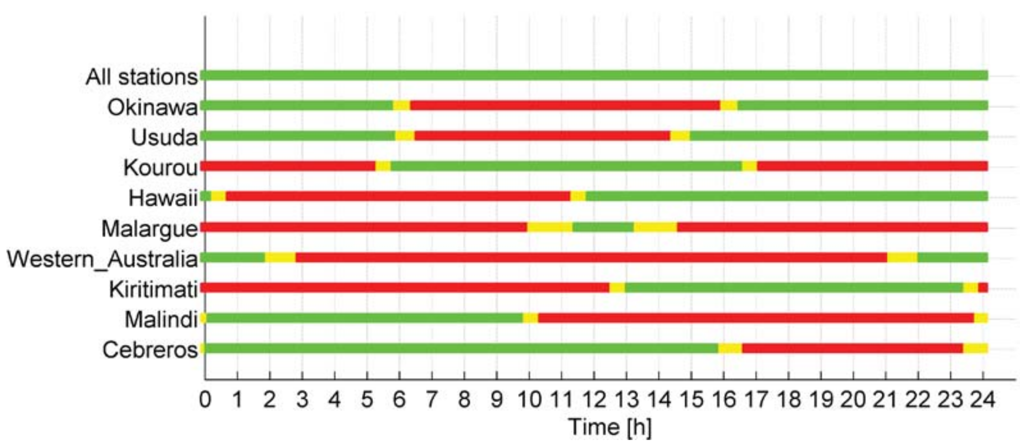

Figure 18-3: ToO station coverage high declination case

legend:

- red: no visibility
- yellow: visibility above 5° inclination
- green: visibility above 10° inclination

18.2.1.4.3 Small ground stations futuristic approach

The time until launch in 2028 could be used to assess alternative approaches to the building of small ground stations. Here are some of the possible improvements foreseen from today's perspective:

- COTS dish and COTS drive
- Lower grade front end
- PC based signal processing based on open source software
- Reliability TBD, redundancy concept perceivable
- Order of magnitude lower price?

Note: A similar approach is currently applied for a small S-band station in ESOC. The achievable reliability will have to be assessed. (For Proba, small dedicated S-band stations based on COTS have been successfully used operationally.)

18.2.1.4.4 ToO ground station sites

Note: the following discussion considers 24h uplink access for the ToO-response. Although this is desirable it is not strictly necessary according to the formulation of the requirement, and the performance achieved even with gaps in the coverage – see the ToO-analysis in §7.1.3.

Figure 18-1, Figure 18-2, and Figure 18-3 show the seasonal visibility of the ATHENA SC from different possible ground station locations. Because of the high amplitude of the halo orbit there is a strong variation of the inclination at which the ground stations can see the SC. The orbital period of the halo orbit is slightly longer than half a year. The plots represent the extreme case of inclination variation over the year (i.e. maximum north/south orbit excursions are in phase with highest/lowest declination).

The following combinations of ToO stations are possible for 24h ToO access:

- **Equatorial Sites:**
  e.g.: Kourou – Malindi – Kiritimati
- **Distributed Sites:**
  e.g.: Malargüe – Malindi - Usuda
- **Distributed Sites:**
  e.g.: 3 ESTRACK deep space sites + TBD:
  (Malargüe – Cebreros – New Norcia
  + choice of Usuda/Okinawa/Hawaii).

3 equatorial sites **Kourou – Malindi – Kiritimati** are geometrically the most straight forward solution for the ToO station locations. A terminal is already available in Malindi. Kourou is not planned to exist anymore as ESTRACK site at the times of ATHENA. Kiritimati would require special arrangements with the Kiritimati state. (The current JAXA antenna there is S-band only). It should also be noted that equatorial sites require a high level of systems maintenance. Equatorial sites are currently only considered as a backup option for the ATHENA ToO network.

The distributed sites **Malargüe – Malindi - Usuda** are another geometrically nice ToO network option, providing 24h access with just 3 stations. It would require to put up an additional small ground station at Malargüe and a cooperation with JAXA with a JAXA small station put up in Usuda. (The available X-band antenna in Usuda would not be available for ATHENA (verbal info from JAXA).) As there is currently no commitment from JAXA and there is only a very narrow variation possible for the station in Japanese longitude, this option is currently only considered as a backup option for the ATHENA ToO network.

4 distributed sites **Malargüe – Cebreros – New Norcia** + choice of **Okinawa/ Hawaii** are proposed as the baseline ATHENA ToO network. On the one hand it is based on the ESTRACK deep space station sites, where maintenance and communications line availability is granted and where the placing of such terminals is planned anyway for LEOP SC acquisition. The NNO-2 class terminals at **Malargüe** and **Cebreros** are planned but not committed by infrastructure due to budget limitations. It is assumed that a favourable co-financing deal can be made for ATHENA if a common interest of the ATHENA project and the ESTRACK infrastructure can be identified. As a backup to the co-financing option of NNO-2 class terminals it is assumed that EQUA-LEOP class terminals can be located at **Malargüe** and **Cebreros**, 100% financed by the ATHENA project, this would provide a reduction in the purchase cost at the expense of a lower data-rate (higher contact duration would be necessary with inherited impact of ToO response time).

A fourth station needs to be added to the ESTRACK station sites. It is assumed here that there is interest from other space agencies, in particular from JAXA and/or NASA. The basic network located at the ESTRACK deep space sites offers the possibility to be rounded off by an existing or new small X-band station at Okinawa (via JAXA) or Hawaii (via NASA). It is assumed that this fourth station is provided on a no exchange of funds basis.

18.2.1.4.5 Use of HGA on board and mixed network of small dedicated ground stations and scheduling of large stations

It may be difficult to establish a dedicated small station network that always guarantees 24h ToO access. A pragmatic approach could be to establish a basic network with a minimum number of dedicated (small) stations and to treat the remaining coverage gaps by the scheduling on a best effort basis of existing multi mission ground stations. In particular this could take advantage of the ESTRACK LEOP network as it will exist at the times of ATHENA. There could be three classes of availability for ATHENA ToOs:

1) Priority could be given to ATHENA ToOs over any current communications.
   Note: This is technically feasible but it is expected that it would be very difficult to get the agreement of the respective affected other missions
2) Short wait time: Stations for near Earth orbit have typically short passes and will become available with a high probability within short time (~10 minutes). This may be in particular relevant for polar stations, e.g. Svalbard as well as Troll provide permanent visibility for maximum respectively minimum declinations and could be used to supplement a basic network at moderate latitudes.
   Note: These stations are typically equipped for the Earth Observation X-band and would need to be equipped for the space exploration X-band. The upgrade cost would have to be borne by ATHENA.

3) Ad-hoc scheduling of station for ATHENA ToO in case that station is currently idle (which will happen with a certain probability).

The combination of a basic network with scheduling of existing stations may provide for a reasonable success rate even if the basic small station network would fall short of the required 80% success rate. Prerequisite would be that a respective real time station scheduling function is established at the ECC.

18.2.1.5 ToO Operations Concept

The prerequisite for the ToO operations concept is a SC HGA always pointed to Earth and configured for TC reception. This enables the use of small ground stations for ToO communications.

Small ground stations are located at sites distributed over the world to enable for 24h access to the SC. 4.5 m class small stations will be used with priority for LEOPs and are available for ATHENA otherwise.

The small ground stations are operated by ESOC ECC.

ToO operation steps:

- Early warning from SOC (alerts MOC team while accepting that some of those alerts may be premature)
- Small ground stations are pointed to SC by ECC based on SOC alert (whether stations will be used or not) => ground stations are not on critical path
- ToO operations at MOC by SPACON. SPACONs are cross trained for astronomy family of missions.

  Notes:

  1) This requires simple SC operations, see 18.2.1.6 SC Prerequisites below.

  2) SPACONs from other missions are assumed to be available for nominal working hours and for 50% of time outside nominal working hours. To guarantee 24h service for the rest of the time there is the option of SPACONS on call (=>2h possible delay) or the ATHENA project pays for the respective permanent SPACON availability (=> cost impact).
- Downlink of HK (real time and stored events) to check SC status prior to manoeuvre TC (HK compression is applied if required due to limitation of link budget.)
- Intelligent planning concept is applied to plan ToO operations. (Technically ideal solution: MOC and SOC use same tool to identify operations constraints => planning in one step)
- Check and uplink of ToO timeline
- Suspension of nominal timeline, continuation timeline after ToO to be planned next working day
- Slew of SC to new target, new instrument setup (and possibly switch of instruments) during slew
- Start of ToO observations.

18.2.1.6 SC Prerequisites

The ToO operations are handled by SPACONs, i.e. these are relatively simple operations according to procedures that can be performed without the need for an in-depth understanding of the SC and the ground systems. This approach makes intrinsic assumptions on the SC design:

- Switchable data-rates to ensure compatibility with a selection of (small) ground stations
- New ranging standard compatible with high data rate RD[40].

Note: Although not directly required by the ToO concept, the overall load on the ESTRACK network shall be minimised.

- Autonomous pointing by SC according to quaternion commanded by ground. This requires knowledge of attitude on board and autonomous actuator management on board, both of which are state of the art
- No constraints by second level requirements:
  - No momentum dump management needed (i.e. wheel capacity sufficient to not risk an unplanned momentum dump)
  - If ToO slew by thrusters: Balanced thrusters to not mess up orbit maintenance
  - No problems with sensors and instrument during slew attitudes (e.g. no startracker blinding)
  - No thermal or power constraints for slew attitudes
  - No science data rate and data storage margin constraints
  - No need for calibrations of fine pointing attitude
  - Operational margins (no constraints even in presence of small problems)
- Highly agile SC
- Instrument autonomy to adapt settings to new (barely known) target (e.g. adaptation to count rate)
- Simple timeline management (new approaches by 2028 to exchange operation modules by drag and drop ?)
- File management (FITS files TBC) for science data and meta data management (science files include data from TCs (i.e. via link to mission planning system), SC data pool, and instrument HK) to ease post processing and simplify management overhead
- File management on board to ease timeline planning for data storage
- CFDP on uplink and downlink to simplify ToO communications
- Capable FDIR: Should identify constraints and preclude operations that might result in safe mode (i.e. not executes such commands)
- State of the art satellite operating system, possibly based on MO services (replacing PUS).

Note: The increased level of SC autonomy will require a respective verification effort.

18.2.2 Futuristic Operations Approach

The operations concept could take advantage from the existence of a small station network for general operations. As the network provides for 24h access to the SC, the flight operations team could access the SC for monitoring and control purposes whenever best suited for the flight ops team. This could reduce the number of SPACONs required and it could relax the operations for the overall family of missions if applied to all the missions of the family.

The science data would be downlinked automatically via a deep space station. This downlink would be supported by a CFDP protocol. (Note: In a high demand situation for the deep space stations this option could allow for a flexible scheduling of the bulk downlinks and increase the possible overall load of the deep space station network).

This approach would be highly beneficial if there would be a larger number of parallel L2 missions.

18.3 Baseline Design

18.3.1 Operations Tasks Overview

Mission Operations will commence at separation from the launcher and will continue until the end of the mission, when ground contact to the SC will be aborted. Mission Operations will comprise the following tasks:

- Mission Analysis
- Mission Planning
- SC and payload status monitoring
- SC control, based on the Flight Operations Plan and the short-term plan
- Instrument operations execution based on operations requests issued by the Science Operations Centre (SOC)
- Orbit determination and control using tracking data (Doppler and ranging) and implementing orbit manoeuvres
- Attitude determination and control by processing attitude sensor data and by commanding updates of control parameters in the AOCS
- On-board S/W maintenance (full maintenance of OBCPs and installing software patches provided by industry and instruments)
- Provision of communication resources (Ground Stations and Lines)
- Data Archiving and Distribution
- Maintenance of ESA ground facilities and network.

18.3.2 Monitoring and Control Concept

The operations activities for ATHENA will be conducted according to the following general concept:

- An intensive preparation activity is set up prior to launch and prior to procedure changes to ensure for safe and efficient operations. Procedures are developed and operations systems are upgraded or newly developed. Procedures and systems are tested and validated. The operations team is trained. To this purpose dedicated test and simulation campaigns are set up.

- The mission planning consists of: Long Term, Medium Term and Short Term planning. The Long Term Plan (months) fixes manoeuvres, pointing and ground station long term planning, the Medium Term Plan (minimum 4 weeks in advance) fixes the configuration and provides firm station planning, and the Short Term plan contains the actual command sequences covering several days, established a week in advance, uplinked at least 2 passes before execution).
- Note: It is assumed that by the time of the ATHENA launch advanced planning systems will be state of the art. The same planning system core should be used at the SOC and the MOC. It should in particular enable to perform a quick planning and checking of the constraints for the ToO operations. For the short term plan it shall support a streamlined planning concept that minimises managerial overhead by forwarding planning data as required into the science files. On board these data are supplemented by as flown data which are also to be included as meta data in the science files. The science files on board are assumed to be in a format that eases the ground processing (e.g. FITS files).
- All operations will be conducted by ESA/ESOC according to procedures laid down in the Flight Operations Plan (FOP).
- The ATHENA mission operations will be conducted with SC controllers during the short daily coverage of 3h. Analysts and engineers are working nominal hours. Engineer on call support is provided for all passes for trouble shooting.
- ToOs are handled by SPACONs. SPACONs are cross trained within the astronomy family of missions to handle ATHENA ToOs. It is assumed that SPACONs of the family of mission are present at ESOC during nominal working hours and for ~ 50% of the remaining times. For the remaining time there are two options: SPACONs on call (up to 2h delay after prewarning to take on duties) or SPACONs permently present and paid by ATHENA.
- ToOs are performed based on a highly automated procedure and they change the medium term planning only in so far, as other observations are replaced. Replanning of nominal observations after the ToO is performed during nominal working hours.
- During the first period after launch (i.e. LEOP duration 3 days) 24 hours operations per day will be conducted with on site presence of maintenance capability for all services. Presence of project and industrial support with decision authority is required on site.
- During transfer and commissioning 12h shifts of the Flight Operations team and Flight Dynamics are provided including weekends. Presence of project, industrial, and payload support with decision authority is required on site.
- All ATHENA operations will be conducted by uplink of a master schedule of commands for later execution on the SC. This schedule will contain all commands necessary to undertake the SC and instruments operations in a predictable fashion. The master schedule will be prepared by a Mission Planning System.

- SC control data are available in real time during passes. Science data are delivered off line.
- Ground station operations (including those required for ToOs plus respective coordination with partner agency for externally provided ToO ground station(s)) is provided by the ESOC ECC. The ECC is manned 24h/day.

18.3.3 Ground Segment Implementation

The current general ESA/ESOC infrastructure is described in RD[43]. The following subchapters only describe the aspects on which the ATHENA implementation differs from the general infrastructure.

18.3.4 General Infrastructure Concept

The ATHENA operations infrastructure will be based on the general ESA/ESOC operations infrastructure with a maximum sharing and reuse of facilities and tools made available from former Observatory missions such as GAIA, or EUCLID. For the ATHENA timeframe the infrastructure will have further evolved integrating state of the art technology advances. Specific customisations will be implemented as required for ATHENA.

18.3.5 Ground Stations and Communications Network

The ground stations network to be used for ATHENA during early LEOP will be composed of the deep space X-band stations Malargüe (35m), Cebreros (35 m), and New Norcia 35 m, possibly augmented by smaller 4.5m stations at the same sites (e.g. NNO-2). The precise definition of the ESTRACK LEOP network at the time of ATHENA is TBD. The LEOP network for ATHENA will guarantee close to 24 hours coverage of the SC during this critical period and will provide an initial acquisition capability to cope with insertion errors.

It is assumed to use 2 deep space stations for the transfer phase. The science observation phase will use a single 35m antenna. The choice of this antenna is TBD and there may be a seasonal switch between southern (Malargüe or New Norcia) and northern (Cebreros) sites. 3h daily passes plus one 8h pass every month (for orbit maintenance) are provided.

Ranging compatible with the high data rate modulation will be provided, according to RD[40]. The associated network shall provide a capability of 3.5 Mbps continuous data traffic with data buffering at the ground station.

18.3.6 Flight Control Systems

The ATHENA Flight Control System will consist of the facilities listed below:

- Procedure generation system (currently based on MOIS, to be replaced by TBD for ATHENA)
- Mission Planning System (common development with SOC is envisaged capable of integrated planning at a single site, in particular capable of quick ToO planning)
- Mission Control System (Details are TBD, because ground system has to mirror on board system, which by the time of ATHENA may be based on MO services. As a

minimum a full file management and transfer capability is assumed on board and on ground)

- A mini-Mission Control System (mini-MCS) in ESA/ESOC on a separate power line for LEOP and for the nominal mission is part of the baseline
- Real time simulator using the then current ESA/ESOC simulator platform (currently: SIMSAT)
- The complexity of the deployment operations may require operations access to an engineering model to verify the procedures and to enable for troubleshooting
- On-board Software Maintenance (OBSM) facility for platform and payload
- Data Dissemination System (DDS) for HKTM, science and auxiliary data distribution
- ToO system to generate ToO commands.

18.3.7 Flight Dynamics

The Flight Dynamics system (currently based on ORATOS) is a multi-mission system. It is implemented in the Flight Dynamics room and operated by a team that looks after a family of missions.

An ATHENA dedicated ToO system will be installed in the DCR that allows the calculation of the parameters for a ToO manoeuvre operated by a SPACON. The input will be a new pointing and respective payload setting calculated by the SOC that replaces other pointings in the mission schedule. (Note: This requires a 24h/day active SOC.)

SC timing will be provided as auxiliary data. The tools used will be based on the developments for GAIA.

18.4 Options

SPACONs:	On-call service or permanent presence
ToO:	2 additional stations: Co-funded NNO-2 class stations at deep space sites or ATHENA dedicated small stations (EQUA-LEOP class)

19 TECHNICAL RISK

19.1 Risk Management Process

Risk management is an organised, systematic decision making process that efficiently identifies, analyses, plans, tracks, controls, communicates, and documents risk in order to increase the likelihood of achieving the project goals. The procedure comprises four fundamental steps RD[44]:

- Step 1: Definition of the risk management policy which includes the project success criteria, the severity & likelihood categorisations, and the actions to be taken on risks
- Step 2: Identification and assessment of risks in terms of likelihood and severity
- Step 3: Decision and action (risk acceptance or implementation of mitigating actions)
- Step 4: Communication and documentation.

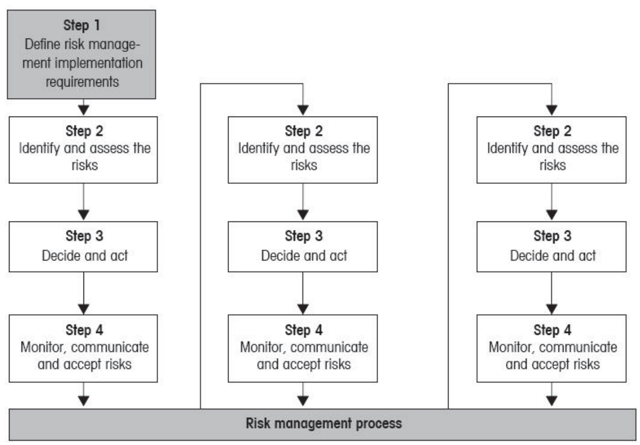

Figure 19-1: ECSS-M-ST-80C, 2008 Risk Management Process

19.2 ATHENA Risk Management Policy

The CDF risk management policy for ATHENA aims at handling risks which may cause serious science, technical, schedule and/or cost impact on the project.

19.2.1 Success Criteria

The success criteria with respect to the science, technical, schedule, and cost objectives are presented in Table 19-1:

Domain	Success Criteria
Science	SCI1. Mission accomplishes the key science goals defined in RD[10]
Technical	TEC1. The SC operates successfully over the designated mission lifetime.
	TEC2. No performance degradation owing to SPF, and no failure propagation.
	TEC3. A mission reliability of >85% at the end of the nominal operations phase
	TEC4. Adhere to Space Debris mitigation requirements, and performance of a successful

Domain	Success Criteria
	controlled de-orbit at EoL TEC5. Launch on an ESA-mandated L-class launcher (A5 ECA)
Schedule	SCH1. Launch date before end of 2028 SCH2. TRL≥5 at the time of mission adoption (end 2018-mid 2019) SCH3. Low development risk during Phase B2/CD.
Cost	COS1. CaC for ESA≤1000M€2 (2013 EC).

Table 19-1: Success Criteria

19.2.2 Severity and Likelihood Categorisations

The risk scenarios are classified according to their domains of impact. The consequential severity level of the risks scenarios is defined according to the worst case potential effect with respect to science objectives, technical performance objectives, schedule objectives and/or cost objectives.

In addition, identified risks that may jeopardise and/or compromise the ATHENA mission will be ranked in terms of likelihood of occurrence and severity of consequence.

The scoring scheme with respect to the severity of consequence on a scale of 1 to 5 is established in Table 19-2, and the likelihood of occurrence is normalised on a scale of A to E in Table 19-3.

Score	Severity	Science	Technical	Schedule	Cost
5	Catastrophic	Failure leading to the impossibility of fulfilling the mission's scientific objectives	Safety: Loss of life, life-threatening or permanently disabling injury or occupational illness; Severe detrimental environmental effects. Loss of system, launcher or launch facilities	Delay results in project cancellation	Cost increase result in project cancellation
4	Critical	Failure results in a major reduction (70-90%) of mission's science return	Safety: Major damage to flight systems, major damage to ground facilities; Major damage to public or private property; Temporarily disabling but not life- threatening injury, or temporary occupational illness; Major detrimental environmental effects Dependability: Loss of mission	Critical launch delay (24-48 months)	Critical increase in estimated cost (100-200 M€)
3	Major	Failure results in an important reduction (30-70%) of the mission's science return	Safety: Minor injury, minor disability, minor occupational illness. Minor system or environmental damage Dependability: Major degradation of the system	Major launch delay (6-24 months)	Major increase in estimated cost (40-100 M€)
2	Significant	Failure results in a substantial reduction (10-30%) of the mission's science return	Dependability: Minor degradation of system (e.g.: system is still able to control the consequences) Safety: Impact less than minor	Significant launch delay (3-6 months)	Significant increase in estimated cost (10-40 M€)
1	Minimum	No/ minimal consequences (<10% impact)	No/ minimal consequences	No/ minimal consequences (1-3 month delay)	No/ minimal consequences (<10 M€)

Table 19-2: Severity Categorisation

Score	Likelihood	Definition
E	Maximum	Certain to occur, will occur once or more times per project.
D	High	Will occur **frequently**, about 1 in 10 projects
C	Medium	Will occur **sometimes**, about 1 in 100 projects
B	Low	Will occur **seldom**, about 1 in 1000 projects
A	Minimum	Will **almost never** occur, 1 in 10000 projects

Table 19-3: Likelihood Categorisation

19.2.3 Risk Index & Acceptance Policy

The risk index is the combination of the likelihood of occurrence and the severity of consequences of a given risk item. Risk ratings of very low/low risk (green, yellow), medium risk (orange), and high/very high risk (red) were assigned based on the criteria of the risk index scheme (see Figure 19-2). The level of criticality of a risk item is denoted by the analysis of the risk index. By policy high and medium risks are not acceptable and must be reduced (see Figure 19-3).

Likelihood					
E	E1	E2	E3	E4	E5
D	D1	D2	D3	D4	D5
C	C1	C2	C3	C4	C5
B	B1	B2	B3	B4	B5
A	A1	A2	A3	A4	A5
	1	2	3	4	5 Severity

Figure 19-2: Risk Index

Risk Index	Risk magnitude	Proposed Actions (during assessment phase)
E4, E5, D5	Very High Risk	Unacceptable risk: implement mitigation actions (either likelihood reduction or severity reduction through new baseline) with appropriate party.
E3, D4, C5	High Risk	Unacceptable risk: see above.
E2, D3, C4, B5	Medium Risk	Unacceptable risk: implement mitigation actions with responsible party.
E1, D1, D2, C2, C3, B3, B4, A5	Low Risk	Acceptable risk: control, monitor.
C1, B1, A1, B2, A2, A3, A4	Very Low Risk	Acceptable risk: see above.

Figure 19-3: Proposed Actions

19.3 Risk Drivers

The following risk drivers have been considered in the identification of specific risk items:

- New technology
- Environmental conditions
- Design challenges
- Reliability issues, single point failures (SPFs)
- Major mission events.

19.4 Top Risk Log

Top risk items have been identified at the mission (ESA), SC (prime), and instruments (Consortium) levels. Please refer to Table 19-7 for a complete list of identified top risks and their corresponding suggested mitigating actions. Risk index results are summarised in the top risk index charts below:

Mission Risk (ESA)

Likelihood					
E			MI01		
D		MI09	MI02, M08, ,MI12	MI10	
C			MI03, MI04, MI05, MI06, MI07	MI11	
B			MI13, MI14		
A					
	1	2	3	4	5
					Severity

Table 19-4: Top Risk Index Chart Mission (ESA)

2

SC Risk (Prime)

Likelihood					
E					
D	SC10	SC05	SC02, SC09, SC12		
C		SC01, SC03, SC04		SC11	
B		SC07			SC06, SC08
A					
	1	2	3	4	5
					Severity

Table 19-5: Top Risk Index Chart SC (Prime)

Instruments Risk (Consortium)					
Likelihood					
E		IN03			
D					
C				IN01, IN02	
B					
A					
	1	2	3	4	5
					Severity

Table 19-6: Top Risk Index Chart Instruments (Consortium)

#	RI	Class.	Risk	Cause	Cons.	Mitigation Actions (on-going)	Mitigation Option(s)
Mission Risk (ESA)							
MI01	E4	Technical	A5ECA/ME not available in 2028 timeframe, causing a re-definition of the mission to be compatible with A6 launcher.	Unavailability of A5 ECA/ME at the launch date (2028), due to retirement of A5 ECA/ME from service. Unknown A6 performance/fairing size may have impact on mission feasibility with current design.	[1] Imposition of the more mass constrained A6 as the baseline launch vehicle for ATHENA assessment phase. Latest info is a 12m fairing length is still OK, but mass performance reduced from 6.5t to 5.3t to L2 - so estimate 'critical' (TBC) effect on science. [2] A new development for an equivalent type of large custom adaptor for the A6.	[1] A5 ECA baseline and Atlas 500 backup imposed as applicable launch vehicles. Can be 'costless' to go to one of these solutions (could be a NASA contribution to ATHENA, within the stipulated 20% cap), but political dimension needs to be considered. [2] Investigation of A6 performance to L2, and alternative launch scenarios (apogee raising sequence, Lunar Gravity Assist) - to be reported in the CReMA.	[1] Twin A6 launch with (more-or-less) identical SC, one nominal instrument per SC [ref: A5 mitigation document, ATHENA-ESA-TN-0001]. [2] Reserve A5 ECA/ME for 2028 launch. Cost is TBD [ref: A5 mitigation document, ATHENA-ESA-TN-0001].
MI03	C3	Schedule	Late X-IFU models (all models up to FM) delivery to Prime.	Unforeseen problems with MAIVT of X-IFU.	WCPE of causing a major delay in launch and associated major increase in ESA CaC (as liable to Prime for timely provision of CFI).	[1] Ensure satisfactory PL Consortium definition of facilities/effort/schedule to produce X-IFU {PRR/SRR}.	[1] Organise the Prime schedule so that CFI FM (and earlier models) provision occurs as late as possible.

#	RI	Class.	Risk	Cause	Cons.	Mitigation Actions (on-going)	Mitigation Option(s)
MI04	C3	Schedule	Late WFI models (all models up to FM) delivery to Prime and impact on AIV/T..	Delays on MAIVT o WFI availability .	WCPE of causing a major delay in launch and associated major increase in ESA CaC (as liable to Prime for timely provision of CFI).	[1] Ensure satisfactory PL Consortium definition of facilities/effort/schedule to produce WFI {PRR}.	[1] Organise the Prime schedule so that CFI FM (and earlier models) provision occurs as late as possible.
MI05	C3	Schedule	Late mirror module (MM) delivery to Prime and impact on AIV/T..	Delays with development and/or MAIVT of MM.	This has a potential worst-case effect of causing a major delay in launch and associated major increase in ESA CaC (as liable to Prime for timely provision of CFI).	[1] [C216-006MM] - MM ruggedisation [2] [C216-128MM] - SPO Manufacturing facility design [3] [C216-127MM] - SPO AIT [4] C216-117MM] - True Wolter [5] [C216-007MM] - Petal Breadboard	[1] Organise the Prime schedule so that CFI FM (and earlier models) provision occurs as late as possible. [2] Transfer responsibility for MM production to Prime responsibility after development (2018 onwards).
MI06	C3	Science	Mass, power and volume changes leading to incompatibility of X-IFU instrument resource requirements with envelope provided by the SC.	Normal development activities might result in changes in mass, volume or power requirements.	Before proceeding to definition, reduce the size of the X-IFU to fit the instrument onto the SC, leading to a major loss of science.	- Detailed follow-up of development to ensure mass, power and volume constraints are kept within design margins.	-
MI07	C3	Science	Mass, power and volume changes leading to incompatibility of WFI instrument resource requirements with envelope provided by the SC.	Normal development activities might result in changes in mass, volume or power requirements.	Before proceeding to definition, reduce the size of the WFI to fit the instrument onto the SC, leading to a major loss of science.	Detailed follow-up of development to ensure mass, power and volume constraints are kept within design margins.	

#	RI	Class.	Risk	Cause	Cons.	Mitigation Actions (on-going)	Mitigation Option(s)
MI09	D2	Science	ToO-response requirement not met.	[1] ToO response requirement very expensive/difficult to meet. [2] The cost of a 24h coverage by ESA DSA is too high (18<=25 M€) depending on 15/35m support.	Reduced number of GRBs followed up within 4 hours of alert, leading to a significant reduction in the science return (10-30%) associated with SG4.1, 5.2.	[1] Setup of ToO-response model and T/O to accurately understand the capability versus cost T/O of various candidate mission architectures for ToO-response [ref]	[1] Discussion with SST on importance of requirement (will be exercised once SST is formed). [2] Study alternative solutions such as the S/X Terminal at NNO-2 plus the development of two additional terminals (CEB-2 and MLG-2) for ~24h coverage at the cost of ~4M€ per terminal.
MI10	D4	Technical	Violation of A5 ECA/ME PL static moment requirement by SC design.	[1] ATHENA CoG static moment during assessment/definition violates requirement.	Reduced telescope size and/or instrument size, leading to a WCPE major (30-70%) reduction in science return (partial mitigation by longer observations.) A switch to larger adapter will have an impact on cost and AIVT.	[1] Phase 0/A study (i.e. confirm proposal design). [2] Monitor the total mass & mass distribution closely throughout the design exercise.	[1] Switch to larger adapter; New development of large custom (A6) adapter [2] Lower mass at the top of the stack
MI11	C4	Schedule	Delays or technical challenges in the international cooperation elements of ATHENA impact on the development cost and schedule of the mission.	[1] International cooperation mission with certain external risks which are uncontrollable for ESA. [2] International contributions up to 250M EUR may be needed to realise project.	Major launch delay by 6-24 months.		[1] Establish a close cooperation with partner agency with regular progress meetings. Create a trusting and open environment enabling improved communication flow and quicker problem notification.

#	RI	Class.	Risk	Cause	Cons.	Mitigation Actions (on-going)	Mitigation Option(s)
							[2] Adequate funding of dedicated ESA interface team with partner agency
MI12	D3	Technical	SC degradation due to excessive radiation exposure.	L2 periodically transfers from within the magnetotail, plasma sheet, and solar wind depending on the intensity and direction of the solar wind.	Major degradation of the system	[1] Provide detailed radiation environment assessment and study mitigation options including shielding , rad-hard component selection, etc.	
MI13	B3	Technical	Incompatibility of the propulsion system (CDF design) with mission ΔV requirements.	Operational contingency ΔV budget not accounted for in overall mission ΔV budget.	Major degradation of the system	[1] Revisit the need to include an operational contingency ΔV budget in the mission ΔV budget. [2] Re-size propulsion system to account for additional ΔV needs due to operational contingency.	
M14	B3	Science	Radiation environment impact on science return	L2 radiation environment uncertainty	Major degradation of science return (lower proton environment for background count in focal plane)		Built on lessons learnt of radiation environment in L2 thanks to knowledge acquired by Hershel and Plank
SC Risk (Prime)							

#	RI	Class.	Risk	Cause	Cons.	Mitigation Actions (on-going)	Mitigation Option(s)
SC01	C2	Science	FoR requirements not met.	Not practical to implement a telescope sun-shield which can protect against straylight for +-34.5 degree excursions from canonical.	Reduced number of GRBs followed up within 4 hours of alert, leading to a significant reduction in the science return (10-30%) associated with SG4.1, 5.2. Small increase in complexity of operational planning.	-	[1] Reduce FoR requirement; will necessitate compensation with mission lifetime and/or improved ToO-response speed (which is very unlikely!)
SC02	D3	Science	Telescope HEW requirements not met.	[1] Difficulty in achieving HEW requirements for MM (probably the most important) [2] µvibration requirements not met for AOCS [3] Problems in achieving mounting accuracy MM>MS [4] Contamination	Major reduction in the science return (30-70%)	[1] Develop ironclad budget for HEW across SC, and ensure requirements are properly flown-down to MM development team, SC Prime etc. Several TDAs to improve MM-performance: [2] TDA for SPO AIT to be awarded in 2014 [ref: C216-127MM] [3] TDA for true wolter development [ref: C216-117MM] [4] TDA for MM ruggedisation [ref: C216-006MM] [5] Enforce proper contamination budget at the outset of the assessment phase.	-
SC03	C2	Science	Telescope A_eff requirements not met.	[1] Focal length reduction due to accommodation problems. [2] Contamination during mission lifetime [3] Unable to accommodate physical area needed (3m diameter)	Significant reduction in the science return (10-30%)	[1] Enforce proper contamination budget at the outset of the assessment phase. [2] TDA on inner SPO module to reduce the inner MM radius, allowing better A_eff, particularly at higher energies [ref: C216-008MM]	-

#	RI	Class.	Risk	Cause	Cons.	Mitigation Actions (on-going)	Mitigation Option(s)
SC04	C2	Technical	MM shock-vibration environment too high.	[1] MM location and load-path in proximity to LV I/F plane causes high shock-loads to be transmitted to the MMs. [2]MM shock testing in 05.2014 resulted in detached plates.	Minor degradation of the system.	[1] TDA with MOOG [ref: C220-001FT] to be awarded Q32014 to develop vibration/shock isolation solutions to reduce applicable shock/random vibration at MM I/F as much as possible. Look into shock damping at LVA I/F or locally. [2] Shock testing underway in frame of ruggedisation TDA [ref: C216-006MM].	[1] Implement MOOG SoftRide system at LVA I/F plane [2] Implement localised shock/vibration reduction measure at SC/MS or MS/MA I/F.
SC05	D2	Technical	SC unable to fit inside fairing.	[1] FPA too large (MIP, radiator area…)	Reduction in FL and therefore A_eff leading to a significant reduction in the science return (10-30%).	-	[1] CDF study to assess MIP feasibility and accommodation [2] CDF study to assess radiator area requirements against new power dissipations.
SC06	B5	Science	Failure in telescope cover deployment (cover will almost certainly be needed).	[1] Most likely mechanism/pyro failure.	Catastrophic (mission lost, no science possible).	-	[1] CDF study to assess telescope cover design & deployment [2] Enforce actuator redundancy and proper RAMS engineering on cover release design.
SC07	B2	Science	Failure in telescope sunshield deployment.	[1] Most likely mechanism/pyro failure.	WCPE significant loss of science (10-30%) - one half of nominal FoR still available (TBC subject to stowed/partial position not generating straylight or FoV blockage).	-	[1] CDF study to assess telescope sunshade design & deployment [2] Ensure stowed/partial deployment does not have any adverse effect beyond FoR reduction.
SC08	B5	Science	Failure in MIP (only applicable for MIP ISM options, not the CDF baseline).	[1] Most likely mechanical. Note that ~300 targets per year [ref: proposal], and cycling constraints of X-IFU cooling chain	WCPE catastrophic loss of science (stuck in intermediate position) - note that	-	[1] CDF study to assess MIP design & feasibility, and possibility to launch in

#	RI	Class.	Risk	Cause	Cons.	Mitigation Actions (on-going)	Mitigation Option(s)
				(leading to frequent switching with WFI) mean ~several thousand cycles of the MIP over the mission lifetime (i.e. we note that the cooling-chain cycling constraint on the X-IFU will STRONGLY drive the cycling requirements on the MIP).	intermediate position is the launch (locked) position so represents a critical SPF. [2] If stuck at one of the locked instrument positions, then not so serious.		viewing position (i.e. remove launch-lock SPF) [2] Develop continuous cooling chain for X-IFU to drastically reduce the number of cycles needed (combined with appropriate planning). [3] Emphasise MIP design & development during industrial assessment & definition studies. [4] Switch to tilting MAM - this allows launch-lock position to be on X-IFU FP.
SC09	D3	Schedule	Delay in manufacturing the ~675 MM required for the telescope mirror.	[1] Up-scaling the manufacturing process and facility to flight production volumes. [2] SPO manufacturing complexity (cleanliness, tolerances, alignment, etc.).	WCPE Major 6-24 month delay in MM delivery to the MS-Prime for integration into the MS.	[1] TDA on SPO AIT [ref: C216-127MM] [2] TDA on SPO manufacturing facility design [ref: C216-128MM] [3] Various TDAs on Bessy and Panter upgrade.	
SC10	D1	Cost	SC pointing requirements (particularly Astrometry) not met by a design w/o OBM (On-Board Metrology).	[1] Insufficient definition of the pointing requirements. [2] Overly optimistic design in early phases.	Need for implementation of OBM system with associated design and procurement costs, leading to a minor (0-10ME) cost increase [reference IXO cost estimate report OBM 3-5ME].	[1] Consolidate pointing/astrometry requirements during Assessment Phase.	-

#	RI	Class.	Risk	Cause	Cons.	Mitigation Actions (on-going)	Mitigation Option(s)
SC11	B5	Science	Failure in MMA.	[1] Most likely mechanical. [2] Low TRL and limited heritage at component level only. [3] Complex design and critical SPF on mechanical parts (2x bearing sets design).	WCPE catastrophic loss of science (stuck in inter-mediate position) [2] If stuck at one of the instrument positions, then not so serious.	[1] Launch lock position is on X-IFU FP. [2] SPF free with 6DOF Hexapod. [3] Invest in technology and testing with dedicated TDA.	
SC12	D3	Technical	Incompatibility of AOCS design with large disturbance torques generated by solar pressure.	[1] Large offset between the SC's centre of pressure and its centre of mass. [2] Large solar array wings located at the lower portion of the SC.	[1] Major redesign of the system and/or AOCS sizing. [2] Impact on science observations.	[1] Check whether AOCS design is able to cope with large disturbance torques [2] Re-evaluate solar array solution to reduce offset between the centre of pressure and the centre of mass.	
Instruments (Consortium)							
IN01	C4	Technical	Energy resolution requirement not met.	[1] Detector temperature requirement not met due to µvibration. [2] Problems with detector development.	WCPE is critical reduction in the science return (30-70%).	[1] Consortium technology development. [2] TDA on 50mK [ref: C221-00MT] will investigate this effect (also seen on JAXA ASTRO-H); TDA to be awarded 2014. [3] TDA on cryogenic vibration isolators to be awarded 2014 [ref: C221-005FI].	-
IN02	C4	Technical	Failure of cryo-chain.	-	Critical reduction in the science return (30-70%) - WFI still available.	Cryo-chain TDAs (various) on-going	[1] Increase redundancy in cryo-chain. [2] Impose Q-branch control on CC development (under ESA-control anyway).
IN03	E2	Schedule	European cooling chain not available on time.	[1]Pre-development delayed. [2] Problems discovered late in the programme.	Delay in the programme.	Cryochain TDAs (various) on-going.	[1] Maintain alternative coolers for the various elements of the cooling chain. [2] Advance testing at X-IFU level. [3] Lessons learnt form

#	RI	Class.	Risk	Cause	Cons.	Mitigation Actions (on-going)	Mitigation Option(s)
							previous ESA/non ESA cryo missions. [4] Sufficient margin in the schedule (1 year).

Table 19-7: Risk Log

19.4.1 Risk Log General Conclusions

- High risks are typical of a phase A project. Areas with lack of definition or little previous experience pose a priori more risk to the mission and therefore are the ones with more risk reduction potential
- Experience shows that all risk items with a critical risk index (red/orange area) must be analyzed and proposals for risk treatment actions elaborated
- In the end, ideally all risk items should reach a level of justifiable acceptance
- The risk management process should be further developed during the project definition phase in order to refine the risk identification/analysis and provide evidence that all the risks have been effectively controlled.

19.5 MIP vs. MMA Risk Trade

A comparative risk assessment was performed for the various mechanical solutions proposed to switch the focal plane between the X-IFU and WFI instruments. The risk trade compared options by summing up the following risk contributors: TRL, heritage (in space), failure tolerance, and probability of failure (fault avoidance). All risk contributors were equally weighted (w=1), and risk factors of r=5, r=2, and r=1 were assigned for high, medium, and low risk respectively for each one of the risk contributors in a given option. Factors were assigned based on expert judgement after consultation with the mechanisms discipline specialist(s). The analysis results contributed to the systems trade-off carried out for the selection of a baseline mechanism.

19.5.1 Options Definition

The options considered in the comparative risk assessment are gathered here below:

- MIP translational 1 DOF
- MIP rotational
- MMA 1 DOF (2x bearing sets)
- MMA 6 DoF (hexapod)

Details of each of these options and the system level trade-off performed are provided in the chapter 7.2.1.

19.5.2 Analysis, Results, and Conclusions

Results show that all options are high risk given their low TRL (3), limited heritage in space, and complexity.

In terms of heritage, there are fewer applications of spindle for translational actuators as compared to other components such as the motors, gearboxes, and bearings. Some heritage for MIP can be found in the Chandra X-ray telescope science platform mechanism and for MMA in the GAIA tip-tilt mechanism. It is to be noted that there are several technology development activities in the planning to raise the TRL to 4 by 2016 for both the MIP and MMA solutions.

As for failure tolerance, the only option capable of coping with a single mechanical failure would be the hexapod. However, certain performance degradation is expected and should be assessed in detail to ensure that it is with the acceptable limits.

Regarding fault avoidance, more complex options with more components score higher risk. The preferred option from this standpoint is the MMA 1DOF 2x Bearing Sets which is the “simplest” option.

Overall there is a slight preference for the hexapod solution since it provides certain failure tolerance against mechanical failures despite its more complex design as compared to the MMA 1 DOF 2x bearing set design. Complete results of the payload mechanism risk trade are summarised in Figure 19-4.

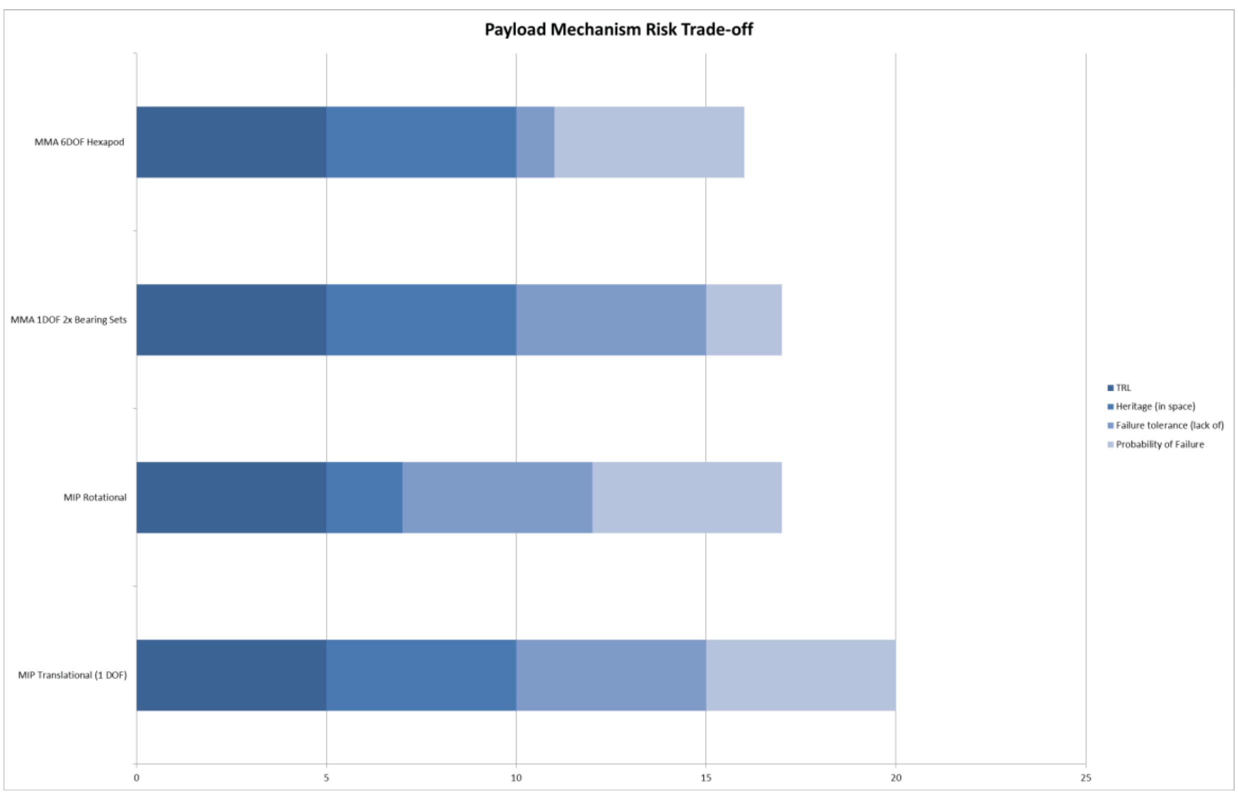

Figure 19-4: Results of the Comparative Risk Assessment

20 PROGRAMMATICS/AIV

20.1 Requirements and Design Drivers

The main requirements and design drivers for the ATHENA Mission from a programmatics point of view are:

- Launch date in 2028
- Phase B2/C/D starting beginning 2020
- TRL 6 achieved by beginning of Phase B2
- Phase A/B1 starting in June 2015
- Optical cleanliness requirements (impacting facilities selection)
- AIT flow driven by mirror module manufacturing, integration and testing.

20.2 Assumptions and Trade-Offs

- Modular satellite environmental testing (Upper and Lower Module)
- Thermal control hardware, harness etc. installation on platform before mirror installation
- New hardware need qualification models (as a minimum EQM units)
- Nothing below TRL 6 at beginning of Implementation Phase (latest: System PDR)
- Movable Mirror Assembly: Hexapod mechanism selected.

20.3 Options

No options were considered for the programmatics assessment.

20.4 Technology Requirements

The Technology Readiness Levels (TRL) present a systematic measure, supporting the assessments of the maturity of a technology of interest and enabling a consistent comparison in terms of development status between different technologies.

The different TRL as defined in RD[47] are shown in Table 20-1:

TRL	ISO Definition	Associated Model
1	Basic principles observed and reported	Not applicable
2	Technology concept and/or application formulated	Not applicable
3	Analytical and experimental critical function and/or characteristic proof-of concept	Mathematical models, supported e.g. by sample tests
4	Component and/or breadboard validation in laboratory environment	Breadboard
5	Component and/or breadboard critical function verification in a relevant environment	Scaled EM for the critical functions

6	Model demonstrating the critical functions of the element in a relevant environment	Full scale EM, representative for critical functions
7	Model demonstrating the element performance for the operational environment	QM
8	Actual system completed and "flight qualified" through test and demonstration	FM acceptance tested, integrated in the final system
9	Actual system completed and accepted for flight ("flight qualified")	FM, flight proven

Table 20-1: TRL scale

Table 20-2 shows an indication of the development time depending on the current TRL. According to the European Space Technology Master Plan, to prepare the contractual basis for multi-annual programs it takes about 18 months to reach political agreement on financial ceiling. This has also been included in the table.

TRL	Duration
5-6	4 years + 1.5 year
4-5	6 years + 1.5 year
3-4	8 years + 1.5 year
2-3	10 years + 1.5 year
1-2	12 years + 1.5 year

Table 20-2: TRL – development duration

TRL Summary:

- Service Module
  - The identified TRL range from 6 to 9
  - For a number of equipment no TRL has been identified (e.g. transponder, HGA, LGA, RFDU, TWT, EPC, CDMU) yet
- X-Ray Field Unit
  - The identified TRL Range from 2 to 5
- Wide Field Instrument
  - The identified TRL range from 3 to 6
- Movable Mirror Assembly (MMA)
  - The identified TRL range from 4 (Linear Actuator) to 9
  - For a number of units no TRL is identified, but these are units which can be developed in the frame of normal project development (mirror cover, structures, baffles, TCM)

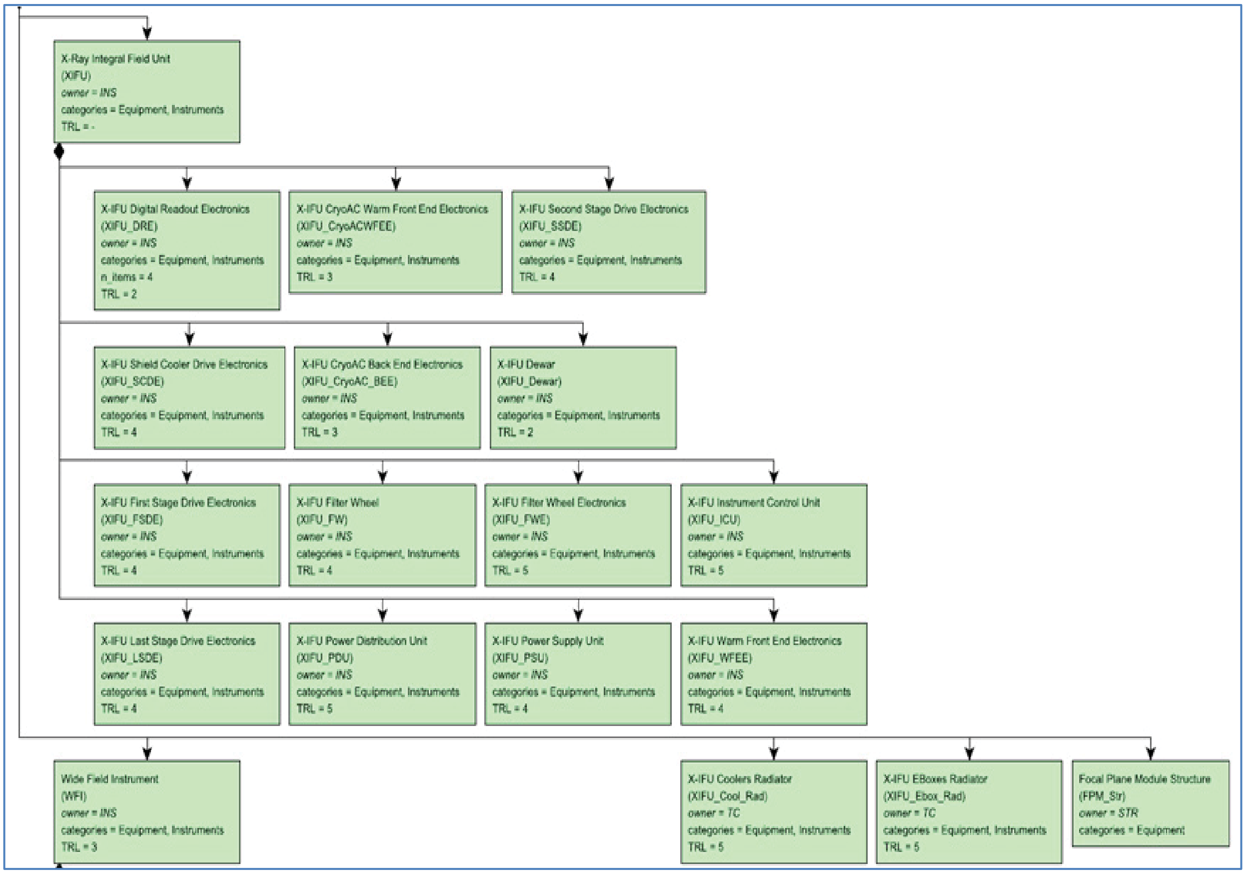

Figure 20-1: TRL X-Ray Field Unit

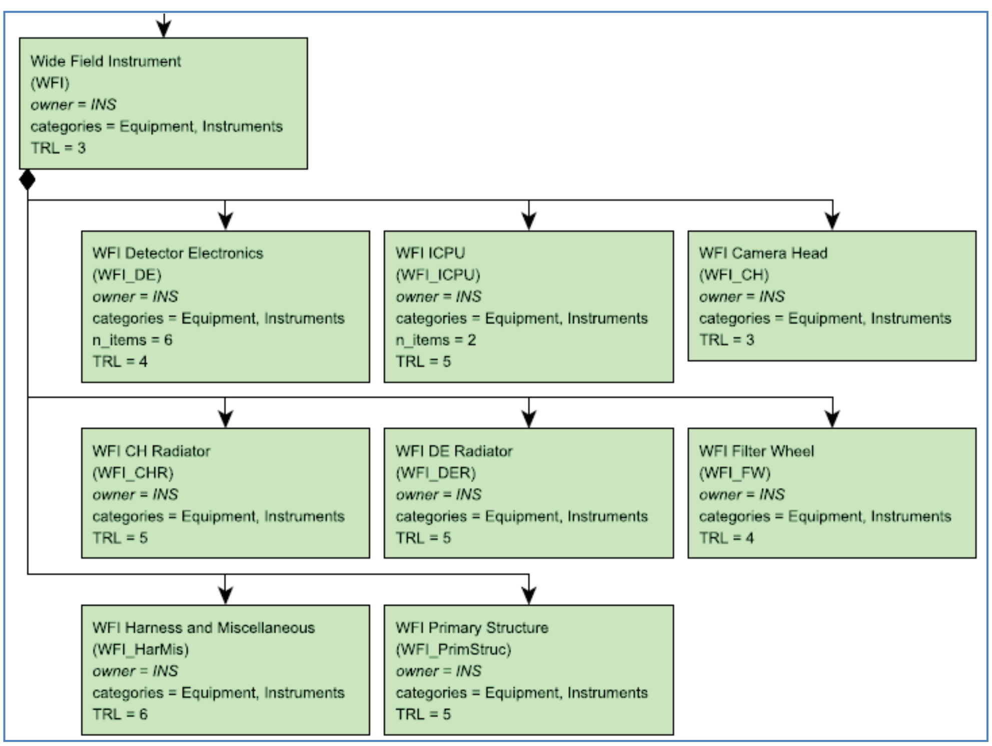

Figure 20-2: TRL Wide Field Instrument

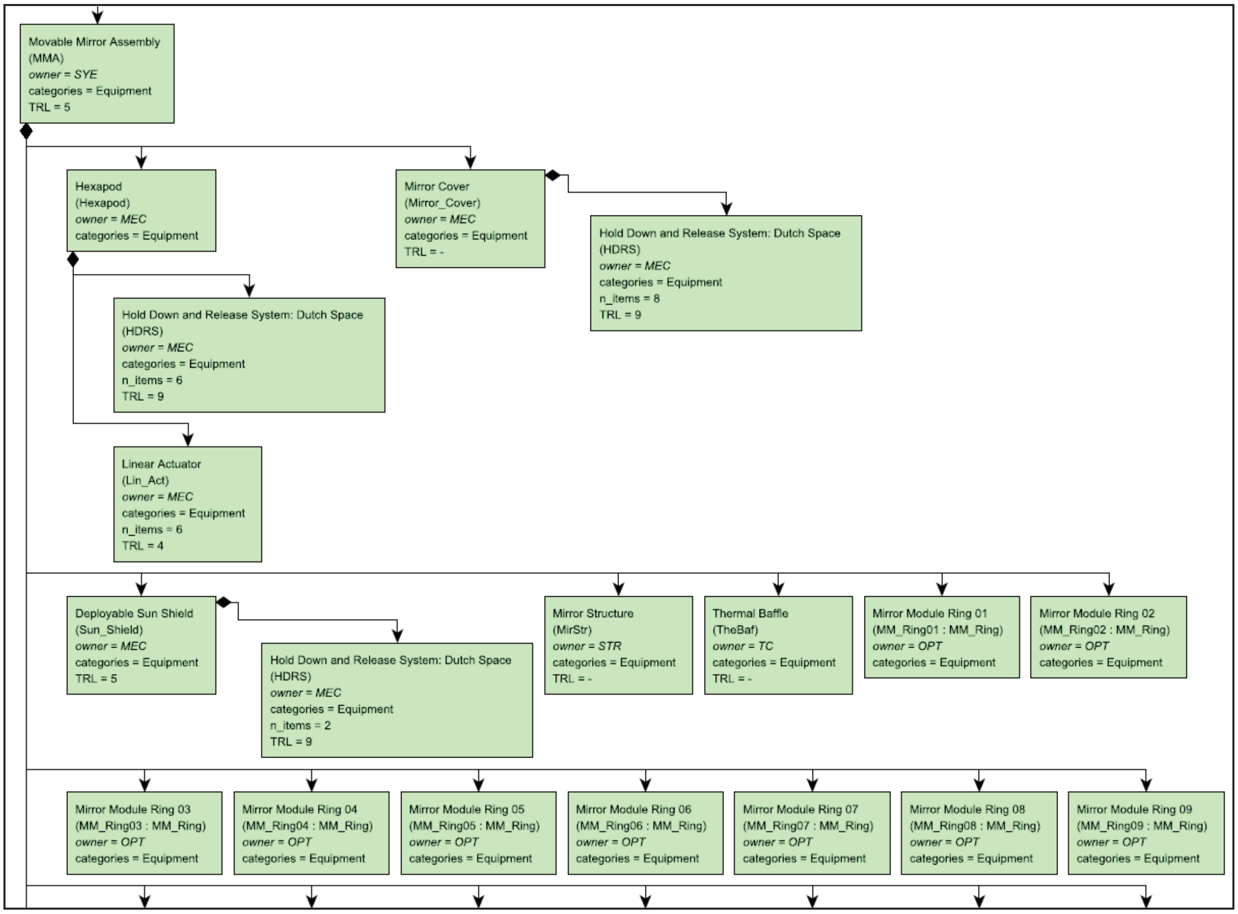

Figure 20-3: TRL MMA

20.5 Integration and Verification Approach

The mirror modules production and assembly process is independent from the rest of the satellite integration and is expected to last about 24 months.

The mirror module integration is expected to be from the top of the MMA. Thermal control hardware and any other harness shall be installed before the mirror modules as far as possible.

Measuring the alignment stability and verifying the Hexapod mechanism performance is a challenge for which details are still to be defined. Whether an alignment measurement system is needed in-flight is still to be determined.

Environmental testing of ATHENA is expected to be only possible on separate modules, SVM and FPA (XMM approach), i.e. Upper Module and Lower Module, plus the central telescope tube element.

Sine vibration testing in 1 piece may be feasible with Hydra (but testing by modules seems more efficient).

A suitable X-ray test facility needs to be found for the Mirror Assembly.

20.6 Model Philosophy

Key elements for the model philosophy are:

- Mirror module manufacturing and testing:
  - Maximising modules production and test rates
  - Availability of X-ray Facility mandatory
  - Qualification and FM production concepts as per IXO study
- Spacecraft STM, AVM and PFM
  - Complemented by QM or EQM for equipment at TRL 6 before B2-C/D.

20.6.1 Satellite STM

For structural and thermal qualification the build of an STM is required which is structurally and thermally representative of flight HW, including mass properties and interfaces. The integration and tests are expected to be organized by modules (Upper and Lower Module) due to the spacecraft size.

- Structural tests
  - Sine and acoustic vibration tests (sine test may be accommodated on the full S/C)
  - Test of mechanism for mirror adjustment after environmental exposure: active (Hexapod) mechanism needed (flight quality, may become a spare of flight model mechanism)
  - Demonstrating mirror integration
  - Shock test and data acquisition for assessment
  - Test of venting mechanism, Deployable Sunshield, Antenna Deployment and Pointing Mechanisms
  - Solar Arrays Deployment Mechanism test
  - Tests that would need the complete S/C:
    - Alignment Mirror to FPA (by laser and mirror devices)
    - Light tightness
    - Thermal distortion
- Thermal Test
  - Correlation of the TMM
  - Verification of FPA and SVM
  - Venting Verification.

20.6.2 Satellite AVM

The Avionics Verification Model (AVM) is built according to the concept of a flat-sat (on a test bench) with EM or EBB units, representative cables, connectors and harness routing. It will be used for:

- Functional tests
  - OBSW versions test
  - Functional testing

- Mission sequence test
- Environmental tests
  - EMC conducted emission and susceptibility
- Compatibility tests
  - SVT-0 (not qual.)
  - RF Compatibility (Suitcase)
  - FOP-SW Validation (not qual.)
- Test support to Mission (not qual.)

Figure 20-4: Mars Express AVM

20.6.3 Satellite PFM

The satellite qualification will be completed and acceptance tests will be performed with the Protoflight Model (PFM). As for the STM the environmental acceptance tests are expected to be organised by modules (Upper and Lower Module). The tests to be performed are:

- Functional tests
  - OBSW loading/regression tests
  - Functional testing
  - Mission sequence test
- Environmental tests
  - EMC conducted (and radiated, if so EMC Facility is needed) emission and susceptibility, auto-compatibility
  - Sine and acoustic vibration tests (sine test may be accommodated on the full S/C)
  - Clamp band release test
  - Deployment tests (all deployable) and mechanisms test

- Test of mirror adjustment mechanism after environmental exposure
- Thermal Vacuum Test
- Tests that would need the complete S/C:
  - Alignment Mirror to FPA – (by laser and mirror devices)
  - Light tightness
  - Thermal distortion

- Compatibility tests
  - SVT-1, 2

20.7 Test Matrix

Test description	ATB	STM		PFM		
		UM	LM	UM	LM	UM+LM
Handling/Integration		X	X	X	X	
Mechanical Interface		X	X	X	X	
Mass Property		X	X	X	X	
Electrical Performance	X			X	X	X
Functional Test	X			X	X	X
Deployment Test		X	X	X	X	
Telecommunication Link	X				X	
Alignment		X	X	X	X	X
Static Load		X	X			
Shock/Separation		X	X		X	
Sine Vibration		X	X	X	X	tbd
Modal Survey		X	X	X	X	
Acoustic		X	X	X	X	
Outgassing		X	X	X	X	
Thermal balance		X	X			
Thermal vacuum				X	X	
Grounding/Bonding		X	X	X	X	X
EMC conducted emission and susceptibility	X			X	X	
EMC radiated emission and susceptibility				X	X	
RF testing					X	

Table 20-3: Test Matrix

Note:

If mechanical tests e.g. sine vibration or acoustic test can be performed with the composite of Upper Module and Lower Module, then the two module level tests can be replaced by the combined test.

20.8 Schedule

Master Schedule:

- Phase 0 (7 month) ending with the Mission Definition Review (MDR) in January 2015
- Phase A ITT, 7 month, partly overlapping with Phase 0
- Phase A, 24 month, followed by PRR of 1.5 month
- ITT for Phase B1, 10 month, partly overlapping with Phase A
- Phase B1, 12 month, followed by SRR of 2 month
- ITT for Phase B2/C/C/D, about 8 month
- Phase B2, 18 month, followed by System PDR and Instrument PDR (together 3 month)
- Phase C 24 month, followed by CDR of 2 month
- Phase D, 48 month, with a Qualification Review in between (after 30 month) and followed by an Acceptance Review of 2 month and 6 month ESA contingency
- Phase E1, 3 month, including launch.

Notes:

1. The Master Schedule in Figure 20-5 identifies mission phase durations which only seem to deviate from spacecraft phase durations identified above. The mission phases include additional instrument activities and times for reviews, ITTs and consolidation of project selection.
2. Latest information identified an extension of the S/C Phase A from 24 month to 30 month. This has not been implemented yet in the schedules below.

ID	Task Name	Start	Finish	Duration	Predecessors
1	[WBS_1.0] ATHENA+ Mission	Mon 20/01/14	Tue 12/09/28	173.73 mons	
2	[WBS_1.0.X] Call for L2 Proposals	Mon 20/01/14	Thu 12/06/14	4.72 mons	
18	[Milestone] Mission Phase 0 KO	Thu 12/06/14	Thu 12/06/14	0 mons	8
19	[WBS_1.0.0] Mission Phase 0	Thu 12/06/14	Fri 29/05/15	11.41 mons	
20	Phase 0 Work	Thu 12/06/14	Wed 14/01/15	7 mons	
27	Phase A Industrial ITT	Mon 10/11/14	Fri 29/05/15	6.59 mons	
46	AO for Payload and SGS Provision	Wed 28/01/15	Thu 14/05/15	3.45 mons	
53	[Milestone] Mission Phase A KO	Fri 29/05/15	Fri 29/05/15	0 mons	45
54	[WBS_1.0.1] Mission Phase A	Mon 01/06/15	Fri 01/12/17	29.77 mons	
55	[WBS_1.0.1.1] Phase A Project Management	Mon 01/06/15	Wed 07/06/17	24 mons	53
59	[WBS_1.0.1.2] S-PRR	Thu 08/06/17	Mon 24/07/17	1.5 mons	58
60	[Milestone] S-PRR Completion	Mon 24/07/17	Mon 24/07/17	0 mons	59
61	[WBS_1.0.1.3] I-PRR	Thu 08/06/17	Mon 24/07/17	1.5 mons	59SS
62	[Milestone] I-PRR Completion	Mon 24/07/17	Mon 24/07/17	0 mons	61
63	[WBS_1.0.1.4] Phase B1 Industrial ITT	Tue 31/01/17	Fri 01/12/17	9.95 mons	
77	[Milestone] Mission Phase B1 KO	Fri 01/12/17	Fri 01/12/17	0 mons	76
78	[WBS_1.0.2] Mission Phase B1	Mon 04/12/17	Fri 04/10/19	21.82 mons	
95	[Milestone] Mission Phase B2 KO	Fri 04/10/19	Fri 04/10/19	0 mons	94
96	[WBS_1.0.3] Mission Phase B2	Mon 07/10/19	Tue 13/07/21	21 mons	
102	[Milestone] Phase C KO	Tue 13/07/21	Tue 13/07/21	0 mons	101
103	[WBS_1.0.4] Mission Phase C	Wed 14/07/21	Thu 21/09/23	26 mons	
109	[Milestone] Mission Phase D KO	Thu 21/09/23	Thu 21/09/23	0 mons	105
110	[WBS_1.0.5] Mission Phase D	Fri 22/09/23	Mon 12/06/28	56 mons	
121	[Milestone] Mission Phase E1 KO	Mon 12/06/28	Mon 12/06/28	0 mons	120
122	[WBS_1.0.6] Mission Phase E1	Tue 13/06/28	Tue 12/09/28	3 mons	
128	[Milestone] Launch	Mon 04/09/28	Mon 04/09/28	0 mons	125

Figure 20-5: Master schedule

ID	Task Name	Start	Finish	Duration	Predecessors
130	[WBS_1.1] SC	Fri 29/05/15	Tue 12/09/28	157.59 mons	
131	[Milestone] SC Phase A KO	Fri 29/05/15	Fri 29/05/15	0 mons	53
132	[WBS_1.1.1] SC Phase A	Mon 01/06/15	Wed 07/06/17	24 mons	131
133	[Milestone] S-PRR Completion	Mon 24/07/17	Mon 24/07/17	0 mons	60
134	[Milestone] SC Phase B1 KO	Fri 01/12/17	Fri 01/12/17	0 mons	77
135	[WBS_1.1.2] SC Phase B1	Mon 04/12/17	Thu 06/12/18	12 mons	134
136	[Milestone] S-SRR Completion	Wed 06/02/19	Wed 06/02/19	0 mons	81
137	[Milestone] SC Phase B2 KO	Fri 04/10/19	Fri 04/10/19	0 mons	95
138	[WBS_1.1.3] SC Phase B2	Mon 07/10/19	Mon 12/04/21	18 mons	137
139	[Milestone] S-PDR Completion	Fri 11/06/21	Fri 11/06/21	0 mons	99
140	[Milestone] SC Phase C KO	Tue 13/07/21	Tue 13/07/21	0 mons	102
141	[WBS_1.1.4] SC Phase C	Wed 14/07/21	Fri 21/07/23	24 mons	140
142	[Milestone] Receipt of EFM from X-IFU	Fri 21/07/23	Fri 21/07/23	0 mons	171
143	[Milestone] Receipt of STM from X-IFU	Mon 24/07/23	Mon 24/07/23	0 mons	172
144	[Milestone] Receipt of EFM from WFI	Fri 21/07/23	Fri 21/07/23	0 mons	194
145	[Milestone] Receipt of STM from WFI	Mon 24/07/23	Mon 24/07/23	0 mons	195
146	[Milestone] S-CDR Completion	Thu 21/09/23	Thu 21/09/23	0 mons	106
147	[Milestone] SC Phase D KO	Thu 21/09/23	Thu 21/09/23	0 mons	109
148	[WBS_1.1.5] SC Phase D	Fri 22/09/23	Fri 08/10/27	48 mons	147
149	[Milestone] S-QR Completion	Wed 03/06/26	Wed 03/06/26	0 mons	112
150	[Milestone] Receipt of X-IFU FM	Thu 03/09/26	Thu 03/09/26	0 mons	178
151	[Milestone] S-AR Completion	Thu 09/12/27	Thu 09/12/27	0 mons	117
152	[Milestone] SC Phase E1 KO	Mon 12/06/28	Mon 12/06/28	0 mons	121
153	[WBS_1.1.6] SC Phase E1	Tue 13/06/28	Tue 12/09/28	3 mons	152
154	[Milestone] FRR Completion	Fri 11/08/28	Fri 11/08/28	0 mons	126
155	[Milestone] LRR Completion	Mon 04/09/28	Mon 04/09/28	0 mons	127
156	[Milestone] Launch	Mon 04/09/28	Mon 04/09/28	0 mons	128

Figure 20-6: Spacecraft schedule

ID	Task Name	Start	Finish	Duration	Predecessors
158	**[WBS_1.2] X-IFU**	**Thu 14/05/15**	**Tue 12/09/28**	**158.09 mons**	
159	[Milestone] X-IFU Phase A KO	Thu 14/05/15	Thu 14/05/15	0 mons	52
160	[WBS_1.2.1] X-IFU Phase A	Fri 15/05/15	Tue 23/05/17	24 mons	159
161	[Milestone] I-PRR Completion	Mon 24/07/17	Mon 24/07/17	0 mons	62
162	[Milestone] X-IFU Phase B1 KO	Mon 24/07/17	Mon 24/07/17	0 mons	62
163	[WBS_1.2.2] X-IFU Phase B1	Tue 25/07/17	Fri 27/07/18	12 mons	162
164	[Milestone] I-SRR Completion	Wed 06/02/19	Wed 06/02/19	0 mons	83
165	[Milestone] X-IFU Phase B2 KO	Wed 06/02/19	Wed 06/02/19	0 mons	83
166	[Milestone] X-IFU DM completed	Wed 06/02/19	Wed 06/02/19	0 mons	83
167	[WBS_1.2.3] X-IFU Phase B2	Thu 07/02/19	Mon 15/02/21	24 mons	165
168	[Milestone] I-PDR Completion	Tue 13/07/21	Tue 13/07/21	0 mons	101
169	[Milestone] X-IFU Phase C KO	Tue 13/07/21	Tue 13/07/21	0 mons	168
170	[WBS_1.2.4] X-IFU Phase C	Wed 14/07/21	Fri 21/07/23	24 mons	169
171	[Milestone] X-IFU STM delivery to SC Prime	Fri 21/07/23	Fri 21/07/23	0 mons	170
172	[Milestone] X-IFU EFM delivery to SC Prime	Mon 24/07/23	Mon 24/07/23	0 mons	170
173	[Milestone] I-CDR Completion	Tue 22/08/23	Tue 22/08/23	0 mons	108
174	[Milestone] X-IFU Phase D KO	Tue 22/08/23	Tue 22/08/23	0 mons	107
175	[Milestone] X-IFU QR Completion	Thu 02/04/26	Thu 02/04/26	0 mons	115
176	[WBS_1.2.5] X-IFU Phase D	Wed 23/08/23	Thu 03/09/26	36 mons	174
177	[Milestone] I-AR Completion	Thu 03/09/26	Thu 03/09/26	0 mons	176
178	[Milestone] X-IFU FM delivery to SC Prime	Thu 03/09/26	Thu 03/09/26	0 mons	177
179	[Milestone] X-IFU Phase E1 KO	Mon 12/06/28	Mon 12/06/28	0 mons	152
180	[WBS_1.2.6] X-IFU Phase E1	Tue 13/06/28	Tue 12/09/28	3 mons	179

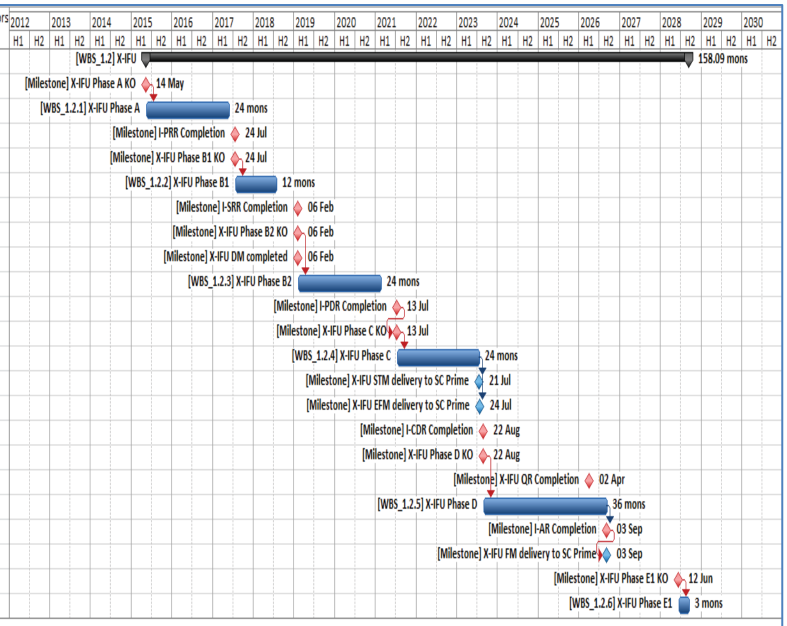

Figure 20-7: Instrument schedule

Note:

The schedules for the instruments X-IFU and WFI are identical and therefore only one is represented here.

ID	Task Name	Start	Finish	Duration
211	Technology Development Activities	Mon 02/11/09	Tue 09/04/19	111.91 mons
212	[Milestone] TRL 6 Deadline	Tue 09/04/19	Tue 09/04/19	0 mons
213	ATHENA-Specific with Highly Critical ATHENA Application	Wed 04/11/09	Mon 16/02/15	62.64 mons
214	C216-006MM [IXO Mirror Module Ruggedisation]	Mon 02/01/12	Mon 30/06/14	29.55 mons
219	C216-008MM [Inner SPO Module]	Mon 20/01/14	Mon 20/01/14	0 mons
220	C216-134MM [Outer SPO Mirror Module]	Mon 20/01/14	Mon 20/01/14	0 mons
221	C216-117MM [True Wolter]	Mon 04/02/13	Wed 01/10/14	19.64 mons
226	C216-125MM [True Wolter CCN]	Mon 20/01/14	Mon 20/01/14	0 mons
227	C216-126MM [SPO EM]	Mon 20/01/14	Mon 20/01/14	0 mons
228	C216-127MM(A) [SPO Assembly, Integration, Test]	Mon 20/01/14	Mon 20/01/14	0 mons
229	C216-127MM(B) [SPO Assembly, Integration, Test]	Mon 20/01/14	Mon 20/01/14	0 mons
230	C216-007MM [MS & Optics Integ. Demonstrator]	Mon 20/01/14	Mon 20/01/14	0 mons
231	C216-135MM [Prep. of coated X-ray MP Prod.]	Mon 20/01/14	Mon 20/01/14	0 mons
232	C216-128MM [SPO Manufacturing Facility Design]	Mon 20/01/14	Mon 20/01/14	0 mons
233	S216-116PA [Multilayer SPO Stack & Test]	Tue 05/03/13	Mon 16/02/15	23.14 mons
239	C216-129FT [Synchrotron beam-time BessyII]	Mon 20/01/14	Mon 20/01/14	0 mons
240	C216-130FT [BessyII Enhanced Performance]	Mon 20/01/14	Mon 20/01/14	0 mons
241	C216-005MM [Panter Upgrade]	Tue 23/02/10	Mon 31/03/14	48.59 mons
245	C216-131FT [Panter Therm. Control & Large Optics Acc.]	Mon 20/01/14	Mon 20/01/14	0 mons
246	T216-022MM [Large X-ray Window Development]	Wed 04/11/09	Fri 13/06/14	54.64 mons
251	C216-132FT [SPO Modelling & Simulation]	Mon 20/01/14	Mon 20/01/14	0 mons
252	C204-110EE [COXPROS - Background Model]	Mon 20/01/14	Mon 20/01/14	0 mons
253	C221-005FI [Cryogenic Vibration Isolators]	Mon 20/01/14	Mon 20/01/14	0 mons
254	C221-006FI [Superconducting Flex Harness]	Mon 20/01/14	Mon 20/01/14	0 mons
255	C221-007FM [Low vib. 15K PT EM inc. CDE]	Mon 20/01/14	Mon 20/01/14	0 mons
256	C221-038FM [2K JT EM inc. CDE]	Mon 20/01/14	Mon 20/01/14	0 mons
257	Generic with Highly Critical ATHENA Application	Mon 02/11/09	Wed 30/09/15	70.09 mons
258	C220-032MC [15K Pulse-Tube Cooler]	Fri 30/04/10	Fri 28/08/15	63.18 mons
264	T220-053MC [2k JT Cooler]	Mon 02/11/09	Fri 29/08/14	57.23 mons
270	C221-00MT [Detector Cooling down to 50mK]	Mon 20/01/14	Mon 20/01/14	0 mons
271	C221-002MT [Perf. Ver/Qual. Of vib. free sorp/JT Cooler	Mon 20/01/14	Mon 20/01/14	0 mons
272	C221-003FI [Hydrogen Phase ESU between 15-20K]	Fri 13/09/13	Wed 30/09/15	24.23 mons
278	C217-031FI [TES Array Optimisation]	Fri 06/06/14	Fri 06/06/14	0 mons
280	C220-001FT [Passive Vibration Control]	Mon 20/01/14	Wed 01/10/14	8.27 mons
322	Specific with Moderately Critical ATHENA Application	Mon 20/01/14	Mon 20/01/14	0 mons
323	C220-038FM [Instrument Selection Mechanism]	Mon 20/01/14	Mon 20/01/14	0 mons
324	Generic with Possible ATHENA Application	Mon 20/01/14	Wed 30/09/15	20.09 mons
325	T201-033ED [Platform & PL Sensor/Actuator Bus Nodes]	Mon 20/01/14	Mon 20/01/14	0 mons
326	C224-001FT [Ultra-low Roughness Mirror Coatings]	Mon 20/01/14	Mon 20/01/14	0 mons
327	C205-106EC [High Accuracy STR]	Mon 20/01/14	Mon 20/01/14	0 mons
328	T205-030C [CMG Based AOCS]	Mon 10/02/14	Wed 30/09/15	19.41 mons
334	Unplanned with Moderately Critical ATHENA Application	Mon 20/01/14	Mon 20/01/14	0 mons
335	On-Board Metrology	Mon 20/01/14	Mon 20/01/14	0 mons
336	SC Mirror Contamination Cover	Mon 20/01/14	Mon 20/01/14	0 mons
337	Fast Planning S/W	Mon 20/01/14	Mon 20/01/14	0 mons
338	Fast Timeline Generation	Mon 20/01/14	Mon 20/01/14	0 mons

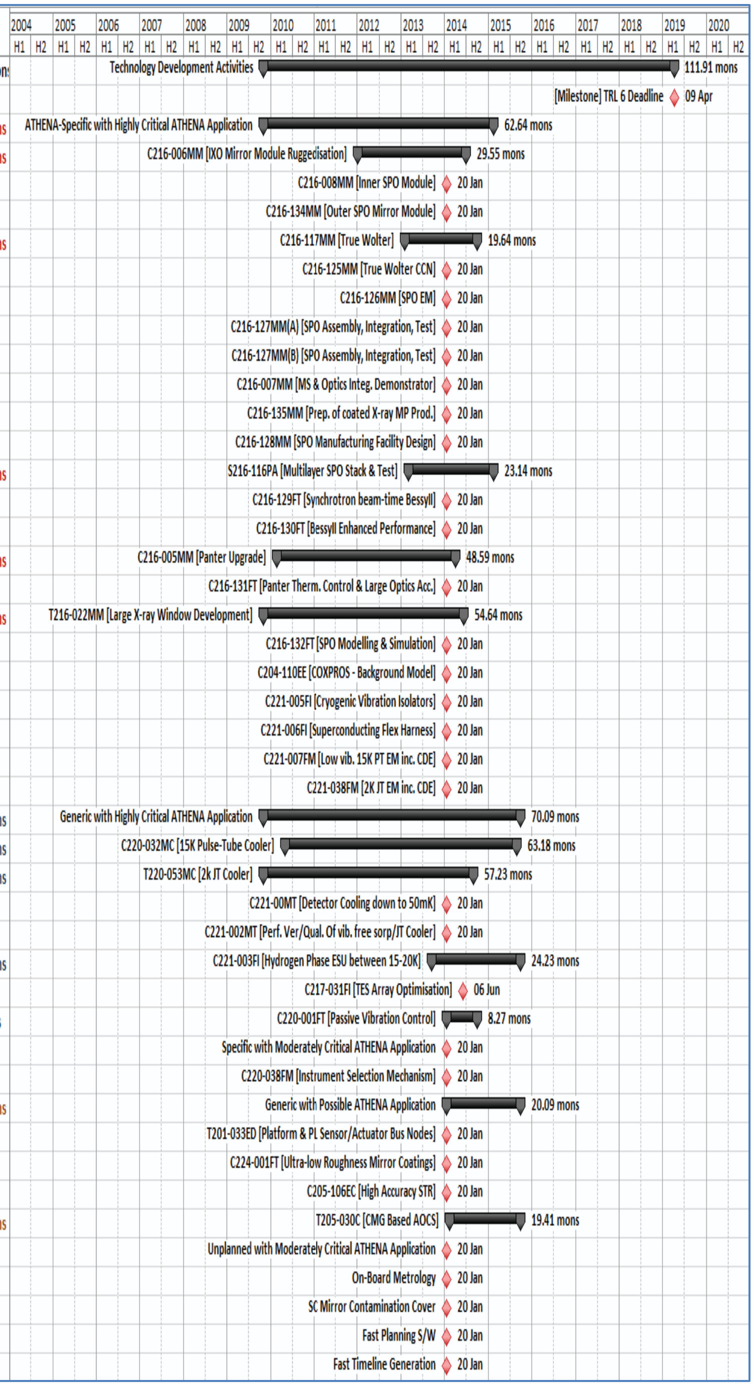

Figure 20-8: Technology development activities

20.9 Summary and Conclusions

The main challenge for this project is to find technical solutions fitting to the cost frame work. Next to that all technologies with low TRL need to be advance such that they reach TRL 6 (RD[47]) before the start of the implementation phase. This could become difficult, although the launch is only required in 2028, because some parts of the X-Ray Field Unit are reported to be only at TRL 2 presently.

For model philosophy at system level an approach with STM, PFM and AVM is recommended. For the environmental testing the proven approach of the XMM project is proposed to be followed splitting the satellite into an Upper Module and a Lower Module.

The mirror modules production, assembly and verification process is independent from the rest of the satellite integration and is expected to last about 24 months. It should be started rather early in the implementation phase.

The integration of the mirror modules must be very well defined and optimised with respect to the overall satellite integration and verification and for the minimisation of contamination risks.

Achievement of a launch date in 2028 is critical because, according to latest Project information and not yet implemented in the presented schedules, the spacecraft Phase A duration will be extended from 24 month to 30 month. The presently identified launch date in September 2028 will shift accordingly unless the duration of other phases will be reduced. The reduction of the ITT phase between Phase A and Phase B1 and between Phase B1 and Phase B2/C/D is hardly possible. An equivalent reduction in Phase B2/C/D seems to be possible however.

22 CONCLUSIONS

22.1 Satisfaction of Requirements

Parameter	ATHENA (as proposed)	ATHENA (CDF baseline design)
System Requirements		
# Instruments	**2**	**2**
On-axis A_eff (~1keV)	**2m^2**	**1.37 m^2**
On-axis A_eff (6keV)	**0.25m^2**	**0.23m^2**
PSF HEW (on axis, <~8keV)	**5"**	**5"**
AKE (a posteriori)	**1" (3σ)**	**1" (3σ)**
ToO reaction time	**<4h 80% of cases**	**<4h 67% of cases (*)**
Inst. Funct. Requirements		
X-IFU e_res	**2.5eV**	**2.5eV**
X-IFU FoV	**5' diameter**	**5' diameter**
WFI e_res	**150eV**	**150eV**
WFI FoV	**40'x40'**	**40'x40'**
Inst. Resource Requirements		
X-IFU (inc. CC)		
Mass (Incl. system margin)	**583 kg**	**583 kg**
Max Power	**1452 W**	**1452 W**
WFI		
Mass (Incl. system margin)	**288 kg**	**288 kg**
Max Power	**684 W**	**684 W**

Table 22-1: Satisfaction of main requirements

The table above quantifies the CDF design in terms of the key performance indicators defined at the onset of the study. A comparison is done against the mission proposed by the ASST prior to the study. It can be noticed that most of the requirements were met with the exception of the effective area and the ToO reaction time.

Note: Recall that the achieved effective area assumes a 1mm rib-spacing. Should 2mm be used, this climbs to 1.51m^2.

Note: The overall requirement to observe GRBs (SG4.1 in RD[10]) is however met, because the SC FoR is 60%, which relaxes the ToO-reaction time requirement (R-MIS-550).

22.2 Satisfaction of CaC

The design-to-cost point of targeting the 2624mm adaptor resulted in, as predicted, a Mission CaC significantly above the envelope. However, during the CDF study period an important programmatic commitment by CNES to take a SI-role for the CC was confirmed, combined with a tentatively agreed CC-architecture as described in chapter 5, mainly using JAXA technology with some European components. Under the assumption that ESA/NASA are also able to agree on significant international contributions to the CaC (significant NASA involvement is already foreseen within the instruments), then the CDF baseline should be broadly-compatible with the 1Bn€ CaC envelope, while retaining in large part of the science-case associated with 2m^2 Effective Area at 1 keV.

Fully recovering the lost 0.5m^2 Effective Area is considered out-of-scope due to the CaC-constraint. Nonetheless, the likely switch to A6 can be considered as a possible opportunity; the motivation for the A6 development is to reduce launch costs, and therefore could release some money currently allocated to the LV (assuming A5 ECA) to the SC, perhaps allowing recovery of ***some*** of the lost Effective Area. However the to-be-assumed LV cost is not clear at present.

22.3 Results of Main Analysis done during the Study

Analysis	Status	Result	Comments
ISM trade-off	**Completed**	**MMA 6-DOF (hexapod) solution chosen**	**Option with best result on system level trade-off looking at the criteria: cost, risk, effective area, angular resolution, ToO reaction time, FoV.**
Ariane 5 ECA accommodation	**Completed**	**Compliant, even without instrument descope**	**Focal length remained at 12 m. FPM was designed for FoR 60% (exclusion angle of 34.5 deg). All necessary radiative surface covered (with additional trimming surfaces). Some electronic boxes were accommodated outside the FPM to minimise volumetric constraints.**
AIT requirements imposed on configuration	**Completed**	**Compliant**	**FMS broken into 3 different parts to improve testability. Special GSE to handle mirror during ground operations.**
Mirror structure material choice	**Completed**	**Compliant**	**Choice of material (Ti) to comply with frequency mode requirements (FEM analysis) and facilitate manufacturing. CTE taken into account for mirror heaters sizing (temperature requirements set by allocation on HEW budget).**
SVM configuration	**Completed**	**Compliant**	**All equipment positioned into an octagonal structure around MAM. CoG distance to CoP taken into account in the design of the AOGNC system and sized for in terms of propellant.**
Pointing requirements and consequences (need for OBM)	**Completed**	**Partially compliant**	**No AKE improvement on ground assumed (6.2" 3σ). Use of OBM deemed necessary for AKE. Pointing budget: APE = 7.4 arcsec PDE = 7.4 arcsec**

			RPE = 1.2 arcsec **AKE = 6.4 arcsec** **Star Trackers, 4 RWs.**
ToO architecture	**Completed**	**Compliant**	**<4h 67% of cases. Meets scientific requirement because FoR = 60%.**
Launcher static moment	**Preliminary**	**Not compliant**	**Estimated with point masses. Modest violation of the 2624 LVA requirement. Mitigation actions proposed.**

Table 22-2: Summary of main analysis done during the CDF study

22.4 Further Study Areas

During the CDF study, a static moment analysis (w.r.t. to launcher interface) was done in order to verify compatibility with the 2624LVA of Ariane 5 ECA. This was done at the system level by using the mass allocation given by the different domains of expertise to their equipment (including equipment level margins –DMM, and system level margins), and using the preliminary placement given by the configuration in the z-axis.

Equipment		Mass (including DMM and system margin) (kg)
FMS		
Venting_Mech	6.00	21.41
(blank)	6.02	674.64
FPM		
FPM_Str	12.40	345.60
WFI		345.60
WFI_CH	12.20	73.58
WFI_CHR	12.80	23.18
WFI_DE_0	12.40	7.78
WFI_DE_1	12.40	7.78
WFI_DE_2	12.40	7.78
WFI_DE_3	12.40	7.78
WFI_DE_4	12.40	7.78
WFI_DE_5	12.40	7.78
WFI_DER	12.80	49.25
WFI_FW	11.90	57.31
WFI_HarMis	12.20	43.92
WFI_ICPU_0	11.00	15.84
WFI_ICPU_1	11.00	15.84
WFI_PrimStruc	12.20	20.02
XIFU		
XIFU_CryoAC_BEE	12.40	3.78
XIFU_CryoACWFEE	12.40	2.16
XIFU_Dewar	12.60	345.04
XIFU_DRE_0	11.00	46.80
XIFU_DRE_1	11.00	46.80
XIFU_DRE_2	11.00	46.80

XIFU_DRE_3	11.00	46.80
XIFU_FSDE	11.00	34.56
XIFU_FW	11.90	12.24
XIFU_FWE	12.40	4.18
XIFU_ICU	11.00	12.67
XIFU_LSDE	11.00	19.44
XIFU_PDU	11.00	3.12
XIFU_PSU	12.40	2.34
XIFU_SCDE	11.00	23.04
XIFU_SSDE	11.00	21.02
XIFU_WFEE	12.40	28.80
XIFU_Cool_Rad	13.00	58.26
XIFU_Ebox_Rad	13.00	24.71
X-IFU_Th_Link	13.00	18.14

Table 22-3: Part of preliminary point mass allocation for static moment estimation

The static moment analysis showed that the CDF baseline design was not compliant with the allowable limit for the 2624 LVA of Ariane 5 (480200 N.m corresponding to 2 gs lateral load for a mass of 7000 kg at 3.5 m). The position of the CoG was estimated at 4.21 m from the launcher interface, which implied a non-compliance with roughly 5% negative margin.

Note: of course the distribution of the system margin in z is a priori not known, so this analysis is indicative only. A parametric model was constructed to evaluate the possible impact of reducing the FPM mass, and/or reducing the focal length in the static moment, which is shown in Figure 22-1.

		Focal length reduction (m)										
		0.00	0.10	0.20	0.30	0.40	0.50	0.60	0.70	0.80	0.90	1.00
FPM mass reduction (%)	0.00%	-4.56%	-4.09%	-3.62%	-3.15%	-2.68%	-2.21%	-1.74%	-1.27%	-0.80%	-0.33%	0.14%
	1.00%	-3.98%	-3.51%	-3.05%	-2.58%	-2.12%	-1.65%	-1.19%	-0.72%	-0.26%	0.21%	0.67%
	2.00%	-3.40%	-2.94%	-2.48%	-2.02%	-1.55%	-1.09%	-0.63%	-0.17%	0.29%	0.75%	1.21%
	3.00%	-2.82%	-2.36%	-1.90%	-1.45%	-0.99%	-0.54%	-0.08%	0.37%	0.83%	1.29%	1.74%
	4.00%	-2.23%	-1.78%	-1.33%	-0.88%	-0.43%	0.02%	0.47%	0.92%	1.37%	1.83%	2.28%
	5.00%	-1.65%	-1.21%	-0.76%	-0.31%	0.13%	0.58%	1.03%	1.47%	1.92%	2.36%	2.81%
	6.00%	-1.07%	-0.63%	-0.19%	0.25%	0.70%	1.14%	1.58%	2.02%	2.46%	2.90%	3.35%
	7.00%	-0.49%	-0.05%	0.38%	0.82%	1.26%	1.69%	2.13%	2.57%	3.01%	3.44%	3.88%
	8.00%	0.09%	0.52%	0.96%	1.39%	1.82%	2.25%	2.69%	3.12%	3.55%	3.98%	4.41%
	9.00%	0.67%	1.10%	1.53%	1.96%	2.38%	2.81%	3.24%	3.67%	4.09%	4.52%	4.95%
	10.00%	1.25%	1.68%	2.10%	2.52%	2.95%	3.37%	3.79%	4.21%	4.64%	5.06%	5.48%

Figure 22-1: Impact of changing FPM mass and/or focal length in the launcher static moment (green depicts compliance, and red non-compliance)

This preliminary analysis showed that, for instance, reducing the FPM mass by 8%, or reducing the focal length by 1 m, would allow compliance to the static moment limit.

Other mitigation options were also mentioned during the study:

- Changing to a larger LVA, which would result in a higher static moment limit
- Changing the placement of the PL electronics in order to lower the CoG, subject to the constraints on their placement identified in chapter 5.4. This exercise showed that a possible optimization of the placement of the electronic boxes (particularly the DREs) can have a significant impact in the position of the CoG.

The CDF baseline ISM (MMA – hexapod) was selected for a number of technical reasons both at mechanism and system-level. However, the CDF study represents only a first-assessment of this critically important trade-off, and the CDF design should not be taken as a starting point for the Phase A study. Note also that the hexapod was sized assuming it will be off-loaded by MGSE during ground operations, and HDRMs during launch. Accordingly, ground-handling aspects should be a key consideration during the Phase A Assessment.

The CDF baseline MAM does not include a dedicated thermal baffle; this results in a high power consumption (~2.5kW) of the MAM heaters to maintain the MMs to their specified temperature stability (20°C±1°C). A thermal baffle should be considered to reduce the power requirement.

The selection of Titanium for the MS was driven by easier manufacture, and avoidance of problems with CME (associated with CFRP). The thermo-elastic performance is considerably worse than for CFRP, but considered acceptable with appropriate temperature control, but this does come at the expense of a high power requirement. As with the selected ISM-baseline, the CDF MA represents only a first-assessment, and should not be taken as a starting point for the Phase A study.

The MAM and PL cleanliness have not been assessed in the CDF study, and this should receive attention during Assessment. The baffling and magnetic diverters have also only been roughly sized, and should be treated with more detail during Phase A.

In addition to the large number of ATHENA-specific and applicable generic technology development activities which were already underway for the key areas of the mission (mainly optics and cooling-chain elements…), this CDF study has identified the need to exploit the on-going High Accuracy STR TDA. Also a TDA to explore the ISM design will be instigated to assess this important element, and the OBM is also under consideration for technology development, pending refinement of requirements and comparison with heritage solutions.

Nascent international contribution discussions are underway, with keen interest from JAXA/NASA to be involved, and the assumption is therefore made that significant international contributions will become available to retire the excess. Parallel to the CDF a report RD[55] aggregating suggestions and possibilities for international collaboration was produced with inputs from the CDF study team, JAXA, NASA and the ASST.

At the time of writing, the Council of Ministers 2014 discontinued the development of A5 ME and approved the development of the A6 launcher. Nominally two variants of A6 are targeted, with the heavy variant (A-64) having a mass capability (10.9t to GTO) and fairing (A5 ME-like) compatible with ATHENA requirements. However, this is a paper launch vehicle at present, and the A6 development should be carefully followed during Assessment.

This Page Intentionally Blank

23 REFERENCES

RD[1] International X-Ray Telescope (IXO) study CDF-082(A) dated December 2008

RD[2] IXO International X-Ray Telescope, CDF-086(A) dated April 2009

RD[3] PLATO Consolidated Report on Mission Analysis (CReMA) 1.1, M. Landgraf and F. Renk, Issue 1.2, April 2010

RD[4] GAIA Consolidated Report on Mission Analysis (CReMA) 4.0 , M. Landgraf and F. Renk, Issue 4.0, April 2010

RD[5] ATHENA (L1) Internal Study Report SRE-PA/2011.033/NR, Issue 1.0 dated 22/06/2014

RD[6] ATHENA PDD (ATHENA-ESA-PDD-0001 draft 07/06/2014)

RD[7] "ATHENA telescope reference design and effective area estimates", SRE-F/2014-033, T. Oosterbroek, Issue 1.0, 04/06/2014

RD[8] "The Optical Design of the ATHENA+ Mirror", R. Willingale et al., 2014

RD[9] ATHENA – ToO Reaction Time Model Description & T/O, ATHENA-ESA-TN-0002, Issue 1.0, 17/11/2014.

RD[10] ATHENA SciRD (Science Requirements Document)

RD[11] ATHENA MRD (Mission Requirements Document)

RD[12] ATHENA SRD (SC Requirements Document)

RD[13] ATHENA ConOps (Concept of Operations)

RD[14] ATHENA – The Advanced Telescope for High ENergy Astrohpyisics, ATHENA ATHENA Science Support Team

RD[15] ATHENA CReMA (Consolidated Report on Mission Analysis)

RD[16] ATHENA MBD (Mission Budgets Document)

RD[17] Ariane-5 User's Manual, Issue 5 Revision 1, July 2011, www.arianespace.com

RD[18] Guidelines for space mechanism ball-bearing design assembly and preloading operations, TEC-MSM/2013/147/ln/LG , Issue 01, 20/09/2013.

RD[19] ADR High Precision Ball Bearings Catalogue, ADR, www.adr-alcen.com.

RD[20] Phytron VSS Extreme Environment Stepper Motors, Phytron, www.phytron.com.

RD[21] CASM–32 Linear units, SKF, PUB MT/P8 12148 EN, 09/2011, http://www.skf.com

RD[22] SEIS Instrument Linear Actuator, ISP System, Presentation at at CCT MAT 2104, 16/09/2014, http://cct.cnes.fr/content/mat%C3%A9riaux

RD[23] Brian P. Trease, Yong-Mo Moon Sridhar Kota, Design of Large-Displacement Compliant Joints, J. Mech. Des., 07/11/ 2004.

RD[24] Jens Müller, Christian Anderau, High Load Low Shock Release Unit (30 kN), ESMATS 2009.

RD[25] J. H. Burge, An easy way to relate optical element motion to system pointing stability, Current Developments In Lens Design And Optical Engineering VII Proc. SPIE 2006.

RD[26] PEPS models forATHENA ATHENA CDF study. Keith Stephenson. svn://subversion.tec.estec.esa.int/users/bgarciag/svn/ecosimpro/MISSIONSCDF_ATHENA_2014

RD[27] ECSS-E-ST-60-10C - Control Performance standard

RD[28] "The Pointing and Alignment of XMM", A. Elfving & G. Bagnasco, Dec 1999, ESA Bulletin 100.

RD[29] "Aspect Camera Assembly overview", Tom Aldcroft, 19/6/2001, URL: *cxc.harvard.edu/mta/ASPECT/aca_training/ACA_overview_CC.pdf*

RD[30] "The Canadian Astro-H Metrology System", Luigi Gallo, Casey Lamberta, Alex Koujelevb, Stephane Gagnonc, Martin Guibert, 2014, Proc. of Space Telescopes and Instrumentation 2014, Vol. 9144.

RD[31] TEC-MPC Chemical propulsion "wiki"" database 23/10/2014

RD[32] Space Propulsion Analysis and Design ed. Humble et al, McGraw-Hill 1996

RD[33] CCSDS File Delivery Protocol (CFDP) CCSDS 727.0-B-4 Blue Book January 2007

RD[34] ECSS-E-ST-50-05C Rev. 1. Space engineering. Radio frequency and modulation. 6th March 2006

RD[35] CCSDS 401.0-B, Radio Frequency and Modulation Systems, Part 1 Earth Stations and SCs, Issue 17. July 2006

RD[36] ECSS-E-ST-50-01C Rev. 1. Space engineering. Space data links - Telemetry synchronization and channel coding. July 2008

RD[37] XMM-Newton RF switch anomaly and recovery in 2008, D. Heger, M.G.F Kirsch, ESA, ESOC, January 2010. http://www.slideshare.net/esaops/heger

RD[38] Performance of GMSK for Telemetry and PN Ranging under realistic conditions, 6th International Workshop on TT&C Systems, ESA-ESOC, 10-13 September 2014

RD[39] ATHENA - ToO Reaction Time Model Description & T/O, TN, ATHENA-ESA-TN-0003, ESA Study Team, issue 1, rev. 0

RD[40] CCSDS 401 (2.4.22A) R-1. Recommendation 2.4.22A (Modulation Methods for Simultaneous Transmission of High Symbol Rate Telemetry and PN Ranging, Space Research 8.45-8.50 Ghz Band, Space-To-Earth, Category A) of CCSDS401 (Radio Frequency and Modulation Systems-Part 1 Earth Stations and SC. April 2014. Presently under elaboration.

RD[41] IXO Ground Segment & Operations Cost Report, Ground Segment & Operations Cost Report, Rainer Timm OPS-HSA, DOP-GS-TN-1011-OPS-HAS, issue 1, revision 1, 06/03/2009

RD[42] CCSDS File Delivery Protocol, Blue book, CCSDS 727.0-B-4, January 2007

RD[43] ESOC Mission Operations Facilities & Services, http://esctoswts04/ewiki/bin/view/EMOFS/WebHome

RD[44] Space Project Management, Risk Management, ECSS-M-ST-80C, 31 July 2008.

RD[45] ECSS-E-ST-10-02C, "European Cooperation for Space Standardization, Space Engineering, Verification", 6 March 2009. http://www.ecss.nl

RD[46] ECSS- E-ST-10-03C, "European Cooperation for Space Standardization, Space Engineering, Testing", 1 June 2012. http://www.ecss.nl

RD[47] "Guidelines for the use of TRLs in ESA programmes", ESSB-HB-E-002, Issue 1, Revision 0, 21 August 2013.

RD[48] TEC-SYC/12/2009/GRE/HJ - ESA Cost Engineering Charter of Services

RD[49] TEC-SYC/GRE/SA/2005/021 - TEC-SYC Cost Risk Assessment Procedure

RD[50] ATHENA – Technology Plan, ATHENA-ESA-PL-0003, Issue 1.0, 12/06/2014.

RD[51] ATHENA Industrial Support Study: Design Document, IXO.RP.ASU.SAT.00021, Issue 1.0, 06/10/2011.

RD[52] IXO Assessment Study: Preliminary IXO Space Segment Design Document, IXO.RP.ASU.SAT.00007, Issue 3.0, 22/07/2010.

RD[53] TAS ATHENA_L1

RD[54] TAS IXO

RD[55] ATHENA – Possibilities for International Collaboration, ATHENA-ESA-PL-0004, Issue 1.0, 12/06/2014.

RD[56] ATHENA – A5 ECA Unavailability Mitigation Options, ATHENA-ESA-TN-0001, Issue 1.0, 20/06/2014.

RD[57] L2 call for proposals reference

RD[58] SSAC Paper reference

RD[59] SPIRIT technology development reference.

RD[60] TEC-SYC Cost Risk Procedure, TEC-SYC/5/2010/PRO/HJ, February 2010

This Page Intentionally Blank

24 ACRONYMS

Acronym	Definition
ACS	Attitude Control System
ADC	Analogue to Digital Converter
ADPM	Antenna Deployment and Pointing Mechanism
ADR	Adiabatic Cooler
AFE	Analogue Front End
AIT/V	Assembly, Integration and Test/Verification
AIV	Assembly, Integration and Verification
AKE	Absolute Knowledge Error
AOCS	Attitude and Orbit Control System
ALM	Additive Layer Manufacturing
APE	Absolute Performance Error
APM	Antenna Pointing Mechanism
ASH	Acquisition and Safe Hold Mode
ASIC	Application Specific Integrated Circuit
ASST	ATHENA Science Support Team
ATV	Automated Transfer Vehicle
AVM	Avionic Verification Model
BB	Bread Board
BCR	Battery charge regulator
BDR	Battery discharge regulator
BEE	Back End Electronics
BoL	Beginning of Life
CaC	Cost at Completion
CC	Cooling Chain
CCD	Charged Coupled Device
CCSDS	The Consultative Committee for Space Data Systems
CDF	Cumulative Distribution Function
CDF	Concurrent Design Facility
CDMU	Command and Data Management Unit

Acronym	Definition
CER	Cost Estimating Relationship
CFDP	CCSDS File Delivery Protocol
CFE	Control Front End
CFEE	Cold Front End Electronics
CFI	Customer Furnished Item
CFRP	Carbon Fibre Reinforced Polymer
CMA	Cost Model Accuracy
CMG	Control Moment Gyro
CoG	Centre of Gravity
CoM	Centre of Mass
ConOps	Concept of Operations
CoP	Centre of Pressure
COTS	Commercial Off The Shelf
CReMA	Consolidated Report on Mission Analysis
CSS	Coarse Sun Sensor
CTE	Coefficient of Thermal Expansion
DCR	Digital Control Room
DDS	Data Dissemination System
DE	Detector Electronics
DE/EP	Digital Electronics/ Events Processing
DEPFET	Depleted P-channel Field Effect Transistor
DMM	Design Maturity Margin
DOA	Degree of Adequacy of the Cost model
DoF	Degree Of Freedom
DRE	Digital Readout Electronics
DSA	Deep Space Antenna
EBB	Elegant BreadBoard
EC	Economic Conditions
ECC	ESTRACK Control Centre
EIRP	Equivalent Isotropic Radiated Power
EMC	ElectroMagnetic Compatability

Acronym	Definition
EoL	End of Life
EoP	Extended Operations Phase
EPC	Electrical Power Conditioner
EPDM	Ethylene propylene diene monomer
EPE	External Project Events
EPS	Electrical Power System
EQM	Engineering and Qualification Model
ESTRACK	European Space TRACKing network
FDIR	Failure Detection Isolation and Recovery
FDM	Frequency Domain Multiplexing
FEE	Front End Electronics
FEM	Finite Element Model
FFBD	Functional Flow Block Diagram
FFOS	Formation Flying Optical Sensor
FL	Focal Length
FM	Flight Model
FMS	Fixed Metering Structure
FOP	Flight Operations Plan
FOP-SW	Flight Operations Software
FoR	Field of Regard
FOS	Flight Operations Ground Segment
FoV	Field of View
FP	Focal Plane
FPA	Focal Plane Assembly
FPGA	Field Programmable Gate Array
FPM	Focal Plane Module
FPS	Fine Point Slew Mode
FRF	Frequency Response Function
G/S	Ground Station
GMM	Geometrical Mathematical Model
GNC	Guidance, Navigations and Control